EVALUATION AND OPTIMAL DESIGN OF SPECTRAL SENSITIVITIES FOR DIGITAL COLOR IMAGING

by

Shuxue Quan

B.S. Beijing Institute of Technology, Beijing, China (1994)

M.S. Beijing Institute of Technology, Beijing, China (1997)

A dissertation submitted in partial fulfillment
of the requirements for the Doctor of
Philosophy degree in Imaging Science
in the Chester F. Carlson Center for Imaging Science
of the College of Science
Rochester Institute of Technology

April 2002

Signature of the author _____

Accepted by _____
Coordinator, Ph.D. Degree Program

COLLEGE OF SCIENCE
ROCHESTER INSTITUTE OF TECHNOLOGY
ROCHESTER, NEW YORK

CERTIFICATE OF APPROVAL

PH.D. DEGREE DISSERTATION

The Ph.D. Degree Dissertation of Shuxue Quan
has been examined and approved by the
dissertation committee as satisfactory for the
dissertation requirement for the Ph.D. degree in
Imaging Science

_____
Dr. Noboru Ohta

_____
Dr. Daniel R. Lawrence

_____
Dr. Roy S. Berns

_____
Dr. Naoya Katoh

_____
Date

THESIS RELEASE PERMISSION
ROCHESTER INSTITUTE OF TECHNOLOGY
ROCHESTER, NEW YORK

EVALUATION AND OPTIMAL DESIGN OF SPECTRAL SENSITIVITIES FOR DIGITAL COLOR IMAGING

I, Shuxue Quan, hereby grant permission to Wallace Memorial Library of R.I.T. to reproduce my dissertation in whole or in part. Any reproduction will not be for commercial use or profit.

_____
Shuxue Quan

_____
Date

EVALUATION AND OPTIMAL DESIGN OF SPECTRAL SENSITIVITIES FOR DIGITAL COLOR IMAGING

by

Shuxue Quan

Submitted to the Center for Imaging Science
in partial fulfill of the requirements for the Ph.D.
degree at the Rochester Institute of Technology

April 2002

ABSTRACT

The quality of an image captured by color imaging system primarily depends on three factors: sensor spectral sensitivity, illumination and scene. While illumination is very important to be known, the sensitivity characteristics is critical to the success of imaging applications, and is necessary to be optimally designed under practical constraints. The ultimate image quality is judged subjectively by human visual system.

This dissertation addresses the evaluation and optimal design of spectral sensitivity functions for digital color imaging devices. Color imaging fundamentals and device characterization are discussed in the first place. For the evaluation of spectral sensitivity functions, this dissertation concentrates on the consideration of imaging noise characteristics. Both signal-independent and signal-dependent noises form an imaging noise model and noises will be propagated while signal is processed. A new colorimetric quality metric, unified measure of goodness (UMG), which addresses color accuracy and noise performance simultaneously, is introduced and compared with other available quality metrics. Through comparison, UMG is designated as a primary evaluation metric. On the optimal design of spectral sensitivity functions, three generic approaches, optimization through enumeration evaluation, optimization of parameterized functions, and optimization of additional channel, are analyzed in the case of the filter fabrication process is unknown. Otherwise a hierarchical design approach is introduced, which emphasizes the use of the primary metric but the initial optimization results are refined through the application of multiple secondary metrics. Finally the validity of UMG as a primary metric and the hierarchical approach are experimentally tested and verified.

DEDICATION

This dissertation is dedicated to my respectable parents, Quan Shixian and Yang Qishun, my beloved wife, Xiaoyun Jiang, my lovely son, Alfred Tony Quan and my dear brothers and sisters.

ACKNOWLEDGEMENTS

First, I would like to thank Professor Dr. Noboru Ohta, my advisor, and a good friend. I have learned a lot from him and enjoyed doing research with him.

I would like to thank Professor Dr. Roy S. Berns for his excellent teaching, guidance and giving me opportunity to verify my theoretical research in his laboratory.

I would like to thank Professor Dr. Daniel Lawrence for his teaching and friendship, also for his will to be my committee chair.

I would like to thank Dr. Naoya Katoh for his guidance and support. He had exciting discussions with Dr. Ohta and me, contributed some good points to this work.

I would like to than Mr. Mitchell Rosen for his support and discussion. He contributed a lot to the patent applications.

I would like to thank Dr. Francisco Imai for his guidance and support. He also helped me setup experiment and process data.

I thank the faculty, staff and students of the Munsell Color Science Laboratory for their comments, discussions and inspirations. Special thanks go to Dr. Mark Fairchild, Dr. Ethan Montag, David Wyble, Colleen Desimone, Val Hemink, Qun Sun, Yongda Chen, Lawrence Taplin, and Ellen Day for their instruction, support and friendship over the years I was part of the Munsell Color Science Laboratory.

I would like to thank Dr. Gaurav Sharma, Dr. Poorvi L. Vora and Dr. Peter D. Burns for their great work, on which part of this dissertation is based.

I would like to thank my parents for their unselfish support that has accompanied me to come to this point. I also thank my brothers and sisters for their hard work and support of my study over years.

Finally, I would like to thank my son, for the joy he brings to me, and my wife, Xiaoyun Jiang, for both her role in my family and in my study. Besides being a Ph.D. candidate, she devoted all the spare time she could squeeze to taking good care of our family.

TABLE OF CONTENTS

LIST OF FIGURES

Figure

LIST OF TABLES

Table

1 INTRODUCTION

1.1 Evaluation and Design of Sensor Sensitivities

Color perception is perhaps the most important approach for human beings to feel the world. It is a lasting desire for human beings to exactly reproduce what they see and keep those beautiful moments forever. More than two thousand years ago, the ancient Chinese philosopher, Mo-tse, did an experiment to illustrate the principal of the light propagation in a beeline and pinhole imaging (Figure 1.1): Let a person stand outside of a house towards a small hole in the wall, when the sunlight shines in through the hole, a headstand image of the person will appear on the white wall where the sunlight is projecting. With science development during the recent one hundred years, today color imaging technology exists in human daily life through books, photography, television, cinema, and a variety of paintings. Modern imaging technology is going through the conventional chemical method to digital electronic imaging method. However, the three primary factors in an imaging process are still the same: object scene, illumination and sensor characteristics.

The typical chemical method is film, and the typical electronic imaging method is charge-coupled device (CCD) or complementary-metal-oxide-semiconductor (CMOS). The discussion in this dissertation will be limited to electronic imaging technology, but most of the evaluation methods and design approaches should be easily generalized to other imaging technologies. Electronic colorimetric measurement or imaging systems include colorimeters, three-channel cameras, scanners and multi-spectral imaging systems. The research object in this dissertation is a “camera,” which refers to a device with electronic sensor, multiple filters and optical system to capture color or spectral information of a surface area, rather than a spot in short time, therefore, three-channel camera, color scanner and multi-spectral imaging system are within the discussion scope of this dissertation.

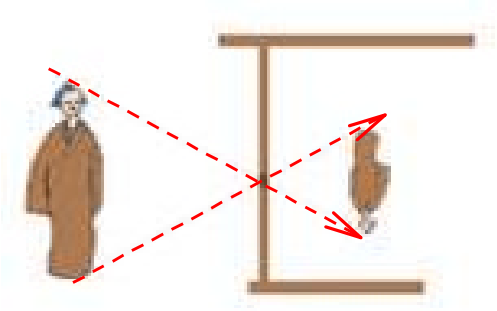

Figure 1.1: Prototype of imaging: pinhole imaging.

The selection of object scene generates multifarious camera applications. Cameras are used from everyday life to space. There are four broad applications: general imagery, scientific, machine vision, and military and space. Consumer or professional cameras for general imagery are designed to operate in real time with an output to match standard display. Digital still cameras, color scanners and digital video cameras fall into this category. People use cameras to take pictures or movies on 2-D or 3-D objects, and print out with a color printer or display with a monitor or television. They are designed and built to simulate the mechanism of the human visual system, but are necessary to consider practical constraints.

Cameras for scientific applications should have low noise, high responsivity, large dynamic range and high resolution. Scientific cameras may quantize signals into 12 or 16 bits with great linearity, with spatial resolution up to 5K-by-5K elements and low dark current and readout noise. These cameras are also used in archiving expensive artworks and rare books, which attracts more and more attention since these paper-based materials fade over time and it is better to archive the color, spectra and shape information as much as possible and as soon as possible.

Camera systems for computer vision consist of controllable light source, camera and computer software that rapidly analyzes digitized images with respect to location, size, flaws and other preprogrammed data. Machine vision functions include location, inspection, gauging,

counting, identification, recognition and motion tracking. The design of these cameras is unnecessary to simulate human eyes.

Finally cameras for military and space applications are interested in detecting, recognizing and identifying targets at long distances or under low light. These cameras may not work in the visible range, but from X-ray, ultraviolet to far infrared and microwave waveband, in order to effectively use the atmospheric window. Information obtained with these cameras is generally hyperspectral images. The evaluation and design of these camera systems are different, and this dissertation concentrates on the trichromatic imaging system for generic imagery use and some discussion on multispectral imaging systems for artwork archiving.

Cameras rely on illumination to capture information of object scene. There are variety of illuminants for a camera to work with, how to estimate the illuminant characteristics that was using from a captured image and how information obtained from under one illuminant is transformed to under another is a challenge, which is called computational color constancy or illuminant estimation. Illuminant estimation has been widely discussed since the “gray-world” algorithm was introduced.

Sensor characteristics, which consist of electronic sensor, color filter and optical lens, are the critical parts in the design of digital color cameras. Since a camera is the input end in a color input-output system, its capability to acquire precise signals under noise environment can make significant contributions to the processing and output image quality. This requires the understanding of human color vision system and how far a camera system can simulate it under real-world constraints.

The human visual system is a complex and partially understood image data acquisition and processing system. Human visual color perception can be roughly described by tri-receptor theory that involves the linear combination of three different photoreceptors with known spectral sensitivities in the visible range. The three receptors are known as the L, M and S cones (for long, medium and short wavelength sensitive). The vision process can be thought of as mapping the infinite-dimensional space of all spectral distributions in the visible range into the three-

dimensional space of tristimulus values. Human visual responses to color stimuli have been determined by psychophysical experiments and are officially recommended as color matching functions by the CIE (Commission Internationale de l'Eclairage).

Many imaging systems are, therefore, set up with three channels and the channel sensitivities are initially designed to approximate the human visual system. However, many of these systems for acquisition and rendering of color imagery still produce color pictures perceptibly different from the original scene. A major reason for this is the difficulty of selection and fabrication of filter sets that are suitable for incorporation into color cameras and scanners. A color quality factor that relates closely to color accuracy is desirable for their evaluation and design. The present research proposes a metric to indicate the degree of goodness of color filters by considering critical practical issues, i.e., recording noise and its amplification in the imaging process and multi-illuminant color correction for minimizing color error in a perceptually uniform color space. The next step is trying to design and produce real filter sets that are either optimum in an absolute, theoretical sense, or close to this optimum but robust to fabrication tolerances at the same time.

Nowadays, light has been described as duality of wave and particle, neither of which can interpret all phenomena related to light. For example, the visible light ranges from 380nm to 780nm, which means light is a "wave," while a type of common noise, shot noise, existed in imaging process, is formed because of the random arrival of photons on the sensor surface, which shows that light is "particle." Traditional approach is to solve light relevant problems by approximating light as an electromagnetic wave whose wavelength is within the visible range, and Maxwell's equations and extensions are applicable to describe all optical effects in nature (except shot noise, etc.). But this approach is tedious, time-consuming and practically infeasible. Most color input and output devices use color-based approach to describe light, with the human visual system as a bridge. Since object's visual property is described with only three numbers, which is very simple, efficient and widely used, loses spectral power distribution information,

which causes problem such as metamerism when illumination changes or output medium changes.

More and more attention is being paid to spectra-based approach, where input signal and output signal are all treated as spectral power distribution. For example, the object surface reflectance is captured spectrally, and rendered or printed spectrally to match the original surface characteristics. They have many advantages than color-based approach, although the corresponding imaging system, printing system, color management system, image rendering and data compression techniques are still in development. Since color-based approaches are still widely used and will unlikely disappear, a multichannel imaging system is proposed whose first three channels emphasize obtaining color-based information and additional channels capture spectra-based information together with the first three channels in this dissertation.

Sensor characterization is a necessary step to evaluate the performance of imaging devices. The characterization procedures usually attempt to determine the relationship between the output signal from a sensor and the object color properties independent of any specific device in some multidimensional space, typically these color properties that are described as three-dimensional color perception value in a device-independent color space (e.g., CIE XYZ, CIELAB). A two-way characterization will be able to predict the color perception values from sensor output as well as predict sensor output from color perception values. Sometimes the object color properties are kept in physical form, i.e. the spectrophotometric measurement. The approaches to do this two-way characterization have been studied extensively, such as polynomial regression, look-up-table and neural network. This characterization is easy to carry out, but it is illuminant-dependent and sample-dependent, while the noise influence is not accounted for.

A more fundamental sensor characterization is to obtain the sensor spectral sensitivity functions through measurement or estimation. The spectral sensitivity functions can then be used to determine the mapping relationship between device output signals and object color perception values for any samples under any interested illumination. Direct measurement of sensor

sensitivities with a spectroradiometer and monochromator takes a long time but gives rather accurate spectra. The noise characteristics of sensor can be measured as well. But in some circumstances, direct measurement is difficult to implement. Estimation with a carefully selected sample set is fast, does not need those expensive instruments and can still give acceptable result, depending on the technique and task. Several estimation approaches will be discussed and the results will be compared with that obtained from measurement. The estimation methods can also be applied to other areas, such as inferring the illumination spectral power distribution if sensor sensitivities are available.

While color accuracy is important for a color input device, noises always exist. The suppression of noise in the imaging process is as important as color accuracy. Due to practical limitations it is necessary to weight the balance between color accuracy and noise propagation. In most of the evaluation and design of sensor sensitivities, noise is either not considered or as white noise, which is not true. Signal-independent noise such as dark or white noise and signal-dependent noise such as shot noise are equally important and worth consideration. The dissertation discusses a typical imaging noise model and noise propagation rules when a device output signal is transformed and processed.

The central work of this research is to introduce a new colorimetric quality factor based on noise analysis. A variety of quality factors for evaluating sensor sensitivities have been introduced. Some are based geometric difference, i.e. Vora and Trussell's m-factor; others are based on minimization of color error metric in uniform color space, i.e. Sharma and Trussell's Figure of Merit, or FOM, which is extensive enough to incorporating most of quality factors in a common framework. The drawback of FOM is that it does not consider a practical imaging noise model. The proposed Unified Measure of Goodness (UMG) takes more practical considerations, such as noise model, multi-illuminant color correction and minimization of color error in uniform color space or color appearance space (Figure 1.2). A new color or image difference formula can also be applied instead of the Euclidean distance color difference DE^*_{ab} based on CIELAB space. This new quality factor would not be suggested as a unique one, but a primary

one, and will allow coexistence of some available quality factors. Final judgment on image quality among a set of optimum candidates would leave to the human visual system, since no one has yet introduced a model to incorporate every effect of the human visual system.

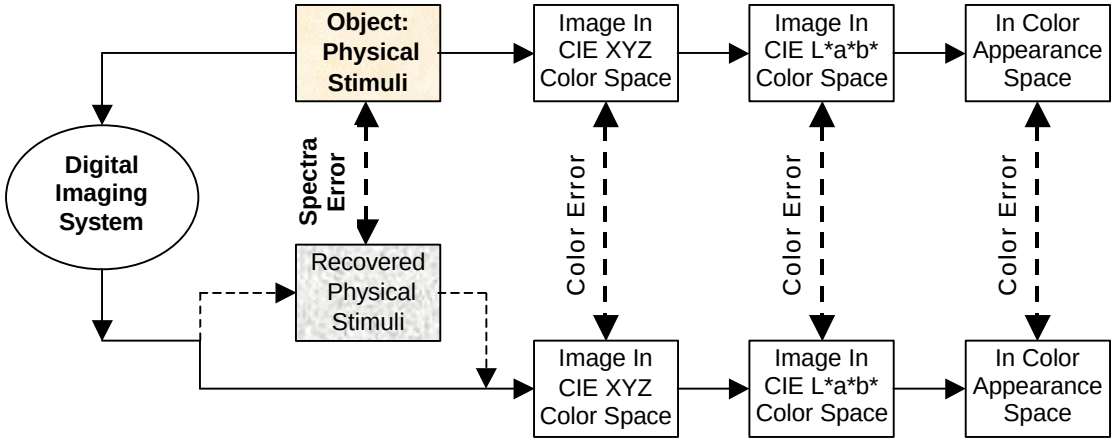

Figure 1.2: Signal capture and conversion in digital imaging system.

The design of colorimetric sensor spectral sensitivities (SS) has been studied extensively in the past. The key point is the selection of an appropriate objective function, but a feasible approach is also important. No research has considered simultaneously these factors: the multiple taking and viewing illuminants, real imaging noise model and noise amplification, and the minimization of color error in a uniform color space. Previous research attempted to obtain an analytical form of optimal sensor sensitivity, or optimize tens or hundreds of variables at the same time while the object function has numerous local optima. This is a backward approach, where the obtained curves have to be approximated again with basic filter components in fabrication process, which will introduce error, possibly big enough to make the optimum meaningless.

The approach proposed in this dissertation will be a forward hierarchical one, and multiple metrics will be used as criteria sequentially rather than only one. Since filters are always obtained with some combinations of given basic filter components, optimal sensor sensitivities are always a function of fabrication parameters, such as the widths of selected filter components.

A complete combination of basic filter components can be obtained by changing the fabrication parameters. Since the proposed UMG takes these important practical factors into account, it will serve as a primary metric to evaluate any possible three channel sensor sensitivities after a pre-selection procedure. A collection of optima candidates will be obtained and be evaluated with additional metrics. Finally, an optimal sensor sensitivity set should also be judged with psychophysical methods, although this dissertation will not tackle this problem. This hierarchical approach basically obtains optimal three channel sensitivities for colorimetric reproduction. This approach is shown in Figure 1.3. Furthermore, by using spectral difference metrics, additional optimal channels can be obtained to make the whole imaging for both high colorimetric and spectral recovery accuracy.

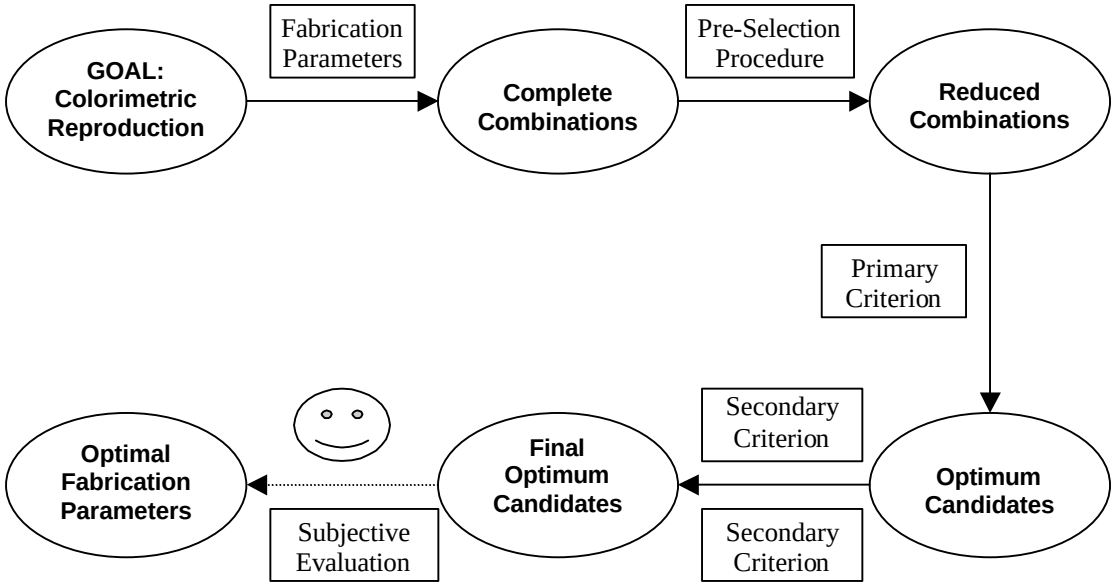

Figure 1.3: Hierarchical approach to the optimal design of spectral sensitivities.

Some issues related to sensor sensitivity design will also be discussed in this dissertation. The first is the optimal peak and width ranges of spectral sensitivities when assuming sensor sensitivity is a gaussian-type function (Here cubic spline function is used.) The second is color correcyiom. Since the matrix embedded in a color input device will only change with a diagonal

correction matrix due to the limited processing capability when taking illuminant changes, how to devise an effective transformation correction matrix is discussed in the dissertation.

1.2 Scientific Contributions

This dissertation proposes solutions to the characterization, evaluation metric and design of spectral sensitivities for digital color imaging devices, particularly for consumer and professional digital camera systems which aim for a better colorimetric performance as well as spectral reproduction performance. The evaluation criterion and design approach can apply to other colorimetric instruments as well with slight modification. In detail, the major contributions are listed as follows.

First, a comparative study on the measurement and estimation methods of spectra is conducted, which is applicable on obtaining sensor spectral sensitivity, illuminant spectral power distribution or reflectance spectra, when two of them are known. When and how far an estimation method can replace measurement is discussed.

Second, a new colorimetric quality factor, unified measure of goodness, is proposed, based on imaging noise model and noise propagation analysis, minimization of average color error in some target color perceptual space, and multi-illuminant color correction. The new quality factor is suggested as a primary criterion to sensor spectral sensitivity evaluation and is flexible on the selection of target color space and color error metric.

Third, a hierarchical approach to the optimal design of sensor spectral sensitivities is proposed. This is a forward approach, directly based on the optimization of filter fabrication parameters. After pre-selection procedure, a collection of optima candidates is obtained with the use of primary criterion. Secondary metrics are used to pick out the final optimum set from among the collection. Practical implementation of this approach generates prevailing advantages.

In addition, without any knowledge on filter fabrication process, the shape of total sensitivity function is assumed as asymmetric gaussian-type function, optimal range of peak and width parameters are obtained by setting quality factor at a reasonable confidence level. The

research finds that the optimal range shrinks when noise is considered and optimal range changes when a different metric is chosen. The optimal range is very helpful to allow some degree of fabrication tolerance.

Finally, primitive results on the transformation correction matrix due to the change of taking illuminant are presented.

1.3 Dissertation Outline

The dissertation is organized as follows. Research reviews are divided into two types. The first type is as Chapter 2, where fundamental concepts on color science and imaging technology are reviewed. Second type of review is specifically related to the corresponding aspect of the dissertation and will be reviewed in the relevant chapters on noise, characterization, metrics and optimal design.

Chapter 2: Background: Color Spaces and Color Perception Difference Metrics

This chapter reviews the general background of color science, particularly for the purposes of evaluation and design of digital imaging devices. The chapter will describe the color matching functions of standard observers, standard color spaces, perceptually uniform color spaces and the latest color appearance space. The color difference metrics cover the development of color difference formulae for large color patches and color images. Vector as the discrete sampling of visible spectra will be used as fundamental approach and relevant notation and terminology is addressed in the chapter as well.

Chapter 3: Color Imaging Devices Characterization

The principle, technology and modeling of color input devices are described in this chapter. And pros and cons of three-channel imaging and multi-spectral imaging technology will be compared. The measurement and estimation technique of spectra distribution, especially the spectral sensitivities will be described and compared. The estimation method includes pseudo-inverse estimation, principal eigenvectors estimation, smoothing estimation, Wiener estimation, and projection-onto-the set estimation.

Chapter 4: Digital Imaging Noise Analysis and Noise Propagation

The proposed quality factor and filter design approach places substantial effort on the analysis of the noise problem in the imaging process. The imaging noise can be classified as signal-independent and signal-dependent noise, both of which are propagated to the output end in the target color space with a series of linear and nonlinear transformation. The output RMS noise is analyzed and the ways to suppress the noise are suggested.

Chapter 5: Evaluation of Digital Imaging Devices

This chapter addresses the available metrics for the evaluation of digital imaging devices. q-Factor and m-factor as geometrical metrics are described, followed by some other sample-dependent metrics such as Figure of Merit. These metrics will be compared with each other.

This chapter will also describe a new quality factor – Unified Measure of Goodness (UMG). By considering the color error minimization in perceptually uniform color space, signal-independent noise and signal-dependent noise, noise propagation and multi-illuminant color correction, UMG is more comprehensive than previous metrics. Details on issues related to this metric, such as the selection of standard samples is discussed.

Chapter 6: Generic Optimal Design and Optimal Filter Paramter Range

The approaches to the design of digital imaging spectral sensitivities will include the minimization of color difference and maximization of certain quality factors. Mathematically feasible approaches such as searching an optimal subset of a discrete set of filters, parameterization of filter characteristics and optimizing additional channel upon available channels are discussed, respectively.

The practical constraints of the optimal design of spectral sensitivities are discussed in the chapter as well. The advantages and problems of the past optimal design approaches are overviewed which enlightens the new quality metric and design approach.

In this chapter, by assuming the preferred spectral sensitivity function as skewed gaussian-type shape, the optimal range of peak wavelength and full-width at half-maximum is determined by setting confidence levels of UMG and other quality factors. When the filter

fabrication process is unknown, these optimal ranges give manufacturers confidence in designing gaussian-type filters for allowance of fabrication tolerances.

Chapter 7: Hierarchical Optimal Design of Spectral Sensitivity Functions

In this chapter, a new hierarchical approach for the practical filter design is proposed. This approach assumes the color filters are directly modeled on practical fabrication parameters, such as filter thickness and components. The parameters are obtained through multiple evaluation procedures sequentially, which consists of pre-selection, UMG evaluation, RMS evaluation and spectral fit evaluation.

Chapter 8: Color Correction in Color Imaging

The digital imaging devices work under various working (taking) illuminants and the information is used to estimate the colorimetric information under target (viewing) illuminants. The color correction issue discussed here mainly deals with the matrix estimation under different illuminant pairs from reference illuminant pair.

Chapter 9: Experiment: Optimal Design of Spectral Sensitivity Functions

In this chapter, the work around the optimal design of spectral sensitivity functions for the Photometrics Quantix digital camera is reported. The optimally designed color filters are fabricated and tested experimentally. The performance of the camera will be compared with some other camera systems.

Chapter 10: Conclusions

This chapter summaries the primary results and conclusions that can be drawn from the research. The scientific contributions are outlined and the directions for future research are also proposed.

As a summary, Figure 1.4 shows the whole research workflow of this dissertation, and the research focuses on the shaded items.

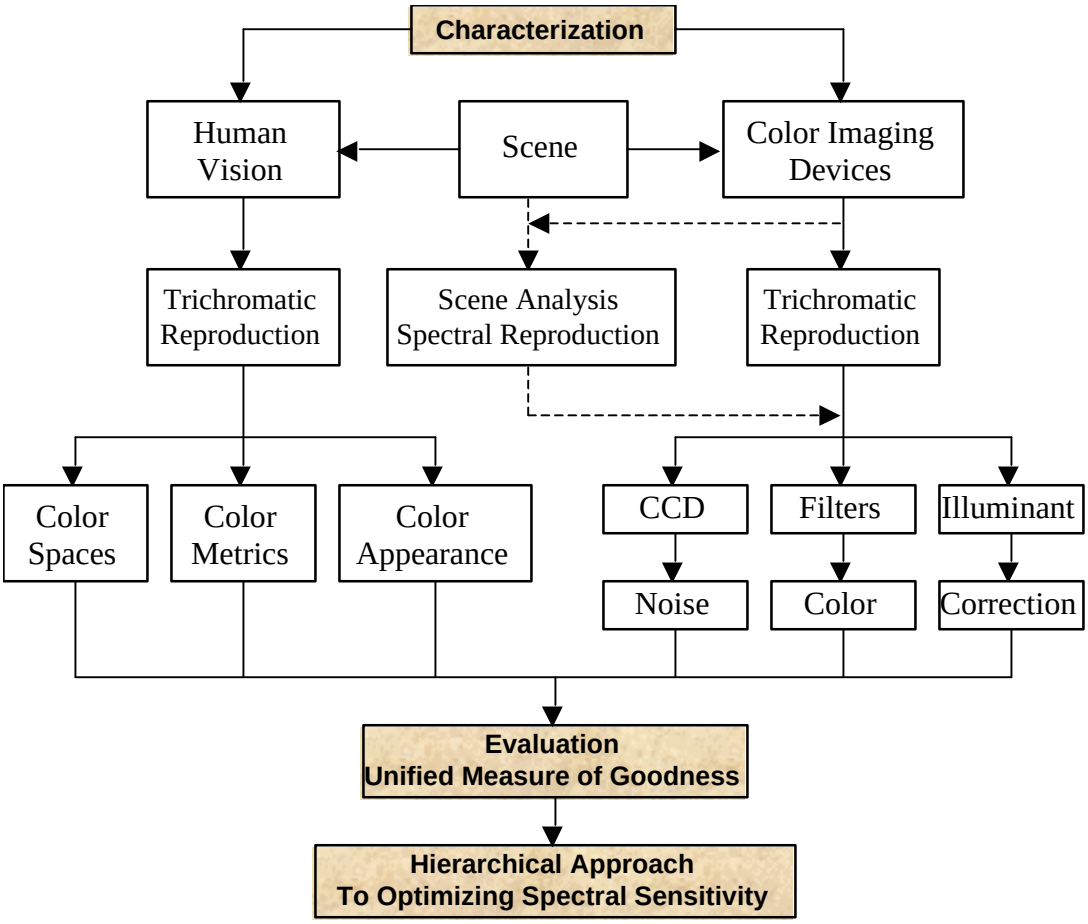

Figure 1.4: Structure of dissertation, concentrating on the shaded items.

2 BACKGROUND: COLOR FUNDAMENTALS

2.1 Spectrum

A spectrum is a physical property that changes along wavelength. Spectra involved in the human visual system usually locate in the visible range (typically 380nm-780nm). A spectral power distribution (SPD) is defined as the power of a light ray per unit wavelength per unit area perpendicular to the propagating direction. By convention, spectral distributions are normalized so that their power at 560nm is defined as unity. The spectral power of an illuminant is defined relative to its power at 560nm. The SPDs of common CIE standard illuminants are widely available. Some spectral curves are quite smooth, such as illuminants A and C; some are quite spiky, such as fluorescent illuminants defined by CIE, whose spikes look like the Dirac functions, containing significant amount of energy within very narrow wavelength intervals. The spectral curves of some illuminants (D65, A, F10 and F10) and a real illuminant simulating A which is used in the research were plotted in Figure 2.1.

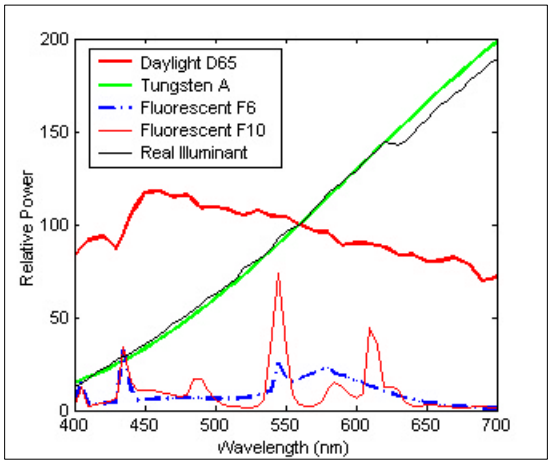

Figure 2.1: Spectral power distributions of some typical illuminants.

2.1.1 Spectral Characteristics of Materials

When light spreads in any medium or interacts with materials, the spectra of light will be altered through reflection, transmission, absorption or scattering. The spectral characteristics of materials appear mainly as follows.

2.1.2 Spectral Reflectance

The spectral reflectance $R(l)$ is defined as the ratio of intensities of the reflected light to the incident light at an object boundary or an interface between two media under specified geometric conditions:

$$R(l) \equiv \frac{I(l)}{I_0(l)} \tag{2.1}$$

where $I(l)$ and $I_0(l)$ are the reflected and incident intensities. Spectral reflectance applies to boundaries of all kinds of materials, including opaque, transparent and translucent.

There are exceptions, such as chameleon, which can change the reflectance of their skin by changing the relevant microphysical structure of its surface, but usually a spectral reflectance is independent of the intensity of the incident light and is an intrinsic property of the material, which is called the spectral linearity. For given reflectance $R(l)$ and the incident light intensity $I_0(l)$, the material surface will alter the light intensity as

$$I(l) = I_0(l)R(l) \tag{2.2}$$

Reflectance can be separate into two components: specular and diffuse reflectance. A more generalized dichromatic reflection model [Tominaga1994&1996] states that light reflected from an object's surface is decomposed into two additive components: the body reflectance and the interface reflectance. Spectral reflectances of many natural materials are usually smooth, such as leaves, flowers, skins, etc.

2.1.3 Spectral Transmittance

Spectral transmittance $T(l)$ is the ratio of the transmitted and incident light intensities:

$$T(l) \equiv \frac{I(l)}{I_0(l)} \tag{2.3}$$

where $I(l)$ and $I_0(l)$ are the intensities of the transmitted and incident lights. A filter with a specified spectral transmittance is particularly useful to change the appearance of a light source in order to obtain a special illumination:

$$I(l) = I_0(l)T(l) \tag{2.4}$$

Quite a few types of optical filters are used commonly [Wyszecki1982]: Absorption filters, glass filters, gelatin filters, liquid filters and liquid crystal tunable filters.

2.1.4 Spectral Absorptance

Spectral absorptance $a(l,\mathbf{r})$ is the percentage of light energy absorbed by a transparent or translucent material within a unit path length of light propagation:

$$a(l,\mathbf{r}) \equiv -\frac{1}{I(l,\mathbf{r})}\frac{dI(l,\mathbf{r})}{dl} \tag{2.5}$$

where $\mathbf{r}$ denotes the location in the material. The energy of light after it travels from $\mathbf{r}_1$ to $\mathbf{r}_2$ with $l = |\mathbf{r}_2 - \mathbf{r}_1|$ can be calculated as

$$I(l,\mathbf{r}_2) = I_0(l,\mathbf{r}_1)\exp\left[-\int_{\mathbf{r}_1}^{\mathbf{r}_2} a(l,\mathbf{r})dl\right] \tag{2.6}$$

If the material is homogeneous, the spectral absorptance is independent of location, $a(l,\mathbf{r}) = a(l)$, and Equation (2.6) becomes

$$I(l) = I_0(l)\exp[-a(l)l] \tag{2.7}$$

This is in fact Bouger-Beer's law. And the internal spectral transmittance can be defined as

$$T_{internal}(l) \equiv \frac{I(l)}{I_0(l)} = e^{-a(l)l} \tag{2.8}$$

2.1.5 Refractive Index

The refractive index of a material is the ratio of propagation velocities of light in the vacuum and the material. For fluids and glass-type materials, the refractive index changes proportionally with l^{-2} and the square of temperature T^2. For example, for water (H_2O),

$$n_{H_2O}(l,T) = -1.8791\times10^{-6}T^2 + 3.1130\times10^{3}\,l^{-2} + 1.3246 \tag{2.9}$$

as shown in Figure 2.2, the refractive index is higher for blue light than for red light. For example, the refractive index of crystal glass declines from 1.57 at 400nm to 1.54 at 800nm. This

effect is small, but is readily observed. Refractive index is assumed constant in the visible range in this research.

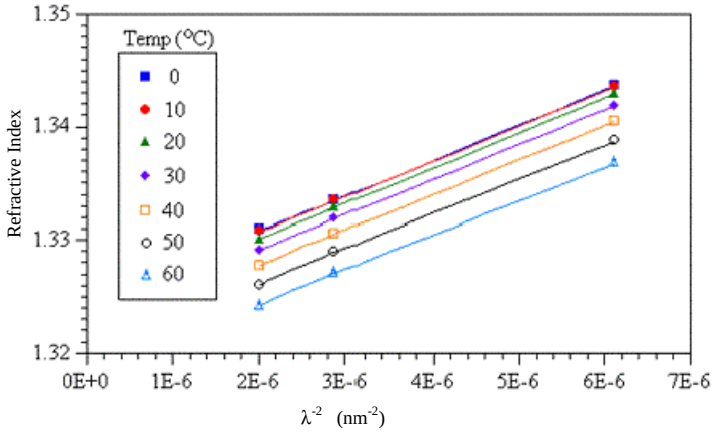

Figure 2.2: Refractive index of water changes with wavelength and temperature.

2.1.6 Combinations of Filters

Absorption filters may be combined in series in order to obtain other and more desirable spectral transmittance characteristics. It is preferred to directly measure the transmittance of a filter combination, but the total transmittance can still be estimated with the available information of internal transmittances and refractive indices of the filter components.

Loss of radiant flux by reflection from the front and back surface of the filter may be computed from Fresnel's law of Reflection. For normal incidence, the fraction $r(l)$ of radiant flux reflected from a surface separating two media is given by

$$r(l) = \left(\frac{n(l) - 1}{n(l) + 1} \right)^2 \tag{2.10}$$

where $n(l)$ is the ratio of refractive indices of the two media. If $n(l)$ is assumed constant in the visible range, $r(l)$ is also constant, let $K_1 \equiv r(l)$.

Now consider a beam of light striking the first surface of a filter. Some of the light ($r(l)$) is immediately reflected from the boundary, the rest of the light starts on its way through the filter and a fraction T_i (the internal transmittance) reaches the other side. Most of the light emerges from the bottom, but some of it is reflected back at the bottom boundary. The light goes

back through the filter and a fraction T_i reaches the top, where the cycle is repeated. Summing up the light emerging from the bottom boundary, which is really the light transmitted by the filter, it was obtained [Allen1980]

$$\begin{aligned} T &= (1-K_1)^2 T_i (1 + K_1^2 T_i^2 + K_1^4 T_i^4 + \cdots) \\ &= (1-K_1)^2 T_i (1 - K_1^2 T_i^2) \end{aligned} \tag{2.11}$$

where T represents the total (or external, as opposed to internal) transmittance.

If the total transmittance is measured, the internal transmittance is obtained by solving Equation (2.11) as

$$\begin{aligned} T_i &= \frac{-(1-K_1)^2 + [(1-K_1)^4 + 4K_1^2 T^2]^{1/2}}{2K_1^2 T} \\ &= \frac{(1-K_1)^4 + 4K_1^2 T^2 - (1-K_1)^4}{2K_1^2 T\{(1-K_1)^2 + [(1-K_1)^4 + 4K_1^2 T^2]^{1/2}\}} \\ &= \frac{2T}{(1-K_1)^2 + [(1-K_1)^4 + 4K_1^2 T^2]^{1/2}} \end{aligned} \tag{2.12}$$

As shown in Figure 2.3(a), if k filters with different thickness d_1, d_2, $\cdots$, d_k are fastened together (optical contact, no air in-between), there is no reflection happened at any interface inside. Let the internal transmittance for each filter in unit thickness is T_i ($i = 1$ to k), the total internal transmittance of the combination is calculated according to Bouger-Beer's Law,

$$T_{i\text{Total}} = \prod_{j=1}^{k} T_j^{d_j} \tag{2.13}$$

The total external transmittance of the combination of the filters can be calculated with Equation (2.11). If the filters are separated by air, as shown in Figure 2.3(b), the total transmittance of the combination is simply approximated as the product of external transmittance of the individual filters [pg. 33 in Wyszecki1982]:

$$T_{\text{Total}} = \prod_{i=1}^{k} T_{\text{Total}}^{i} \tag{2.14}$$

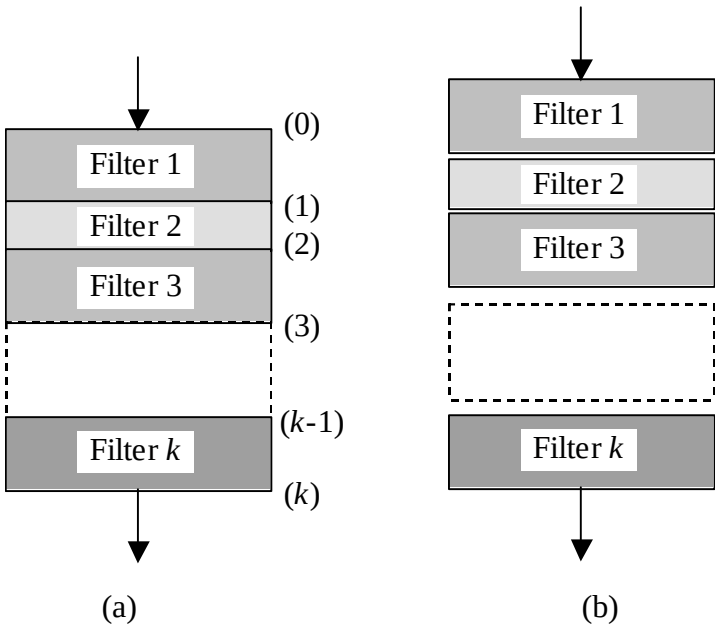

Figure 2.3: (a) Schematic diagram of combination of *k* filters in optical contact; (b) Schematic diagram of combination of *k* filters separated by air.

2.2 Colorimetry

Human vision relies on the stimulation of receptors in the retina of the eye. There are two types of receptors, rods and cones, names according to their shape. Rods detect low levels of illumination and give monochromatic vision. As the amount of light increases, the rods become desensitized and hibernated, and the second class of receptors, cones, begins working. Cones are insensitive to weak incident light. There are three types of cones, which work together and give color vision under normal levels of illumination. Color sensation arises when electromagnetic radiation with wavelengths of between approximately 380nm and 780nm is incident on these receptors and this stimulation is processed and interpreted by the human visual system. Stimuli that cause different colors have different cone signals, the symbols *L*, *M* and *S* are used to represent the three cones with their peak sensitivities in the long, middle and short wavelength regions respectively [pg. 46 in Wandell1995].

The cones integrate light at all wavelengths incident on them, which reduces the information of the entire spectrum of incident light to three signals, one for each type of cone,

resulting in trichromacy. The cone signals are the multiples of the SPD of incident light and spectral sensitivities of cones. CIE defined two sets of color matching functions (CMF) respectively through matching experiments for samples subtending 2° and 10° in 1931 and 1964, which are denoted by $\bar{x}(l)$, $\bar{y}(l)$, $\bar{z}(l)$ (Figure 2.4) and $\bar{x}_{10}(l)$, $\bar{y}_{10}(l)$, $\bar{z}_{10}(l)$, respectively. It is important to note that these functions are not the actual response characteristics of the cones, but linear transformations of them, so that the $\bar{y}(l)$ function is identical to the CIE standard photometric observer function, or luminous efficiency function, $V(l)$, and thereby represents perceived luminance. As the cone responses are made up of the characteristics of the illuminant and the illuminated object, a pair of stimuli without physical properties match could match in colors under one illuminant but mismatch under another, whereby such a pair is called *metameric*, and the property of the visual system is called *metamerism*.

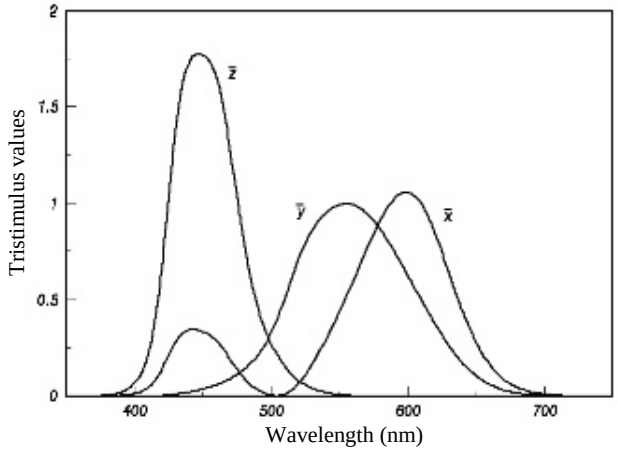

Figure 2.4: CIE color matching functions for 2° observer defined in 1931.

2.2.1 CIE 1931 XYZ System

CIE defined a standard colorimetric observer by providing two different but equivalent sets of color matching functions. The first set of color-matching functions, known as the CIE RGB color-matching functions, $\bar{r}(l), \bar{g}(l), \bar{b}(l)$, is associated with monochromatic primaries at wavelengths 700.0nm, 546.1nm and 435.8nm respectively. The second set, CIE XYZ color-matching functions, $\bar{x}(l)$, $\bar{y}(l)$, $\bar{z}(l)$ is defined as a linear transformation of $\bar{r}(l), \bar{g}(l), \bar{b}(l)$,

so as to avoid negative values at all wavelengths. Definition of XYZ color-matching functions is not for visual purpose, but for computational convenience.

The three numbers corresponding to CIE 1931 standard colorimetric observer's color matching functions constitutes the units of the first CIE color space – CIE XYZ, whose coordinates are referred to as tristimulus values and can be calculated as

$$\begin{aligned} X &= k\int_{l_{\min}}^{l_{\max}} P_l \bar{x}_l \, dl \cong k\sum \bar{x}_l P_l \Delta l = k\sum \bar{x}_l S_l R_l \Delta l \\ Y &= k\int_{l_{\min}}^{l_{\max}} P_l \bar{y}_l \, dl \cong k\sum \bar{y}_l P_l \Delta l = k\sum \bar{y}_l S_l R_l \Delta l \\ Z &= k\int_{l_{\min}}^{l_{\max}} P_l \bar{z}_l \, dl \cong k\sum \bar{z}_l P_l \Delta l = k\sum \bar{z}_l S_l R_l \Delta l \\ k &= \frac{100}{\int_{l_{\min}}^{l_{\max}} S_l \bar{y}_l \, dl} \cong \frac{100}{\sum \bar{y}_l S_l \Delta l} \end{aligned} \tag{2.15}$$

Here S_l is SPD of illuminant, R_l is the object's spectral reflectance factor, P_l stands for the SPD of the physical stimulus at wavelength l and k is a scaling constant. The tristimulus values with CIE RGB color-matching functions can also be obtained in like manner. The Y value is called the *luminance* and correlates with perceived brightness of radiant spectrum. All other CIE-defined color spaces and practical color space are derived from this one by various transformations, i.e. the *standard-RGB* (sRGB, Figure 2.5) color space:

$$\begin{bmatrix} R_{sRGB} \\ G_{sRGB} \\ B_{sRGB} \end{bmatrix} = \begin{bmatrix} 3.2410 & -1.5374 & -0.4986 \\ -0.9692 & 1.8760 & 0.0416 \\ 0.0556 & -0.2040 & 1.0570 \end{bmatrix} \begin{bmatrix} X \\ Y \\ Z \end{bmatrix} \tag{2.16}$$

Two-dimensional chromaticity coordinates can also be derived from XYZ as:

$$\begin{aligned} x &= \frac{X}{X+Y+Z}, \\ y &= \frac{X}{X+Y+Z}, \\ z &= \frac{Z}{X+Y+Z} = 1-x-y \end{aligned} \tag{2.17}$$

Even though the XYZ color space is very useful for quantifying color stimuli, it has one serious shortcoming: equal distances in various parts of the color space represent different perceptual color differences. For example, the length of segments, which represent equal

perceived difference in the blue region differ from those in the green region by a factor of five. In a uniform color space they ought to have the same length.

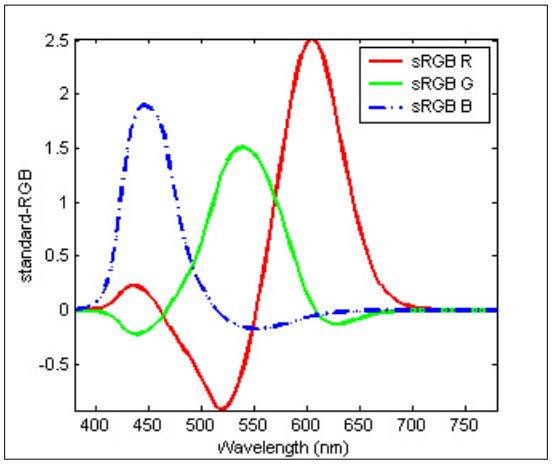

Figure 2.5: ISO Standard RGB color matching functions.

2.2.2 CIE Uniform Color Spaces and CIELAB

Color perception difference is characterized by *just noticeable difference* (JND), the minimum difference required between two stimuli that will elicit a perceived difference. Color space is a system for specifying color in terms of transformations of tristimulus values that can be used to represent colors unambiguously in a 3-D space. If the Euclidean distance between two locations in a color space is proportional to the color perception difference, the color space is a uniform color space, which is desirable for defining tolerances in color reproduction systems. It is widely known that CIE XYZ space is perceptually non-uniform. Many research efforts [as reviewed in Wyszecki1982, Sharma1997a and Berns2000] lead to the CIE 1976 uniform color spaces – CIELUV and CIELAB. CIELUV is still in use, but CIELAB is probably the most widely used color space, although it is not as uniform as it claimed and many attributes of color cannot be predicted. A color is defined in this space by the coordinate values L^*, a^* and b^*, which are transformations of the CIE tristimulus values X, Y and Z:

$$\begin{aligned} L^* &= 116\, f(Y/Y_n) - 16 \\ a^* &= 500[\, f(X/X_n) - f(Y/Y_n)] \\ b^* &= 200[\, f(Y/Y_n) - f(Z/Z_n)] \end{aligned} \tag{2.18}$$

where function $f(\bullet)$ is defined as

$$\begin{aligned} f(x) &= x^{1/3} && x > 0.008856 \\ f(x) &= 7.787x + \frac{16}{116} && x \le 0.008856 \end{aligned} \tag{2.19}$$

where X_n, Y_n and Z_n are the tristimulus values of the reference white. Similarly chroma and hue angle can be defined as

$$\begin{aligned} C_{ab}^{*} &= (a^{*2} + b^{*2})^{1/2} \\ h_{ab} &= \tan^{-1}(b^{*} / a^{*}) \end{aligned} \tag{2.20}$$

The CIELAB space was intended to be a perceptually uniform color space, so that equal distances in the color space represent equal perceived differences in appearance. Color difference is defined as the Euclidean distance between two colors in the color space:

$$\Delta E_{ab}^{*} = \sqrt{(\Delta L^{*})^2 + (\Delta a^{*})^2 + (\Delta b^{*})^2} \tag{2.21}$$

The CIELUV and CIELAB transformations are relatively simple, but they do not result in perfectly uniform perceptual spaces, only approximately uniform. In addition, visual environmental factors such as the ambient illumination, background color etc. also affect color discrimination, but are not included in the transformations. Today application of CIELUV color space wanes and most researches prefer using CIELAB to CIELUV. The discussion in this dissertation will be based on CIELAB color space.

2.3 Color Difference Metrics

Determining the difference between two stimuli is of significant importance in colorimetry and color reproduction. The main objective for designing color difference formulae is to make their results as close to human judgments as possible. CIELAB was proposed as a uniform color space, so the Euclidean distance between the coordinates of two stimuli is considered as the corresponding color difference ΔE_{ab}^{*}. However the color space is not so uniform in fact, advanced color difference formulae were developed to predict human judgment more accurately. Many different formulae have been developed and the work is still going on to improve them.

Metrics for predicting the visibility of color changes of large uniform targets have been used widely to describe tolerances for color reproduction of large samples in the paint and dye industry. The CIELAB metric is a standard that specifies how to transform physical image measurements into perceptual differences. The metric was derived from perceptual measurements of color discrimination of large uniform targets. Though not perfect, the metric has been in use for over twenty years, and it has served as a satisfactory tool for measuring perceptual difference between large uniform patches of colors.

2.3.1 Euclidean Distance on RGB (or XYZ)

The error values were computed as point-by-point vector length of the RGB difference image between an original image and its reproduction:

$$e_{RGB} = \sqrt{(\Delta R)^2 + (\Delta G)^2 + (\Delta B)^2} \tag{2.22}$$

where *DR*, *DG* and *DB* represent the difference in *Red*, *Green*, *Blue* channel values between the original color image and the reproduction. Similarly, in CIE XYZ space, the error is defined as:

$$e_{XYZ} = \sqrt{(\Delta X)^2 + (\Delta Y)^2 + (\Delta Z)^2} \tag{2.23}$$

The Euclidean distance in CIELAB as error metric is already described as Equation (2.21). The error metric in RGB space does not include any information about the device used to present the images. Therefore the error computed using Equation (2.22) is uncalibrated. Using uncalibrated image values to measure perceptual difference is poor practice, because the displayed image can differ depending on the display hardware. The error metric in XYZ space means the device has been calibrated, but since XYZ space is not a perceptual uniform color space, the error measure from Equation (2.23) is expected very different from perceptual difference. Still, because the error measure of Equation (2.23) is commonly used as an initial metric, it is included in this analysis.

A few color and image difference metrics that were used in this dissertation or will be used in the future continuous work were discussed in Appendix A, which include CMC, BFD,

CIEDE94, CIEDE2000 and S-CIELAB. Since the future work will be based on color appearance models, some primary models were analyzed in Appendix B.

2.4 Color Reproduction Types

The purpose of color reproduction is to replicate the physical property or color information of interested objects on another media. For the replication of art paintings, their spectra are desired to be reproduced exactly so that the replication can be looked the same when both are viewed under any illuminant. In everyday light, people want the sky in photography is more bluish, and the grass is more greenish. Therefore the purpose of color reproduction varies greatly depending on specific application. Six different types of color reproduction are often referred, as given by Hunt [Hunt1995, pg. 222]. Figure 2.6 gives a whole image on color reproduction, where spectral reproduction and trichromatic reproduction are shown.

2.4.1 Spectral Color Reproduction

If the spectral power distribution of original and reproduction are identical, a spectral color reproduction is achieved. In this case, the colors should match for all observers under identical viewing condition. Most of the current color photography, color displaying and color printing cannot achieve spectral color reproduction. Spectral color reproduction defines the requirement for independence of illuminant color and observer color vision and is the only way to discount metamerism, therefore it is attracting much more attention now.

2.4.2 Colorimetric Color Reproduction

If computation of tristimulus values on both original and reproduction is the same through using CIE standard observer data, a match is usually made well by real normal observers. The colorimetric color reproduction is defined as the reproduced color has chromaticities and relative luminances equal to those of the original. It does not need the spectra of original and reproduction are the same, on the contrary, it is usual that their spectra may be different drastically, but that difference is eliminated due to metamerism under some illuminant. When

illuminant changes, the match may disappear. This approach enables the usual color-difference formula to be used.

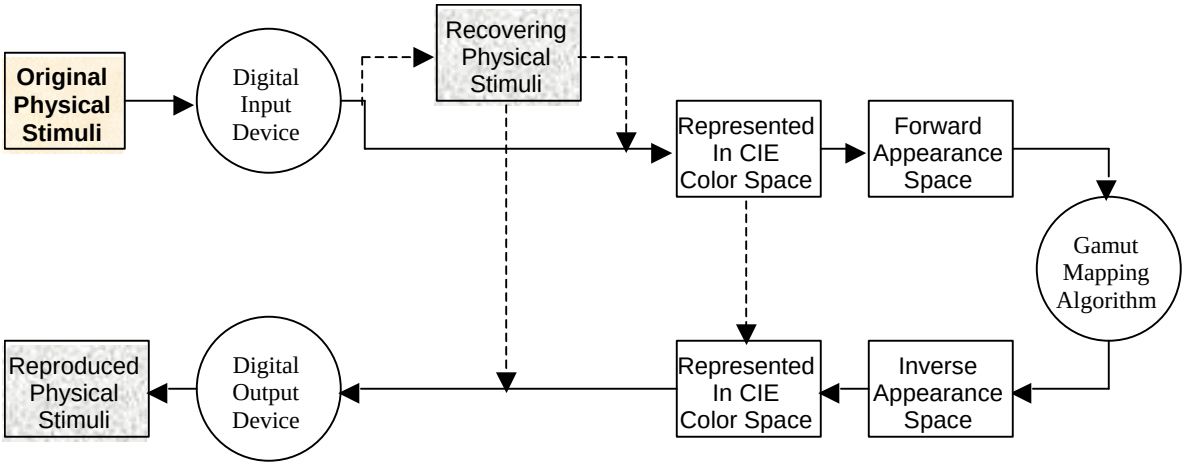

Figure 2.6: Color reproduction types.

2.4.3 Exact Color Reproduction

The exact color reproduction requires that the reproduction of a color in a picture have the same chromaticity and absolute luminance as those in the original scene. This would result in equivalent appearance of the reproduced and original colors providing that the state of adaptation of the eye was the same when viewing the picture as when viewing the original scene.

2.4.4 Equivalent Color Reproduction

The equivalent color reproduction is defined as reproduction in which the chromaticities, absolute luminances of the colors are such that, when seen in the picture-viewing conditions, they have the same appearance as the colors in the original scene. The differences in color or intensity between the original and reproduction illuminants, and the differences in the surround of the original and reproduction are of practical importance to this reproduction.

2.4.5 Corresponding Color Reproduction

The corresponding color reproduction is defined as reproduction in which the chromaticities and relative luminances of colors are such that, when seen in the picture-viewing conditions, they have the same appearance as the colors in the original would have had if they had been

illuminated to produce the same average absolute luminance level as that of the reproduction. It has the same advantage over equivalent color reproduction as colorimetric color reproduction has over exact color reproduction: by relating the colors both in the original and in the reproduction to a reference white, allowance is made for the fact that observers tend to perceive not in isolation but with reference to a framework provided by the environment.

2.4.6 Preferred Color Reproduction

The preferred color reproduction is defined as reproduction in which the colors deviate from equality of appearance to those in the original, either absolutely or relative to white, in order to give a more pleasing result to the viewer. For example blue sky and vivid clothing are usually preferred in real life; color imaging systems can be modified to boost the blueness of sky and chroma of clothing so that the appropriately reproduced colors are preferred to a more consistent reproduction. It may be very important on practice, but it can be considered as a deliberate distortion, which can be represented as a transformation based on psychophysical experiments, to the previous five color reproduction types.

2.4.7 Discussion

All but spectral color reproduction are based on the trichromatic and adaptation characteristics of the human visual system on physical stimuli. The mathematical approaches to achieve these intents are similar, although some depend on the color appearance models, and some depends on observers' preference, which can all be represented as series of linear and nonlinear transformations. Spectral color reproduction is independent of the human visual system to replicate the spectra power distributions of physical stimuli. If spectral color reproduction is obtained, other types of color reproductions can be achieved easily by further transformations. In this study, only colorimetric and spectral color reproductions will be discussed, focusing on the former.

Color reproduction relies on color input and output devices. Device characterization defines the (two-way) relationship between the device color space and the CIE Colorimetry

system. Each device in an imaging chain must be characterized so that the information can be interchanged in a device-independent color space. Even though characterization methods usually depend on the specific device, but some generic approaches can be used for most of input and output devices: linear and polynomial regression, nonlinear gamma correction, look-up-table, neural-networks and full characterization. Input devices characterization, such as camera, will be discussed in detail later; for output devices, such as color printer, color monitor, and LCD, their characterization can be found in literatures respectively [i.e. Berns1993a on CRT].

2.5 Vector-Space Approach to Color Imaging

2.5.1 Color Vision with Matrix Notation

If the spectral power distribution of a physical stimulus is given by $P(l)$, the responses of the three types of cones can be modeled as a vector with three components given by

$$t_i = \int_{l_{\min}}^{l_{\max}} s_i(l) P(l) dl \qquad i = 1, 2, 3; \tag{2.24}$$

where $s_i(l)$ denotes the sensitivity of the i^{th} type of cones or color matching functions, and $[l_{\min}, l_{\max}]$ denotes the visible range outside of which all sensitivities are near zero. Usually a visible range of [400nm, 700nm] or [380nm, 780nm] is specified, depending on if the computation is for simulation purpose or practical application. Notice that although human eyes do not response beyond the visible range, imaging devices that strive for simulating human eyes may have considerable response.

Mathematically the cone response process in Equation (2.24) is described as inner products of stimulus and sensitivity functions, or projection of a spectrum $P(l)$ onto the space spanned by sensitivity functions $\{s_i(l)\}_{i=1}^{3}$, whose subspace is called the *human visual subspace* (HVSS). Computationally, each continuous function in Equation (2.24) may be replaced with discrete sampling, and integral becomes summation. In general, a sampling interval of 10nm or 5nm is accurate enough, but in some applications involving fluorescent illuminants or media, 2nm or 1nm sampling may be necessary.

If all spectra are uniformly sampled to N points across the visible range, Equation (2.24) can be written as

$$\mathbf{t} = \mathbf{S}^T\mathbf{P} \tag{2.25}$$

where the superscript T denotes the transpose operation, $\mathbf{t} = [t_1, t_2, t_3]^T$ represents the cone responses, $\mathbf{S}$ is an $N \times 3$ matrix with $\mathbf{s}_i$, the discrete sampling of $s_i(l)$, as its i^{th} column, and $\mathbf{P}$ is an $N \times 1$ vector of sampling of $P(l)$. If for two stimuli **P** and **Q**,

$$\mathbf{S}^T\mathbf{P} = \mathbf{S}^T\mathbf{Q} \tag{2.26}$$

P and **Q** are *metameric match*, and they are *metamer*s to each other.

From now on, only color matching functions will be used to represent the color response mechanism of cones. Tristimulus values can be written as

$$\begin{aligned} \mathbf{t} &= \mathbf{A}^T\mathbf{P} = \mathbf{A}^T\mathbf{L}\mathbf{r} \\ &= (\mathbf{L}\mathbf{A})^T\mathbf{r} = \mathbf{A}_L^T\mathbf{r} \end{aligned} \tag{2.27}$$

where **A** is the $(N \times 3)$ matrix of CIE XYZ color matching functions, $\mathbf{A} = [\bar{\mathbf{x}}, \bar{\mathbf{y}}, \bar{\mathbf{z}}]$, **L** is the $(N \times N)$ diagonal illuminant matrix with diagonal elements from illuminant vector **l**, with $\mathbf{A_L} = \mathbf{LA}$, and **r** is the ($N$×1) spectral reflectance.

2.5.2 Singular Value Decomposition

The *singular value decomposition* (SVD) means for any real $m \times n$ matrix A, there exist orthogonal matrices

$$U = [u_1, \cdots, u_m] \text{ and } V = [v_1, \cdots, v_n]$$

where u_i and v_i are column vectors, such that

$$U^T AV = \text{diag}(s_1, \cdots, s_p) \equiv \Sigma \qquad p = \min\{m, n\}$$

where $s_1 \geq s_2 \geq \cdots \geq s_p \geq 0$ are the singular values of A and Σ is an $m \times n$ diagonal matrix. The SVD of A can also be written as

$$A = U\Sigma V^T = \sum_{i=1}^{r} s_i u_i v_i^T \tag{2.28}$$

where r is the rank of A and $s_1 \geq s_2 \geq \cdots s_r > s_{r+1} \cdots = s_p = 0$. Furthermore, SVD-related projections can be defined as follows:

If matrices U and V are partitioned as

$$U = [U_r \quad \tilde{U}_{m-r}] \qquad V = [V_r \quad \tilde{V}_{n-r}]$$

then U_r is the range, or fundamental subspace of *A*, $\mathbf{P}_r = U_r U_r^T$ is the projection onto the range of *A*, and $\tilde{V}_{n-r}\tilde{V}_{n-r}^T$ is the projection onto the null space of *A*.

If $m \geq n$, the *thin SVD* of A is

$$A = U_1 \Sigma V^T \tag{2.29}$$

where

$$U_1 = [u_1, \cdots, u_n] \text{ and } \Sigma_1 = diag(s_1, \cdots, s_n) \text{ is a square matrix}$$

Details on SVD can refer to [pg. 69-77 in Golub1996].

Cohen and Kappauf had defined Matrix-*R* [Cohen1985] as:

$$\mathbf{R} = A(A^T A)^{-1} A^T \tag{2.30}$$

It is in fact $\mathbf{R} = U_r U_r^T$, since $A = U_1 \Sigma_1 V^T$, $A^T = V \Sigma_1^T U_1^T$, $A^T A = V \Sigma_1 U_1^T U \Sigma_1 V^T = V \Sigma_1^2 V^T$, thus

$$\begin{aligned}
\mathbf{R} &= U_1 \Sigma_1 V^T (V \Sigma_1^2 V^T)^{-1} V \Sigma_1^T U_1^T \\
&= U_1 \Sigma_1 V^T V \Sigma_1^{-2} V^T V \Sigma_1^T U_1^T \\
&= U_1 \begin{bmatrix} \mathbf{I}_r & \mathbf{0} \\ \mathbf{0} & \mathbf{0} \end{bmatrix} U_1^T \\
&= U_r U_r^T = \mathbf{P}_r
\end{aligned}$$

where Σ_1^{-2} is a diagonal matrix with the first *r* diagonal elements are non-zero and the left *n*-*r* diagonal elements are zero, assuming *A* (and Σ) is a *r*-rank matrix.

If a spectrum *R* is projected onto the fundamental subspace of *A*, a companion spectrum *R** is obtained as

$$\begin{aligned}
R^* &= \mathbf{P}_r R = U_r U_r^T R = \sum_{i=1}^{r} (u_i^T R) u_i \\
&= A(A^T A)^{-1} A^T R
\end{aligned} \tag{2.31}$$

which is called the *fundamental metamer* of *R*, since it can be easily verified that

$$\begin{aligned}
A^T R^* &= A^T A(A^T A)^{-1} A^T R \\
&= A^T R
\end{aligned} \tag{2.32}$$

The spectra difference between *R* and *R** is

$$B \equiv R - R^* = R - U_r U_r^T R = (I_n - U_r U_r^T) R = \mathbf{P}_r^0 R \tag{2.33}$$

where $\mathbf{P}_r^0 = I_n - U_r U_r^T$. Since

$$A^T B = A^T (R - R^*) = A^T R - A^T R^* = \mathbf{0} \tag{2.34}$$

B is called the metameric black of *R*. Therefore all metamers *N* of *R* is given by

$$N = P_r R + P_r^0 B \qquad \text{for any stimulus } B \tag{2.35}$$

Here application of metrix provides good insight into metamerism phenomena.

2.5.3 Linear Models of Spectrum

The linear model of spectrum is to express a spectral function as a linear combination of a set of given basis functions that are linearly independent of each other:

$$S(l_i) = \sum_{j=1}^{m} a_j B_j(l_i) \qquad \text{for } i = 1, 2, \cdots, n \tag{2.36}$$

where $B_j(l)$ denotes the basis functions and a_j are the coefficients. In principle, any linearly independent basis functions can be used. In color imaging applications, the basis functions are derived such that they can represent all spectra of the similar type in low dimension, that is, $m \le n$. Ohta used linear combination of cubic spline functions to represent spectrum [Ohta1983]. Fourier series expansion provides one set of basis functions [Sun2000]. The above singular value decomposition also provides one set of basis functions [Kotera2001]. Principal Component Analysis (PCA) provides another set of basis functions. PCA means that a spectrum having the similar characteristics of an ensemble $\mathbf{M}$ can be represented as linear combination of m eigenvectors together with the mean $\overline{s}_l$ from the ensemble:

$$S_l \approx \overline{s}_l + \sum_{i=1}^{m} a_i \mathbf{e}_i \tag{2.37}$$

where $\{\mathbf{e}_i\}_{i=1}^{m}$ are the first m eigenvectors of variance-covariance of $\mathbf{M}$, m is chosen such that, for example 99% (depends on application and reconstruction accuracy) of total variance is explained by m eigenvectors [pg. 458-512 in Johnson1998]. PCA has been shown as an effective way to reduce the dimensionality of natural reflectance spectra [Maloney1986, Katera1987a, Chang1988, Vrhel1992, Burns1997b, Tajima1998a].

Linear model works well for smooth spectrum. For spectrum with multiple spikes, i.e. fluorescent illuminant spectra, it can be decomposed into two components, one of which is smooth, and the other contains spikes that can be expressed in terms of delta-functions [Trussell1994, Sharma1994, Sun2000]:

$$S(l) = S_{smooth}(l) + S_{spikes}(l) \tag{2.38}$$

$$S_{spikes}(l) = \sum_{i=1}^{p} w_i d(l - l_{0i}) \tag{2.39}$$

where l_{0i} and w_i denote the location and height of the i^{th} of the p spikes. The smooth component can still apply the linear models.

2.6 Conclusions

The fundamentals of color vision and color imaging were described, which consists of spectrum of physical stimulus, color space, color and image difference metrics, color appearance models, some mathematical backgrounds, such as vector space method, linear models, singular value decomposition, principal components analysis. These fundamentals form a basis for color imaging applications, including color device characterization, evaluation and design.

3 CAMERA CHARACTERIZATION

3.1 Introduction

Digital color cameras (including digital still camera, digital video camera and color scanner) capture the spectrum or color information of physical stimuli by filtering the object image through color filters with different spectral transmittances, and transforming the photon signal into electronic signal which finally is quantized into digital counts with electronic sensors.

Figure 3.1 illustrates the major components of a generic digital camera. The optical lens subsystem images the light onto color filters and the detector array. Electronic sensors generally are based on Charge-Coupled Device (CCD) or Active Pixel Sensor (APS) CMOS technology. Color filters allow only specific spectral radiance to pass through. The camera channel is defined as the total effect of color filter and electronic sensor. Usually the optical subsystem is shared by all channels. Depending on the application, the number of channels may be different for different cameras. With the development of spectral imaging, up to eight channels for wideband principal component capture is used, and up to thirty-one channels for narrowband imaging is used, but typical trichromatic cameras have three channels, each of which consists of CCD array and one of red, green and blue filters, respectively. High-end cameras have three CCD arrays, which respond light from beam splitter and require precise mechanical and optimal alignments in order to maintain good registration for images from different channels. Common cameras have only one CCD array, which is shared for all channels, and color filters are arranged as single color filter arrays (CFA) such as Bayer pattern [Kriss1996] (Figure 3.2) in one plane or changed through filter wheel. The CFA arrangement can avoid the problems of registering multiple images, but will decrease the captured image resolution, which may be enhanced through interpolation in the signal processing stage. Some broadcasting cameras have four channels,

cyan, magenta, yellow and green, which are combined to generate red, green and blue signals in order to increase signal-to-noise ratio and minimize aliasing [pg. 96 and 167 in Holst1998].

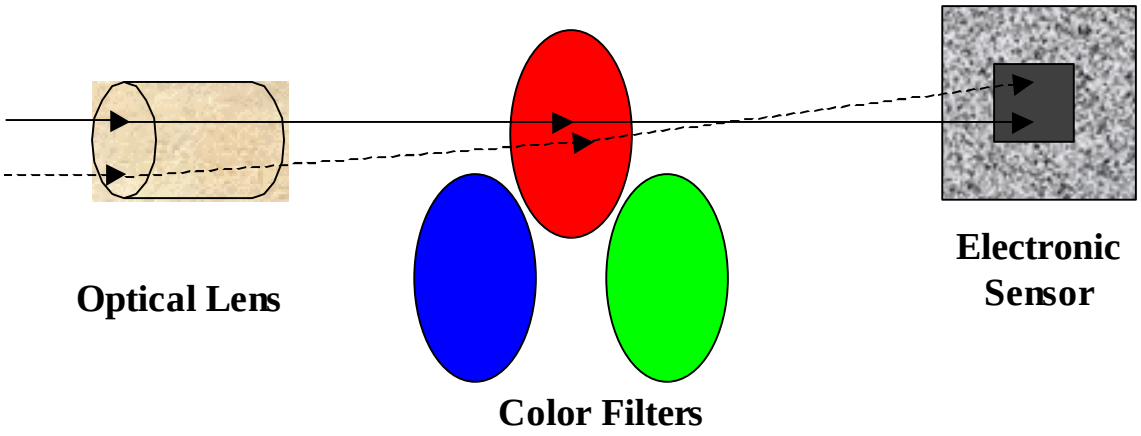

Figure 3.1: Generic components in digital camera.

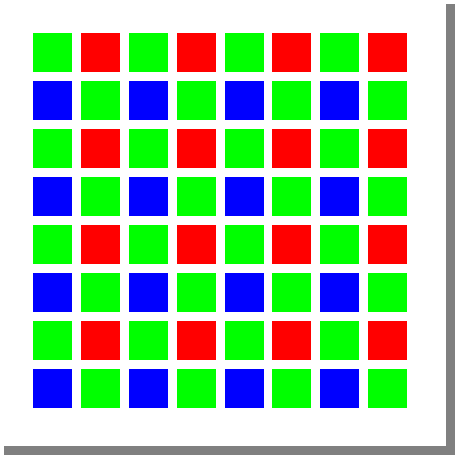

Figure 3.2: Bayer pattern in digital camera.

This chapter begins with a description of camera response models, which will be used throughout of the dissertation, followed by an introduction of conventional camera characterization methods. The camera spectral characterization method is then discussed. Spectral sensitivity functions can be measured or estimated. Measurement gives great accuracy but the process is time-consuming and requires special instruments, while estimation is easy to implement, and in some circumstances, it is accurate enough to replace *in situ* measurement.

This chapter also discusses which estimation method and how far the estimation can replace direct measurement.

3.2 Camera Model

A camera model predicts the image pixel digital counts of spectral power distributions of physical stimuli. It depends on the camera setup. Typical camera setup requires fixation of lens aperture, distance of camera and target, position of light source and minimization of ambient light. Assuming all camera controls are fixed, a generalized camera image formation process can be represented as

$$t_i = F_i(v_i) = F_i\left(\int_{l_{\min}}^{l_{\max}} s_i(l)P(l)dl + x_i\right) \qquad i = 1, 2, \cdots J; \tag{3.1}$$

where v_i is the initial captured raw signal for the i^{th} channel of a specific image pixel, t_i is the final manipulated camera output signal, $P(l)$ is the spectral power distribution of physical stimuli, $s_i(l)$ is the total sensor spectral sensitivity function for the i^{th} channel, x_i is the noise property corresponding to the i^{th} channel, $F_i(\bullet)$ is usually the gamma correction (optional), a monotonically increasing nonlinear function, and J is the number of channels. This model is also true for color scanner, colorimeter, spectrophotometer and spectroradiometer.

While cameras for scientific applications usually give linear output signal, that is, the final output signal is proportional to the intensity of the input physical stimuli, many cameras for common use adopt the idea to boost the image detail in low luminance level by introducing gamma correction [Giorgianni1998].

Successful use of the above model requires sufficient consideration of the nonlinear function $F_i(\bullet)$. $F_i^{-1}(\bullet)$ reverses any added gamma correction, subtracts any camera black, flat-fields the non-uniformity of light illumination on the object surface, as well as correcting for other more subtle non-linearities which may exist. In this dissertation, the camera output signal is assumed being corrected if necessary such that the linear raw signal is obtained. Therefore a linear model on camera response can be rewritten as

$$
\begin{aligned}
t_i &= \int_{l_{\min}}^{l_{\max}} s_i(l)P(l)dl + x_i \\
&= \int_{l_{\min}}^{l_{\max}} s_i(l)L(l)r(l)dl + x_i \\
&= \int_{l_{\min}}^{l_{\max}} f_i(l)d(l)L(l)r(l)dl + x_i
\end{aligned}
\tag{3.2}
$$

where t_i denotes the camera raw signal, $f_i(l)$ is the spectral transmittance of the i^{th} channel color filter, $d(l)$ is the spectral sensitivity of the detector, which usually contains the effect of infrared cutoff and ultraviolet cutoff filters, $s_i(l) = f_i(l)d(l)$, $L(l)$ is the spectral radiance of the taking illuminant, $r(l)$ is the spectral reflectance of object surface.

Like the signal formation process in human eye, assuming all spectra are band-limited, the continuous functions of the wavelength are replaced by samplings of those functions, and the recording process, or the integral can be represented as matrix operation:

$$
t_i = s_i^T L_c r + x_i, \qquad i = 1, 2, \cdots J; \tag{3.3}
$$

where s_i is the $N \times 1$ vector of samplings of $s_i(l)$, r is the $N \times 1$ vector of reflectance samplings, and L_c is an $N \times N$ diagonal matrix with samplings of the taking illuminant, $L(l)$, along the diagonal. Equation (3.3) may be rewritten using matrix vector notation as

$$
t_c = S^T L_c r + x = G^T r + x \tag{3.4}
$$

where $t_c = [t_1, t_2, \cdots, t_J]^T$ is the $J \times 1$ vectors of camera output signals, $S_{N \times J} = [m_1, m_2, \cdots, m_J]$, $x = [x_1, x_2, \cdots, x_J]^T$ is the $J \times 1$ recording noise vector and $G = L_c^T S = L_c S$. In the absence of noise, the camera imaging process can be described as the projection of reflectance spectra onto the column space of $G = L_c S$. Similar to the definition of HVSS, the column space of *G* will be called the *camera imaging subspace* (CIS).

Some cautions must be taken in practical applications. The reflectance spectra of natural objects, the daylight spectra, the tungsten spectra, the transmittance spectra of filters, and the sensitivity function of common electronic devices are typically smooth functions of wavelength and can be sampled with negligible aliasing using a 10nm-sampling interval. However a 10nm-sampling interval is inadequate for fluorescent illuminants which have sharp emission lines in their spectra. A much smaller sampling interval need be used, for example, 2*nm* or 1*nm* sampling, which will drastically increase the dimensionality of the problem and computational

load. Some materials have strong reflection in near-blue region, which may make the lower bound of the visible range (380nm) not low enough. Some color filters have strong transmittance beyond the visible range (Figure 3.3), and typical CCD sensor is also sensitive to infrared spectra, therefore infrared and ultraviolet cutoff filters are required to block the entrance of those radiances.

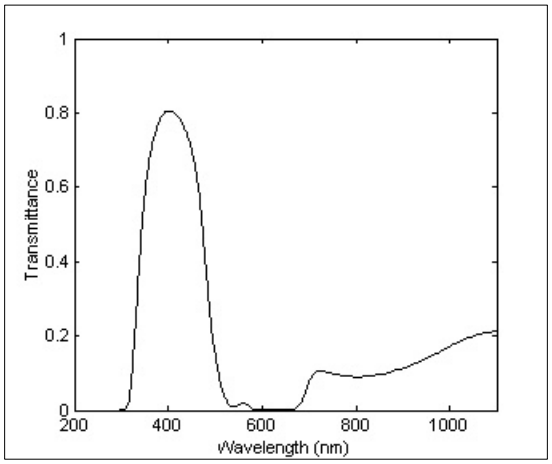

Figure 3.3: Example of spectral transmittance beyond the visible range.

3.3 Review of Camera Colorimetric Characterization

Conventional camera colorimetric characterization establishes the relationship between the camera output signal of physical stimuli and the human visual response (Figure 3.4). A standard test target is necessary in order to carry out the characterization, such as the Macbeth ColorChecker, or selected color patches. The camera output signal is described by device RGB values, and the human visual response is represented with tristimulus values or further interpretations, such as CIELAB values. The device-dependent RGB signals of the standard samples are obtained under taking illuminant L_c . An unknown transformation F_0 will be determined so that the tristimulus values can match the reference tristimulus values determined for viewing illuminant L_v using a colorimeter or spectrophotometer. Since the transformation from CIE XYZ to CIELAB is fixed, and XYZ is not a perceptually uniform color space whereas CIELAB is approximately a uniform color space, the transformation can also be defined so that

the difference between the estimated CIELAB and measured (reference) CIELAB values is minimized. While F_0 defines a forward transformation, F_0^{-1} defines a reverse transformation. Note that the taking illuminant L_c and the viewing or target illuminant L_v may be different, in which case color correction is involved.

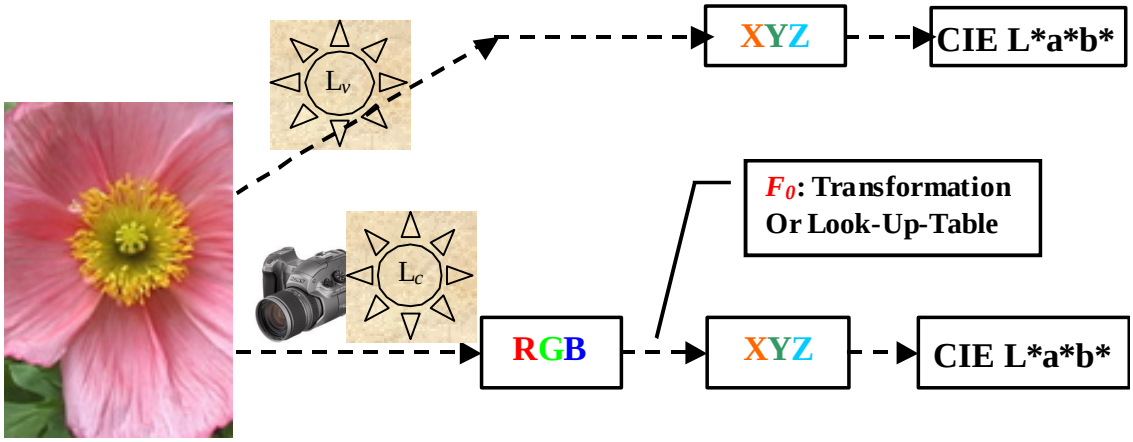

Figure 3.4: Conventional camera characterization approach.

Kang reported color scanner calibration with multiple polynomial regressions [Kang1992a & Kang1992b]. In his method, the scanner RGB responses are at first gray-balanced, and then transferred to the measured XYZ values with polynomial regression, which is obtained with least-squares techniques. Color difference, ΔE^*_{ab}, or ΔE^*_{94} is calculated for both the training set and testing set. The regression terms are symmetrically picked from the Table 3-1.

Table 3–1: Polynomial terms for polynomial regression.

Types	Terms					
Black and white	1					
Linear Terms	R	G	B			
Second-Order Terms	RG	GB	RB	R^2	G^2	B^2
Third-Order terms	R^3	G^3	B^3	RGB		

It was found that the accuracy of the polynomial approximation in the training set improves as the number of terms in the polynomial increases, but that in the testing set the

opposite occurs, which means only lower order polynomials can fit equally well both training and testing sets. In addition, the position of the color used in the training set, not the number of colors, is more important in the color interpretation within a given gamut. The characterization process is also material-dependent, but a unified transformation exists for a specific material.

Hung introduced a colorimetric calibration method in electronic imaging devices using a look-up-table model and interpolation [Hung1993]. By dividing the color gamut into many tetrahedrons and using linear matrices, 3-D forward and backward transformations were performed. In order to reduce the number of measurement points, a nonlinear interpolation technique was also proposed. His simulation found that a $33\times33\times33$ look-up-table was enough to approximate the analytical models yielding color difference $\Delta E^*_{uv} \le 0.5$ and that $5\times5\times5$ color measurements were enough to predict colors in practice ($\Delta E^*_{uv} \approx 0.8$).

Adkins, *et al*. reported color mapping using neural networks [Adkins1993]; Tominaga also introduced a neural network approach to color reproduction in color printers [Tominaga1993]. Usually a feed-forward back-propagation neural network is applied to build a mapping relationship between input signals and output signals (Figure 3.5). Such an artificial neural network, simulating human nerve intelligence, consists of an input layer, multiple hidden layers and an output layer. The circles at the nodes represent processing units (neurons), each of which sends its output to higher layers, receive its input from lower layers and follow a sigmoid learning curve. For a training set, the obtained output signals, after sufficient iterations of learning, should match the measured signals. The minimization of this difference can find the internal parameters in the learning curves, which determine a trained neural network when the difference is acceptably small. After the neural network is trained, it can be used to predict the output signals in the testing set. Since no analytical model or properties of devices are used, the approach can be treated as a *black box* and used to establish any mapping relationship between two attributes, and the mapping could be either forward or backward. Tominaga reported a $3-10-10-3$ network achieved a good accuracy for color reproduction on his printer. Tominaga has also used neural networks to do coordinates conversion between color-specification systems,

i.e. Munsell to CIELAB and vice versa [Tominaga1998]. This approach is straightforward and attractive, but in fact determining the form of the network takes much time through trials, and the minimization process to determine parameters can easily result in oscillation. All these disadvantages make the neural network not used widely in practice.

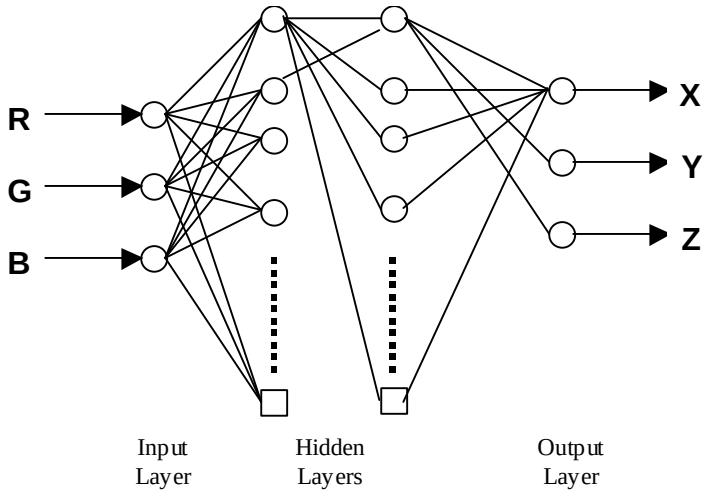

Figure 3.5: Neural network for camera characterization.

3.4 Camera Spectral Characterization

Conventional colorimetric characterization approaches are very useful in practice, but they have limitations: the characterization depends on the viewing and taking illuminants, as well as materials. A fundamental method would be to obtain the spectral sensitivity functions of the color input device. With knowledge of the spectral sensitivities, one can predict the digital counts from the measurement of reflectance spectra, and transfer the digital counts into tristimulus values with any taking and viewing illuminant pairs. The spectral sensitivities can be measured directly, which requires special instruments and takes a long time. In some cases, estimation of those functions through a “quick and dirty” approach is desired provided that the estimation accuracy can fulfill application requirement. In this section, the measurement procedure is introduced at first, followed by the spectral estimation approaches.

3.4.1 Accurate Measurement of Spectral Sensitivities

Accurate knowledge of the spectral sensitivity function for each sensor of the multichannel camera system is necessary for either color correction of different illuminants or the estimation of the surface-spectral reflectance. A coarse measurement of the spectral sensitivity functions of a CCD camera uses a set of interference filters and spectrophotometer [Park1995]. Usually a total of 31 interference filters is needed for the wavelength range of 400nm~700nm with a 10nm interval. The interference filters convert the continuous light spectrum of a lamp into a set of narrow bandwidth light spectra; strictly speaking, these filtered light spectra have a bandwidth of 9~20nm.

For more precise measurement, a monochromator can be used to determine the spectral sensitivity of the camera [Martinez-Verdu2002]. Figure 3.6 shows the setup for measuring the spectral sensitivity of the CCD camera. The monochromator converts the continuous spectrum of a xenon or tungsten lamp into a set of equally spaced monochrome wavelengths through the visible wavelength range of 380nm-780nm with a desired interval. The bandwidth of the generated spectrum could be as narrow as 2-3nm. The monochromatic light is then guided to diffusers, and the diffused light is measured with both the camera and a spectroradiometer. The spectral-sensitivity function of the camera is determined as the ratio of the camera output and the measured radiance at each of the sampling wavelengths. The determined spectral sensitivity function is the product of detector spectral sensitivity and filter transmittance (including optical system and infrared cutoff filter if used).

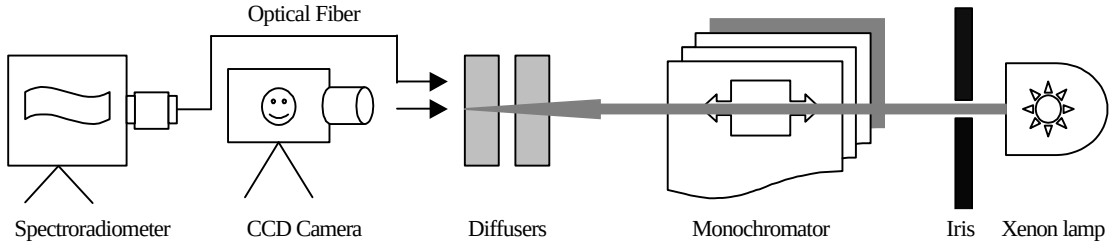

Figure 3.6: Setup for measuring spectral sensitivity of CCD camera.

3.5 Estimation of Spectral Sensitivities

The estimation of spectral sensitivity functions for color input devices is to infer the functions by imaging common reflectance or transmittance targets that are carefully selected under known illumination conditions. Researchers contributed estimation methods, i.e. Pratt and Mancill [Pratt1976], Sharma and Trussell [Sharma1996a], Hubel *et al*. [Hubel1994], Finlayson *et al*. [Finlayson1998], König and Herzog [König2000], and Thomson and Westland [Thomson2001].

3.5.1 Problem Formulation

The imaging process for a *J* channel linear or linearized camera has been written as

$$t_i = r^T L_c s_i + x_i, \qquad i = 1, 2, \cdots J; \tag{3.5}$$

where variables are defined the same as in Equation (3.3). Equation (3.5) can be rewritten as

$$t_c = r^T S + x \tag{3.6}$$

where *S* contains the information of illuminant and sensitivity functions. After *S* is estimated, the sensitivity functions $\{s_i\}_{i=1}^{J}$ can be obtained by dividing illuminant spectra L_c, which is known through measurement with a spectoradiometer. Illuminant information may also be combined with reflectance spectra in order to leave spectral sensitivity alone, i.e.

$$t_i = (L_c r)^T s_i + x_i \tag{3.7}$$

Assuming a target consisting of *K* samples with known reflectance spectra $\{r_k\}_{k=1}^{K}$ is used in the imaging, the captured signal for the i^{th} channel can be obtained from Equation (3.8):

$$\begin{aligned} \mathbf{t}_i &= [r_1, r_2, \cdots, r_k]^T L_c s_i + x_i \\ &= \mathbf{R}^T L_c s_i + x_i \\ &= \mathbf{R}^T S_i + x_i \end{aligned} \tag{3.8}$$

where $\mathbf{t}_i = [t_{i1}, t_{i2}, \cdots, t_{iK}]^T$ is the $K \times 1$ vector of output signals from the i^{th} channel, $\mathbf{R} = [r_1, r_2, \cdots, r_K]$ is the matrix of reflectance spectra of the samples, $x_i = [x_{i1},\ x_{i2},\ \cdots,\ x_{iK}]^T$ is the $K \times 1$ recording noise vector for the i^{th} channel, $S_i = L_c s_i$ is the product of illuminant information and spectral sensitivity. Assuming there is no cross-talk between *K* channels, the problem of estimation for *J* channels can be represented with one uniform equation:

$$\mathbf{T} = \mathbf{R}^T \mathbf{S} + x \tag{3.9}$$

where $\mathbf{T}$ contains *K* values, $\mathbf{S}$ contains *N* unknowns.

3.5.2 Pseudo-Inverse Estimation

If noise is ignored, a simple procedure to estimate the spectral sensitivity would be to solve the least-squares problem:

$$\hat{\mathbf{s}} = \arg\min_{\mathbf{y}} \left\| \mathbf{T} - \mathbf{R}^T \mathbf{y} \right\|, \tag{3.10}$$

where the minimization is performed over all possible $N \times 1$ vectors $\mathbf{y}$.

The solution of this problem is readily obtained in terms of the pseudo-inverse:

$$\hat{\mathbf{s}} = (\mathbf{R}\mathbf{R}^T)^{-1}\mathbf{R}\mathbf{T} = \mathbf{R}^{T\dagger}\mathbf{T} \tag{3.11}$$

where $R^{T\dagger}$ denotes the pseudo-inverse of $\mathbf{R}^T$. In terms of the singular value decomposition (*SVD*), $\mathbf{R} = U\Lambda V^T$, the least-squares solution can be written as

$$\hat{\mathbf{s}} = \sum_{i=1}^{P} \frac{(v_i^T \mathbf{T})}{s_i} u_i \tag{3.12}$$

where $P\left[\leq \min(K, N)\right]$ is the rank of $\mathbf{R}$; $\{s_i\}_{i=1}^{P}$ are the nonzero singular values of $\mathbf{R}$ (in decreasing order); and $\{u_i\}_{i=1}^{P}$ and $\{v_i\}_{i=1}^{P}$ are the columns of U and V, respectively (the left and right singular vectors of $\mathbf{R}$).

The least-squares approach suffers from a serious practical problem in that the spectra of natural objects do not have sufficient dimensionality to yield a good estimate of $\mathbf{S}$. If the noise is assumed to be white, the mean squared estimation error for least squares is given by:

$$E\left\{ \left\| \mathbf{S} - \hat{\mathbf{s}} \right\|^2 \right\} = \sum_{i=P+1}^{N} (u_i^T \mathbf{S})^2 + \sum_{i=1}^{P} \frac{s_e^{\,2}}{s_i^{\,2}} \tag{3.13}$$

where E denotes the expectation operator, and $s_e^{\,2}$ is the noise variance [Sharma1996c].

The matrix of reflectance spectra $\mathbf{R}$ is usually highly ill-conditioned and has only up to seven to eight significant singular values. As a result, even at low levels of noise, the higher order singular values of $\mathbf{R}$ are small compared with $s_e^{\,2}$, and the second summation in Equation (3.13) is large. Therefore, the least-squares solution is highly sensitive to noise and yields extremely poor estimates of the spectral sensitivity at typical noise levels in cameras.

3.5.3 Principal Eigenvector Estimation

The sensitivity of the least-squares solution to noise is greatly reduced if only the singular vectors corresponding to the significant singular values are used in the solution, i.e., if the

singular vectors v_i for which s_i is small are not included in the solution. If the singular values beyond $s_{P'}$ are considered insignificant, the estimate of the sensitivity becomes

$$\hat{\mathbf{s}} = \sum_{i=1}^{P'} \frac{(v_i^T \mathbf{T})}{s_i} u_i \tag{3.14}$$

This solution, referred to as the *Principal Eigenvector* (PE) estimation, is less sensitive to noise than the least-squares solution and usually generates reasonable results.

A few spectral estimation techniques, such as smoothing estimation, Wiener estimation, projection onto convex set (POCS), are summarized in Appendix C.

3.6 Experiments

In this section the experiment of measurement and estimation of spectral sensitivities on a real camera are described. Colorimetric camera characterization was also tested.

A Photometrics Quantix monochromatic CCD camera, model A00K6016, with a Nikon 50mm lens was used in the experiment. The camera uses a Grade 3 CCD sensor, Kodak KAF6303E, with a resolution of3072×2048. It is controlled by Roper Scientific V++ software and outputs 12-bit digital data. A filter wheel is attached to the camera and software controlled. Up to six channels can be inserted, and five channels were examined in the research with infrared cutoff filter, short-blue, blue, green and red filters, respectively. They were designed for colorimetric and spectral reproduction purposes [Quan2001c, Imai2001].

3.6.1 Camera Response Linearity

In order to test the camera response linearity, a Kodak GrayScale was used as the target. The light source was a *ScanLite*, with spectral power distribution very close to CIE illumination A. In order to discount the surface illumination non-uniformity, a large white card with uniform surface was also captured, and the black image was taken by closing the shutter of the camera. A corrected digital count for each channel was calculated as

$$DC' = 4095 \times \frac{DC - DC_{black} + e}{DC_{white} - DC_{black} + e} \tag{3.15}$$

where DC is the digital count of any pixel in the interested area, DC_{black} is the corresponding black image digital count, DC_{white} is the corresponding white image digital count, e is a small number in order to computationally avoid some hot pixels whose black digital counts equal to the white digital counts ($e \approx 10^{-8}$).

Since color filters do not change the linearity property, the experiment tests the linearity for red, green, blue and short blue channels. Results showed that the camera CCD has excellent linearity ($R^2 \geq 0.999$), as plotted in Figure (3.7). Figure 3.8 demonstrates the linearity between captured digital counts and exposure time ($R^2 \geq 0.999$) for each gain setting. More exposure time means more photons are captured and converted to electrons, the signal is proportionally larger due to the linearity of CCD devices. It is expected noise (signal variance) be larger.

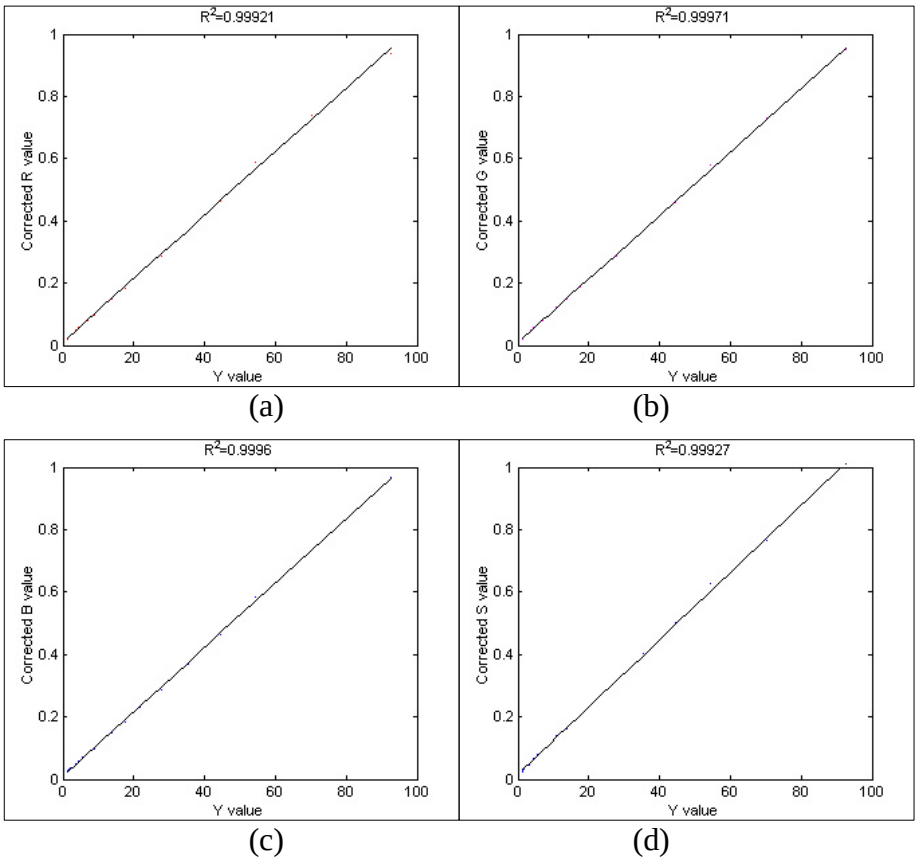

Figure 3.7: Linearity test for four channels: (a) red, (b) green, (c) blue and (d) short blue.

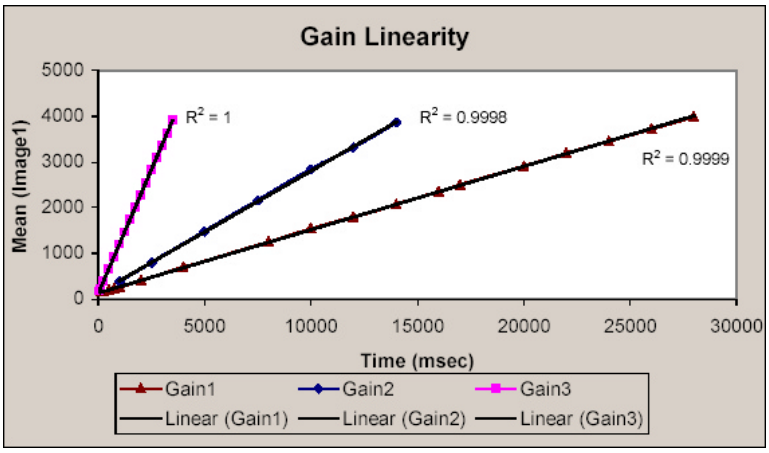

Figure 3.8: Linearity of Quantix CCD: responses versus exposure time.

3.6.2 Camera Spectral Sensitivity Measurement

The Quantix camera was used to capture images of a light source at different wavelengths. At the same time, a spectroradiometer was used to obtain the spectral radiance measurements of the light source. This was carried out for both xenon and tungsten light sources. The spectral power distributions of both light sources are shown in Figure 3.9. The xenon lamp has much higher power than the tungsten lamp; therefore it takes much longer for both spectroradiometer and camera to finish scanning using tungsten illumination. But the spectral power distribution of xenon light is not smooth and may be unstable, thus two trials were done with the xenon lamp.

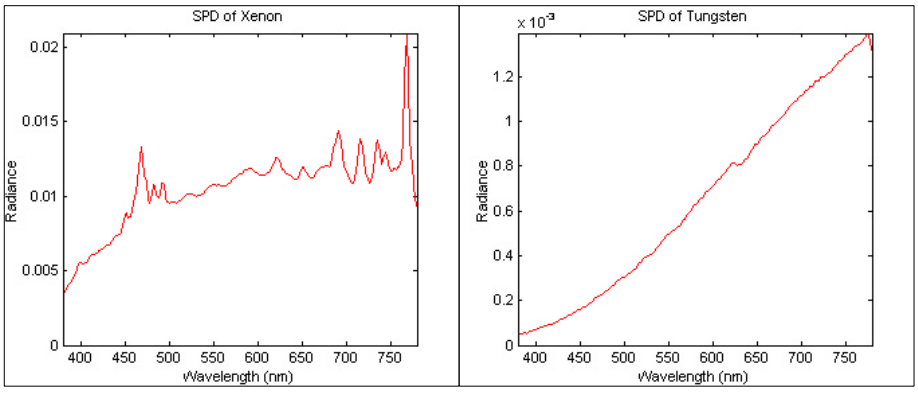

(a) (b)

Figure 3.9: Spectral power distributions of (a) xenon lamp; (b) tungsten lamp.

The experiment was setup as follows. The light rays from the light source passed through a monochromator with 2.5mm entrance and exit slits forming a 10nm passband, monochromatic light illuminated a halon patch. Both the camera and spectroradiometer were located symmetrically and closely on the two sides of the norm of the halon surface and focused on the center of the halon (Figure 3.10). After the camera configuration was fixed, the spectral sensitivity was a combination of the camera CCD, the 50mm Nikon lens and the infrared cutoff filter. Exposure time for xenon and tungsten lamps were 1.4s and 13s, respectively. Imaging and spectral radiance scanning were performed simultaneously at every 10nm from 380nm to 730nm. Once all the images were obtained, the average, maximum, minimum and standard deviation values of digital counts within the small area where spectraradiometer was focused on were calculated, shown in Figure 3.11. The final digital counts were subtracted the black digital counts and were flat-fielded.

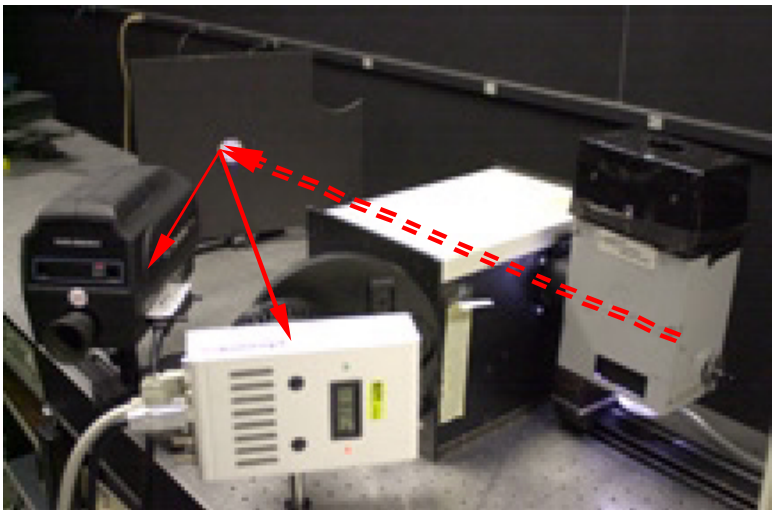

Figure 3.10: Measurement experiment setup.

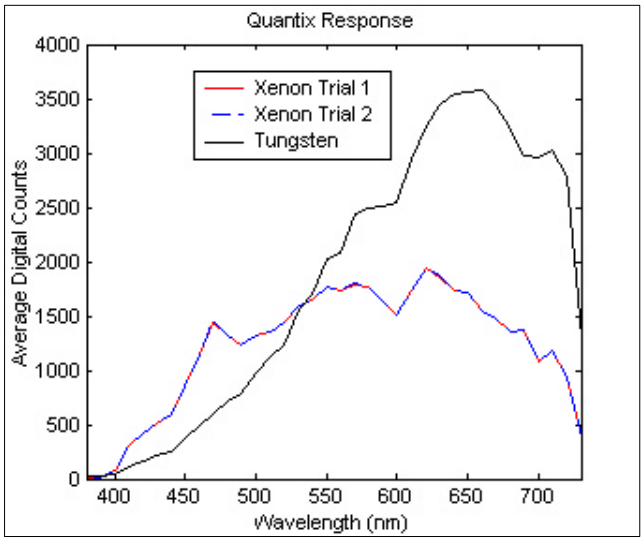

Figure 3.11: Camera response digital counts for each narrowband radiance spectra (xenon measurements overlap with each other).

Finally the total spectral sensitivity of the Quantix camera was calculated by dividing the obtained average digital counts by the spectral radiance of the corresponding narrowband light. The normalized sensitivity curves are shown in Figure 3.12 (a), which are very similar, and the two xenon measurements overlap very well. However, there are obvious differences between the xenon and tungsten measurements in the blue region. This difference was a result of the extremely low intensity for the blue narrowband radiance spectra generated from the tungsten light, which can not be measured accurately by either camera or spectroradiometer. The average of the three measurements with more weights on xenon measurements was regarded as the measured spectral sensitivity, shown in Figure 3.12 (b).

3.6.3 Measurement of Five channels

Since the filter wheel can be removed from the camera base, the transmittance spectra of the filters in each channel can be measured easily, as shown in Figure 3.13 (a). By combining the measured CCD sensitivity SS_{CCD}, the total spectral sensitivity for each channel was obtained. Note that a total infrared cutoff filter was used for all channels by attaching it on front of lens, the sensitivity functions were calculated by Equation (3.16) and shown in Figure 3.13(b).

$$SS_{\text{Total}} = SS_{\text{CCD}} \times T_{\text{IR cutoff}} \times T_{\text{color filter}} \tag{3.16}$$

where $T_{\text{IR cutoff}}$ is the transmittance of infrared cutoff filter, $T_{\text{color filter}}$ is the transmittance of color filter, and SS_{Total} is the total spectral sensitivity.

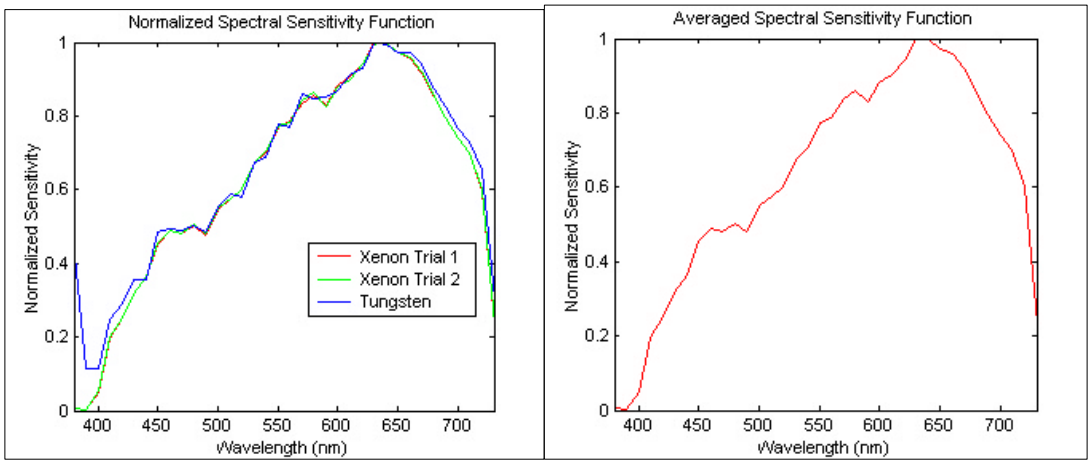

(a) (b)

Figure 3.12: Normalized spectral sensitivity function (a) three trials; (b) weighted average.

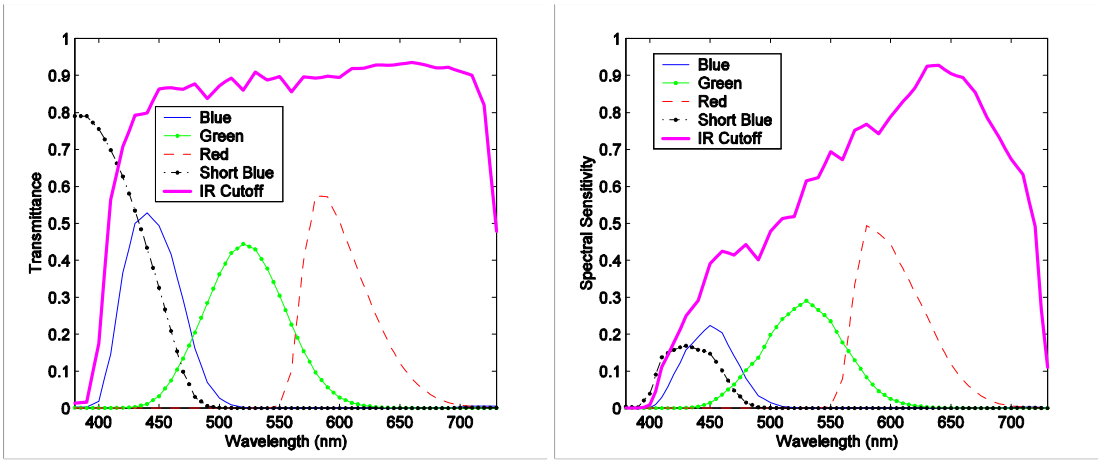

(a) (b)

Figure 3.13: (a) The spectral transmittance of filters for five channels; (b) The total spectral sensitivity functions for five channels.

3.6.4 Colorimetric Characterization

Since the spectral sensitivity functions were measured, it is easy to transform camera signals under any illumination to colorimetric data under any viewing illumination. It is interesting to

see if the practical performance can approximate the simulated performance. In this experiment, the camera is used to take images of the Macbeth ColorChecker. A 3×3 matrix was derived to convert RGB signals into CIE XYZ values by minimizing ΔE^*_{ab} or ΔE^*_{94} between the measured and estimated color information. Red, green and blue channels (RGB) as a set are compared with red, green and short blue (RGS) as a second set. For any set, the conversion matrix was first determined using a pseudo-inverse from RGB signals to XYZ values:

$$\begin{aligned} RGB \bullet M &= XYZ \\ M &= (RGB^T RGB)^{-1} \bullet RGB^T \bullet XYZ \\ &= RGB^{\dagger} \bullet XYZ \end{aligned} \tag{3.17}$$

where $RGB^{\dagger}$ is the pseudo-inverse of RGB. The initial matrix M was refined through nonlinear minimization of ΔE^*_{ab}, and the refined matrix is the final conversion matrix.

While color filters were under design, a channel consisting of CCD sensor and infrared cutoff filter was treated as the CCD sensitivity, therefore a total IR cutoff filter should be in place for the red, green, blue and short-blue channels. In the first test, the IR cutoff filter was not inserted, the color difference performance was calculated in Table 3-2. From the table, the color difference performance was very poor for the RGB filter set, though reasonable using the short-blue filter. Repeating the experiment many times gave similar and consistent color difference performance. Note that RGB was designed as a nearly colorimetric set, and was expected to perform reasonably.

Table 3–2: Color difference performance for RGB and RGS channels.

		Blue, Green, Red		Short-Blue, Green, Red	
		ΔE^*_{94}	ΔE^*_{ab}	ΔE^*_{94}	ΔE^*_{ab}
Mean ΔE	Predicted from SS	0.91	1.79	1.62	2.84
	Calculated from DC	4.09	7.12	2.11	3.60
Max ΔE	Predicted from SS	3.04	7.80	6.24	10.42
	Calculated from DC	18.58	22.19	7.53	12.50

In order to identify the problem, the relationship between predicted and calculated digital counts for each channel was shown in Figure 3.14. It can be seen that short-blue, green and red channels exhibited excellent linearity. Though blue channel deviated the linearity, most patches still followed a straight line. Patches such as No. 2, 17, 15, 7 do not, whose reflectance spectra are plotted in Figure 3.15. Those patches have some similar characteristics: their reflectance is larger in red and infrared region than other regions, where the blue channel has a secondary sensitivity. It was inferred that an infrared cutoff filter should be applied to remove the CCD sensitivity beyond the visible range. After applying IR cutoff filter, new color differences were calculated in Table 3-3. Now the performance of RGB set was reasonable, and the blue channel had a linear relationship between the predicted and captured digital counts (Figure 3.16).

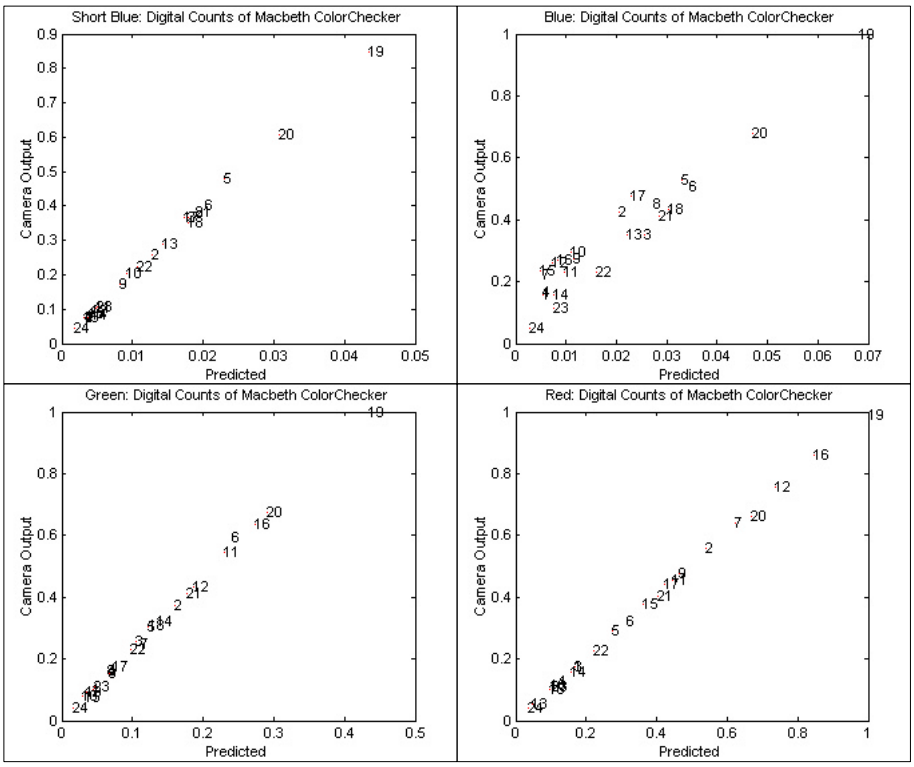

Figure 3.14: Linearity relationship for red, green, blue and short blue channels.

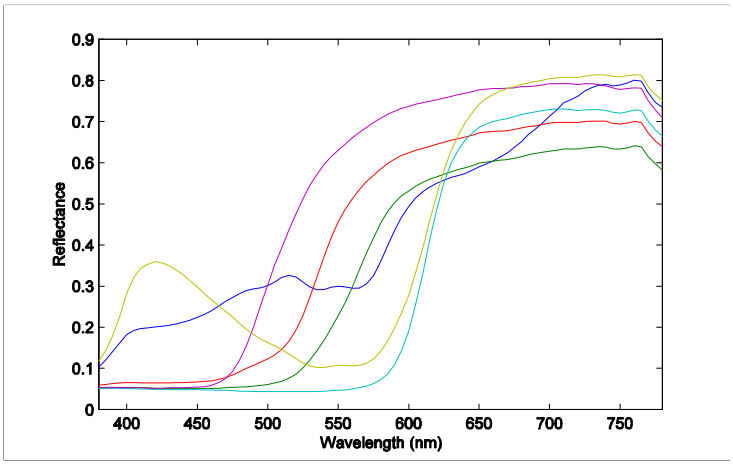

Figure 3.15: Macbeth ColorChecker patches deviated from the linearity for blue channel.

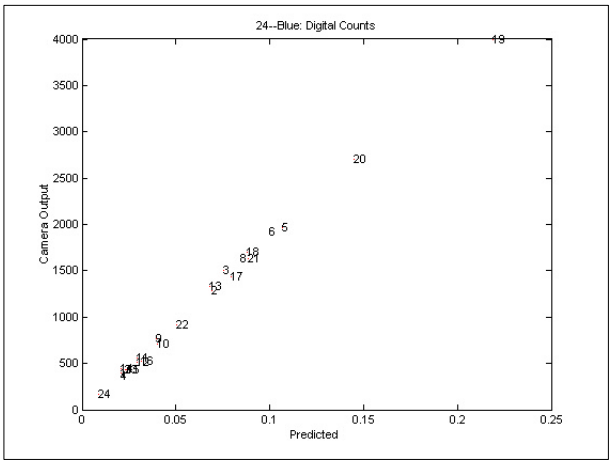

Figure 3.16: Linearity for blue channel after infrared cutoff filter was applied.

Table 3–3: Color difference performance after applying IR cutoff filter.

	Mean ΔE^*_{94}	Mean ΔE^*_{ab}	Max ΔE^*_{94}	Max ΔE^*_{ab}
Predicted RGB (IR for Blue)	1.46	2.86	5.72	9.00
Experimental RGB (IR for Blue)	1.69	3.40	4.86	8.06
Predicted RGS	1.91	3.32	7.81	13.01
Experimental RGS	2.15	3.90	7.02	11.52
Predicted RGB (IR for RGB)	0.98	1.79	3.63	6.02
Experimental RGB (IR for RGB)	1.13	2.13	3.08	5.39

3.6.5 Spectral Estimation

Principal Eigenvectors, Wiener and Projection onto the convex set estimations have been widely tested and been proven to be quite successful [i.e. Hardeberg1998, Vora2001 and Sharma1997c]. PE estimation is comparatively easy to be implemented yet gives reasonable precision if imaging targets are carefully selected. The result shown in Figure 3.17 was obtained to estimate camera spectral sensitivity by imaging Macbeth ColorChecker using a Sony B/W XCH-1125 CCD camera. Totally up to 7 principal eigenvectors are applied to estimate the camera spectral sensitivity. The estimations from 3, 4, 5 or 6 PE are very close to each other and their average was regarded as an estimation of the camera spectral sensitivity. If more PE (i.e. 7) are used, estimated curve is oscillated, which should be avoided practically.

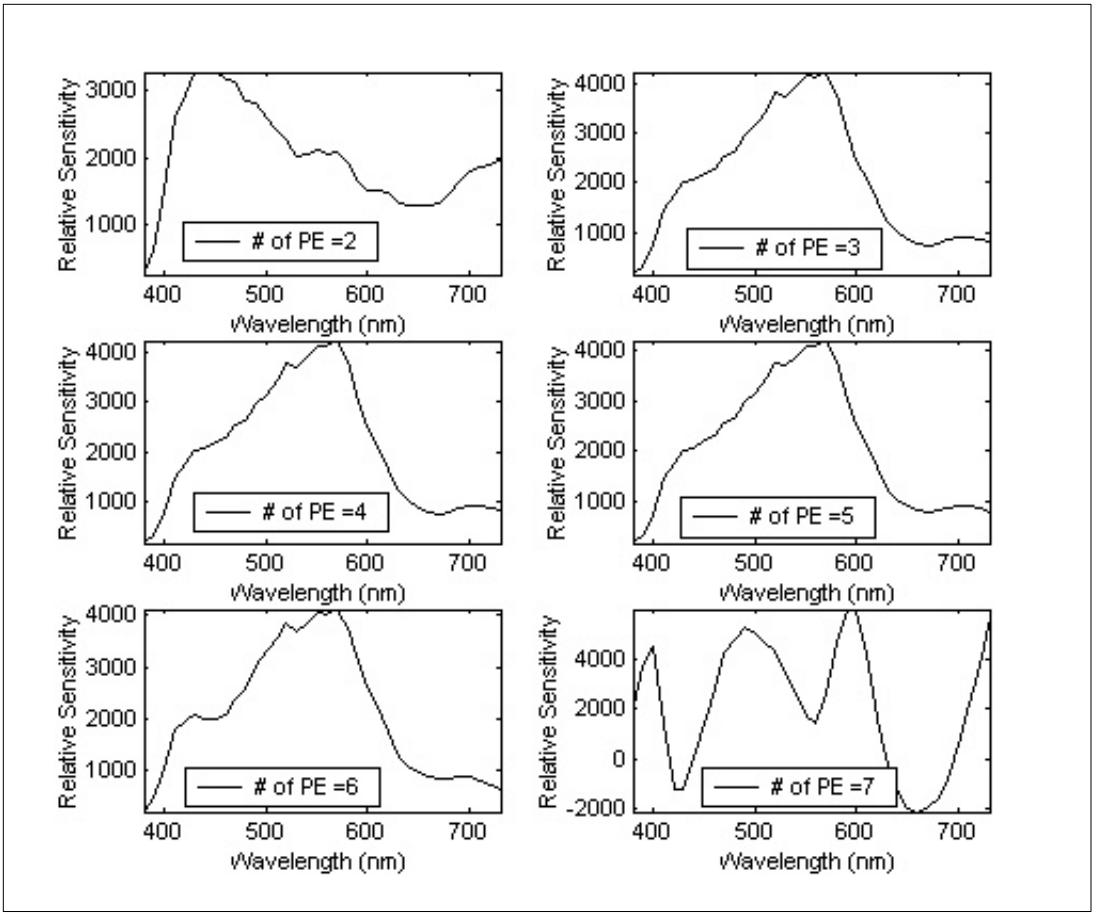

Figure 3.17: PE estimation on XCH 1125 B/W camera

3.7 Conclusions

The colorimetric and spectral characterization methods for color input devices were described in this chapter. The colorimetric characterization builds a relationship between device output signals and color coordinates in a device-independent color space. Linear and polynomial regressions as well as neural network mapping are the typical approaches to carry out conventional device characterization. A spectral characterization of digital imaging devices is realized by directly measuring the device spectral sensitivity functions with monochromator and spectraradiometer. Some typical spectral estimation approaches were discussed in this chapter and an example using principal eigenvector method shows that, depending on the characteristics of imaging targets, illumination, and real sensitivity curves, the estimation methods may be able to achieve the required estimation accuracy.

4 IMAGING NOISE AND NOISE PROPAGATION

Strictly, any system is subject to uncertainty. It is because of the existence of uncertainty that *practice* is the only approach to test a theory. An imaging system takes in physical stimuli with uncertainty and adds more uncertainty in processing stage. This uncertainty is then propagated as long as the signal is processed. The uncertainty created during an imaging process is called imaging noise. It is desirable that a camera can always capture accurate color under a variety of illumination conditions, which depends on the detector noise characteristics, the color filters and signal processing algorithms. This chapter discusses imaging noises in digital imaging applications. A physical noise model will be formed which consists of the major sources of noise. General rules on noise propagation caused by signal processing will be also discussed. Some experimental results on noise measurement will be presented finally.

4.1 CCD Imager Noise Model

4.1.1 Introduction

Compared with chemical imaging methods, CCDs are relatively new devices, first introduced in 1970. An imaging CCD consists of an array of pixel sites that detect incoming light through the photoelectric effect. Electrons generated by the detection process are collected as charge packets in well-defined potential wells. The charge packets thus collected are transferred by externally applied electric signals to one or more output ports, where the charge packets are converted to electrical signals proportional to the charge. The detection, collection, transfer, and conversion operations are accomplished with remarkable efficiency and precision. Modern CCDs have the attributes of large linear dynamic range, relatively high quantum efficiency, excellent charge-transfer efficiency, wide spectral response, and geometric stability.

The light detection capability of CCD is limited by noise. The level of detail in any noise discussion depends on the application. Figure 4.1 shows the typical noise sources at each signal transfer step in CCD. Shot noise is caused by the discrete nature of photons. It occurs when photoelectrons are created and when dark current electrons are present. Additional noise is added when reading the charge (reset noise) and introduced by the amplifier (1/*f* noise and white noise). If the output is digitized, the inclusion of quantization noise may be necessary. Switching transients that are coupled through the clock signals also appear as noise. It can be minimized by good circuit design [Holst1998].

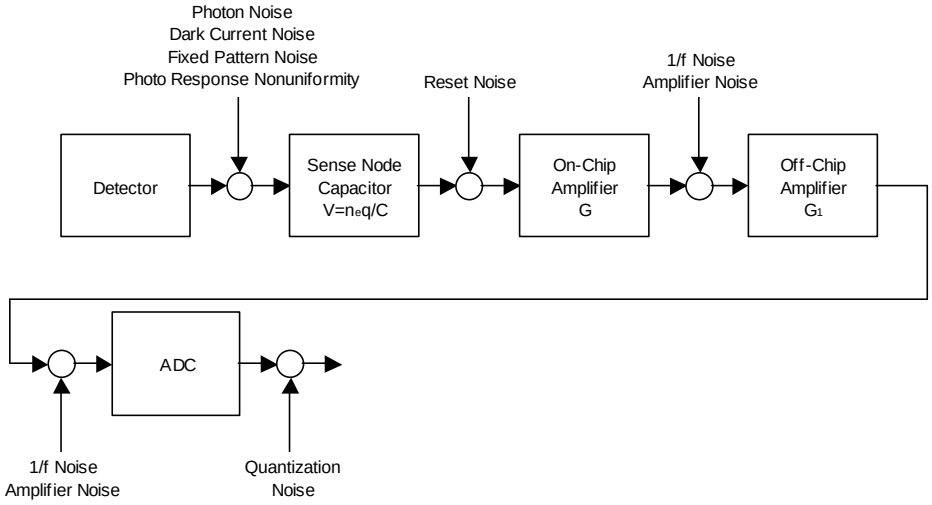

Figure 4.1: Typical noise sources in CCD; parameters are described in [Holst1998].

Although the origin of each noise source is different, they all appear as variations in the image intensity. Photon shot noise produces a temporal variation in the output signal that is proportional to the square root of the signal level elements. Each pixel output will have a slightly different value for a uniform source.

Under ideal conditions, each pixel would have the same dark current and this value is subtracted from all pixels leaving the desired signal. However, dark current also exhibits

fluctuations. Even after subtracting the average value, these fluctuations remain and create fixed pattern noise.

Pattern noise refers to any spatial pattern that does not change significantly from frame-to-frame. Dark current varies from pixel-to-pixel and this variation is called fixed pattern noise (FPN). FPN is caused by differences in detector size, doping density, and foreign matter getting trapped during fabrication. Photoresponse nonuniformity (PRNU) is the variation in pixel responsivity and is seen when the device is illuminated. The noise is due to differences in detector size, spectral response, and thickness in coatings. These “noises” are not noise in the usual sense. PRNU occurs when each pixel has a different average value. This variation appears as spatial noise to the observer. Frame averaging will reduce all the noise sources except FPN and PRNU. Although FPN and PRNU are different, they are sometimes collectively called scene noise, pixel noise, pixel nonuniformity, or simply pattern noise.

When quoting noise levels, it is understood that the noise magnitude is the root-mean-squares (rms) of the random process producing the noise. Noise powers are considered additive. Significant noise sources are limited to the following [Holst1998]:

Photon statistics: This uncertainty is due to the Poisson arrival statistics of the input photons and results in an observational uncertainty whose variance is equal to the mean photon input. Maximum sensitivity in a CCD system is achieved by reducing all other noise sources so that photon statistics dominate output noise at the lowest possible input signal level.

Fixed pattern noise: This noise source arises from variations in gain (photon to electron conversion variations) at individual pixel sites. Modern CCDs reduce this problem through calibration or flat fielding schemes to make corrections to the output data to reduce the effect of fixed pattern noise.

Dark current noise: Dark current results from electrons that are generated at the pixel sites as the result of thermal action. Dark current can be reduced to negligible levels by CCD design and processing techniques, proper bias of the device and cooling.

4.1.2 Quantization Error

Image quantization is the encoding of each sample of a continuous sampled signal, e.g. radiance, as one of a limited number of discrete values. This represents a loss of information in that an error is introduced when the quantized signal is interpreted as, or compared with, the original continuous sample. The simplest and most common procedure is uniform quantization. Here each sample is compared to a set of levels that are equally spaced over the available signal range, and assigned to the nearest one. Non-uniform quantization is also common, as part of image compression [Pratt1991] or as a step to compensate for later elements in an imaging system, such as the photometric response of a CRT display [Giorgianni1998]. Non-uniform quantization is usually implemented in two steps: a primary uniform quantization followed by a discrete transformation.

Historically image quantization has been analyzed as both a source of stochastic and deterministic error. These two views of the same signal transformation arise from differing imaging objectives. For systems where objectives can be cast in terms of signal detection and statistical information preservation, such as medical imaging, reconnaissance and astronomy, then the error introduced by quantization is often seen as an added signal-independent stochastic source with an approximately uniform probability distribution. The width of this distribution is equal to the quantization interval Δv [sees Burns1997b and Holst1998] corresponding to the range of a rounding error, i.e. $-\Delta n/2 \le e \le \Delta n/2$. For a random variable of uniform or rectangular distribution, and width parameter *Dn*, the variance is given by

$$s^2 = \frac{\Delta n^2}{12} \tag{4.1}$$

Therefore, the rms quantization noise is

$$s = \frac{\Delta n}{\sqrt{12}} \tag{4.2}$$

For the case of uniform quantization using *b* bits (2^b discrete levels) to encode each pixel, the interval has a width $(n_{\max} - n_{\min})/2^b$. Equation (4.2) then becomes

$$s = \frac{(n_{\max} - n_{\min})}{2^b \sqrt{12}} \tag{4.3}$$

where the available signal range is $v_{max} - v_{min}$. As an example, the quantization noise introduced by 8-bit encoding is $0.0011(v_{max} - v_{min})$, or 0.29 digital counts on a (0-255) scale.

Viewing error introduced by signal quantization as a stochastic noise source ignores the fact that all the resulting pixel values are rounded to a *finite number* of levels. When viewed, a quantized image, particularly in slowly-varying regions or graphical elements, shows the discrete levels as artifacts that detract from the image information. Consequently, it is the effective quantization interval that is often compared with (visually) detectable intensity or color-differences. For many applications the requirement that each quantization interval is not visible, i.e., not introduce visible artifacts, is more stringent than one based on a comparison of the rms quantization noise with image fluctuations from other sources, such as scene content and image detection.

When image signals are quantized prior to other signal processing, the resultant error can be propagated through the signal path in a similar way to that used for stochastic error propagation. In this dissertation, uniform quantization is assumed for camera signal digitizing; therefore the quantization error will not be included in the noise analysis.

4.1.3 CCD Imaging Noise Model

One purpose of this work is to minimize the propagation of input noise. The noise sources are not necessary to be diagnosed specifically but need only be classified as signal-independent and signal-dependent types which are represented by primary noises. The constant dark noise with random fluctuation represents the signal-independent noise and shot noise represents the signal-dependent noise. The fixed noise variation from pixel-to-pixel is assumed to have been corrected externally (i.e. flat fielding).

For this purpose, Figure 4.2 shows a simple model for a CCD imager, whereby a certain fraction, h, of the incident photons are detected. Ignoring dark noise for the moment, this mechanism can be written as

$$o = h \cdot i \tag{4.4}$$

where *i* and *o* are the exposure and detected signals, respectively. If the mean input exposure is m_i, then the mean output, in electrons, is

$$m_o = h \cdot m_i \tag{4.5}$$

where h is the effective quantum efficiency (the primary quantum efficiency and any net loss mechanisms that reduce the mean number of signal charge electrons that are read out, amplified, quantized, etc.) which is a function of wavelength. Note that it is assumed that, over the visible wavelength range, a single free electron is generated for each absorbed photon. The arrival statistics of uniform exposure (per area and over time) are governed by Poisson statistics, and for this discrete probability distribution the variance is equal to the mean, $s_i^2 = m_i$. For output signal, the mean is $m_o = h \cdot m_i$, and the variance should be $s_o^2 = h^2 \cdot s_i^2 = h^2 \cdot m_i$. Since photon noise will be observed even with perfect image detection, it is the lowest noise level to which actual imager performance can be compared.

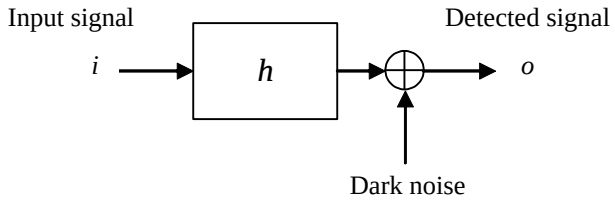

Figure 4.2: Physical model for electronic image detection.

Another noise component included in this analysis scope is dark noise, so-called because it is characterized by signal fluctuations in the absence of light exposure. There are several physical origins of this noise source, such as spontaneous thermal generation of electrons, and it is modeled as a constant-variance, zero-mean random variable (The uniform constant is assumed to have been subtracted) added to the detected signal. If both dark and shot noises are included as statistically independent stochastic sources the resulting noise variance is

$$s_o^2 = s_d^2 + h^2 m_i = s_d^2 + h^2 s_i^2 \tag{4.6}$$

where the dark noise variance is s_d^2. Note that for average signal levels where shot noise is dominant, the variance is proportional to the mean signal and the rms noise is $s_o \cong h\sqrt{m_i}$. The

noise model described as Equation (4.6) is often used for electronic image captures. From Equation (4.6), it is expected that when the signal level is low, the noise is dominated by dark noise, and when the signal level is high, the noise is dominated by shot noise, which is proportional to the signal level.

4.2 Noise Propagation

Noise is generated in the imaging stage. When the signal is transformed, noise is propagate simultaneously. The theory of error propagation through physical measurements is well established. This section outlines the basic principles of error propagation and how it can be applied to color transformation in signal processing within a digital camera.

4.2.1 Multivariate Linear Transformation

Transformation of statistical moments related to multivariate linear transformation has been discussed widely [Johnson1998]. A common color-signal transformation is a matrix operation, e.g.,

$$y = Ax \tag{4.7}$$

where a set of input signals $[x_1, x_2, ..., x_n]$ is written as $x = [x_1, x_2, ..., x_n]^T$ and the output is $y = [y_1, y_2, ..., y_m]^T$. The superscript, *T*, indicates matrix transpose, and *A* is the (*m*×*n*) matrix of transformations. If each member of the set $\{x\}_{i=1}^{n}$ is a random variable, the second-order moments can be written as a covariance matrix:

$$\Sigma_x = \begin{bmatrix} s_{11} & s_{12} & \cdots & s_{1n} \\ s_{21} & s_{22} & & \\ \vdots & & \ddots & \\ s_{n1} & & & s_{nn} \end{bmatrix} \tag{4.8}$$

where $s_{ii} = s_{x_i}^2$, and the covariance between x_i and x_j is s_{ij} . If the set of signals $\{x\}_{i=1}^{n}$ are statistically independent, Σ_x is diagonal. The resulting covariance matrix for *y*, from multivariate statistics, is given by

$$\Sigma_y = A\Sigma_x A^T \tag{4.9}$$

Equation (4.9) can also be written as an equivalent set of linear equations. For example, Wyszecki and Stiles addressed such matrix transformations and their effect on color-matching ellipsoids [Wyszecki1982].

4.2.2 Multivariate Nonlinear Transformation

When multivariate signals are transformed and combined nonlinearly, the resulting transformations of the covariance matrix and mean vector can be approximated by linear combinations with Taylor Series [Burns and Berns in Burns1997a, mathematical background can be found in Magnus1999]. Fairchild devised the variance (s_V^2) of a bivariate function as a function of the variances ($s_x^2,\ s_y^2,\ r_{xy}$) of its variables [Fairchild1991]:

$$s_V^2 = \left(\frac{\partial V}{\partial x}\right)^2 s_x^2 + \left(\frac{\partial V}{\partial y}\right)^2 s_y^2 + 2\, r_{xy} \left(\frac{\partial V}{\partial x}\right)\left(\frac{\partial V}{\partial y}\right) s_x s_y \tag{4.10}$$

Equation (4.10) can be rewritten in matrix form:

$$s_V^2 = \begin{bmatrix} \frac{\partial V}{\partial x} & \frac{\partial V}{\partial y} \end{bmatrix} \begin{bmatrix} s_x^2 & r_{xy} s_x s_y \\ r_{xy} s_x s_y & s_y^2 \end{bmatrix} \begin{bmatrix} \frac{\partial V}{\partial x} & \frac{\partial V}{\partial y} \end{bmatrix}^T \tag{4.11}$$

In general, Equation (4.11) can be extended to multiple multivariate nonlinear transformations. If the input signals have covariance matrix, Σ_x and each of the signals is transformed,

$$\begin{aligned} y_1 &= f_1(x_1, x_2, \cdots, x_n) \\ y_2 &= f_2(x_1, x_2, \cdots, x_n) \\ &\vdots \end{aligned} \tag{4.12}$$

where *f* may represent a compensation for detector response, or a nonlinear transformation between color spaces. Let the matrix derivative operator be

$$J_f(x) = \begin{bmatrix} \frac{\partial y_1}{\partial x_1} & \frac{\partial y_1}{\partial x_2} & \cdots & \frac{\partial y_1}{\partial x_n} \\ \frac{\partial y_2}{\partial x_1} & \ddots & & \\ \vdots & & \ddots & \\ \frac{\partial y_m}{\partial x_1} & & & \frac{\partial y_m}{\partial x_n} \end{bmatrix} \tag{4.13}$$

where each element of $J_f(x)$ is evaluated at the mean, $(m_{x_1}, m_{x_2}, \cdots, m_{x_n})$. This operator is called the Jacobian matrix [Magnus1999]. The transformation of the covariance matrix due to Equation (4.13) is given by

$$\Sigma_y \cong J_{f(x)} \Sigma_x J_{f(x)}^T \tag{4.14}$$

Equation (4.14) is an extension of Equation (4.11) and can also be rewritten as

$$s_{yii} = \sum_{j=1}^{n} \left(\frac{\partial f_i}{\partial x_i}\right)^2 s_{xjj} + 2\sum_{j=1}^{n-1} \sum_{k=j+1}^{n} \frac{\partial f_i}{\partial x_j} \frac{\partial f_i}{\partial x_k} s_{x_{jk}} \tag{4.15}$$

Equation (4.15) is the form most often used, where s_{xij} are the elements from the variance-covariance matrix Σ_x. In practice, the calculation of Jacobian matrix is better obtained through a numerical approach:

$$J_f^{(ij)} = \frac{\partial y_i}{\partial x_j} = \frac{y_i^{(-e)} - 2y_i^{(0)} + y_i^{(+e)}}{e} \tag{4.16}$$

where

$$\begin{aligned} y_i^{(+e)} &= y_i(x_1, \cdots, x_{j-1}, x_j + e, x_{j+1}, \cdots, x_n) \\ y_i^{(-e)} &= y_i(x_1, \cdots, x_{j-1}, x_j - e, x_{j+1}, \cdots, x_n) \\ y_i^{(0)} &= y_i(x_1, \cdots, x_{j-1}, x_j, x_{j+1}, \cdots, x_n) \end{aligned} \tag{4.17}$$

and where e is a small number, such as 10^{-4}. For a very complex transformation, *i.e.* CIEDE2000, the numerical method is more effective. The numerical method will be demonstrated in this chapter.

4.2.3 Cascading of Transformations

Many color-signal transformations can be seen as a cascading of the above types of transformations. In general, if a signal $\mathbf{y}$ is transformed sequentially from input signal $\mathbf{x}$:

$$\mathbf{y} = F_2\left(F_1(\mathbf{x})\right) \tag{4.18}$$

where F_1 and F_2 are transformation functions. Assuming the functions are all first differentiable, the uncertainty of $\mathbf{y}$ can be obtained through the cascading of Jacobian matrices:

$$\Sigma_{\mathbf{y}} = J_{F_2}\left(F_1(x)\right) J_{F_1}(x) \Sigma_x J_{F_1}^T(x) J_{F_2}^T\left(F_1(x)\right) \tag{4.19}$$

Such kind of transformation cascading is quite common in camera signal processing and can be extended to any number of transformations.

4.3 Noise Amplification Analysis for Digital Camera

The noise propagation from camera output signals to tristimulus values is demonstrated here, which is followed by the transformation to CIELAB coordinates. These are important and common transformations, and can also be prototypes for image processing steps found in many electronic imaging systems.

The camera signal can be represented as

$$t_c = G^T r \tag{4.20}$$

where r is the sample reflectance, G contains camera spectral sensitivities and taking illuminant, and t_c is the camera output signal. If there is any error in the measurement of reflectance spectra, which can be written as Σ_r, the resulting uncertainty in camera signal will be

$$\Sigma_{t_c} = G^T \Sigma_r G \tag{4.21}$$

To transform the camera signals to approximations of CIE tristimulus values (X, Y, Z), the following matrix operation is often used:

$$\mathbf{t} = \mathbf{M}\mathbf{s} \tag{4.22}$$

where $\mathbf{s} = [R \quad G \quad B]^T$, $\mathbf{t} = [X \quad Y \quad Z]^T$, $\mathbf{M}$ is a 3×3 conversion matrix. In most practical cases, the imager spectral sensitivities cannot be expressed as a linear combination of CIE color matching functions. Thus Equation (4.22) allows only an approximation to the tristimulus values. The matrix $\mathbf{M}$ will be a function of the spectral power distribution of illuminant and imager spectral sensitivities, and is chosen to minimize a particular weighting of colorimetric difference between the estimated and measured tristimulus values.

As discussed in the previous section, imaging detectors are subject to stochastic error due to, for example, photon arrival statistics (shot noise), thermally generated electrons, readout electrons and signal amplification. The detected signals, **s**, will therefore include variation from many sources, and can be modeled as a set of random variables. The transformed signal, **t**, contains a corresponding error that will be a function of the variation in **s**, and the matrix transformation, **M**. Results for the error-propagation analysis provide a way of predicting the statistics of the noise due to the image detection step in terms of the output transformed signal.

The second-order statistics of a set of detected signals subject to a stochastic error can be described by the covariance matrix,

$$\Sigma_s = \begin{bmatrix} s_{RR} & s_{RG} & s_{RB} \\ s_{RG} & s_{GG} & s_{GB} \\ s_{RB} & s_{GB} & s_{BB} \end{bmatrix} \tag{4.23}$$

where the diagonal elements are the variance values of the *R*, *G* and *B* signals. In general the elements of Σ_s will be functions of the detected signal. The resulting covariance matrix for the transformed signals is

$$\Sigma_t = \mathbf{M}\Sigma_s\mathbf{M}^T \tag{4.24}$$

Similarly, the propagation of the signal covariance through nonlinear transformations can be approximated by applying a derivative matrix. If the CIELAB coordinates are expressed as a vector, $c = [L^* \; a^* \; b^*]^T$, and the Jacobian Matrix of the multivariate transformation is written as

$$\mathbf{J} = \begin{bmatrix} 0 & \partial L^*/\partial Y & 0 \\ \partial a^*/\partial X & \partial a^*/\partial Y & 0 \\ 0 & \partial b^*/\partial Y & \partial b^*/\partial Z \end{bmatrix} \tag{4.25}$$

then

$$\Sigma_{L^*a^*b^*} = \mathbf{J}\Sigma_t\mathbf{J}^T \tag{4.26}$$

The Jacobian matrix has been further derived as [Fairchild1991, Sharma1997b, Burns and Berns 1997a]

$$J_{Lab} = J_0 D(t) \tag{4.27}$$

where

$$J_0 = \begin{bmatrix} 0 & 116 & 0 \\ 500 & -500 & 0 \\ 0 & 200 & -200 \end{bmatrix} \tag{4.28}$$

and

$$D(t) = \begin{bmatrix} v(x, x_n) & & \\ & v(y, y_n) & \\ & & v(z, z_n) \end{bmatrix} \tag{4.29}$$

where

$$v(a,b)=\begin{cases}\frac{1}{3}a^{-\frac{2}{3}}b^{-\frac{1}{3}} & \frac{a}{b}>0.008856\\ 7.787b^{-1} & \frac{a}{b}\le 0.008856\end{cases}$$

In general, the RMS (root-mean-square) noise in CIELAB space is defined as a function of diagonal elements of the variance-covariance matrix.

$$s_{L^*a^*b^*}=\sqrt{s^2_{L^*}+s^2_{a^*}+s^2_{b^*}} \tag{4.30}$$

Burns and Berns derived another RMS noise metric [Burns1997a]

$$\begin{aligned}E[\Delta E^*_{ab}] &= E\left[\sqrt{\Delta L^{*2}+\Delta a^{*2}+\Delta b^{*2}}\right]\\ &\approx \sqrt{s^2_{L^*}+s^2_{a^*}+s^2_{b^*}}-\frac{s^2_p}{8(s^2_{L^*}+s^2_{a^*}+s^2_{b^*})^{3/2}}\end{aligned} \tag{4.31}$$

where

$$s^2_p=2(s^4_{L^*}+s^4_{a^*}+s^4_{b^*})+4(s^2_{L^*a^*}+s^2_{L^*b^*}+s^2_{a^*b^*})$$

Equation (4.31) may be a more appropriate formula to calculate RMS noise, since the influence of off-diagonal elements in the variance-covariance matrix are considered.

4.4 Experiments and Results

4.4.1 Measurement of Noise Characteristics

The noise properties of the Quantix camera have been measured in an experiment. First the dark noise can be measured by taking dark images while the camera shutter is closed. The exposure time varied from 10 seconds to 10 minutes. While the camera temperature is kept cool (~-25°F, or -37°C), the dark current was very stable, as shown in Figure 4.3.

The parameters of the noise model can be estimated as follows. Using the camera to take multiple images of a uniform object which is illuminated uniformly, the variance of the images can be obtained. The average digital counts may be varied by using several neutral density filters. In a well-controlled condition, the variances of digital counts against average digital counts are shown in Figure 4.4. From the figure, it shows that the variance increases with average digital count monotonically. The noise level also depends on the gain value. If gain is

larger, noise is larger, which is consistent with the noise propagation analysis. The variance of the signal-independent noise is negligibly small, which means the noise of the Quantix camera is dominated by signal-dependent noise. The usual assumption of white noise in an imaging process conflicts with this result. Similar result on shot noise can be found at [Hosoi1999].

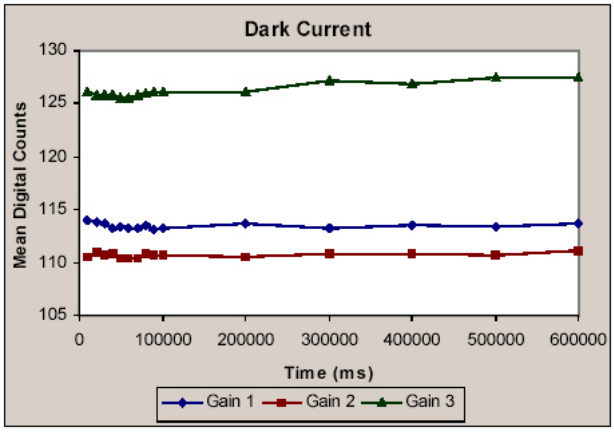

Figure 4.3: Measurement of Dark noise in Quantix camera.

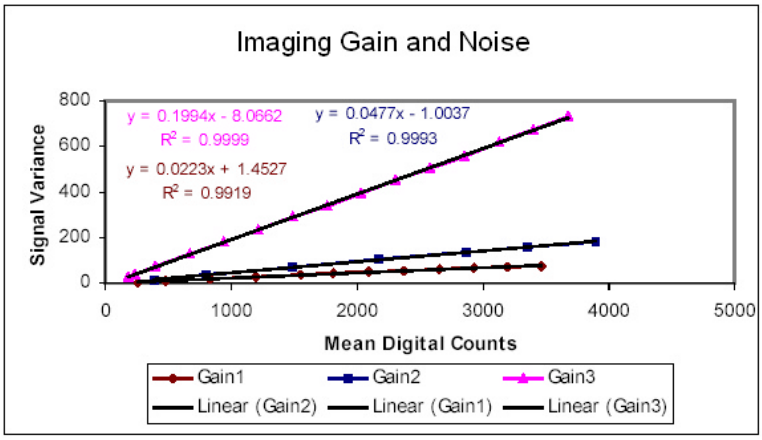

Figure 4.4: Verification of noise model.

In a second experiment, A Kodak GrayScale was captured with four channels of Quantix camera. The average digital counts were those of all B/W patches, and standard deviation of digital count was calculated for each patch in each selected area. Their relationship is plotted in Figure 4.5. A direct conclusion from the figure is that if the signal level is high, the noise level is

also high, but the noise level in this figure is dependent on both the CCD imaging noise and the non-uniformity of test targets.

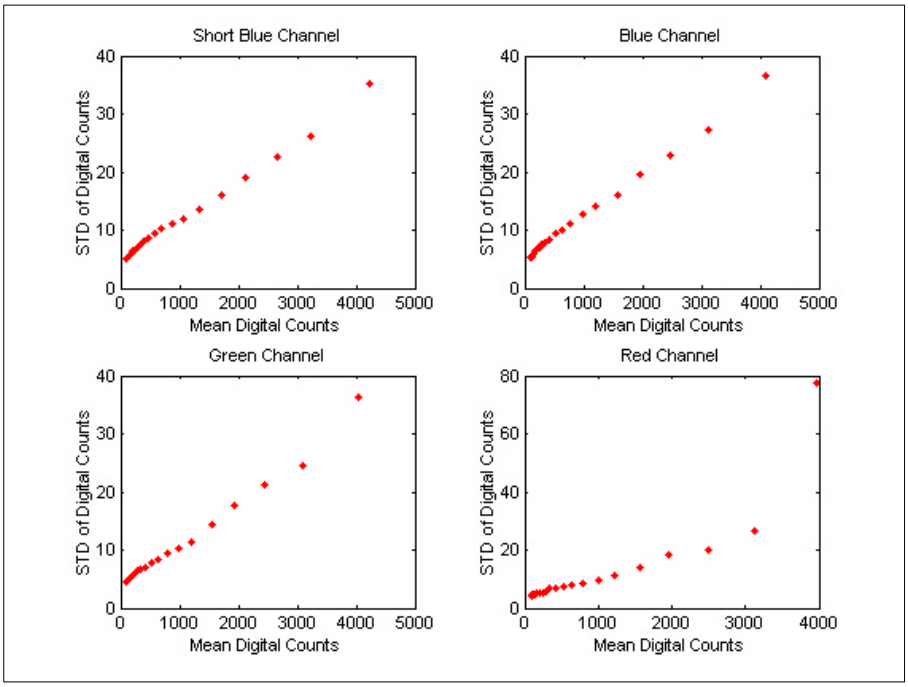

Figure 4.5: Standard deviation (STD) of digital counts versus average digital counts.

4.4.2 Calculation of Jacobian Matrix

In this section, the calculation of Jacobian matrix from CIE XYZ to CIELAB is demonstrated with both an analytical approach and numerical approach. In this example, the tristimulus values of the patch #13 (blue) of the Macbeth ColorChecker was calculated under CIE illuminant A as well as the tristimulus values of the corresponding white point. The Jacobian matrix was calculated analytically with Equations (4.27)-(4.29), that is M_1 in Table 4-1. In the numerical approach, the CIELAB values of $T_0 = [X, Y, Z]$ and $T_1 = [X + e_0, Y, Z]$, $T_2 = [X, Y + e_0, Z]$, and $T_3 = [X, Y, Z + e_0]$ were calculated, as well as $T_{-1} = [X - e_0, Y, Z]$, $T_{-2} = [X, Y - e_0, Z]$, and $T_{-3} = [X, Y, Z - e_0]$, where e_0 is a very small number, such as 0.001. The Jacobian matrix can be calculated with Equations (4.16)-(4.17), denoted as M_2 in Table 4-1. The difference of M_1 and M_2 is negligible. The calculation of the Jacobian matrix for the transformation from XYZ to LAB using the numerical approach showed little advantage than an analytical approach, but for

transformations such as the color difference formula CIEDE2000 or color appearance model CIECAM97s, the analytical approach is almost impossible, while the numerical approach can be easily implemented through calculation of function values of input values with small deviation.

Table 4–1: Calculation of the Jacobian matrix from CIE XYZ to CIELAB.

Tristimulus Values XYZ	5.90	5.17	10.01
White Point $X_nY_nZ_n$	108.53	100.00	37.70
Analytical Approach			
Jacobian Matrix M_1	0	2.786	0
From Analytical	10.698	-12.009	0
Approach	0	4.804	-4.282
Numerical Approach			
$L_0a_0b_0$	27.214	3.169	-54.020
$L_{-1}a_{-1}b_{-1}$	27.214	3.062	-54.020
$L_{-2}a_{-2}b_{-2}$	27.186	3.289	-54.068
$L_{-3}a_{-3}b_{-3}$	27.214	3.169	-53.977
$L_{+1}a_{+1+}b_{+1}$	27.214	3.276	-54.020
$L_{+2}a_{+2}b_{+2}$	27.242	3.049	-53.972
$L_{+3}a_{+3}b_{+3}$	27.214	3.169	-54.063
Jacobian Matrix M_2	0	2.786	0
From Numerical	10.698	-12.009	0
Approach	0	4.804	-4.282

4.4.3 Calculation of Signal-to-Noise Ratio

The signal-to-noise ratio (SNR) is defined as

$$\mathrm{SNR} = 10\log_{10}\left(\frac{s^2}{n^2}\right) \tag{4.32}$$

where s^2 is the expected signal energy, and n^2 is the expected noise energy.

Let the noise model in Equation (4.6) be divided by the square of maximum signal $m_{\max}$,

$$\frac{s_o^2}{m_{\max}^2} = \frac{s_d^2}{m_{\max}^2} + \frac{h^2}{m_{\max}} \cdot \frac{m_i}{m_{\max}}, \text{ or } s_o'^2 = s_d'^2 + k \cdot m_i' \tag{4.33}$$

where $s_o' = s_o / m_{\max}$, $s_d' = s_d / m_{\max}$ are the normalized shot and dark noise RMS, $m_i' = m_i / m_{\max}$ is the normalized input signal ($0 \le m_i' \le 1$) and $k = h^2 / m_{\max}$ is the normalized quantum efficiency.

For instance, let the shot-noise level correspond to a maximum signal of 60000 e^-/pixel, the RMS dark noise is equivalent to 50 e^-, and the quantum efficiency (h) of CCD is 0.98 [pg. 72 in Burns1997b]. The total noise is then represented as

$$s^2 = s_d^2 + h^2 \cdot m = 50^2 + 0.98^2 m \tag{4.34}$$

The normalized noise model can be represented as

$$s_o'^2 = \frac{50^2}{60000^2} + \frac{0.98^2}{60000} m_i' \approx 6.94\times10^{-7} + 1.60\times10^{-5} m_i' \tag{4.35}$$

In Equations (4.33) and (4.35) only measured macro statistical information is enough to estimate the noise parameters. According to Equation (4.32), the SNR is calculated as

$$\text{SNR} = 10\log_{10}\frac{m_i'^2}{s_o'^2} = 10\log_{10}\frac{m_i'^2}{6.94\times10^{-7} + 1.60\times10^{-5} m_i'} \tag{4.36}$$

The signal-to-noise ratio changes with the level of input signal, as shown in Figure 4.6. It shows that the SNR of CCD camera increases as the input signal increases. But it should be kept in mind that if the signal is too strong, CCD will saturate, and the SNR will not increase any more.

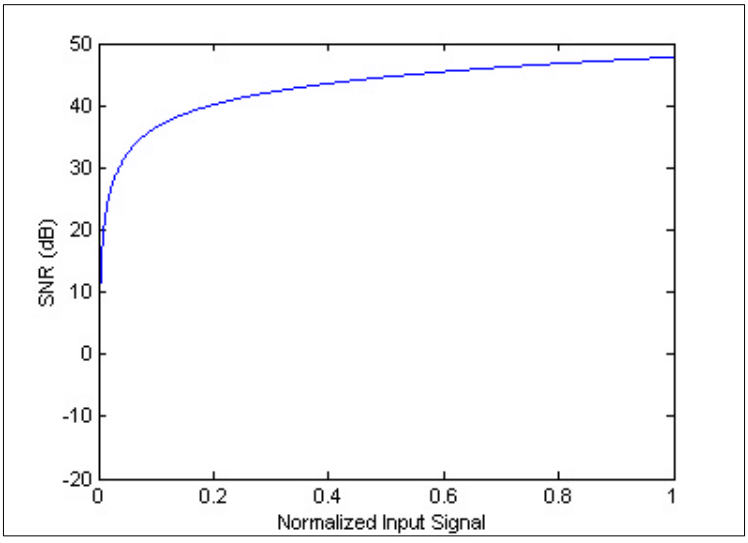

Figure 4.6: SNR of CCD camera as a function of input signal

4.5 Conclusions

There are many noise sources in digital electronic imaging, but the consideration of noise types depend on the specific application. In this application, CCD imaging noise is modeled as sum of signal-independent noise and signal-dependent noise, represented by Gaussian-distributed dark noise and Poison-distributed shot noise respectively. Experimental noise measurement and characterization verifies that this model fulfills the requirement. The noise in the input end will be propagated and amplified while signals are transformed step-by-step. Noise is described by its mean and variance, which can be calculated through first and second order moments of random variables. Noise propagation rules are obtained with linear transformation and nonlinear transformation. The RMS noise in the target space can be formulated as a function of the variance-covariance matrix in the target color space. Some signal transformation and noise propagation instances usually found in color imaging are described briefly.

5 EVALUATION OF SPECTRAL SENSITIVITIES

5.1 Introduction

Human visual color perception can be described by tristimulus theory that involves the linear combination of three different photoreceptor types with known spectral sensitivities in the visible range. The CIE has characterized the standard human visual color perception with color-matching functions for a standard observer and defined standard color spaces, including perceptually non-uniform CIE XYZ and uniform CIELAB spaces. These standards are fundamental for colorimetry and for the transformation and sharing of color information. Color input devices such as cameras and scanners that seek for colorimetric color reproduction (including color appearance match) of object colors must take into account the characteristics of the human visual system in their design and in the understanding of the output data from the physical sensors.

Many imaging devices are therefore set up as three channel systems with their channel spectral sensitivities (SS) initially designed to mimic human visual responses. The spectral sensitivities for color imaging devices (digital cameras, color scanners etc.) should satisfy the Luther condition [Luther1927], that is, device spectral sensitivities need not be exact duplicates of the color-matching functions but need only be their nonsingular linear transformation. Although these input devices have reached reasonable performance today, their color reproduction is still perceptibly different from the original scene. Major reasons for this are the difficulties of selection and fabrication of transmittance filter sets that are suitable for color imaging devices. Basically two primary factors - the non-Luther condition due to the practical limitations in manufacturing color filters and the intrinsical imaging noise in the imaging process, limit their color accuracy. The optimal design of the spectral sensitivity functions should

account for both aspects. Therefore, a criterion for evaluating and optimally designing the spectral sensitivities by considering all these factors is desirable.

The concept of the so-called “quality factor” was first introduced by Neugebauer [Neugebauer1956]. Quite a few quality metrics have been proposed up to now. All these metrics for evaluating and designing spectral sensitivities striving for colorimetric reproduction fall into two primary categories. The first type describes the geometrical difference between the subspaces of color matching functions and spectral sensitivity functions. These quality factors are often sample-independent and do not consider the imaging noise, but only consider the difference through linear transformation. Typical metrics are Neugebauer’s q-factor for the evaluation of a single imaging channel, Vora-Trussell’s extension, m-factor [Vora1993a] for the evaluation of multispectral system with an arbitrary number of channels and the CQF (“Color Quality Factor”) [described in Sharma1997b] already used in the industry for the evaluation of entire imaging system.

The second type describes the minimal color error for a set of user-defined samples of reflectance spectra in CIE color spaces. The linear transformation from RGB signal to XYZ values is determined by minimizing the color error and a data-dependent metric can be defined using this procedure. Imaging noise may or may not be considered during the minimization. In this category, there are Shimano’s Q_{st} and Q_{sf} metrics [Shimano2000a] minimizing the average color error in CIE XYZ space without noise consideration, Tajima’s several indices [Tajima1996] taking account of object color spectral characteristics of principle components, Hung’s CRI (Color Rendering Index) [Hung2000], and Sharma-Trussell’s Figure of Merit (FOM) [Sharma1997b], which was probably the most extensive and complicated quality factor minimizing the color error in a perceptually uniform color space while taking account of the white noise in the recording process. Quite a few simpler quality factors can be attributed to the special forms of FOM.

FOM has been extended to Unified Measure of Goodness (UMG) so that it includes both the signal-independent and signal-dependent imaging noise (dark noise and shot noise) as well as

multi-illuminant color correction, to be described in the following section. Tajima's quality indices ("*T*-factor") do not rely on satisfying the Luther condition but instead determine how well a set of filters can be used to reconstruct object color spectral characteristics [Tajima1996]. His metric is based on the assumption that each object spectral reflectance characteristic can be restored from three sensor signals provided that almost all object spectral reflectance can be well represented by three or four principal components.

Notice that the data-dependent metrics may perform well for specific data sets and may not perform well for some other data sets. Selection of the standard set in the computation should be cautious and consistent. The twenty-four Macbeth ColorChecker patches were used as standard samples in the computation because of an enough number of colors involved and also the widespread use of this target in similar research. Alternatively, the Vrhel-Trussell dataset [Vrhel1994b].covers many more samples and will also be used as a standard object color set

Both *q*-factor and *m*-factor are based on the description of the geometrical difference between the subspaces of color matching functions (CMF) and spectral sensitivity functions (SS). This description is elegant though incomplete for the real world by neglecting various noise issues. In this chapter *q*-factor and *m*-factor are used as example quality metrics for evaluating sensitivity functions. The approach described is methodologically applicable to the use of any other quality factors and for consideration of other practical issues, such as recording noise and color correction across multiple illuminants.

Q-factor and *m*-factor are relatively simple and are based on the key point of evaluating deviation of a single or a set of SS from a set of CMF. While Vora and Trussell presented a systematic and complete description of their *m*-factor, their somewhat complicated mathematics is simplified through the use of a least-squares approach to their derivation. As peak position and width of spectral sensitivities are two primary parameters for describing spectral sensitivity function shapes, these are used as optimization parameters. A hypothetical SS model with parameters of peak position and width has been developed. Optimal values are easily chosen

from finite combinations by changing peak position and width discretely. Further optimization of spectral sensitivity function shapes can be based on the results obtained herein.

The higher the quality factor for an imaging device, the higher the quality of the color signals that are expected from that device. Higher quality color signals should result in more accurate color reproduction, assuming all other properties are equal. One approach to improve colorimetric accuracy, other than satisfying the Luther condition with three channels, is to use an increased number of color channels. As the number of color filters is increased, additional information about the object color is obtained, but cost and fabrication difficulty are also increased. Four-channel systems may prove a good tradeoff between cost, fabrication difficulty, noise reduction and color fidelity. This chapter demonstrates a method to compute the optimal sensitivity of the additional channel by maximizing the total m-factor of the system.

In this chapter, the hypothetical spectral sensitivity model is described first. The model consists of a parameterized cubic spline function with a single peak. A discussion on the physical meaning of q-factor and m-factor follows along with an evaluation of spectral sensitivities using these metrics. Then data-dependent metrics including Q_{st}, Q_{sf} and FOM, are briefly introduced. Finally, the new data-dependent metric, UMG, which incorporates noise model described in Chapter 4, will be derived and discussed. Throughout, finite dimensional representations of all continuous spectral functions are used. All spectral distributions are assumedly sampled at 10nm intervals from 400nm to 700nm and represented as 31-element column vectors. For certain color reproduction situations such as imaging onto photographic paper, this range might not be enough, but the method can be easily extended to take advantage of larger ranges.

5.2 The Hypothetical Spectral Sensitivity Function Model

The spectral sensitivity of a color channel is defined as the product of a detector spectral sensitivity and the transmittance of a filter. In general, a channel spectral sensitivity function is assumed to be a smooth single-peaked curve in the visible range with values strictly limited to be between 0 and 1. A value of 0 means that no radiation at that wavelength is detected, and a value

of 1 means that 100% of all such radiation will be detected. The peak position and width are two critical parameters and vary considerably for real spectral sensitivities used in color reproduction, many of which can be approximated by smooth cubic spline functions with peak positioned at $l = l_0$ and width parameter *w*, written as:

$$C(l) = \begin{cases} \dfrac{w^3 + 3w^2(w - |l - l_0|) + 3w(w - |l - l_0|)^2 - 3(w - |l - l_0|)^3}{6w^3} & |l - l_0| \le w \\ \dfrac{(2w - |l - l_0|)^3}{6w^3} & w \le |l - l_0| \le 2w \\ 0 & |l - l_0| \ge 2w \end{cases} \quad (5.1)$$

where *w* is the half-width of the cubic spline function at one-fourth height (the corresponding full width at half maximum is about 1.414*w*). Linear combinations of cubic spline functions were used to simulate color film spectral sensitivity functions by Ohta [Ohta1983] and estimate spectral reflectance by Park and Huck [Park1977]. Figure 5.1 shows a spectral sensitivity function of a green channel whose peak wavelength locates at 550nm and width 2*w* is 80nm.

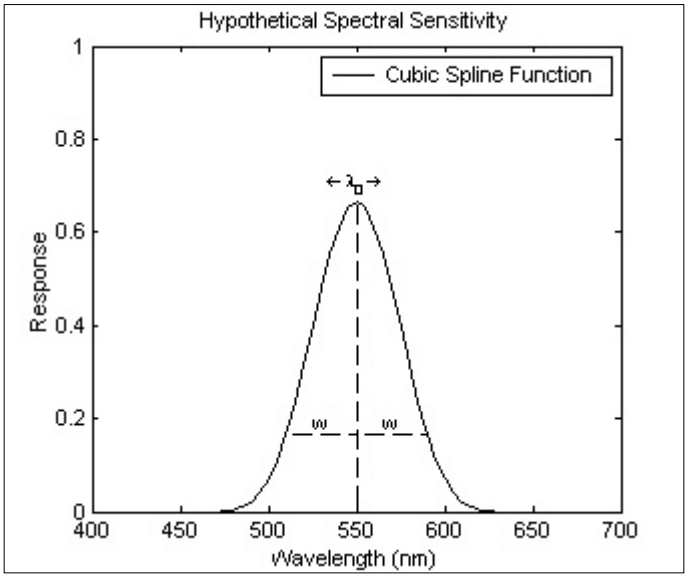

Figure 5.1**:** Typical hypothetical spectral sensitivity function modeled as smooth single-peaked symmetric function.

5.3 The *q*-factor for Individual Spectral Sensitivity

As discussed in Chapter1, it is common that the camera spectral sensitivity functions are not the linear combinations of CIE color matching functions. Therefore it is valuable to have a metric that evaluates how far an SS deviates from a linear combination of color matching functions.

Let $\bar{x}(l)$, $\bar{y}(l)$, $\bar{z}(l)$ be the CIE color matching functions and A=[$\bar{x}(l)$, $\bar{y}(l)$, $\bar{z}(l)$] is defined as human visual subspace (HVSS). In an attempt to measure the goodness of SS, *Neu*gebauer's *q*-factor for a spectral sensitivity function *m* can be defined as follows:

Assume *m* can be mostly approximated by the linear combination of CMF (*Af*), where *f* is a 3×1 vector, that is, $\mathbf{min}\Delta = \|Af - m\|_F^2$, where the Frobenius norm for matrix $X \in R^{m\times n}$ is defined as the square root of summation of all element squares in *X*:

$$\|X\|_F = \sqrt{\sum_{i=1}^{m}\sum_{j=1}^{n}|x_{ij}|^2}$$

This is a least-square problem, and $f = (A^TA)^{-1}A^Tm$ can be obtained with pseudo inverse operation. Thus the minimal residue:

$$\begin{aligned}\Delta_{\min} &= \|Af - m\|_F^2 = (Af - m)^T(Af - m)\\ &= (f^TA^T - m^T)(Af - m) = f^TA^TAf - m^TAf - f^TA^Tm + m^Tm\\ &= m^TA(A^TA)^{-1}A^TA(A^TA)^{-1}A^Tm - m^TA(A^TA)^{-1}A^Tm - m^TA(A^TA)^{-1}A^Tm + m^Tm\\ &= m^Tm - m^TA(A^TA)^{-1}A^Tm\end{aligned} \tag{5.2}$$

and

$$\begin{aligned}\frac{\Delta_{\min}}{\|m\|^2} &= \frac{m^Tm - m^TA(A^TA)^{-1}A^Tm}{m^Tm} = 1 - \frac{m^TA(A^TA)^{-1}A^Tm}{m^Tm}\\ &= 1 - q(m)\end{aligned} \tag{5.3}$$

where

$$q(m) = \frac{\|A\cdot(A^TA)^{-1}A^T\cdot m\|^2}{\|m\|^2} = \frac{m^TA(A^TA)^{-1}A^Tm}{m^Tm} \tag{5.4}$$

which is equivalent to Neugebauer's definition of *q*-factor for spectral sensitivity *m*.

As an extreme case, for example, spectral sensitivity $m(i)$ is chosen as a *d*-function peaked at the i^{th} sampling wavelength between 400nm and 700nm, $m(i) = (0,\ 0,\ \ldots,\ 1,\ \ldots,\ 0)^T$,

where i is the position of 1 in the N-element vector (i.e. N=31 for 10nm interval). The corresponding q-factor can be obtained as $diag(A(A^TA)^{-1}A^T, i)$, which is the i^{th} diagonal element of the matrix $A(A^TA)^{-1}A^T$. Figure 5.2 shows the q-factors of a series of spectral sensitivities $m(i)$ as d-functions where i changes from 1 to N. The q-factor curve presents three peaks at about 450nm, 540nm and 600nm with corresponding q-factors 0.2263, 0.1756 and 0.1858. Of course, such q-factors are relatively low, as they should be for d-function spectral sensitivities. Note that the q-factor of full-pass spectral sensitivity function $m(i) = (1,\ 1,\ \ldots,\ 1)^T$ is about 0.7224.

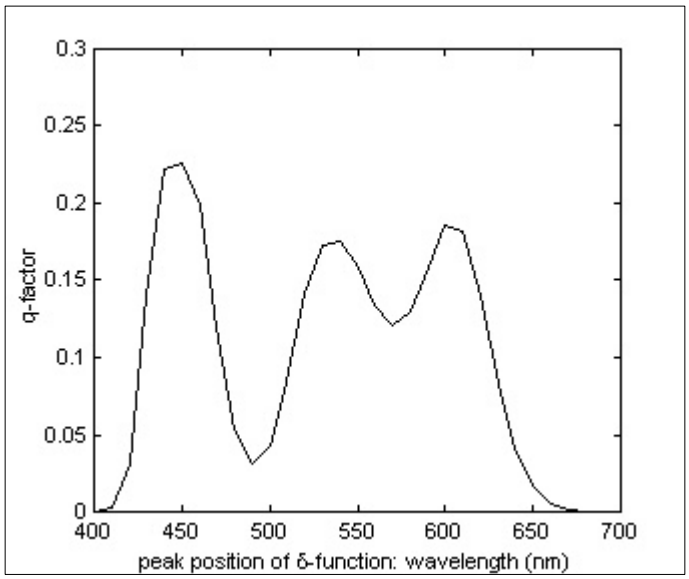

Figure 5.2: q-Factors of narrow band spectral sensitivity functions modeled as δ-functions when CIE 2° color matching functions are used.

q-*F*actor values are limited in the range $0 \le q(m) \le 1$, with unity representing a perfect linear combination of CMF. If the value of $q(m)$ is much less than unity, the filter measurement does not give much colorimetric information about the measured signal, and hence the SS is not appropriate for color capture. The q-factor is a reasonable quality measure for determining whether spectral sensitivities are contained in the range of *HVSS*, because $\|m\|^2(1-q(m))$ indicates the square of the Euclidean distance of m from *HVSS* as derived above.

Now the q-factors of the hypothetical spectral sensitivity functions are evaluated. The peak position l_0 of the cubic spline function changed from 400nm to 700nm by 10nm (31

different positions), and the width parameter *w* changed from 10nm to 90nm by 20nm (5 different widths). For each combination, the corresponding *q*-factor can be calculated through Equation (5.2).

Figure 5.3 shows how the *q*-factors change as with the peak position l_0 and the width parameter *w* of the hypothetical spectral sensitivity. In the figure, when *w* is not so large, for example, *w*≤70nm, each curve gives a series of varying *q*-factors and there are 3 obvious peaks of *q*-factor curve. The peak positions of SS with maximal *q*-factors are almost consistently located at 450nm, 540nm and 600nm. These are the same positions favored by the *d*-function sensitivities.

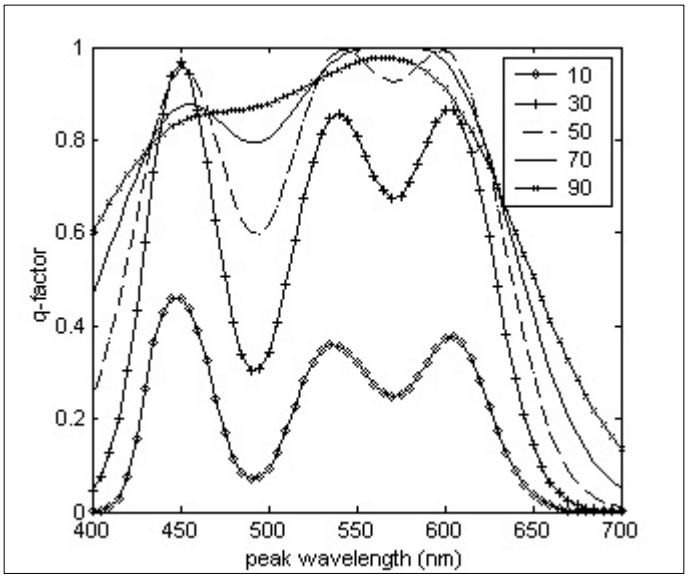

Figure 5.3: *q*-Factors of hypothetical SS with different peak l_0 and width *w* (10, 30, 50, 70, 90nm): Optimal peak wavelength tends to locate at around 450, 535 and 600nm.

For these wavelength positions, there exist optimal widths that maximize the *q*-factor. The optimal width can be found to be about 40nm for sensitivities with peak wavelength of 450nm and about 50~60nm for those with peak wavelength of 540nm and 600nm. Figure 5.4 shows how the maximum *q*-factor changes with width. When the width becomes large enough, say 100nm, the three peaks of *q*-factor curve disappear and the shape becomes flat. On the contrary, the *q*-factor in the middle part of the curve is not very small but changes slowly along

peak wavelength, so it is unfavorable to choose very wide spectral sensitivity for color reproduction. In fact, when the width is small enough, the sensitivity function can be modeled as a *d*-function, while it gets wider and wider, the sensitivity is close to a full-pass function. So the curve is very similar to that in Figure 5.2 when width is small and the curve becomes full-pass when it is large. In an extreme condition when $w \to \infty$, the SS is a full-pass function, and, as mentioned above, the *q*-factor becomes approximately 0.7.

5.4 The *m*-Factor for a Set of Spectral Sensitivities

A major disadvantage of the *q*-factor is that it was designed to evaluate only a single SS. A measure that extends the idea of the *q*-factor to evaluate a set of spectral sensitivities is useful. For three-channel imaging devices, averaging *q*-factors of the individual channels may be of value in some cases, but only when certain assumptions are made. For a general three-channel evaluation with no *a priori* information about the relationship between the channel sensitivities, *q*-factor cannot be relied on to evaluate a system of spectral sensitivities. A trivial example to demonstrate this is a three-channel system with all three SS being identical to the luminance function $\overline{y}(l)$. Although all three channels will have a perfect *q*-factor of 1, and the average of the three would still be 1, the system will be completely useless for color reproduction since the resultant signals will be monochrome.

A further argument against use of the *q*-factor for evaluating filter sets is that for channels numbers greater than three, averaging *q*-factors becomes meaningless. Some studies suggest that more than three spectral sensitivities may be useful to improve the quality of the color reproduction [Ohta1991, Vrhel1994a]. First, in many cases, three parameters are not enough to define sufficiently an *N*-dimensional visual stimulus for color correction. Second, the constraint of feasibility on the spectral sensitivities might imply that no set of three feasible spectral sensitivities could fully span the HVSS, although a set of four feasible spectral sensitivities could be constructed to do well. When more than three parameters (four spectral sensitivities, for example) are necessary, the *q*-factor is not an effective measure of the goodness. For example,

suppose that $\{s_1, s_2, s_3, s_4\}$ is a set of spectral sensitivities. It is possible that the *HVSS* is contained in the span of the set of four spectral sensitivities, but $q(\mathbf{s}_i)<1$ for i=1, 2, 3, and 4. Such a system could provide perfect color capture, although the individual q-factors may not be high.

Let S denote the matrix of r spectral sensitivities, $S=[s_1\ s_2\ \ldots\ s_r]$ and $A=[a_1\ a_2\ \ldots\ a_s]$ denote the human visual space (color matching functions) to be approximated. An orthonormal basis for A is defined by $U=[u_1\ u_2\ \ldots\ u_a]$. Such a basis may be obtained by the Gram-Schmidt orthogonalization procedure. The number of orthonormal vectors, a, is the rank of A and a equals s if A is a linearly independent set (s=3 since It is easy to know that A is linearly independent). Similarly, an orthonormal basis for S is defined by $O=[o_1\ o_2\ \ldots\ o_b]$. Also notice that b is the rank of S and that b equals r if S is a linearly independent set. The orthonormal basis U and O need not represent realizable spectral sensitivities. It can be derived that $S(S^TS)^{-1}S^T = OO^T$ and $A(A^TA)^{-1}A^T = UU^T$ [SVD analysis in Chapter 2].

A purpose of this work is to approximate A by the linear combination of S, that is, to minimize $\Delta = \|A-SQ\|_F^2$, where Q is the linear combination coefficient matrix to be optimized. This is a least-squares problem as well. Similarly, $Q=(S^TS)^{-1}S^TA$ can be obtained through a pseudo inverse operation. And the corresponding minimal residue:

$$\begin{aligned}\Delta_{\min} &= \|A-SQ\|_F^2 = \text{Trace}\{(A-SQ)^T(A-SQ)\} = \text{Trace}\{(A^T-Q^TS^T)(A-SQ)\}\\ &= \text{Trace}\{A^TA-Q^TS^TA-A^TSQ+Q^TS^TSQ\}\\ &= \text{Trace}\{A^TA-A^TS(S^TS)^{-1}S^TA-A^TS(S^TS)^{-1}S^TA+A^TS(S^TS)^{-1}S^TS(S^TS)^{-1}S^TA\}\\ &= \text{Trace}\{A^TA-A^TS(S^TS)^{-1}S^TA\}\\ &= \text{Trace}\{A^TA\}-\text{Trace}\{A^TS(S^TS)^{-1}S^TA\}\end{aligned} \quad (5.5)$$

therefore,

$$\begin{aligned}\frac{\Delta_{\min}}{\|A\|_F^2} &= \frac{\text{Trace}\{A^TA\}-\text{Trace}\{A^TS(S^TS)^{-1}S^TA\}}{\text{Trace}\{A^TA\}} = 1-\frac{\text{Trace}\{A^TS(S^TS)^{-1}S^TA\}}{\text{Trace}\{A^TA\}}\\ &= 1-m_A(S)\end{aligned} \quad (5.6)$$

where

$$m_A(S) = \frac{\text{Trace}\{A^TS(S^TS)^{-1}S^TA\}}{\text{Trace}\{A^TA\}} \quad (5.7)$$

is a measure of goodness for a set of spectral sensitivities S to approximate color matching functions A, and Trace{X} is the sum of diagonal elements of X. When multi-illuminants are involved, S and A may be redefined as:

$$\begin{aligned} S &\Rightarrow \begin{bmatrix} L_1 S & L_2 S & \ldots & L_k S \end{bmatrix} \\ A &\Rightarrow \begin{bmatrix} L_1 A & L_2 A & \ldots & L_k A \end{bmatrix} \end{aligned} \tag{5.8}$$

where L_1, L_2, ..., L_k are the diagonal matrices of the spectral power distributions of the illuminants involved. Since quality factor $m_A(S)$ can be applied to multiple taking illuminants and viewing illuminants among L_1, L_2, ..., L_k, name it as M-factor for convenience. When only one illuminant is present and the orthonormal subspace U is used instead of A,

$$\begin{aligned} &\text{Trace}\left\{U^T U\right\} = \text{Trace}\{I_a\} = a, \\ &\text{Trace}\left\{U^T S (S^T S)^{-1} S^T U\right\} = \text{Trace}\left\{U^T O O^T U\right\} = \left\|O^T U\right\|_F^2 = \left\|U^T O\right\|_F^2 \\ &= \text{Trace}\left\{O^T U U^T O\right\} = \sum_{i=1}^{b} o_i{}^T U U^T o_i = \sum_{i=1}^{b} q(o_i) \end{aligned} \tag{5.9}$$

therefore,

$$m_U(S) = \frac{\text{Trace}\left\{O^T U U^T O\right\}}{\text{Trace}\{U U^T\}} = \frac{\text{Trace}\left\{O^T U U^T O\right\}}{a} = \frac{\sum_{i=1}^{b} q(o_i)}{a} \to m_U(O) \tag{5.10}$$

which is Vora and Trussell's m-factor for a set of SS. This can be rewritten as:

$$\begin{aligned} m_U(S) &= \frac{\text{Trace}\left\{O^T U U^T O\right\}}{a} = \frac{\text{Trace}\left\{S^T U U^T S \cdot (S^T S)^{-1}\right\}}{a} \\ &= \frac{\text{Trace}\left\{S^T A (A^T A)^{-1} A^T S \cdot (S^T S)^{-1}\right\}}{a} \end{aligned} \tag{5.11}$$

In Equation (5.11), $S^T U U^T S$ is the q-factor matrix. The diagonal elements are the q-factors of the original SS. The off-diagonal elements are the inter-product pseudo q-factors. $r = S^T S$ is the correlation between the original spectral sensitivities. The operation $r^{-1} = (S^T S)^{-1}$ is a de-correlation process; that is, it removes the correlation between the set of spectral sensitivies to obtain a "pure" uncorrelated (orthonormal) SS and facilitate the calculation of a goodness metric. Hence, the sum of q-factors $\sum_{i=1}^{r} q(m_i)$ cannot be used instead of $\sum_{i=1}^{a} q(o_i)$ as a measure because spectral sensitivities with a high value of correlation $C_{ij} = \left\|s_i{}^T s_j\right\| \Big/ \left(\left\|s_i\right\| \cdot \left\|s_j\right\|\right)$

between different channels (i and j) may have high individual q-factors but poor joint performance. Ensuring that the spectral sensitivities O are orthogonal removes the correlation effect C_{ij} and therefore minimizes the distance between subspaces of HVSS and spectral sensitivity functions.

5.4.1 Evaluating Spectral Sensitivities with m-Factor

Now the aforementioned hypothetical spectral sensitivities are evaluated with m-factor criterion. The three spectral sensitivities for color imaging devices are denoted as Red (R), Green (G) and Blue (B). For this evaluation the peak positions l_0 are now limited such that Red can vary between 580-680nm, Green can vary between 480-580nm and Blue can vary between380-480nm by 10nm steps. Considering all possible R, G, B mutual combinations, a potential total of 1331 (11^3) sets of spectral sensitivities exist. Width parameters w can also vary. The width w was allowed to change from 10nm to 100nm by 10nm steps, generating a potential total of 13310 (10×1331) combinations.

Each R, G, B peak combination is associated with 10 width settings. A brute force search ensured where every width setting for every R, G and B peak positions was evaluated. It was found that for almost every R, G, B peak combination, the maximal m-factor was almost always associated with width w=50nm. From Table 5-1 and Figure 5.4, it is shown that the global optimal peak position was found at 600nm for R, 540nm for G and 450nm for B with optimal width of 50nm. This result is consistent with the properties of q-factors of a series of spectral sensitivities. Three spectral sensitivities with high q-factors have high m-factor if they are as uncorrelated as possible. Some other combinations of spectral sensitivity functions such as {610nm, 530nm and 460nm} have comparatively high m-factors as well, but the peaks of those combinations are very close to the three principle peaks.

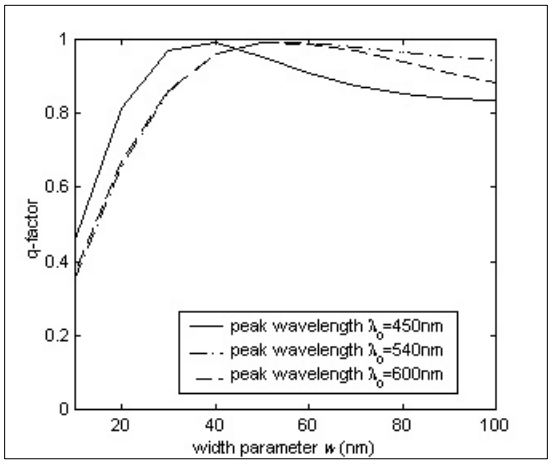

Figure 5.4: The effect of width on maximal *q*-factor: The optimal bandwidth of blue channel (40nm) is less than that of red and green channels (50~60nm).

Table 5–1: Peak positions of spectral sensitivities with maximal *m*-factor.

Width (nm)	Maximal *m*	Blue Peak (nm)	Green Peak (nm)	Red Peak (nm)
10	0.380	450	540	600
20	0.713	450	540	600
30	0.895	450	540	600
40	0.965	450	540	600
50	0.978	450	540	600
60	0.963	450	540	600
70	0.935	460	540	600
80	0.901	470	530	600
90	0.865	490	510	600
100	0.824	490	510	600

The width of the spectral sensitivities affects their *m*-factor. There exists an optimal width for the maximal *m*-factor when the three peak positions are fixed. Here again, in Figure 5.5, the optimal width *w* is around 50nm and the corresponding maximal *m*-factor=0.9779.

When the peak positions and widths of two spectral sensitivities are fixed, and only one SS changes its peak position, how does their *m*-factor change? Since *m*-factor is an extension of *q*-factor, the peak positions should be consistent with that obtained from the evaluation with *q*-factor. Figure 5.6 shows this point. The peak position l_0, of one SS was changed say, 380-480nm

by 10nm, while the other two peak positions were fixed where the maximal *m*-factor were obtained (540nm, 600nm). The calculations show that the behavior of *m*-factor carried by changing only one SS among the set is just like that of *q*-factor in that wavelength interval. Once again, the peak positions of SS having maximal *m*-factor are found at about l_0 = 450nm, 530~540nm, and 590~610nm for Blue, Green and Red channel sensitivities.

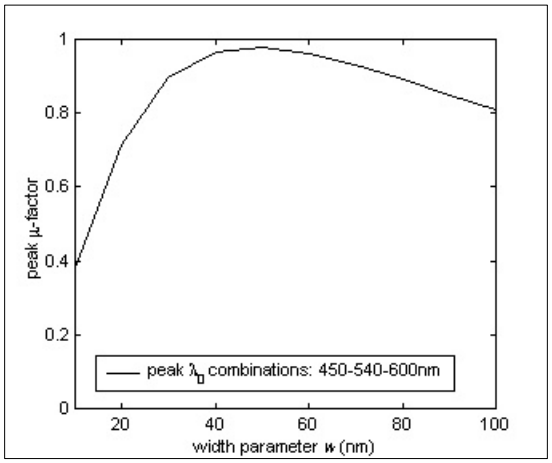

Figure 5.5: Effect of width of sensitivity function on peak *m*-factor; optimal *w* is about 50nm.

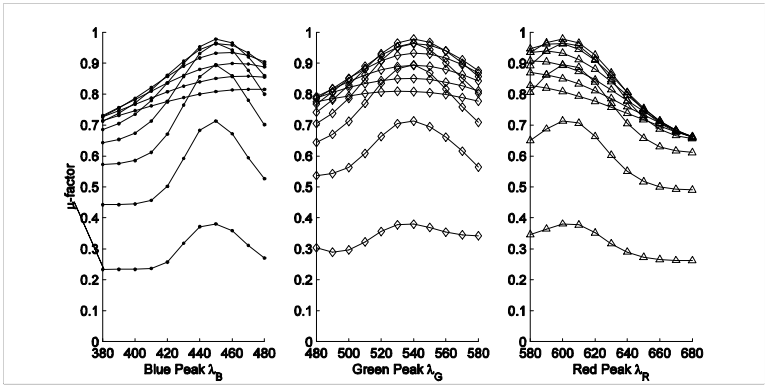

Figure 5.6: *m*-Factors of a set of SS: One SS changes its peak position, while the peak positions of the other two SS are fixed, that is, change one of the peak wavelengths (450nm, 540nm, 600nm) from -50nm to 50nm in intervals of 10nm and vary width parameter from 10nm to 100nm in intervals of 10nm for each peak wavelength variation.

5.4.2 More Discussion on *m*-Factor

Since spectral sensitivity functions and their number affect the accuracy of recording an original image, the use of more than three channels in the recording process is an alternative approach

when three channels cannot fully span the human visual space effectively (low *m*-factor) due to cost or manufacturing difficulty. Previous research has suggested that the use of four channels improves color difference performance [Vrhel1994a]; but unfortunately the obtained shapes of filter transmittances are uneven, which places difficulty in the fabrication process. The following simulated example demonstrates how a fourth channel could improve the total *m*-factor of color imaging devices while the obtained sensitivity functions are smooth. Assume the three spectral sensitivities have width parameter of 50nm and peak positions of 650nm, 550nm and 450nm individually. The system *m*-factor is 0.742. A fourth hypothetical spectral sensitivity varying in peak position from 400nm to 700nm by 10nm steps, and width from 10nm to 100nm by 10nm steps was evaluated, 310 combinations in total, as represented by each dot in Figure 5.7, where each curve donotes the sensitivities with the same width parameter. The maximal *m*-factor of the four-channel system is found to be 0.973, and the fourth sensitivity has width of 60nm and peak position of 590nm. The corresponding *q*-factors for the four spectral sensitivities are 0.953, 0.982, 0.297 and 0.997 respectively.

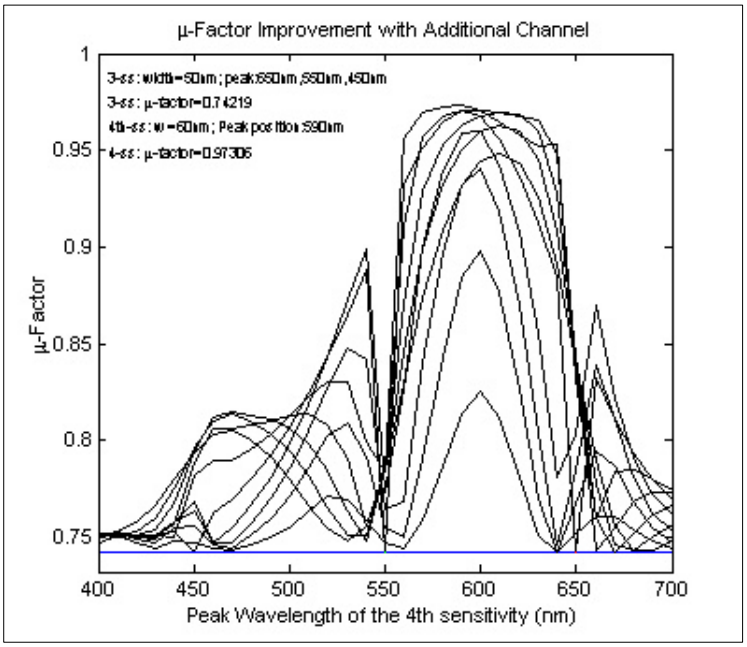

Figure 5.7: Choose the optimal fourth spectral sensitivity by maximizing the total *m*-factor of four channels from among all combinations when the spectral sensitivity functions of three channels are given.

Since *m*-factor is not based on a perceptually uniform color space, such as CIELAB, a high *m*-factor doesn't always lead to a small color difference. In Figure 5.8, all aforementioned 13,310 virtual spectral sensitivity sets were generated and simulated to capture Vrhel and Trussell's object color spectra ensemble [Vrhel1992] without noise distortion. A CIE ΔE^*_{94} color difference between the measured and estimated CIELAB coordinates were calculated for each object color patch, and an average color difference was obtained over the whole ensemble for each set of hypothetical sensitivity functions. It was found that a higher *m*-factor does not always lead to a smaller average color difference. But the average color difference in CIELAB over an ensemble of reflectance is usually highly correlated with the *m*-factor of the camera system when the *m*-factor is close to one. *m*-Factor is roughly linearly related to average ΔE^*_{94} if $m \geq 0.95$. However, color imaging devices with poor *m*-factor may still generate a satisfactory color reproduction [Tajima1996]. Another issue of *m*-factor is that it doesn't consider the recording noise, which always exists in real world devices and will contaminate the camera output signal creating a distribution of color differences not addressed by the quality factors such as *q*-, and *m*-factors.

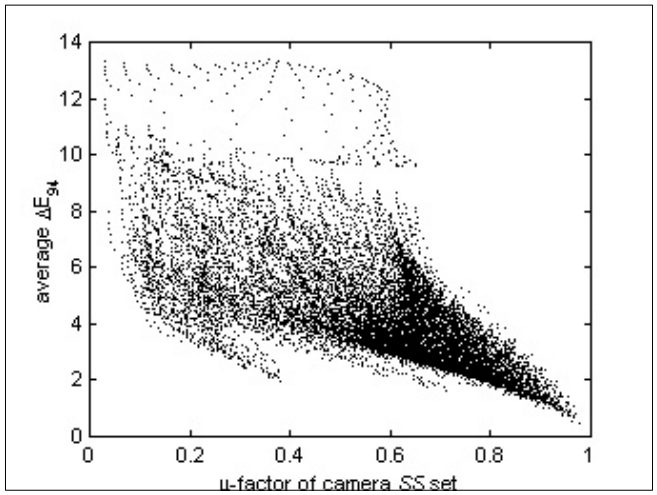

Figure 5.8: Relationship between *m*-factor and average color difference (DE^*_{94}) between reference and estimation of an ensemble of reflectance spectra, here Vrhel-Trussell data set is considered as object colors to be captured with 13,310 sets of three-channel hypothetical spectral sensitivity functions.

5.4.3 Conclusions on *q*-Factor and *m*-Factor

The goodness metrics of spectral sensitivities including Neugebauer's *q*-factor for individual SS and Vora and Trussell's *m*-factor for a set of SS were analyzed through least-squares approach in the chapter. Hypothetical spectral sensitivities with varied peak position and width parameter were evaluated with these criteria. For these hypothetical sensitivities, the optimal peak wavelengths for Red, Green and Blue spectral sensitivity functions were determined to be around 450nm, 540nm and 600nm. The optimal width parameters were found to be around 50nm with that of the Blue channel (40nm) being a little smaller than that of the Red and Green channels (50~60nm). These results will be useful for designing practical filters. It is known that the disadvantage of *q*-factor has been overcome by *m*-factor, but the latter does not consider some practical issues such as imaging noise. Also, these merit functions are not based on a perceptual uniform color space. The ultimate solution to the design of spectral sensitivities relies on complete consideration on these real world factors.

5.5 Q_{st} and Q_{sf}

When a camera is used for imaging a set of reflectance spectra, the camera signala can be transformed into CIE XYZ to match the accurate CIE XYZ values of those samples. The transformation can be simply obtained with a pseudo inverse, and the minimized mean-squared difference of tristimulus values can be separated into two parts. Shimano defined Q_{st} as the ratio of these two parts [Shimano2000a], which is equivalent to the following form:

$$Q_{st} = \frac{\text{trace}(A_L A_L^T K_r G (G^T K_r G)^{-1} G^T K_r)}{\text{trace}(A_L A_L^T K_r)} \tag{5.12}$$

A brief derivation of Equation (5.12) has been attached in Appendix D. If color matching functions are replaced with orthonormal color matching functions, an orthonormal color quality factor Q_{sf} is defined, which is equivalent to the following form:

$$Q_{sf} = \frac{\text{trace}(U_L U_L^T K_r G (G^T K_r G)^{-1} G^T K_r)}{\text{trace}(U_L U_L^T K_r)} \tag{5.13}$$

where

$$K_r = E\{rr^T\} = \frac{1}{n_{samples}} \sum_{i=1}^{n_{samples}} r_i r_i^T \tag{5.14}$$

is the correlation matrix for the ensemble of object reflectance spectra. A_L ($= L_{view}$ A) and G ($= L_{take}M$) already include the illuminant factor inside, and U_L is the orthonormal fundamental vectors derived from A_L. A is the color-matching functions matrix, typically the CIE 1931 2° $[\bar{x}, \bar{y}, \bar{z}]$, and M is the spectral sensitivity functions matrix. Both Q_{st} and Q_{sf} are the data-dependent metrics for spectral sensitivity functions. In the experiment, Vrhel and Trussell's data set, which contains 354 object colors, is used when the statistics of reflectance spectra is necessary.

5.6 Figure of Merit

Sharma and Trussell's Figure of Merit (FOM) has been recognized as the most extensive colorimetric quality factor [Sharma1996b]. With the same notation used in Chapter 3, FOM is defined by minimizing the mean-squared color error e between camera response t_c and reference measurement t in a target color space which is perceptually uniform:

$$e(A_L, G, B) = E\left\{\left\|F(t) - F(\hat{t})\right\|^2\right\} \quad \text{where } \hat{t} = Bt_c \tag{5.15}$$

This color error is approximated with local linearization such that closed-form expressions can be obtained. The linear matrix B which transforms camera output signal into tristimulus values is determined through optimization, and the minimized mean squared linearized color error has been derived as

$$e_{\min} = a(A_L) - t(A_L, G) \tag{5.16}$$

Finally, the figure of merit q_{FOM} is defined as the ratio

$$q_{\text{FOM}} = \frac{t(A_v, G, K_r, K_h)}{a(A_v, K_r)} \tag{5.17}$$

where

$$0 \le t(A_v, G, K_r, K_h) \le a(A_v, K_r) \tag{5.18}$$

$a(\cdot)$ and $t(\cdot)$ are two functions, which can be interpreted as the total and recovered colorimetric information of object color respectively, K_r and K_h are the correlations of the reflectance

spectra set and the random noise. A simple modification to FOM, named as Measure of Goodness (MG) is realized as:

$$q_{MG} = 1 - \sqrt{1 - \frac{t(A_v, G, K_r, K_h)}{a(A_v, K_r)}} = 1 - \sqrt{1 - q_{FOM}} \tag{5.19}$$

Here the average color difference of an ensemble of spectra varies linearly against quality factor. The imaging noise is assumed to be white noise (zero mean and independent of signal) in Equations (5.15)-(5.17). The above *q*-factor, *m*-factor, Q_{st} and Q_{sf} are special cases of FOM [Sharma1997b].

5.7 Unified Measure of Goodness

The detailed derivation of Unified Measure of Goodness is described in Appendix E. This colorimetric quality factor is an extension of FOM by taking account of the following properties: Minimization of average color difference over an ensemble of standard reflectance samples in uniform color space; The input signal together with noise, which includes shot noise and dark noise is propagated into the target color space, a linear matrix is obtained by optimization based on the noise propagation property. A scheme corresponding to multi-illuminant color correction is further proposed. All these properties are *unified* into a single metric – *Unified Measure of Goodness* (UMG).

Figure 1.2 illustrated the generic signal transformation in a camera. The captured signal can be used to estimate the original signal represented in a perceptually uniform color space or color appearance space that considers viewing condition. Assuming the average color difference between the estimation and reference of original signal which can be written as Euclidean distance in target color space is minimized:

$$e = E\left\{\left\|F(t) - F(F_0 t_c)\right\|^2\right\} \tag{5.20}$$

where F_0 linearly transforms camera output signals into CIE XYZ values, t is the measured CIE XYZ values, t_c is the camera output signal with noise contaminated, and

$$F(\bullet) = F_n(\cdots F_2(F_1(\bullet))) \tag{5.21}$$

sequentially transform tristimulus values into target color space, such as CIELAB, or CIECAM97s with series of transformations $F_{0, \ldots} F_n$. If $F_1 \ldots F_n$ are linear or nonlinear but approximately differentiable with continuous first partial derivatives, a first-order Taylor series provides a fairly accurate locally linear approximation for each of them:

$$F_i(x+\Delta x) - F_i(x) = J_{F_i}(x)\Delta x \tag{5.22}$$

With the law of chains for first derivatives,

$$F(x+\Delta x) - F(x) = \prod_{i=1}^{n} J_{F_i}(F_i(\cdots F_1(x)))\Delta x = J_F(x)\Delta x \tag{5.23}$$

Therefore,

$$e \cong E\{\left\| J_F(t)(t - F_0 t_c)\right\|^2\} \tag{5.24}$$

By minimizing this color error, the optimal linear matrix F_0 can be determined, and a new measure for single viewing-taking illuminant pair can be defined:

$$e_{\min} = a(A_L) - t(A_L, G) \tag{5.25}$$

and

$$q(A_L, G, F) = \frac{t(A_L, G)}{a(A_L)} \tag{5.26}$$

$$q = 1 - \sqrt{1 - q(A_L, G, F)} \tag{5.27}$$

Since the taking (recording) and viewing illuminants may be different, a quality factor for any taking and viewing illuminant pair is defined. For particular application, if a set of illuminants $\{L_{v_1}, L_{v_1}, \cdots, L_{v_n}\}$ is chosen as the viewing illuminant, and another set of illuminants $\{L_{t_1}, L_{t_1}, \cdots, L_{t_m}\}$ is chosen as the taking illuminant, one can define a quality factor matrix M as follows:

$$? = \begin{bmatrix} q_{11} & q_{12} & q_{13} & \cdots & q_{1m} \\ q_{21} & q_{22} & q_{23} & \cdots & \vdots \\ q_{11} & q_{11} & q_{11} & \cdots & \vdots \\ \vdots & \vdots & \vdots & \ddots & \vdots \\ q_{n1} & q_{n2} & q_{n3} & \cdots & q_{nm} \end{bmatrix} \tag{5.28}$$

The comprehensive quality factor UMG for the taking-viewing-illuminant pair may be defined as the weighted average of elements of the above matrix:

$$\Theta = \frac{1}{nm}\sum_{i=1}^{n}\sum_{j=1}^{m} w_{ij} q_{ij} \tag{5.29}$$

where w_{ij} is the weight preset by camera manufacturers for the corresponding quality factor q_{ij} defined for viewing-taking-illuminant pair (L_{v_i}, L_{t_j}), and $\sum_{i=1}^{n}\sum_{j=1}^{m} w_{ij} = 1$.

The advantage of UMG is that, choosing different target color space, or different color difference formula, a normalized measure of merit is obtained on a set of spectral sensitivities. It is preferred that the value of evaluation can be proportional to human visual judgment. Therefore a UMG takes advantages of CIEDE2000, S-CIELAB and color appearance models is desirable. Currently, color difference is chosen as Euclidean distance in a recognized uniform color space, i.e. CIELAB. A typical linear relationship between UMG without noise consideration and the average color difference of an ensemble of object samples is shown in Figure 5.9.

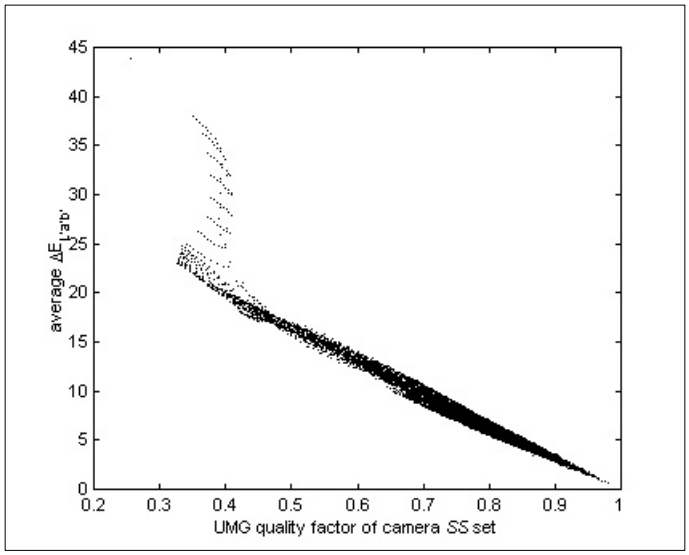

Figure 5.9: Typical Relationship between average color difference and UMG.

Table 5-2 compares the difference between the available quality factors and UMG. UMG has been a most complete consideration of practical issues in data-dependent metrics. If the samples are representative, it can be expected to replace data-independent metrics. The only disadvantage of UMG is that the evaluation of sensitivities takes much more time.

Table 5–2: Comparing variety of quality factors.

Items	Quality Factors Based on Geometrical Difference		Quality Factors Based on Sample-Dependent Color Error		
	q-Factor	*m*-Factor	Q_{st}-Q_{sf}	FOM	UMG
Number of Channels	1	Multiple	Multiple	Multiple	Multiple
Orthonormal CMFs	Yes	Yes	Yes (Q_{sf})	-	-
CIE XYZ Color Space	-	-	Yes	-	-
CIELAB ΔE Based	-	-	-	Yes	Yes
CIELAB ΔE Linearity	-	-	-	-	Yes
Multi-illuminant Strategy	-	Possible extension	Possible extension	Possible extension	Yes
Noise Consideration	-	-	-	Yes	Yes
Signal-dependent Noise	-	-	-	-	Yes
Practical Optimization	-	Yes	-	-	Yes

5.8 Standard Samples

For metrics such as Q_{st}, Q_{sf}, FOM or UMG, a representative ensemble of object reflectance spectra are required. Hardeberg, *et al*. used all 1269 Munsell patches as a target for characterizing electronic cameras [Hardeberg1998]. They also compared the results with 20 optimally or heuristically chosen patches from the Munsell book. The heuristically chosen set was obtained by simply selecting the most saturated patch from each of the 20 hue pages of the Munsell book, and the optimal set was chosen through a procedure of selection of the most significant target patches (for details, seethe paper). Both sets listed with their Munsell notation in Table 5-3, and a a^*-b^* plot can show that the optimally chosen set approximately uniformly distributes patches in the a^*-b^* plane.

Table 5–3: Munsell patches chosen as standard targets for camera characterization.

Optimal Set (20 Patches)		Heuristic Set (20 Patches)	
7.5RP 9/2	10B 6/10	5R 5/14	5BG 6/8
5R 4/14	10Y 8/4	10R 6/12	10BG 6/8
7.5Y 8/12	7.5YR 8/8	5YR 7/12	5B 6/8
2.5G 7/10	10RP 8/6	10YR 7/12	10B 6/10
5P 2.5/6	10R 3/2	5Y 8/12	5PB 5/12
10R 7/12	7.5PB 5/12	10Y 8/12	10PB 5/10
7.5RP 6/10	10Y 8.5/6	5GY 8.5/10	5P 5/10
2.5B 5/8	10PB 4/10	10GY 7/10	10P 5/12
10P 3/8	10YR 3/1	5G 7/10	5RP 5/12
7.5R 7/4	7.5YR 6/4	10G 6/10	10RP 5/12

In general, color cameras are used to record human portraits (skin tones), natural object colors (surface reflectance), and man-made object surfaces from natural materials. So the standard object reflectance spectra used in quality factors should contain representative samples from those reflectance categories, i.e. the Vrhel-Trussell data set. This data set includes a total of 354 samples: (1) The reflectance spectra of 120 DuPont paint chips. The DuPont paint chips are the solid color selections of the DuPont Color Sampler from DuPont Transportation products, and can be ordered from any DuPont Refinish Sales Centers; (2) The spectral reflectance of the 64 Munsell chips in Munsell book notation, including 9 patches from the Macbeth Color Checker chart. The reflectance spectra of the 170 natural and man-made materials measured *in situ*, covering surface reflectance of trees, leaves, human skins, and clothing. The variety of objects in this dataset should be enough for testing and designing camera spectral sensitivities.

The problem now is that, are the samples in Vrhel-Trussell set more than enough? A pre-selected smaller data set, which represents the reflectance characteristics of this rather big data set, would be desired. Options come to the 24 Macbeth ColorChecher patches and the 15 CIE13.1 color rendering patches. Some studies by Hung [Hung2000] show that the 15 CIE 13.1 patches can represent the real world well enough. But Macbeth ColorChecker is a widely accepted target for color imaging studies and can be readily found. It would be a better choice if

the 24 patches can represent the 354 Vrhel-Trussell patches. The first three principal components of both sets are calculated and plotted in Figure 5.10 and the corresponding variance interpreted by them are shown in Figure 5.11.

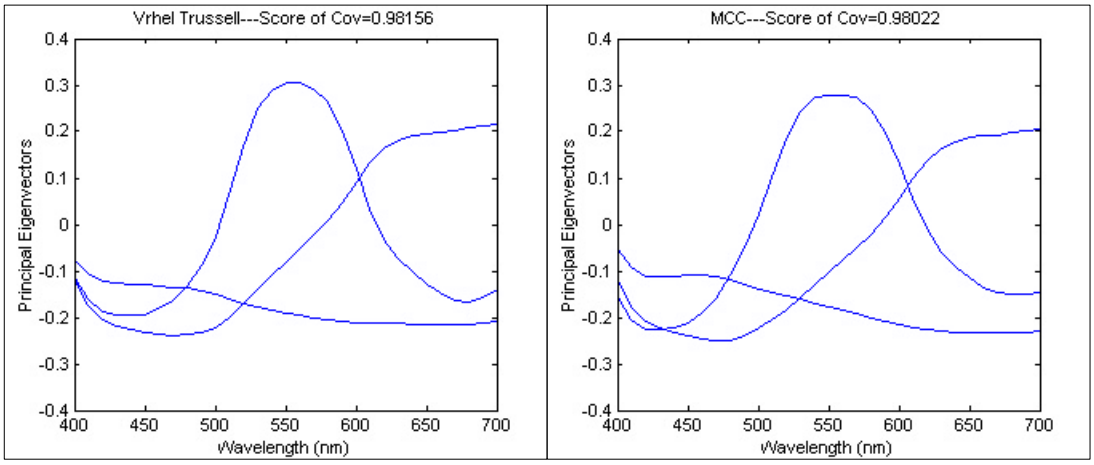

(a) (b)

Figure 5.10: Principal components of (a) Vrhel-Trussell data set; (b) Macbeth ColorChecker.

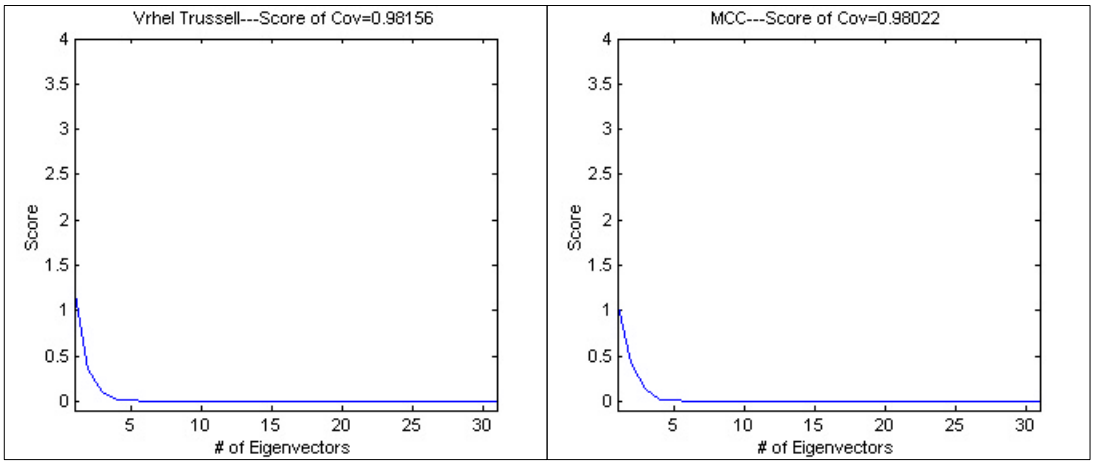

(a) (b)

Figure 5.11: Eigen-values of the principal components (a) Vrhel dataset; (b) Macbeth.

The similarity between the two sets of principal components from the two data sets in terms of *m*-factor (extended to represent the difference between two subspaces) is 0.9931. The spectra of two data sets were reconstructed with these two sets of principal components. The

spectral difference between original and reconstructed is calculated and shown in Table 5-4. There is little difference for the two principal component sets in terms of reconstruction error. The gamut of Vrhel-Trussell patches and Macbeth ColorChecker in CIELAB space is plotted in Figure 5.12. From the plots, Vrhel-Trussell data set covers a larger area, but Macbeth ColorChecker patches averagely distributed within most area. In brief, Macbeth ColorChecker can roughly take the place of Vrhel-Trussell data set as an effective standard target in this application.

Table 5–4: Spectra difference (RMS) between original and reconstruction reflectance.

Reconstruction Comparison	Vrhel-Trussell Data Set (354)	Macbeth ColorChecker (24)
PCs obtained from Vrhel Data	0.0350	0.0368
PCs obtained from MCC Data	0.0367	0.0362

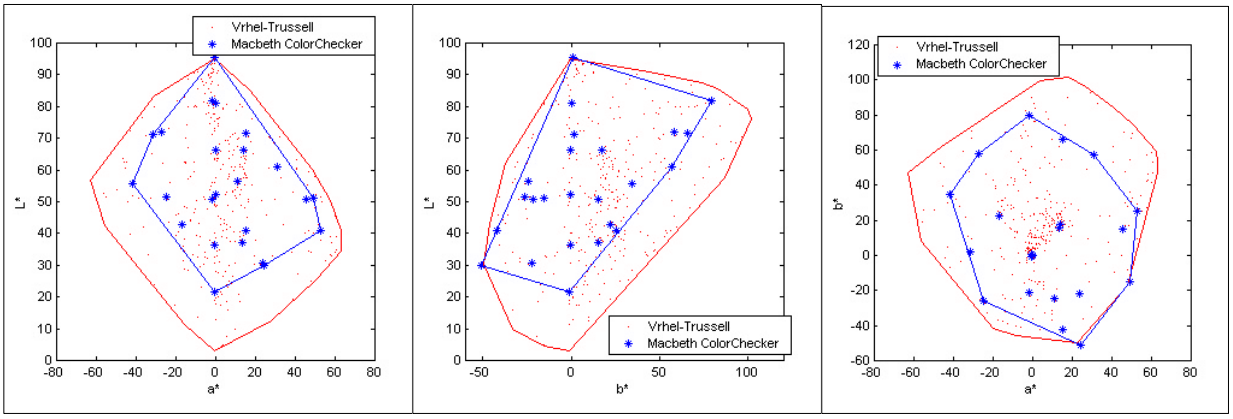

(a) (b) (c)

Figure 5.12: CIELAB coordinates of Vrhel-Trussell and Macbeth ColorChecker datasets: (a) L^*-a^* plane; (b) L^*-b^* plane; (c) a^*-b^* plane.

5.9 Relationship between UMG, m-Factor and RMS Noise

UMG with or without noise consideration, m-factor and RMS noise describe different aspects in color imaging. UMG without noise consideration indicates the performance of a spectral sensitivity set that does not satisfy Luther condition. UMG with noise consideration gives the

comprehensive performance if the sensitivity set does not satisfy the Luther condition and noise in the recording process is propagated as RMS noise in the target color space. m-Factor only indicates the performance of spectral sensitivity set that does not satisfy Luther condition. There may exist some kind of relationship between these quality metrics. In this study, 500 sets of spectral sensitivity functions (optimum candidates) are generated from the combination of Schott glass filters (as described in experiment 2 at Chapter 9). A variety of colorimetric quality factors, RMS noise in CIELAB or XYZ space and average color difference of an ensemble of object colors were calculated. The goal of the study was also to provide validity basis for the hierarchical approach to the optimal design of spectral sensitivities to be described in Chapter 7. The recording noise in a camera RGB signal is assumed to be white noise plus signal-dependent shot noise with parameters specified as in Section 4.4.3 ($m_h = 0$, $s_d^2 = 50e^-$, $m_{\max} = 60,000e^-$ and $h = 0.98$).

Without considering the imaging noise, the color difference comes from the fact that the spectral sensitivity functions are not satisfying the Luther condition. Therefore the UMG evaluation without noise consideration indicates the degree of deviation from Luther condition. Also the average color difference reflects the degree of deviation from Luther condition. Figure 5.13 shows that a monotonic (roughly linear) relationship exists between UMG without noise consideration and average color difference. The monotonic relationship is due to the fact when noise is not considered, UMG represents the minimized average color difference.

When noise was considered, UMG values and the average color difference were calculated for the 500 sets. Due to the simultaneous existence of noise and non-Luther condition, the relationship between UMG with noise consideration and average color difference does not follow a strict linear relationship (Figure 5.14). Compared with Figure 5.13, here the average color difference represents both the part due to deviation of the Luther condition and the part due to imaging noise propagation from device RGB space to CIELAB color space. Therefore here the average color difference is larger than that in Figure 5.13.

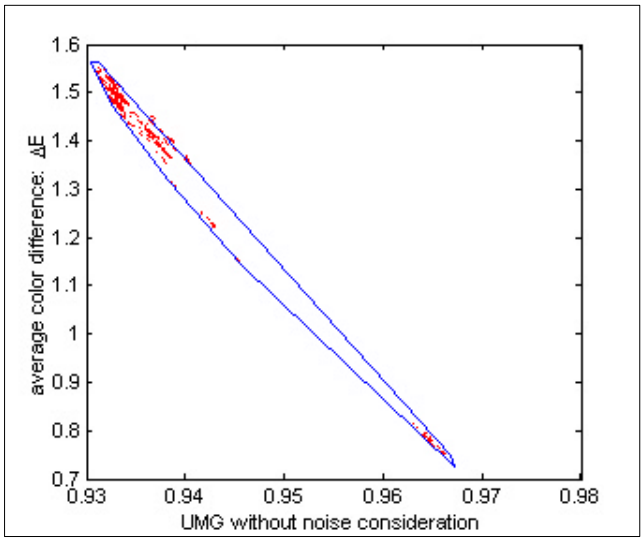

Figure 5.13: Relationship between UMG without noise consideration and averageDE^*.

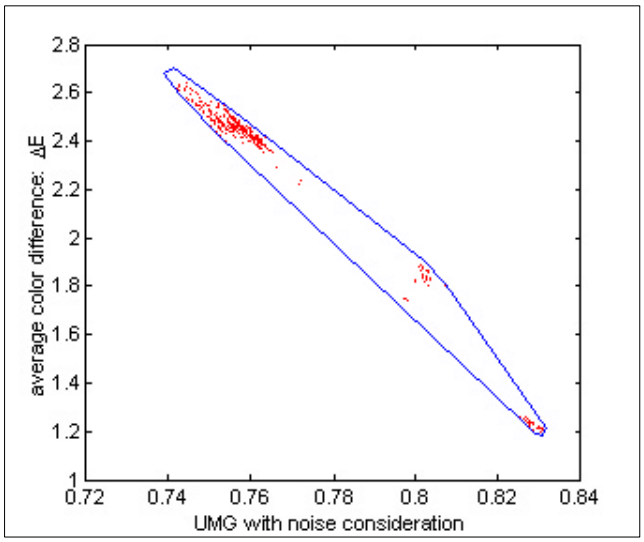

Figure 5.14: Relationship between UMG with noise consideration and average DE^*.

Equations (4.30)-(4.31) gave two definitions of RMS noise, one is just the square root of the sum of diagonal elements of the variance-covariance matrix, and the other was defined by Burns and Berns [Burns1997b]. Since the diagonal noise term dominates in Burns-Berns noise equation, there should be no substantial difference from two formulae. Noise calculated from the two equations in fact were very close (Figure 5.15). This fact suggests that only one RMS noise formula is required.

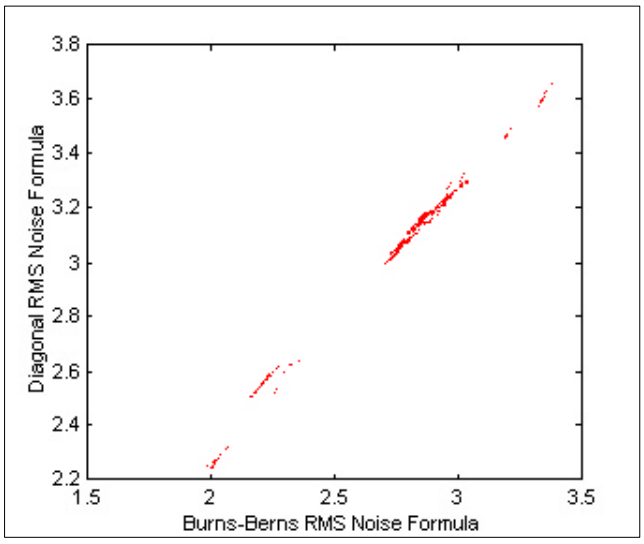

Figure 5.15: Relationship between two definitions of RMS noise.

It is expected that the larger the value of UMG without noise consideration, the smaller the RMS noise. But it is not always like this. The relationship between UMG without noise consideration (ideal UMG) and RMS noise in CIELAB color space is located within a two-dimentional area (Figure 5.16). The same UMG does not correspond to the same RMS noise performance. This is reasonable, since sensitivity sets with the same UMG without noise consideration (or m-factor) have different degree of noise amplification. Those spectral sensitivity sets that have large ideal UMG values and small RMS noise values (the spectral sensitivity sets represented in red dots on the lower right part of the enveloped area) are preferred as optimum candidates. Some typical spectral sensitivities sets have been labeled with their internal indices for comparison purpose in Figure (5.16).

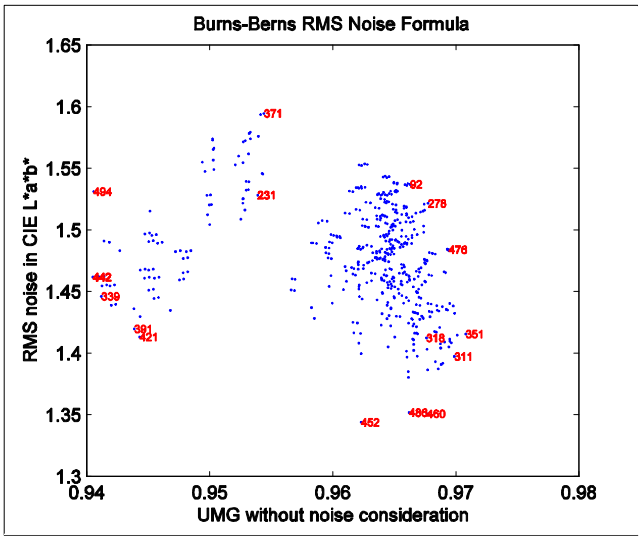

Figure 5.16: Relationship between UMG without noise consideration and RMS noise.

If the relationship between UMG with noise consideration and RMS noise is plotted, it is found that they fulfill a monotonic relationship (Figure 5.17), which is similar to Figure 5.14. If noise is considered, UMG is a comprehensive evaluation of color difference because of the non-Luther condition and suppression of noise propagation. Therefore if UMG has a monotonic relationship with minimum average color difference (Figure 5.14), it should also have a monotonic relationship with RMS noise in CIELAB space (Figure 5.17).

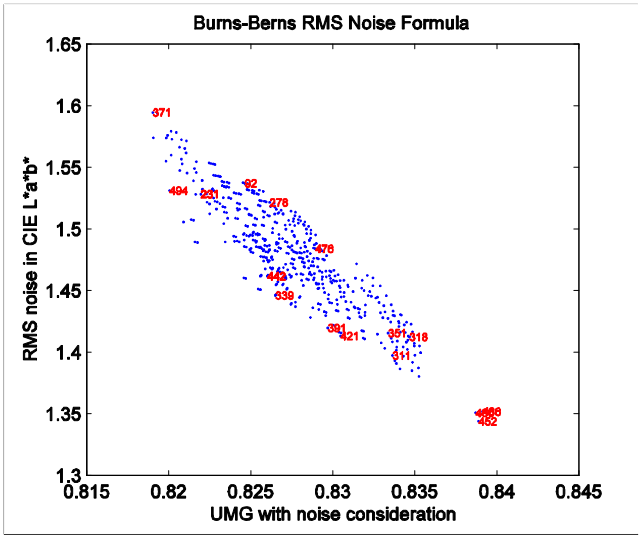

Figure 5.17: Relationship between UMG with noise consideration and RMS noise.

If comparing Figures (5.16) and (5.17), those spectral sensitivity sets having the smallest RMS noise in Figure (5.16), such as #452, now have the largest values of UMG with noise consideration in Figure (5.17). This shows that UMG with noise consideration is a good indicator of noise performance for spectral sensitivities.

The RMS noise was calculated in CIE XYZ space, the UMG without noise consideration and RMS noise were located within an two-dimensional area (Figure 5.18). This plot is similar to Figure 5.16, since CIELAB is just additional noise propagation from CIE XYZ. The sensitivity sets located on the lower right of the enveloped area are preferred (better color, less noise).

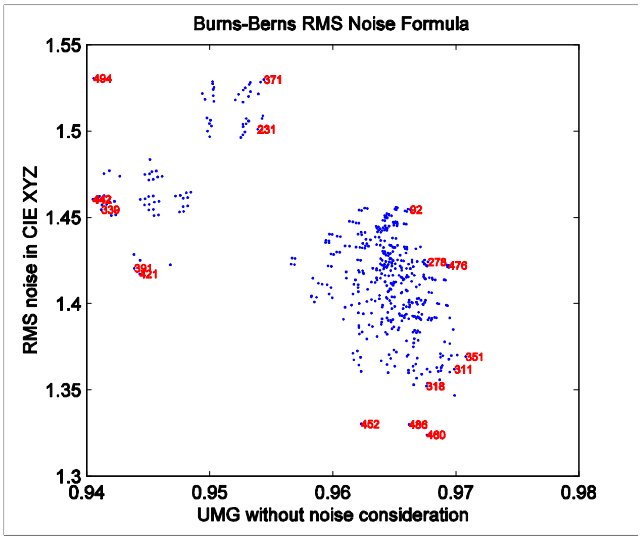

Figure 5.18: Relationship between UMG without noise consideration and RMS noise in XYZ.

The relationship between RMS noise in CIELAB space and m-factor is plotted in Figure 5.19. Since m-factor and UMG without noise consideration are equivalent (only describing the satisfaction of the Luther condition), the figure shows similarity to the relationship between RMS noise and UMG without noise consideration. Figure 5.19 is similar to Figure 5.16. Those sensitivity sets with higher m-factor and lower RMS noise are desired.

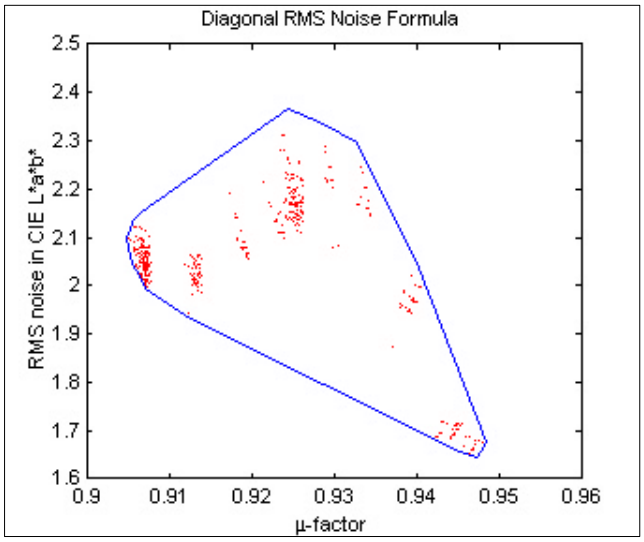

Figure 5.19: Relationship between *m*-factor and RMS noise.

Both UMG without noise consideration and *m*-factor indicate the degree of satisfaction of the Luther condition. It may be expected that they have linear relationship. The relationship between UMG without noise consideration and *m*-factor is shown in Figure 5.20. Little linear relationship exists between them, although the trend is that the larger the UMG without noise consideration, the larger *m*-factor.

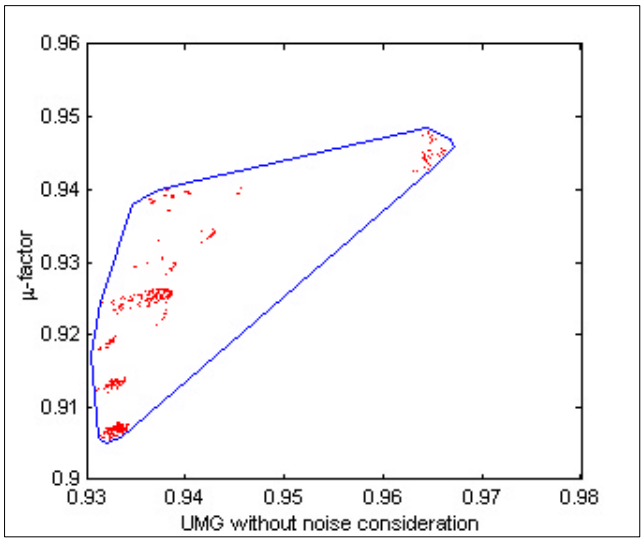

Figure 5.20: Relationship between UMG without noise consideration and *m*-factor.

5.10 Conclusions

The performance evaluation metrics of spectral sensitivity functions were discussed in this chapter. Colorimetric quality factors have been found to be appropriate measures to describe various aspects of spectral sensitivity functions. q-Factor and m-factor are simple metrics to describe how the sensitivity functions approximate color matching functions in geometrical space. They were formulated with least-squares approach and used to explore the characteristics of hypothetical spectral sensitivities. FOM emerged as the most extensive metric, but the only shortcoming is that it lacks the capability to handle signal-dependent noise. The proposed UMG metric is more like a practically useful metric as an improvement of FOM. A practically verified noise model and multi-illuminant color correction are embedded in this metric. Besides that, UMG can be implemented in color appearance space and with new color and image difference formulae other than Euclidean distance in CIELAB color space.

6 GENERIC APPROACHES TO THE OPTIMAL DESIGN OF SPECTRAL SENSITIVITIES

6.1 Introduction

In chapter 5, the performance evaluation metrics of spectral sensitivities were described, including average color difference, *q*-factor, *m*-factor, Q_{st} and Q_{sf}, FOM and UMG. While evaluation is very interesting, it is more desirable to use the performance evaluation metrics as objective functions to search for a set of optimal spectral sensitivities for digital imaging devices. Since the freedom of designing spectral sensitivities mostly is just the color filters selection, it has also been designated as a filter design problem.

A lot of efforts have been put on the filter design before. Ohta started the evaluation and optimization of sensitivities in subtractive imaging systems [Ohta1981b, Ohta1983]. Wolski, *et al*. reviewed the major work done before them [Wolski1996], including Davies and Wyszecki [Davies1962], Engelhardt and Seitz [Engelhardt1993], Vora and Trussell [Vora1993a and Vora1993b], and Vrhel and Trussel [Vrhel1994a]. Tsumura, *et al*. optimized three channel gaussian-shaped filters with noise presence by simulated annealing to minimize CIE color difference [Tsumura1997]. Wolski, *et al*. also optimized the sensor response functions for colorimetry of reflectance and emissive objects under multiple illuminants, and the optimization was carried out in CIELAB color space with a smoothness constraint. Sharma and Trussell also did optimal searching of transmittance filters [Sharma1998], but not with their proposed FOM metric; they were looking for the nonnegative filters in the presence of white noise in the similar but improved way as Vrhel and Trussell [Vrhel1994a].

In this chapter, some general constraints on spectral sensitivities are discussed, followed by the literature review on filter design, and propose three practically feasible approaches. By assuming that spectral sensitivity functions approximate gaussian-type functions (asymmetric

cubic spline functions), the optimal region of peak positions and widths can be obtained by setting a confidence level on quality factors. The region is compared with each other when a different quality metric is used.

6.2 Physical Constraints on Spectral Sensitivities

The optimal design of spectral sensitivities is usually to search for a set of filters by maximizing some pre-defined measure of goodness while satisfying the physical constraints emerging from practical fabrication processes. The measure of goodness such as the *m*-factor defined by Vora *et al*, the figure of merit by Sharma or the defined UMG can be used as criteria. The constraints usually imposed on camera spectral sensitivities are:

(1) *Non-negativity and boundedness*:

The transmittance or spectral sensitivity at each wavelength is non-negative; the transmittance at each wavelength cannot exceed one or some other constant. Different boundedness constraint may be exerted according to the real world.

$$0 \le s_{(R,G,B)}(l_i) \le 1 \tag{6.1}$$

(2) *Smoothness*:

The second derivative of the physical sensitivity can be used as a measure of curvature and therefore as a measure of smoothness of the sensitivity.

$$\begin{aligned} &\left|s(l_{i-1}) - 2s(l_i) + s(l_{i+1})\right| \le \Delta_i \\ &\Delta_i \le \Delta_{\max} \end{aligned} \tag{6.2}$$

where Δ_i is the smoothness tolerance at wavelength l_i, and $\Delta_{\max}$ is the maximal smoothness tolerance for all wavelengths.

(3) *Single Peak* (optional, preferred):

The transmittance of the filter has one global peak, and without multiple local peaks. There is more chance to fabricate a single-peaked filter than a multi-peaked filter.

These constraints are more or less applied on the estimation or optimal design of spectral sensitivities. But true spectral sensitivity functions, in fact, may not satisfy all of them. For

example, the blue sensitivity of a Kodak digital cameras DCS200 or DCS420 is multi-modal with more than one peak and are not smooth at all [Vora1997c]. Other constraints such as the range of the first derivative of the spectral sensitivities, symmetry etc. may also be included depending on specific problems.

6.3 Literature Review on Filter Design

Some work on color filter or spectral sensitivity design is reviewed briefly here.

Ohta developed a numerical method, based on a linear and nonlinear optimization technique, for deriving optimum spectral sensitivity functions under practical constraints in subtractive color photography [Ohta1983]. Although chemical imaging method has been replaced with digital electronic imaging technology, the ideas presented in this paper are still useful today, such as linear model of spectrum, smoothness and single peak constraints, etc.

Vora and Trussell proposed methods to find an optimal set filters from Kodak Wratten filters in terms of m-factor, they also parameterized filter transmittance spectra as linear combination of gaussian functions, the parameters of which were determined by maximizing the m-factor of the filter set [Vora1993b, 1997a]. The influence of filter deviation due to fabrication on the filter performance was also analyzed [1997b]. Since m-factor reflects only the geometrical difference between subspaces of color matching functions and filters, it is a good metric to demonstrate filter optimization [Quan2000c], but it is inappropriate as a metric to find a practically optimal filter set used in the real world [Quan2001c].

Chen and Trussell used filters to alter the device sensitivities and designed an optimal filter set that maximizes Vora's measure of goodness for multi-illuminant color imaging [Chen1995]. The filters are parameterized with gaussian functions.

Engelhardt and Seits described their attempt at designing and producing dielectric filter sets that are either optimum in an absolute, theoretical sense, or close to this optimum but robust to fabrication tolerances at the same time [Engelhardt1993]. Although noise was considered, their design was not systematic.

Vrhel and Trussell described a method of computing transmittances of filters that minimized the mean-squared tristimulus error [Vrhel1994a]. The obtained filters may have negative portions, which are unacceptable to use in a real system.

Vrhel and Trussell outlined a new method of designing color filters that accounted for the presence of noise in the recording process [Vrhel1995a]. This approach used a minimum-mean-squared orthogonal-tristimulus error formulation. Closed-form solutions for optimal filters at various signal-to-noise ratios were determined, and the relation of the number of filters to the color error was examined. The constraint of filter non-negativity was also formulated, but only a near optimal solution was obtained based on the unconstrained solution due to the nonlinear power constraint. In addition, the obtained filters have jaggy shape and multiple secondary peaks, which increase the likelihood of fabrication difference.

Sharma and Trussell slightly modified the Vrhel-Trussell approach and transformed the problem with only non-negativity constraints [Sharma1998]. A numerical optimization scheme was utilized to determine the optimal solution, indicating significant improvement over Vrhel-Trussell method. The obtained optimal filters were also not smooth.

Wolski, *et al*. described the design of color recording filters for a device capable of both reflective and emissive measurements [Wolski1995, Wolski1996]. They minimize mean-squared error (MSE) in a linearized perceptually uniform color space. Regularization terms were used to enforce smoothness on the designed transmittances and provided robustness in the presence of noise and component variations in the filters. Since noise was not explicitly included in the analysis, the weighting of the regularization term was determined empirically.

Wu and Allebach optimized two filters for multi-exposure multi-illuminant system following Wolski and Allebach's approach [Wu1999]. Two theoretical filters and two combined filters from Kodak Wratten filters were obtained. Still noise was not considered.

Haneishi, *et al*. designed gaussian-shaped filters for recovering spectra of artworks. The filters are obtained by minimizing spectra difference with Wiener estimation [Haneishi1997]. Noise was not considered in this study. Later on, Hosoi, *et al*. described a method to select two to

six filters from very limited number of given filters for spectral recovering with noise consideration [Hosoi1999]. The noise was measured and spectral reflectance was recovered by minimizing mean squared error of spectra with Wiener estimation. The Wiener estimation approach was also widely used by Vrhel and Trussell in [Vrhel1994a] and [Vrhel1995a].

Quan *et al* reported a systematic filter design method for colorimetric reproduction [Quan2001c]. This method will be described in detail later. Recently the approach has also been extended to achieve reflectance spectral recovering for a multispectral camera.

6.4 Generic Design Approaches of Spectral Sensitivities

Since each spectral sensitivity function has 31 variables (assume the visible range defined on 400nm-700nm with an interval of 10nm), an optimization problem with nearly 100 variables for designing a three-channel camera is very difficult to be implemented in reality. It still can be done theoretically, but It is hard to judge if the obtained optimum is really optimal since the optimization is much likely to be trapped in local valleys. Some simplification is necessary in practice. Based on the analysis of others' research as cited above, three practically feasible approaches on filter or sensitivity function design are described as follows.

6.4.1 Optimal Subset of Discrete Set of Filters

A simple formulation of the optimization problem is to determine the "best" set of K filters from a set of existing filters. Suppose the set $\boldsymbol{S}$ is the set of existing filters from which the best subset M_0 of K filters is to be chosen. UMG may be maximized with respect to subsets of $\boldsymbol{S}$, of size K, by exhaustive searching K filters at a time. If N is the size of set $\boldsymbol{S}$, such a search will involve $C_N^K = N!/[K!(N-K)!]$ times of evaluations of the measure of goodness. For instance, Vora selected optimal three-filter subset from the Kodak Wratten Filter Set [Vora1993b], in terms of m-factor. The optimal set of the filters (23A, 48A and 52) has m-factor of 0.912.

Another example is to choose the best three hypothetical spectral sensitivities [Quan2000a] from the complete combinations of cubic spline functions with varied peak

wavelength and width. With exhaust searching, one can obtain the three hypothetical spectral sensitivities (*R*: peak (590nm), width *w*=60nm; *G*: peak (550nm), width *w*=60nm; and *B*: peak (450nm), width *w*=40nm), which contribute a UMG without noise consideration of 0.990, as shown in Figure 6.1(a). It is the highest among the discrete spectral sensitivity sets with cubic spline shape. One can calculate the color difference of each sample in the Vrhel object color ensemble [Vrhel1992] between the measured reflectance spectra and the predicted one with this hypothetical optimal spectral sensitivity set. Under daylight D65, the overall average CIELAB color difference is 0.35, as shown in Figure 6.1(b). Based on criteria of either quality factor or average color difference, it is an optimal spectral sensitivity set.

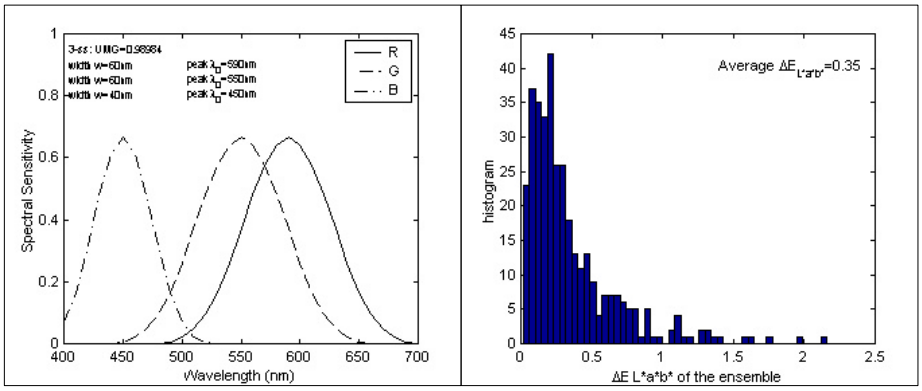

(a) (b)

Figure 6.1: (a) An optimal set of spectral sensitivities by computing every possible combination; (b) Histogram of color difference of all samples of an ensemble.

6.4.2 Parameterization of Filter Characteristics

One way of incorporating a manageable dynamic range and smoothness for filters is by modeling each filter in terms of smooth, nonnegative functions with a few parameters. SS can be modeled other than cubic spline functions, i.e. single gaussian or linear combination of multiple gaussians. Other functions, such as sinusoidal functions can also be used. It is feasible that each filter has no more than 5 or 7 parameters (degree of freedom), resulting in tractable formulations of the optimization problem and in physically realizable filters. The functions were chosen for ease of implementation and efficiency of the optimization routine. For instance,

$$S_i(l) = \exp(-\frac{(l - l_{i1})^2}{2s_{i1}^2}) + a_i \exp(-\frac{(l - l_{i2})^2}{2s_{i2}^2}), \quad i = \text{R, G, B} \tag{6.3}$$

where l_{i1}, l_{i2} are peak positions, s_{i1}, s_{i2} are width parameters, a_i is the weight for the secondary sensitivity. The resulting "optimal" filters will be sums of gaussian functions.

Once again it is likely that the merit function has many local maximum, which implies that a particular solution is a function of the starting point and not necessary the really optimal set of filters. To minimize this effect, thousands of trials are attempted with different initial points used. The resulting sensitivity set is the one with maximal quality factor among those trials. Figure 6.2(a) is result of optimization of parameterization of filter characteristics. Each sensitivity function has two parameters (peak position, half width), totally six for three sensitivities. It can be seen that the range of optimal peak position and width from those thousands of trials spreads widely but clusters on a few points in Figure 6.2(b, c). The optimal peak positions are around 450, 545 and 600nm, and the optimal width parameters are 40nm for blue, 50-60nm for green and red channels.

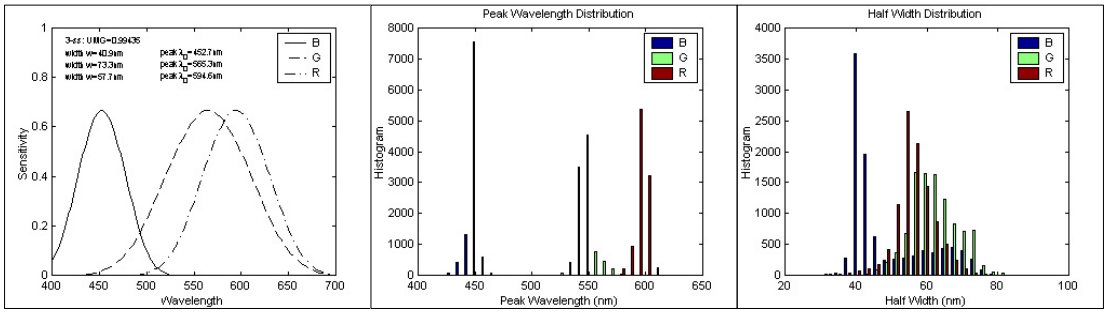

(a) (b) (c)

Figure 6.2: (a) Optimization result of parametrization approach. Histogram of (b) optimal peak wavelengths and (c) optimal half widths after thousands of repeated optimization.

6.4.3 Only One Channel Needs Optimization

There are cases when two or three spectral sensitivities are given and only one more is free to search for an optimal one. In this case, one has 31 variables totally (still too many), however the problem is much easier. The above two approaches may still be applied, but a direct optimization

towards the 31 variables could be an interesting trial in practice, while a local optimal result is still likely to be obtained. In the following example, given three sensitivities with UMG of 0.765, a fourth channel is designed so that the total quality factor is improved. The fourth SS satisfies the general three constraints with a smoothness tolerance of 0.025 (this number can be adjusted to make a tradeoff between smoothness and freedom). The unique peak position of the fourth SS slides from 400nm to 700nm by 10nm, totally 31 possible positions (since it is unknown which wavelength it should locate at). Final UMG of the set consisting of four SS can be as high as 0.937. The peak position of the fourth spectral sensitivity locates at about 610nm (Figure 6.3).

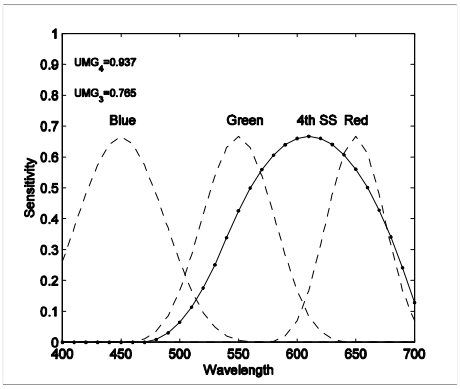

Figure 6.3: Assume three sensitivities are given, for instance, cubic spline functions peak at 450nm, 550nm and 650nm with width parameter *w* of 60nm, 50nm, 40nm. A fourth sensitivity is optimized according to the physical constraints described above.

6.4.4 Discussions and Conclusions

It is hard to tell which kind of spectral sensitivity is easy to be fabricated in practice, the one with parameterized shape or the one with arbitrary shape but satisfaction of the common constraints. Generally, optimization of the spectral sensitivity with predefined shape yields smooth curve and high quality factor but may omit those beyond this shape, which could be optimal set as well. Global optimization without shape limitation is likely trapped in local minima and produce intractable curve. Optimization through computing combination of discrete set is tedious, but it produces feasible solution from the available filters. As a next stage, more constraints from

industrial viewpoints will be incorporated and full trials will be carried out by actually fabricating the optimal filters.

6.5 Fabrication Tolerance and Optimal Region of Filters

6.5.1 Introduction

The optimal design of color filters is essential to color imaging devices in the reproduction of object colors. Camera designers pay attention to colorimetric accuracy, noise sensitivity and illuminant invariance. Filters are often specified through minimizing color differences between the measurements and estimations for an ensemble of object colors. For instance, color differences might be derived through the calculation of mean squared color differences in uniform color spaces like CIELAB [Sharma1997b, Vrhel1994a]. Sometimes color quality factors such as *m*-factor proposed by Vora and Trussel [Vora1993a] are used in color filter specification approaches.

However, the manufacturing process will finally determine whether the optimal filter is really feasible. If a filter design can be built but slight deviations cause its performance to deteriorate drastically, then such a filter could be a poor choice for putting it in a mass-produced product. Better smoothness of the ideal filtration function will increase the possibility of closeness between the ideally designed and practically fabricated filters. However small deviations from the desired curve may still cause loss of image quality. This paper proposes a new criterion for the optimal design of color filters based on fabrication tolerance. Ranges of sensitivity function parameters that describe comparatively optimal filters are sought instead of a unique “absolutely” optimal filter. The larger the parameter range, the more tolerant the filter is to slight manufacturing errors.

A variety of color quality factors have been proposed and developed for various goals. The quality factors that will be used in this study are Neugebauer’s *q*-factor [Neugebauer1956], Vora and Trussell’s *m*-factor [Vora1993a], Shimano’s Q_{st} and Q_{sf} [Shimano2000a] and Sharma and Trussell’s Figure of Merit and its extension. For all these quality factors, the perfect score is that

of 1. No comparison has been done yet in the literature on the optimal ranges obtained from these metrics at the same level.

The width and peak wavelength of sensitivity functions are important variables in color reproduction. General sensitivity function is modeled as asymmetric cubic spline function as Equation (6.4), as shown in Figure 6.4. The geometric peak wavelength l_0, left half-width w_1 and right half-width w_2 are the three primary parameters.

$$C(l)=\begin{cases}\dfrac{w_2^3+3w_2^2(w_2-|l-l_0|)+3w_2(w_2-|l-l_0|)^2-3(w_2-|l-l_0|)^3}{6w_2^3} & 0\le l-l_0\le w_2\\ \dfrac{w_1^3+3w_1^2(w_1-|l-l_0|)+3w_1(w_1-|l-l_0|)^2-3(w_1-|l-l_0|)^3}{6w^3} & -w_1\le l-l_0\le 0\\ \dfrac{(2w_2-|l-l_0|)^3}{6w_2^3} & w_2\le l-l_0\le 2w_2\\ \dfrac{(2w_1-|l-l_0|)^3}{6w_1^3} & -2w_1\le l-l_0\le -w_1\\ 0 & \text{otherwise}\end{cases} \tag{6.4}$$

Alternatively the function can be represented with these three parameters: peak wavelength l_0 (as above), width parameter *w* and skewness parameter Δw, where

$$\begin{aligned} w_1+w_2&=2w\\ w_2-w_1&=2\Delta w\end{aligned} \tag{6.5}$$

It follows that

$$w=\frac{w_1+w_2}{2} \tag{6.6}$$

$$\Delta w=\frac{w_2-w_1}{2} \tag{6.7}$$

where Δw describes the degree of skewness in the spectral sensitivity function. For symmetrical functions, $\Delta w=0$. For more complicated spectral sensitivity shapes, lower and upper bound of spectral sensitivity functions may be introduced. Many real sensitivity functions have secondary peaks, so it may prove important to include those. Other real-world structure may be modeled in

some future study, as well. The simple curves have shown, so far, to be reasonable representations of filters believed to be easily fabricated.

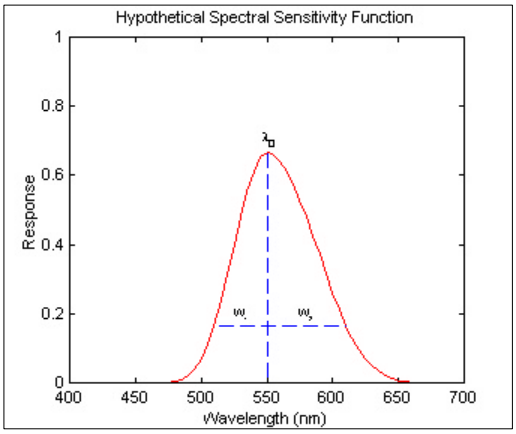

Figure 6.4: Hypothetical spectral sensitivity: Peak l_0, left and right widths are w_1 and w_2.

By shifting peak wavelength of the cubic spline function from 400nm to 700nm, channel sensitivities from blue to red are simulated. By modifying the width parameters, the bandwidth of sensitivity functions is modified. For the analysis, the possible geometrical peak wavelength for blue channel was varied from 400nm to 500nm, green channel from 500nm to 600nm and red channel from 550nm to 650nm, all in intervals of 10nm. The width parameter, w, was tested between 10nm and 110nm in increments of 10nm. The skewness parameter, Δw, was varied between –5nm and 5nm by increments of 5nm. By calculating all of these combinations, one can choose the combinations whose quality factors satisfy some pre-defined minimum conditions, such as $q(m) \geq 0.98$. In order to compare the optimal ranges from different quality factors, these parameters were held constant:

$$\Delta w_R = \Delta w_G = \Delta w_B = 0nm$$

$$w_R = 50nm \quad w_G = 70nm \quad w_B = 40nm$$

6.5.2 Optimal Range Obtained with *q*-Factor

Neugebauer's q-factor has been discussed in Section 5.3 and is mathematically described by Equation (5.4). If some confidence level is given, this metric will give a parameters region where

spectral sensitivities with parameters located in this region is preferred. Figure 6.5 shows a contour plot of Neugebauer's *q*-factor relative to varying peak wavelength of hypothetical spectral sensitivities. The optimal range of $q>0.95$ is found to be the contour as shown in Figure 6.5. For results where *q* is high, e.g. $q>0.95$, two separate width-peak continuous areas are found. These show blue region to be limited, while the red-green region to be quite large and connected. Neugebauer's *q*-factor does not treat the three filters as a system, so for this factor the simultaneous selection of optimal three sensitivity functions cannot be obtained.

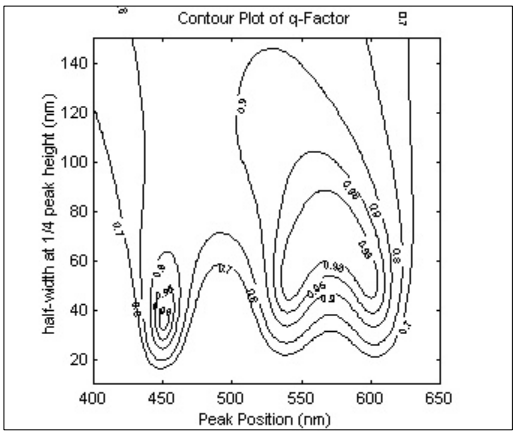

Figure 6.5: Optimal range defined by *q*-factor.

6.5.3 Optimal Range Obtained with *m*-Factor

Vora and Trussell's *m*-factor has been discussed in Section 5.4, where Equation (5.7) defines a quality factor $m_A(\cdot)$ in terms of original CIE 1931 XYZ color matching functions, and Equation (5.10) defines a quality factor $m_U(\cdot)$ in terms of the orthonormal color matching functions.

The optimal ranges defined by $m_A(M)$ and $m_U(M)$ are different, since different weights are used in the functions. Figure 6.6(a) demonstrates the use of $m_A(M)$. It shows the optimal range of peak positions when $m_A(M) \geq 0.95$, standard CIE 2° $[\overline{x}, \overline{y}, \overline{z}]$ color matching functions and illuminant D65 is used. $m_U(M)$ is used in making Figure 6.6(b) and Figure 6.7. These figures show the optimal range of peak positions when $m_U(M) \geq 0.95$ and illuminants equi-energy, D65 and A are used. Within the $m_U(M)$ figures, it can be plainly seen that the regions have only minor difference between the illuminant changes. Much larger differences are noted

between the use of $m_A(M)$ and $m_U(M)$. Figure. 6.6(a) shows the peak of green could be less than 500nm if the peak wavelengths of blue and red are appropriate, and there exist conditions where the peak wavelength of red could be higher than 650nm. Both metrics limit the peak position of blue sensitivity to some interval, about 435nm~450nm, and m_U also limits the optimal peak wavelength of red to 570nm~600nm. Detailed analysis shows the boundary of the region changes when the illuminant changes.

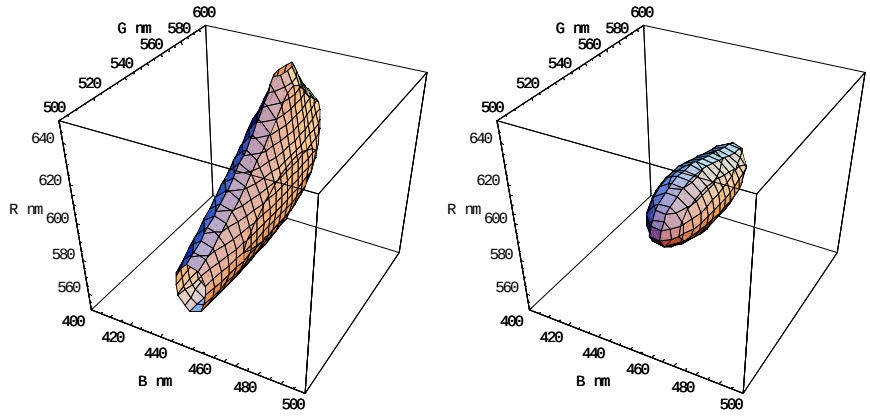

(a) (b)

Figure 6.6: (a) $m_A(M)$≥0.95 when D65 is used; (b) $m_U(M)$≥0.95 when EE illuminant is used.

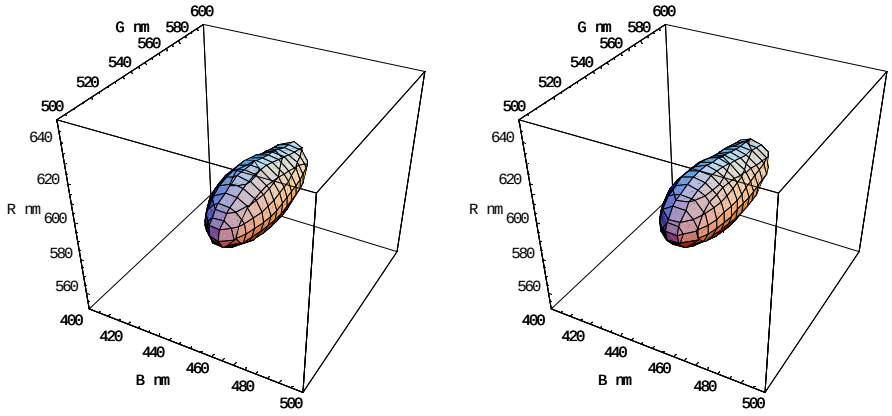

(c) (d)

Figure 6.7: (a) $m_U(M)$≥0.95 when D65 is used; (b) $m_U(M)$≥0.95 when A is used.

6.5.4 Optimal Range obtained with Q_{st} and Q_{sf}

The real object reflectance would be very helpful in transforming camera signal into the colorimetric values. By minimizing the mean-squared error between the estimated and measured tristimulus values, Shimano's Q_{st} and Q_{sf} quality factors have been discussed in Section 5.5 and described by Equations (5.12) and (5.13) respectively.

The optimal range obtained with Shimano's Q_{st} and Q_{sf} are be shown in Figure 6.8. While Vora and Trussell's *m*-factor misses some good sensitivity functions [Tajima1996, Shimano2000b], here both two measures here try to "beautify" all spectral sensitivity sets. If the threshold is chosen as 0.95 or 0.98, every combination in the peak position cube will qualify "optimal." Instead, here a threshold of 0.9995, which is very close to 1, is chosen to define the optimal space. Shimano's papers [Shimano2000a and 2000b] also demonstrate that most quality factor values he calculated are very close to 1 even when different object reflectance set is used. Comparing Figure 6.8(a) and (b), they are obviously different, which is similar to the difference to that between Figures 6.6(a) and 6.7(a). Since a threshold of 0.9995 is used, it will be difficult to discriminate which sensitivity set is better if quality factors of both sets are larger than 0.9995. The optimal range of blue in Figure 6.8(b) is wider than that in Figure 6.7(a), while that of red is narrower. Similar feature can be found between Figures 6.6(a) and 6.8(a).

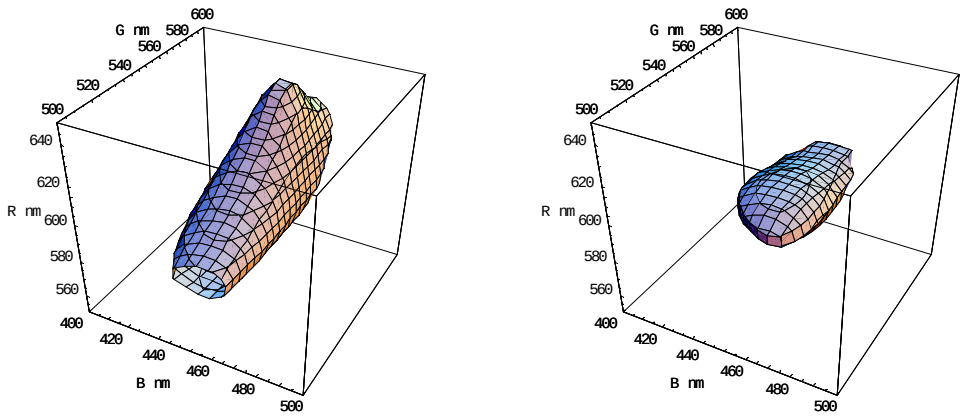

(a) (b)

Figure 6.8: (a) $Q_{st} \geq 0.9995$ when D65 is used; (b) $Q_{sf} \geq 0.9995$ when D65 is used.

6.5.5 Optimal Range obtained with FOM/MG

Sharma and Trussell's Figure of Merit (FOM) [Sharma1997b, reviewed in Section 5.6] is based on the optimization within CIELAB color space, which is considered as a more perceptually uniform color space than CIEXYZ. It also takes the signal-independent random noise into account. This quality factor should be more coincident with the real world. Like Shamano's metrics, it also depends on the selection of recording and targeting illuminants, as well as the statistical characteristics of the ensemble of object reflectance. FOM is described by Equation (5.17) and its simple modification MG which leads to a linear relationship has been described by Equation (5.19).

For comparison with figures obtained previously, if noise is ignored, the noise correlation matrix $K_h = 0$, the optimal range is obtained. For comparison, illuminants D65 and A will be used in the calculation of optimal range. Figures 6.9 demonstrate the results when illuminant D65 and A are used with FOM, and Figures 6.10 demonstrate the results when illuminant D65 and A are used with MG. At a level of 0.98 in Figure 6.9, the optimal ranges of peak wavelengths tend to be quite large for both D65 and A. The optimal peak wavelength of blue is extended from 420nm to 480nm, but that of green could be from less than 500nm to 600nm, and that of red could be from 560nm to more than 650nm. The difference between Figures 6.9(a) and (b) shows that the peak wavelength of red could be even higher for A, since A has higher spectral power distribution in red wavelength than D65. Figures 10(a) and (b) show that $\mathrm{MG} \geq 0.95$ is a more strict condition than $\mathrm{FOM} \geq 0.98$. Since MG has a linear relationship to CIELAB, it would be a more effective choice for selecting the peak wavelengths of sensitivity functions. Probably $\mathrm{MG} \geq 0.90$ is a good condition to determine the region in practice.

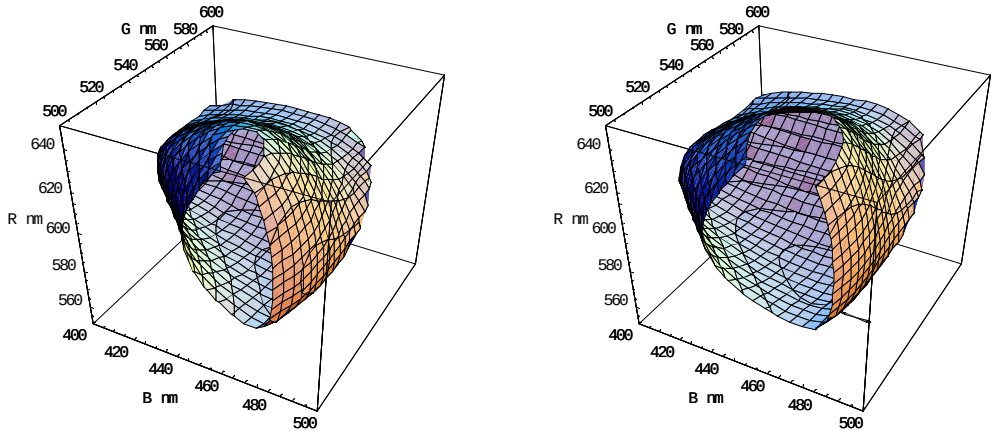

(a) (b)

Figure 6.9: (a) FOM≥0.98 when D65 is used; (b) FOM≥0.98 when A is used.

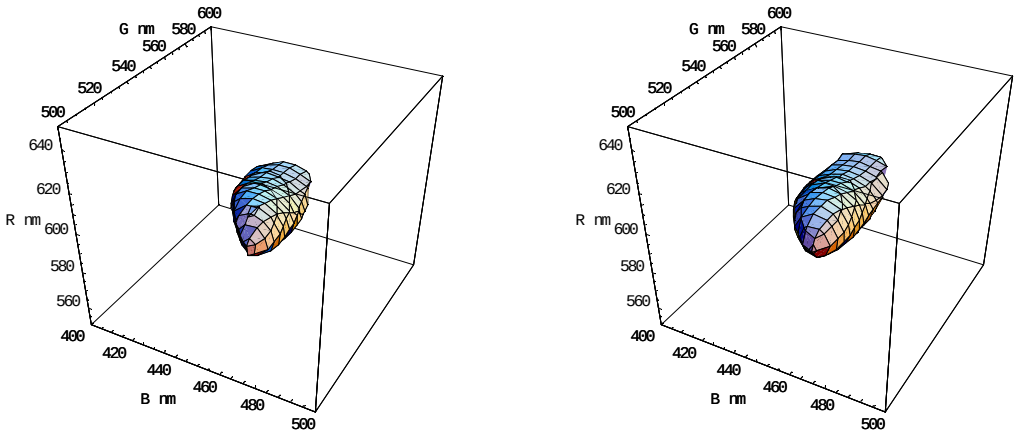

(a) (b)

Figure 6.10: (a) MG≥0.95 when D65 is used; (b) MG≥0.95 when A is used.

6.5.6 Conclusions

In this chapter, several color quality factors have been explored to obtain the optimal peak positions of spectral sensitivities when their widths and skewness have been given. The optimal regions are different from each other, which demonstrates that one should exercise caution in the use of quality factors. The following has been concluded:

(1) The region of optimal peak positions is continuous. For sensitivity functions with peak parameters which sit within a large region of high factors, the fabrication tolerance would be relatively high. For other sensitivity curve parameters the same can be said.

(2) The region of optimal peak positions becomes larger when the quality factor level is lowered. The region with lower quality factor value will include that with higher quality factor value.

(3) The shape of the region depends on the choice of the width parameter and skewness. Details are being summarized in US patent application [Quan2001d].

(4) m-Factor tends to be overly discriminating, while Q_{st} is likely to include everything. If color difference is the final judge, then the region obtained with FOM or MG is more promising.

(5) The value of most quality factors is more or less affected by the statistics of the data set and the characteristics of illuminants. In the future, these factors and noise amplification will be considered for real-world sensitivity optimization.

6.6 Conclusions

Generic approaches to the optimal design of spectral sensitivity functions are described. Some basic constraints on spectral sensitivity functions or color filters are described for optimization purposes. Direct optimization on around one hundreds variable would meet practical problem. The practically feasible approaches are the optimal subset searching among a set, parameterization of spectral sensitivity functions such that the optimization is implemented with a small number of variables, and optimization of single spectral sensitivity functions upon available channels in which case the optimization is also implemented with a small number of variables. In the second part of this chapter, by assuming the spectral sensitivity function is asymmetric gaussian function, the optimal region of peak positions and widths of spectral sensitivity functions are obtained by setting certain quality factor a confidence level. The region is found to be a continuous solid in high dimension and has some other properties. The region provides fabrication tolerance if the filter fabrication process is unknown.

7 HIERARCHICAL APPROACH TO THE OPTIMAL DESIGN OF SPECTRAL SENSITIVITIES

7.1 Introduction

Reviewed in chapter 6, the optimal design of spectral sensitivities had been studied extensively. Notice that all of those efforts were successful in some aspects, but also have some individual disadvantages. A satisfactory solution should take account of both data-independent and data-dependent performance, as well as signal-independent and signal-dependent noise, and the objective function of optimization should be implemented within a perceptually uniform color space or color appearance space. Furthermore, mismatch appears when approximating the virtual optimal curves with manufacturer's filter component set at fabrication process. This will induce error so that the fabricated curves are deviated from the ideally optimal ones, which may make the theoretically optimal set practically not optimal at all. The optimal design approach would optimize the imaging channels directly as a parameterized model of the filter manufacturing process, e.g. the selection and thickness of the filter components used in each channel. This research will initiate a new strategy to optimize filters for a high-end digital camera. In this scheme, it is unnecessary to assume the spectral sensitivities be smooth, since in strict sense most are not smooth at all, while the designed spectral sensitivities are guaranteed to be non-negative, since the given filter components are always non-negative.

Figure 7.1 illustrates the general processing pipeline for camera output signals. In general, the raw camera output signals will be transformed in sequence into the standard target color space. The white balance process is optional for scientific cameras. Conversion matrix F_0 transfers the camera RGB signals to standard CIE XYZ values. Additional transformations can be connected to transfer XYZ values into uniform color space, or even color appearance space. In alternative scenario, the XYZ values can be transformed to standard RGB space in order to

match reproduction on a standard CRT monitor. Image quality and analysis is carried out in the standard color space.

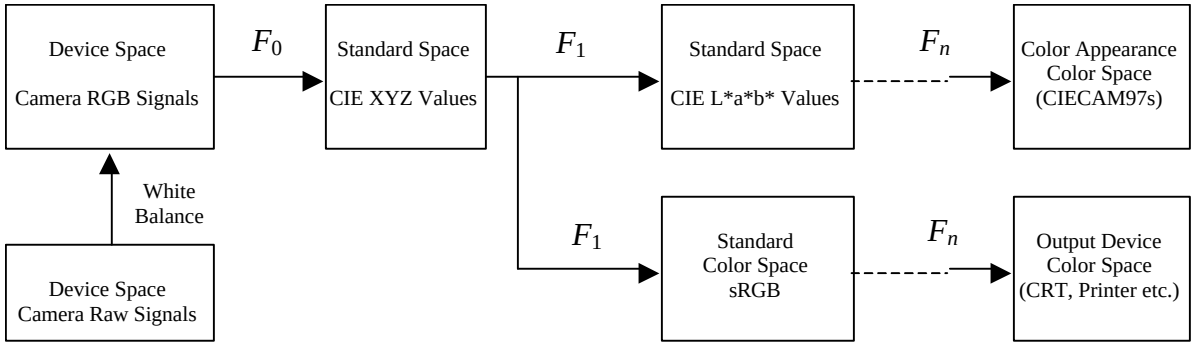

Figure 7.1: Processing pipeline of digital camera signal, where F_s are transformations.

7.2 Imaging Properties Analysis

Chapter 5 showed that each metric usually describes one aspect of characteristics of spectral sensitivity functions. It is risky to evaluate the performance of a set of spectral sensitivity functions as a system with unique image quality metric. Various aspects of spectral sensitivities from designed filters need be evaluated fully before manufacturing. Usually the optimal design of camera spectral sensitivities requires consideration of properties as follows.

Spectral fit: The CIE color matching functions are approximated by asymmetric gaussian functions, linear combination of them, or the combinations of real color filter components with a 3×3 matrix. The merit function can be the mean-squared spectra difference $\|R - R_1\|^2$, where R denotes the reference spectra, and R_1 denotes the approximation spectra, or some pre-defined quality factors, such as *q*-factor and *m*-factor. Davies and Wyszecki approximated CIE 1931 standard color matching functions with the sensitivity of photocell and selected filters [Davies1962] by separately minimizing the spectral difference between color matching functions and the combined sensitivity functions (photocell plus filter layers). They did not evaluate the three sensitivity functions as a whole system. Instead, *q*-factor and *m*-factor can give good evaluation on how far CIE color matching functions have been approximated with

those spectral sensitivity functions. Spectral fit does not account for the human visual perception performance, although a perfect fit shows of course no difference to human visual perception.

Colorimetric performance of a set of object color spectra: In order to obtain a set of spectral sensitivity functions (filters plus detector sensitivity), a mid-size set of standard object color spectra is input into the camera system, the average color difference, maximal color difference and standard deviation are then calculated as criteria for specific spectral sensitivity set. Variety of color difference formulae may be evaluated in uniform color space or in color appearance space, i.e. CIECAM97s. Different color input device may perform differently in terms of color difference scale, so a normalized color difference metric should be used.

Image noise minimization: UMG (refer to Chapter 5 or conceptual description later) is based on minimizing the mean-squared color error in perceptually uniform color space, (eventually in color appearance space) and is essentially different from other quality factors by taking into account both signal-independent and signal-dependent noises and their amplification in target color space when the raw signal is transformed from device-RGB space to CIE XYZ space, then to CIELAB space etc. Some "optimal" spectral sensitivity sets after noise analysis may not be truly optimal, and thus will not work well since noise is amplified too much through those transformations.

Color reproduction accuracy: Maximizing the pre-defined quality factor "UMG" which means minimizing and normalizing the average color difference for a set of spectra samples in CIELAB color space while the noise in original device-RGB space is propagated into CIELAB color space.

RMS noise (granularity): square root of the variance of the signal in target color space. When the raw RGB signals are contaminated with noise, which can be transformed into CIE XYZ space, then into CIELAB space, following the noise propagation rules in chapter 4, the RMS noise of X, Y, and Z, as well as L^*, a^*, and b^* can be calculated. Another paradigm is that the noise in raw device-RGB space is propagated into XYZ color space, then into sRGB color space, if sRGB space is the target color space.

The total color difference includes two aspects (Figure 7.2), one is already defined above, coming from RMS noise, the other comes from the fact that the sensitivity functions do not satisfy the Luther condition, that is, SS are not the linear combinations of color matching functions. The influence of the total color difference can be calculated as the sum of the two portions, or as comprehensive equation as follows:

$$e_0(A_L, G, F_0) = (E\{\|F(t) - F(\hat{t})\|^2\})^{1/2} = (E\{\|F(t) - F(F_0(t_c + h))\|^2\})^{1/2} \quad (7.1)$$

where $\hat{t} = F_0(t_c + h)$ is the estimated tristimulus vector from the output of camera. F is the CIE transformation from XYZ to LAB, t is tristimulus vector, $t_c + h$ is the camera RGB signal vector which includes noise (currently, shot noise and dark noise are considered). F_0 is a linear matrix, determined through optimization of Equation (7.1) and the expectation operation is taken on both the noise term and sample statistics.

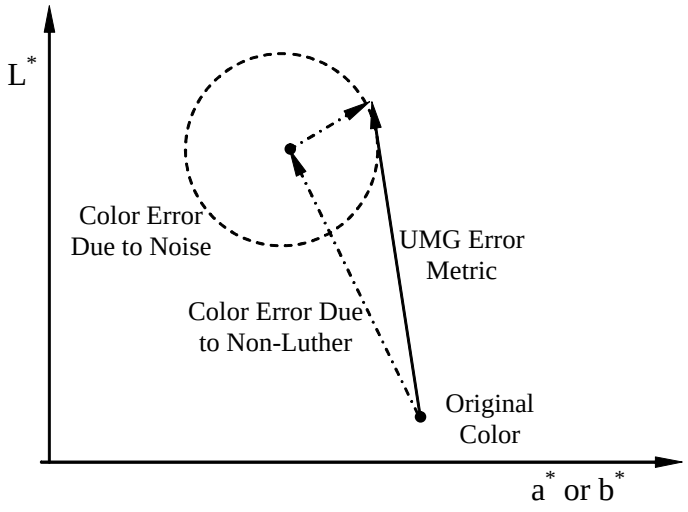

Figure 7.2: Color error sources (non-Luther condition and noise).

There should be balance between color and noise. A comprehensive metric should be the weighted average of color difference and RMS noise. If a manufacturer thinks the reduction of RMS noise is more important, more weight should be put onto it.

Quantization minimization for a defined encoding scheme: For quantization, linear uniform quantization is the simplest choice to digitize signal, in this sense, higher quantization

can reach more accurate signal encoding. But if only 8-bit quantization can be used, linear uniform quantization might be replaced with nonlinear quantization or even vector quantization, both of which could be implemented to reduce the signal encoding error (which is inevitable). It is unknown that whether non-uniform quantization is widely used in camera signal encoding since complicated quantization method is generally used for data compression. Error introduced by quantization is often seen as an added signal-independent stochastic source with an approximately uniform probability distribution. Error introduced by signal quantization is modeled as a stochastic noise source though signal values are rounded to a finite number of levels. The effective quantization interval is often compared with (visually) detectable intensity or color-differences. For many applications the requirement that each quantization interval is not visible, i.e., not introduce visible artifacts, is more stringent than one based on a comparison of the rms quantization noise with image fluctuations from other sources, such as scene content and image detection. Quantization error can also be propagated through the signal path in a similar way to that used for stochastic error propagation.

7.3 Hierarchical Optimization Approach

Although most spectral sensitivity optimization approaches reviewed in Chapter 6 generate color filters to be approximated with manufacturer's basic filter set, it is not a good strategy to do so, since the approximation will result in spectral error, making the "optimal" non-optimal. It is better to let the optimization procedure be a direct model of the fabrication parameters of basic filter set. In this way, no obvious post-approximation error will be introduced. Based on the above analysis, a hierarchical approach is proposed to solve the issue of camera spectral sensitivities optimization. The imaging properties considered are as follows:

1. UMG: average color difference in uniform color space, CCD noise model and noise propagation
2. m-Factor or UMG without noise consideration: spectral fitting
3. RMS noise: minimization of granularity noise

4. Other indices, i.e. minimization of quantization error

Since these merit functions describe different aspects of the optimal sensitivity set. It is a good idea to incorporation all of them into single metric. Currently, UMG ("Unified Measure of Goodness") considers the image noise minimization as well as the colorimetric performance of a set of object color spectra. And quantization error is not considered in this project at this moment by assuming the quantization will be carried out with 12- or 14-bit, which can be considered roughly "continuous." Preliminary experimental results showed that a comprehensive evaluation with both sample-dependent and sample-independent metrics is necessary to obtain optimal set. If an ultimate metric is going to be introduced, different weights should be used instead of equal weight. And strictly, the weights should be determined through objective and subjective methods. It is feasible to optimize those parameters simultaneously, but it may take too much time. Experimental results showed that some of the merit functions are really time-consuming but very effective, such as UMG. In this condition, the range of evaluation with UMG should be greatly reduced while most of the possible optimal candidates are left within this range.

Step-by-step refinement of optimum candidates are preferred. By choosing one or two important properties, one can obtain a collect of optimal sets, other parameters will be determined by comparison among this collect of optimal sets. The spectral sensitivity functions with gaussian shapes are often seen and chosen because of their less noise propagation probability. In previous chapter, the optimal width and peak position of gaussian type functions are found to be in a limited continuous solid. Therefore pre-selection of spectral sensitivities can be started by estimating the width and peak positions first, followed by selecting those sensitivity functions with plausible peak positions and width parameters. The peak wavelength is estimated by just finding the wavelength where peak sensitivity is located, or the gravitational center of the sensitivity curve. The full-width at half peak is obtained by finding the two half-peak ends in the spectral sensitivity curve.

Since multiple evaluation metrics are available, it is difficult to optimize all those indices at the same time. It is even more difficult to numerically assign different weights for those

metrics when a comprehensive objective function is necessary (as linear combination of multiple measures), which should be determined through subjective image quality evaluation procedure. A feasible approach might be to optimize the most important index in the first place, which considers more practical conditions than the others, and obtain a collection of optimal results. By comparing the other indices among the collection according to their degree of importance, the final desired optimal sets are obtained, as shown in Figure 7.3. First, a complete combination of possible filter sets are generated by changing the fabrication parameters of given basic filter components, by assuming most desirable shapes are like gaussian functions, find those combinations which have estimated widths and peak positions located within the optimal range. The combinations usually are reduced greatly.

Then evaluating these combinations with UMG metric with noise consideration, obtain a small collection of spectral sensitivity sets with highest UMG values. Evaluating those small collections of spectral sensitivity functions with spectral fitting metric such as m-factor, and simultaneously evaluating the RMS noise properties of these sets, give a two-dimensional decision to obtain final optimal candidates. The best of the candidates may be subjectively evaluated to pick out the finest (manufacturing cost and the filter stability can be evaluated in this stage as well), otherwise just select the set with highest comprehensive metric value.

Again, it might be a good idea to optimize one primary aspect, and then compare the secondary aspect among those optimized sets. Subjective method may be used to judge which levels of the two aspects are comparable, which is left as future work.

It is worth noting that Liu, Berns and Shu introduced an optimization algorithm for designing colored glass filters to simulate CIE illuminant D65 [Liu1991], where a multistage logical decision method is proposed to obtain the optimal selection of filters. The framework of the method shared some similarity with the hierarchical approach to the design of colorimetric filters.

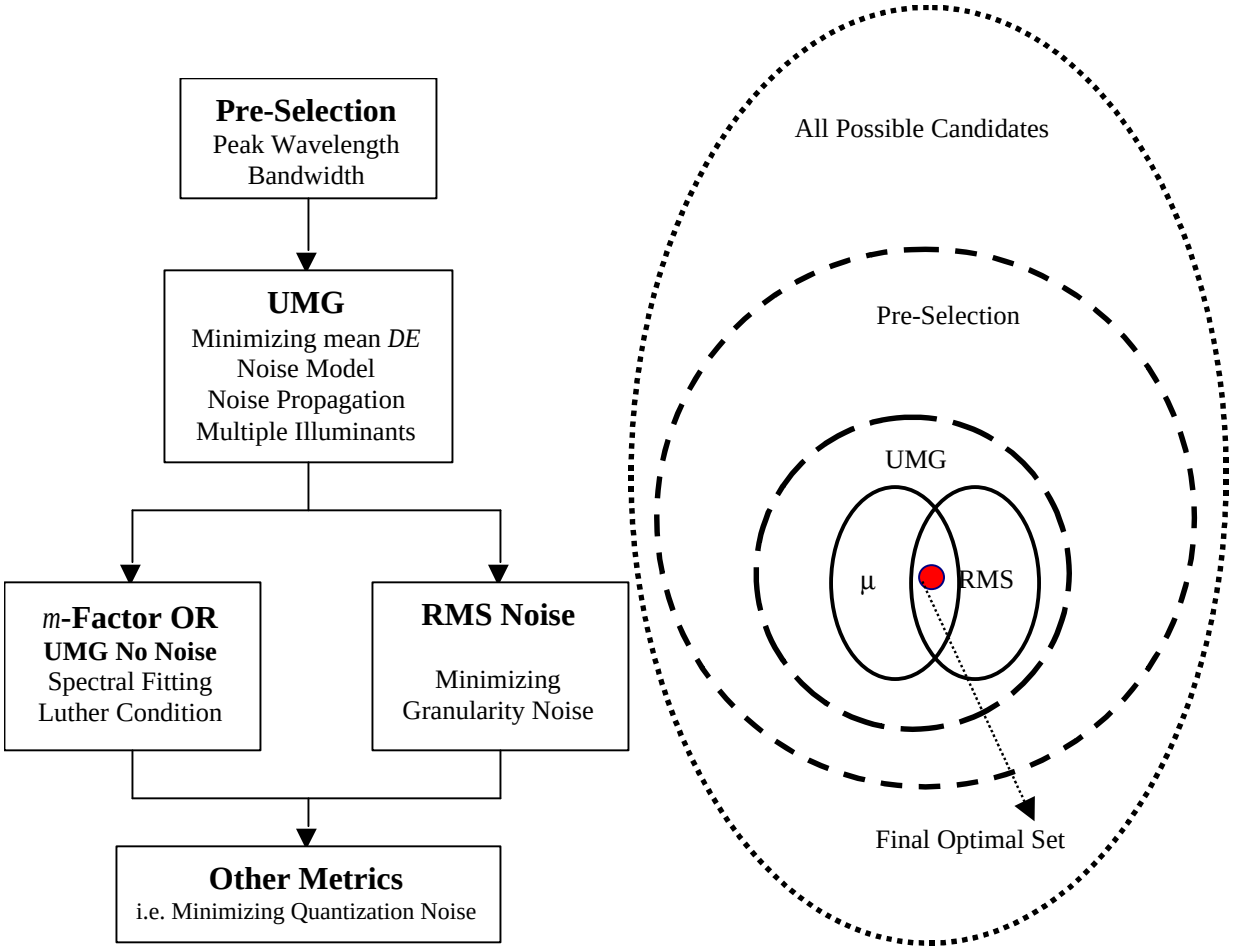

Figure 7.3: Hierarchical approach to search the optimal spectral sensitivity function set.

7.4 Conclusions

This chapter outlined a practically feasible and systematic approach to the optimal design of spectral sensitivities for colorimetric reproduction. The hierarchical approach takes advantages of multiple metrics to describe the various aspects of spectral sensitivities. The approach is further extended to design spectral sensitivity functions for spectral reproduction, as described in Appendix F. The approach has been pratically applied to design multiple imaging channels for the Quantix camera. The experiments and results will be discussed in Chapter 9.

8 COLOR CORRECTION IN COLOR IMAGING

8.1 Introduction

Illumination affects the recorded or observed colors of objects. Objects in pictures taken under tungsten light will tend to be reddish and they tend to appear pale under fluorescent light. These color shifts due to the illuminant changes in the image needed be corrected to the expected color under some reference illuminant. The human visual system has the ability to discount the color shift due to illuminant change, which is referred to as color constancy [see reviews in Barnard1999, Rutherford2000], and color constancy is usually incomplete [Wandell1995, pg. 156 in Fairchild1998, also in Brainard1997b & Brainard1998, Kraft1999].

One of the most important tasks for digital camera is illuminant estimation, that is, to infer the illuminant information from upon the scene it captures or diminish the affect of the illumination to obtain data which more precisely reflects the physical content of the scene. The method is called computational color constancy [see reviews in Barnard1999]. The gray world assumption is the simplest approach to estimate illuminant. In this chapter, the task is not illuminant estimation, but the correction of color shifts once the illuminant is known through measurement or estimation. The color shifts due to the illuminant changes can be represented as a difference between the tristimulus values under different illuminants (Figure 8.1). If the surface reflectance spectra can be estimated from the tristimulus values under reference illuminant, it is possible to acquire the tristimulus values under any test illuminant. Some work was done in this area [Vrhel1992], but its accuracy is limited to the number of channels.

The UMG metric emphasizes certain specific taking and target illuminant pairs, but in practice, the taking illuminant for a camera may be numerous and the target illuminant in general is limited to a few standard illuminants. In camera signal processing, generally one transformation matrix is embedded for a pair of reference taking and target illuminants. It is

impossible to calculate and store an illumination related matrix for all the illuminations that might occur when using the camera. For any other illuminant, a color correction matrix to adjust the camera signal into the target signal under reference illuminant is calculated *in situ*. This chapter discusses how to choose this correction matrix due to the illuminant change. Since cameras transform RGB signals to XYZ values, the conversion matrix may happen in the RGB space or XYZ space, which gives different performance.

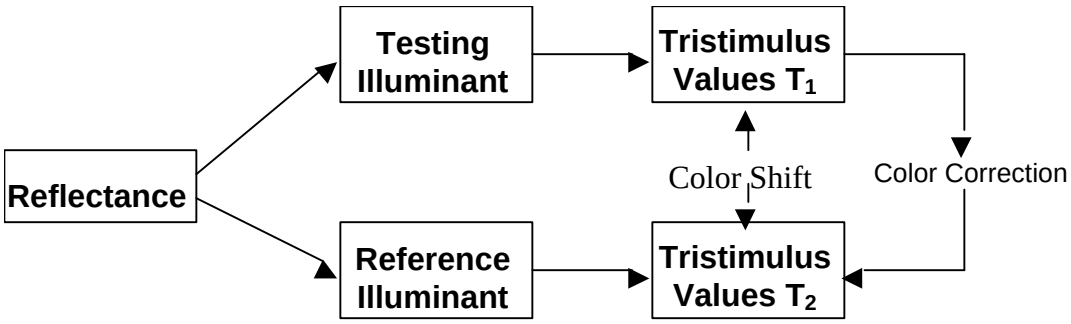

Figure 8.1: Correction of color shifts due to illuminant changes.

8.2 Color Correction Methods

8.2.1 White Point Mapping (WPM)

This method assumes that the proportional color shift due to the illuminant changes occurs in each color, and uses the relationship of testing white and reference white to determine the quantity of color correction. The correction matrix is defined as

$$D = \begin{bmatrix} \frac{X^{w}_{reference}}{X^{w}_{testing}} & & \\ & \frac{Y^{w}_{reference}}{Y^{w}_{testing}} & \\ & & \frac{Z^{w}_{reference}}{Z^{w}_{testing}} \end{bmatrix} \tag{8.1}$$

such that

$$T_2 = D \cdot T_1 \tag{8.2}$$

where $T^{w}_{reference} = [X^{w}_{reference}, Y^{w}_{reference}, Z^{w}_{reference}]$ and $T^{w}_{testing} = [X^{w}_{testing}, Y^{w}_{testing}, Z^{w}_{testing}]$ are the tristimulus values of the reference white and testing white, T_2 and T_1 are tristimulus values of object under reference and testing illuminants. The elements of *D* may also be determined through least-squares method, in which case, the coordinates of white (and gray-scale) may shift, Finlayson and Drew proposed white-point preserving approach to solve this problem [Finlayson1997].

8.2.2 Principal Components Method

Vrhel and Trussell introduced this correction method initially [Vrhel1992], based on a standard assumption on natural reflectance spectra, that is, naturally occurred reflectance spectra can be adequately approximated by the linear combination of a small number of eigenvectors generated from a typical ensemble of spectra [Maloney and Wandell, 1986]:

$$R = \bar{R} + \sum_{i=1}^{m} a_i \mathbf{b}_i = \bar{R} + \mathbf{B}a \tag{8.3}$$

where matrix **B** contains the eigenvectors, **a** are the coefficients, $\bar{R}$ is the mean spectrum of the ensemble. The tristimulus values under testing illuminant is calculated as

$$T_1 = A^T L_T \mathbf{B}a + A^T L_T \bar{R} = A^T L_T \mathbf{B}a + \bar{T}_1 \tag{8.4}$$

where $\bar{T}_1 = A^T L_T \bar{R}$. From Equation (8.4) the coefficients can be calculated by

$$a = (A^T L_T \mathbf{B})^{-1} (T_1 - \bar{T}_1) \tag{8.5}$$

Therefore the tristimulus values under reference illuminant corrected by principal components method is

$$\begin{aligned} T_2 &= A^T L_R \mathbf{B}a + A^T L_R \bar{R} \\ &= A^T L_R \mathbf{B}(A^T L_T \mathbf{B})^{-1}(T_1 - \bar{T}_1) + \bar{T}_2 \end{aligned} \tag{8.6}$$

Arai *et al* introduced color correction method based on the spectral reflectance estimation using a neural network [Arai1996]. Since the processing capability within a camera unit is limited, and the signal transformation need be processed quickly, this study will discuss only white-point-conversion-type correction method.

8.3 General Camera Signal Processing

The signal is transformed as described in Figure 8.2. The camera raw signal is first white-balanced, and then transformed to CIE XYZ values, additional matrix may be used to transform signal into CIELAB or standard RGB space that matches standard monitor.

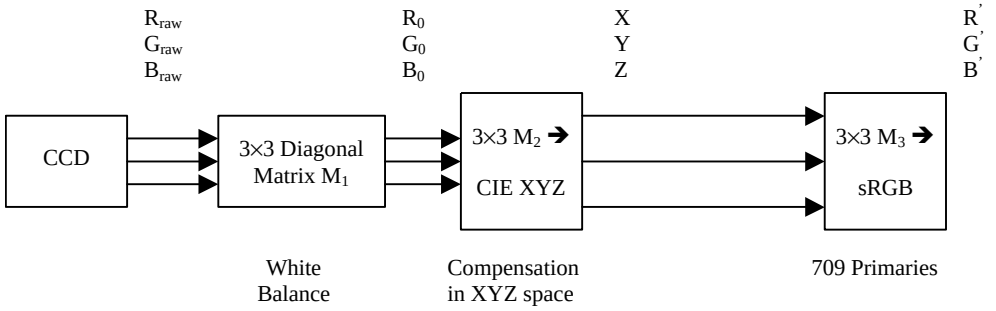

Figure 8.2: Generic signal transformation in a CCD camera.

The matrices are calculated as follows. M_1 can be calculated by white balancing. The camera output signal of illuminant white is assumed to be the same for each channel, assuming K is the normalized constant (=255 for 8-bit camera),

$$R_{0w} = S_R^T L_c \quad G_{0w} = S_G^T L_c \quad B_{0w} = S_B^T L_c \tag{8.7}$$

where R_{0w}, G_{0w}, and B_{0w} are the camera raw signal for illuminant white.

$$k_R = K \Big/ S_R^T L_c \,,\; k_G = K \Big/ S_G^T L_c \,,\; k_B = K \Big/ S_B^T L_c \tag{8.8}$$

Therefore,

$$M_1 = \begin{bmatrix} k_R & & \\ & k_G & \\ & & k_B \end{bmatrix} = \begin{bmatrix} K \Big/ S_R^T L_c & & \\ & K \Big/ S_G^T L_c & \\ & & K \Big/ S_B^T L_c \end{bmatrix} \tag{8.9}$$

Conversion matrix $B_{opt} = M_2 M_1$ is obtained through optimization by maximizing quality factor, such as UMG, or minimizing average color difference. So matrix M_2 can be easily obtained as:

$$M_2 = B_{opt} M_1^{-1} \tag{8.10}$$

The matrix M_3 transforms the CIE XYZ tristimulus values to sRGB values; this is a static matrix and is specified as:

$$M_3 = \begin{bmatrix} 3.2406 & -1.5372 & -0.4986 \\ -0.9689 & 1.8758 & 0.0415 \\ 0.0557 & -0.2040 & 1.0570 \end{bmatrix} \tag{8.11}$$

8.4 Correction with the Same Taking and Viewing Illuminants

For color correction in color imaging, the following matrix operations are used commonly:

$$\begin{bmatrix} a_1 & a_2 & a_3 \\ b_1 & b_2 & b_3 \\ c_1 & c_2 & c_3 \end{bmatrix} \begin{bmatrix} & M_d & \end{bmatrix} = \begin{bmatrix} a_1 a & a_2 b & a_3 g \\ b_1 a & b_2 b & b_3 g \\ c_1 a & c_2 b & c_3 g \end{bmatrix} \tag{8.12}$$

and

$$\begin{bmatrix} & M_d & \end{bmatrix} \begin{bmatrix} a_1 & a_2 & a_3 \\ b_1 & b_2 & b_3 \\ c_1 & c_2 & c_3 \end{bmatrix} = \begin{bmatrix} a_1 a & a_2 a & a_3 a \\ b_1 b & b_2 b & b_3 b \\ c_1 g & c_2 g & c_3 g \end{bmatrix} \tag{8.13}$$

where color correction matrix is

$$M_d = \begin{bmatrix} a & & \\ & b & \\ & & g \end{bmatrix} \tag{8.14}$$

In this study, at first, the variation of the optimal 3×3 conversion matrix due to illumination changes will be investigated. The CIE D65 illuminant will be given as reference, any other illuminants, like CIE A, F2 and F6 will be specified as testing illuminants. Average color difference and maximal color difference will be calculated for a standard data set also when the illuminant changes. The standard data set used here are Vrhel-Trussell reflectance data set with 354 samples, alternative data set can be Macbeth ColorChecker with 24 samples.

A total of three sets of RGB spectral sensitivities will be tested. One is the set designed for Quantix camera, or the fabricated sensitivity set based on the design (their shape can be found in Chapter 3 as red, green and blue channels, or Figure 9.6(b) in Chapter 9). The other two sets are the Sony 1CCD3SS and 3CCD3SS spectral sensitivity functions, as shown in Figure 8.3.

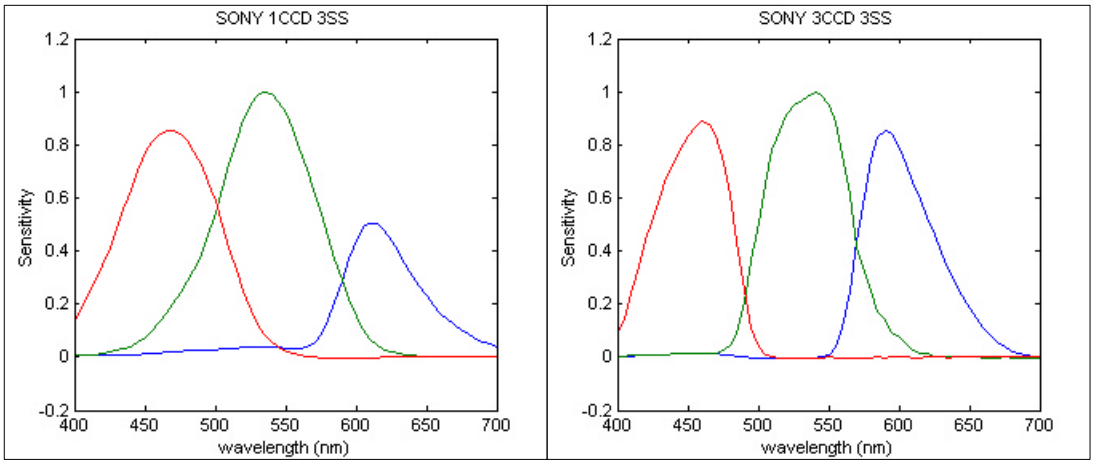

(a) (b)

Figure 8.3: Sony spectral sensitivity function sets: (a) 1CCD 3SS; (b) 3CCD 3SS.

In this chapter, the notation "A→B" means the colorimetric information under illuminant A is converted to that under illuminant B. In general, the theoretical 3×3 matrix that transforms the raw RGB signals to standard signal in standard color space, e.g. CIE XYZ in the processing pipeline of digital camera signal will change when taking and viewing illuminants change from D65 to other illuminants. Table 8-1 to 8-4 show that the conversion matrix does not change too much for specific set of spectral sensitivities, and the color difference performance is also roughly the same when both taking and viewing illuminants change from one type to another. Simply, the matrix derived from D65→D65 can be applied when the taking and viewing illuminants are the same. The performance is shown in Table 8-5. In this table, since the conversion matrix is only truly optimal for D65→D65, it is only approximately optimal for other illuminant pairs, therefore the color difference performance for these illuminant pairs is not as good as for D65→D65. It can be seen that for Quantix SS and Sony 3CCD 3SS single matrix is suitable, but for Sony 1CCD 3SS, the color difference is very large for F2→F2 and F6→F6. Table 8-1 and 8-2 also indicate that the fabricated filters have slightly worse color difference and color correction performance than the theoretical designed counterpart. Correction calculations from now on will only consider the fabricated filters.

Table 8–1: The performance of the designed filter sets for Quantix camera.

Illuminant Pair	Optimal 3×3 Matrix **M** RGB➔XYZ			Mean ΔE^*_{ab}	Mean ΔE^*_{94}	Max ΔE^*_{ab}	Max ΔE^*_{94}
D65-D65	1.7514	0.6106	1.8081	1.34	0.75	6.50	2.76
	0.7889	3.1024	-0.5414				
	-0.0298	0.1186	12.3948				
A-A	1.7101	0.8089	1.0726	1.61	0.84	10.91	4.94
	0.7231	3.4242	-1.7108				
	-0.0459	0.1891	12.1939				
F2-F2	1.7099	0.7028	2.0795	1.27	0.71	6.86	3.04
	0.7988	3.3007	-0.5200				
	-0.0096	0.0717	12.8581				
F6-F6	1.7010	0.7378	2.0913	1.24	0.69	6.81	2.98
	0.7969	3.3298	-0.5282				
	-0.0091	0.0687	12.8870				

Table 8–2: The performance of the fabricated filter sets for Quantix camera.

Illuminant Pair	Optimal 3×3 Matrix **M** RGB➔XYZ			Mean ΔE^*_{ab}	Mean ΔE^*_{94}	Max ΔE^*_{ab}	Max ΔE^*_{94}
D65-D65	2.0792	0.5755	1.8392	1.71	0.96	8.61	3.48
	0.9813	3.1417	-0.9797				
	-0.0332	0.0998	12.8149				
A-A	2.0675	0.7204	1.2593	1.87	0.99	9.23	4.17
	0.9129	3.4942	-2.3506				
	-0.0440	0.1581	12.5883				
F2-F2	1.9834	0.7016	2.0942	1.53	0.86	8.55	3.70
	0.9786	3.4072	-0.9816				
	-0.0140	0.0588	13.4068				
F6-F6	1.9715	0.7404	2.1018	1.48	0.84	8.44	3.63
	0.9759	3.4456	-0.9967				
	-0.0134	0.0567	13.4457				

Table 8–3: The performance of the SONY 3CCD 3SS Spectral Sensitivities.

Illuminant Pair	Optimal 3×3 Matrix **M** RGB➔XYZ			Mean ΔE^*_{ab}	Mean ΔE^*_{94}	Max ΔE^*_{ab}	Max ΔE^*_{94}
D65-D65	1.4646	0.2121	0.2566	1.50	0.81	8.67	3.57
	0.7155	0.9917	-0.0332				
	-0.0108	0.0386	1.8947				
A-A	1.4721	0.2241	0.2319	1.72	0.90	8.98	3.41
	0.6899	1.0541	-0.1138				
	-0.0084	0.0401	1.9119				
F2-F2	1.3951	0.2582	0.3169	1.42	0.78	8.65	3.98
	0.7282	1.0536	-0.0276				
	-0.0035	0.0218	2.0242				
F6-F6	1.3887	0.2711	0.3173	1.39	0.77	8.62	3.94
	0.7297	1.0610	-0.0319				
	-0.0033	0.0216	2.0300				

Table 8–4: The performance of the SONY 1CCD 3SS Spectral Sensitivities.

Illuminant Pair	Optimal 3×3 Matrix **M** RGB➔XYZ			Mean ΔE^*_{ab}	Mean ΔE^*_{94}	Max ΔE^*_{ab}	Max ΔE^*_{94}
D65-D65	1.8119	0.4364	-0.0266	2.82	1.63	18.19	5.98
	0.7768	1.1087	-0.2887				
	0.0588	-0.1362	1.5351				
A-A	1.5070	0.7113	-0.4143	3.04	1.56	25.88	6.37
	0.5928	1.2728	-0.5252				
	0.0141	-0.0806	1.3391				
F2-F2	2.0158	0.5787	-0.0159	2.72	1.36	24.32	6.67
	0.8590	1.1878	-0.2805				
	0.0446	-0.1050	1.7436				
F6-F6	2.0304	0.5898	-0.0279	2.72	1.36	24.13	6.68
	0.8646	1.1949	-0.2917				
	0.0426	-0.0952	1.7537				

Table 8–5: Using optimal matrix from illuminant pairs D65-D65 as conversion matrix for A-A, F2-F2 and F6-F6 to calculate color difference.

1CCD 3SS

Illuminants	ΔE^*_{ab}	ΔE^*_{94}	Max ΔE^*_{ab}	Max ΔE^*_{94}	$B_{opt}=M_1M_2$		
D65-D65	2.82	1.63	18.19	5.98	1.8119	0.4364	-0.0266
A-A	4.77	2.85	17.51	8.03	0.7768	1.1087	-0.2887
F2-F2	10.24	6.52	47.94	17.69	0.0588	-0.1362	1.5351
F6-F6	11.56	7.11	58.82	19.27			

3CCD 3SS

	ΔE^*_{ab}	ΔE^*_{94}	Max ΔE^*_{ab}	Max ΔE^*_{94}	$B_{opt}=M_1M_2$		
D65-D65	1.50	0.81	8.67	3.57	1.4646	0.2121	0.2566
A-A	2.02	1.06	12.21	5.19	0.7155	0.9917	-0.0332
F2-F2	4.62	3.01	12.43	6.51	-0.0108	0.0386	1.8947
F6-F6	4.76	3.10	12.84	6.75			

Quantix

	ΔE^*_{ab}	ΔE^*_{94}	Max ΔE^*_{ab}	Max ΔE^*_{94}	$B_{opt}=M_1M_2$		
D65-D65	1.71	0.96	8.61	3.48	2.0792	0.5755	1.8392
A-A	2.12	1.08	11.98	3.72	0.9813	3.1417	-0.9797
F2-F2	5.63	3.74	12.42	9.17	-0.0332	0.0998	12.8149
F6-F6	5.95	3.96	13.03	9.69			

8.5 Correction with Different Taking and Viewing Illuminants

8.5.1 Introduction

The color correction when taking and viewing illuminants are different can be illustrated in Figure 8.4. In the figure, D65 is referred as a standard taking and viewing illuminant, raw signal from camera is converted to CIE XYZ through white balance (M_1) and compensation matrix (M_2), where $B_{opt}=M_2M_1$ is obtained through optimization. For any other illuminants (CIE A, F2, F6), the same conversion matrix B_{opt} will be used, but a second diagonal correction matrix is concatenated in order to correct color under the other illuminant into CIE XYZ values under

D65. This diagonal correction matrix M_d is similar to the widely used von-Kries transformation and may be placed before or after the conversion matrix, as shown by Equations (8.12)-(8.13).

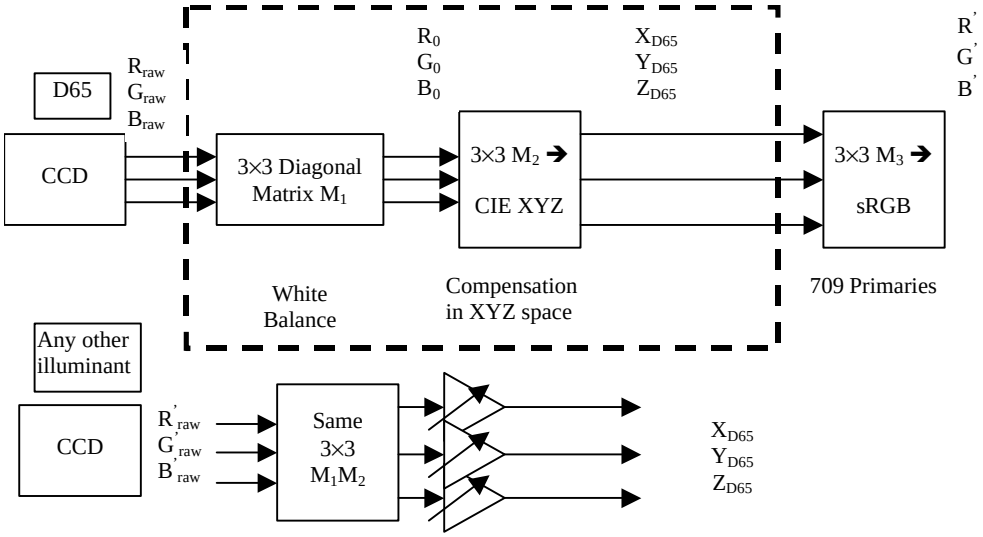

Figure 8.4: Color correction when taking and viewing illuminants are different.

8.5.2 Optimal Matrix for Each Illuminant Pair

An individual optimal matrix can be obtained for each taking and viewing illuminant pairs respectively by minimizing mean color difference for an ensemble of object colors. Table 8-6, 8-7 and 8-8 show the matrices and color difference performance for three sets of spectral sensitivity functions. The color difference is averagely the same if optimal matrix is applied for each illuminant pair. The optimal matrices B_{opt} for different illuminant pairs vary drastically due to the curve shape and relative scale of the spectral power distribution of illuminants.

Table 8–6: Using optimal matrix to calculate DE^* performance (1CCD 3SS).

	$B_{opt}=M_1M_2$			Mean ΔE^*_{ab}	Mean ΔE^*_{94}	Max ΔE^*_{ab}	Max ΔE^*_{94}
D65-D65	1.8119	0.4364	-0.0266	2.82	1.63	18.19	5.98
	0.7768	1.1087	-0.2887				
	0.0588	-0.1362	1.5351				
A-D65	0.9247	0.7122	-0.1508	5.27	2.93	31.83	10.86
	0.3061	1.4256	-0.5579				
	0.0466	-0.1768	3.6560				
F2-D65	16.0222	2.3794	1.2306	3.42	1.89	21.53	7.55
	5.6982	8.0864	-0.8934				
	0.3594	-0.5844	19.0750				
F6-D65	16.9809	2.2188	1.5463	3.55	1.98	22.08	7.91
	6.0297	7.9169	-0.6255				
	0.3759	-0.5957	21.4572				

Table 8–7: Using optimal matrix to calculate DE^* performance (3CCD 3SS).

	$B_{opt}=M_1M_2$			Mean ΔE^*_{ab}	Mean ΔE^*_{94}	Max ΔE^*_{ab}	Max ΔE^*_{94}
D65-D65	1.4646	0.2121	0.2566	1.50	0.81	8.67	3.57
	0.7155	0.9917	-0.0332				
	-0.0108	0.0386	1.8947				
A-D65	0.9219	0.3511	0.7563	1.44	0.85	8.79	4.20
	0.4133	1.2560	0.0878				
	-0.0133	0.0428	5.7819				
F2-D65	10.0173	0.4993	3.9350	1.99	1.14	13.80	7.07
	4.1648	7.8429	1.1907				
	-0.2481	0.7619	22.9432				
F6-D65	10.3671	0.3070	4.4914	2.17	1.27	14.69	7.58
	4.2680	7.6833	1.5895				
	-0.2783	0.8081	25.7413				

Table 8–8: Using optimal matrix to calculate DE^* performance (Quantix).

	$B_{opt}=M_1M_2$			Mean ΔE^*_{ab}	Mean ΔE^*_{94}	Max ΔE^*_{ab}	Max ΔE^*_{94}
D65-D65	2.0792	0.5755	1.8392	1.71	0.96	8.61	3.48
	0.9813	3.1417	-0.9797				
	-0.0332	0.0998	12.8149				
A-D65	1.2883	1.1463	4.3616	1.34	0.77	7.89	4.69
	0.5192	4.1697	-1.5123				
	-0.1021	0.2377	37.8571				
F2-D65	14.2956	0.4823	28.4139	1.95	1.12	13.28	7.03
	5.4244	25.5059	2.9155				
	-0.4908	2.3351	152.5723				
F6-D65	14.7914	-0.2142	32.3669	2.10	1.23	14.04	7.53
	5.5403	25.1184	5.7701				
	-0.5481	2.4949	171.0496				

8.5.3 XYZ Correction Matrix before Transformation

It has been found that, when taking and viewing illuminants are the same, (D65➔D65, A➔A, F2➔F2, and F6➔F6) the optimal matrix obtained from D65➔D65 can roughly satisfy the other three cases. If a new diagonal matrix converts the white point of illuminants A, F2 and F6 to that of D65, which is similar to von Kries transform, the diagonal matrix may be qualified as the color correction matrix. The white point are calculated "as is" without normalization from spectral sensitivity (SS) in camera RGB space or color matching functions (CMF) in CIE XYZ space. If calculated in XYZ space, the matrix can be written as:

$$M_d = \begin{bmatrix} X_{w_{D65}} / X_{W_{Other}} & & \\ & Y_{w_{D65}} / Y_{W_{Other}} & \\ & & Z_{w_{D65}} / Z_{W_{Other}} \end{bmatrix} \tag{8.15}$$

$$M_{\text{optimal Other}\rightarrow\text{D65}} = M_{\text{optimal D65}\rightarrow\text{D65}} M^{XYZ}_{correction} \tag{8.16}$$

Calculation results of correction matrix and color difference are listed in Table 8-9, 8-10 and 8-11. The color difference from correction matrix in this way is unacceptable: for each set of SS, the average color difference (in shaded items) is about or over 10 units.

Table 8–9: XYZ correction matrix before transformation matrix (3CCD 3SS).

	White Point from CMF1931			Diagonal Elements in Color Correction Matrix M_d			ΔE^*_{ab}	ΔE^*_{94}	Max ΔE^*_{ab}	Max ΔE^*_{94}
D65	2005.814	2112.730	2296.673				1.50	0.81	8.67	3.57
A	2364.500	2155.824	766.932	0.848	0.980	2.995	19.50	12.46	31.58	30.89
F2	290.400	292.827	197.215	6.907	7.215	11.646	11.67	7.50	26.17	19.93
F6	284.995	292.808	176.328	7.038	7.215	13.025	11.71	7.48	28.06	19.84

Table 8–10: XYZ correction matrix before transformation matrix (1CCD 3SS).

	White Point from CMF1931			Diagonal Elements in Color Correction Matrix M_d			ΔE^*_{ab}	ΔE^*_{94}	Max ΔE^*_{ab}	Max ΔE^*_{94}
D65	2005.814	2112.730	2296.673				2.82	1.63	18.19	5.98
A	2364.500	2155.824	766.932	0.848	0.980	2.995	32.66	20.58	76.08	49.39
F2	290.400	292.827	197.215	6.907	7.215	11.646	8.74	5.54	31.83	20.84
F6	284.995	292.808	176.328	7.038	7.215	13.025	9.71	6.13	36.08	23.09

Table 8–11: XYZ correction matrix before transformation matrix (Quantix).

	White Point from CMF1931			Diagonal Elements in Color Correction Matrix M_d			ΔE^*_{ab}	ΔE^*_{94}	Max ΔE^*_{ab}	Max ΔE^*_{94}
D65	2005.814	2112.730	2296.673				1.71	0.96	8.61	3.48
A	2364.500	2155.824	766.932	0.848	0.980	2.995	23.27	15.13	43.03	39.19
F2	290.400	292.827	197.215	6.907	7.215	11.646	15.11	9.84	37.79	27.58
F6	284.995	292.808	176.328	7.038	7.215	13.025	15.71	10.22	41.93	28.65

8.5.4 RGB Correction Matrix before Transformation

The ratio of raw signals in RGB space from the testing illuminant and CIE D65 is calculated as the diagonal elements of the color correction matrix M_d, and do the color correction:

$$M_d = \begin{bmatrix} R_{w_{D65}} / R_{w_{Other}} & & \\ & G_{w_{D65}} / G_{w_{Other}} & \\ & & B_{w_{D65}} / B_{w_{Other}} \end{bmatrix} \tag{8.17}$$

$$M_{\text{optimal Other}\rightarrow\text{D65}} = M_{\text{optimal D65}\rightarrow\text{D65}} M_{correction}^{RGB} \tag{8.18}$$

The process can be illustrated as

$$\begin{bmatrix} R_{Other}^{white} \\ G_{Other}^{white} \\ B_{Other}^{white} \end{bmatrix} \xrightarrow[\substack{\text{von-Kries-Type} \\ \text{Color Correction}}]{M_d} \begin{bmatrix} R_{D65}^{white} \\ G_{D65}^{white} \\ B_{D65}^{white} \end{bmatrix} \xrightarrow[\substack{\text{Optimized} \\ \text{Transformation} \\ \text{From D65}\rightarrow\text{D65}}]{M_{3\times3}} \begin{bmatrix} X_{D65}^{white} \\ Y_{D65}^{white} \\ Z_{D65}^{white} \end{bmatrix}$$

Corresponding calculation results of correction matrix and color difference are list in Tables 8-12 to 8-14. This time, it is found that, the optimal matrix from D65➔D65 together with the color correction matrix M_d obtained from the ratio of the RGB raw signals of the testing illuminant and CIE D65 can be a good choice to obtain the reasonable conversion. It is also true that the color difference performance for A➔D65 is better than that for F2➔D65 and F6➔D65 consistently for three sets of camera spectral sensitivities. The Sony 3CCD 3SS set performs the best, followed by the designed Quantix spectral sensitivities, and the Sony 1CCD 3SS.

Table 8–12: RGB correction matrix before transformation matrix (3CCD 3SS).

→D65	White Point from SS			Diagonal Elements in Color Correction Matrix M_d			ΔE_{ab}^*	ΔE_{94}^*	Max ΔE_{ab}^*	Max ΔE_{94}^*
D65	943.480	1481.338	1194.680				1.50	0.81	8.67	3.57
A	1371.828	1189.018	385.307	0.688	1.246	3.101	2.73	1.77	14.55	7.78
F2	154.914	173.717	96.695	6.090	8.527	12.355	5.80	3.09	20.67	10.77
F6	152.401	173.971	86.020	6.191	8.515	13.888	6.47	3.47	21.91	12.26

Table 8–13: RGB correction matrix before transformation matrix (1CCD 3SS).

→D65	White Point from SS			Diagonal Elements in Color Correction Matrix M_d			ΔE_{ab}^*	ΔE_{94}^*	Max ΔE_{ab}^*	Max ΔE_{94}^*
D65	647.639	1803.822	1574.265				2.82	1.63	18.19	5.98
A	1010.238	1441.250	623.507	0.641	1.252	2.525	6.87	4.25	29.96	14.46
F2	80.253	213.182	120.766	8.070	8.461	13.036	8.01	4.54	38.84	17.46
F6	76.915	211.947	107.414	8.420	8.511	14.656	8.69	4.95	39.78	19.75

Table 8–14: RGB correction matrix before transformation matrix (Quantix).

→D65	White Point from SS			Diagonal Elements in Color Correction Matrix M_d			ΔE^*_{ab}	ΔE^*_{94}	Max ΔE^*_{ab}	Max ΔE^*_{94}
D65	665.851	517.308	177.248				1.71	0.96	8.61	3.48
A	971.801	401.629	59.209	0.685	1.288	2.994	3.91	2.40	19.04	10.37
F2	110.872	58.102	14.576	6.006	8.904	12.160	7.52	4.13	22.60	13.49
F6	109.501	57.548	12.982	6.081	8.989	13.653	8.45	4.65	26.28	15.79

8.5.5 RGB Correction Matrix after Transformation

If color correction matrix is applied after the 3×3 conversion matrix, similar strategy can be performed. The ratio of the camera raw signals of illuminant color for the testing illuminant and CIE D65 is set as the color correction matrix, and

$$M_{optimal\quad Other\rightarrow D65} = M^{RGB}_{correction} M_{optimal\ D65\rightarrow D65} \tag{8.19}$$

The color difference performance is calculated and found very large; perhaps the physical meaning of this approach is wrong.

8.5.6 XYZ Correction Matrix after Transformation

If the color correction matrix is modeled as the ratio of the XYZ values of the illuminant color for testing illuminant and D65, and placed after the optimized color transformation, the color difference performance is much better than 8.5.3. The signal transformation is shown below.

$$\begin{bmatrix} R^{white}_{Other} \\ G^{white}_{Other} \\ B^{white}_{Other} \end{bmatrix} \xrightarrow[\substack{\text{Optimized} \\ \text{Transformation} \\ \text{From D65}\rightarrow\text{D65}}]{M_{3\times3}} \begin{bmatrix} X^{white}_{Other} \\ Y^{white}_{Other} \\ Z^{white}_{Other} \end{bmatrix} \xrightarrow[\substack{\text{von-Kries-Type} \\ \text{Color Correction}}]{M_d} \begin{bmatrix} X^{white}_{D65} \\ Y^{white}_{D65} \\ Z^{white}_{D65} \end{bmatrix}$$

$$M_{optimal\quad Other\rightarrow D65} = M^{XYZ}_{correction} M_{optimal\ D65\rightarrow D65} \tag{8.20}$$

The color correction performance, which is listed in Table 8-15, 8-16 and 8-17, is reasonable, but is not as good as that obtained in Section 8.5.4. There are two reasons. First, the optimal transformation fit illuminant D65→D65 the best; it has been shown in Table 8-5 that although the matrix is applicable to other illuminant pairs, but it is not optimal to do so. Second, the von-Kries-type of transformation is more accurate for sharper sensors [Finlayson, Drew and

Funt in Finlayson1994]. All spectral sensitivity functions discussed here are comparatively sharper sensors than CIE XYZ color matching functions, color correction is more useful in RGB space and gives better color difference performance.

Table 8–15: XYZ correction matrix after transformation matrix (3CCD 3SS).

	Mean ΔE^*_{ab}	Mean ΔE^*_{94}	Max ΔE^*_{ab}	Max ΔE^*_{94}
D65	1.50	0.81	8.67	3.57
A	7.59	4.50	24.00	13.56
F2	6.19	3.66	18.13	8.28
F6	6.36	3.79	18.56	9.12

Table 8–16: XYZ correction matrix after transformation matrix (1CCD 3SS).

	Mean ΔE^*_{ab}	Mean ΔE^*_{94}	Max ΔE^*_{ab}	Max ΔE^*_{94}
D65	2.82	1.63	18.19	5.98
A	9.06	5.86	33.20	15.25
F2	13.17	7.78	58.18	17.21
F6	14.60	8.44	68.89	18.74

Table 8–17: XYZ correction matrix after transformation matrix (Quantix).

	Mean ΔE^*_{ab}	Mean ΔE^*_{94}	Max ΔE^*_{ab}	Max ΔE^*_{94}
D65	1.71	0.96	8.61	3.48
A	7.33	4.40	24.73	12.38
F2	7.49	4.46	18.46	9.36
F6	7.88	4.74	19.32	9.89

8.6 Weighting Functions

It is desired that some kind of neat modification to the correction matrix can increase the performance of color correction than that obtained in Section 8.5. In the simulation, weighting function has been used to modify the color correction matrix M_d.

$$M_d = \begin{bmatrix} \dfrac{W_l L_{D65} S_R}{W_l L_{Other} S_R} & & \\ & \dfrac{W_l L_{D65} S_G}{W_l L_{Other} S_G} & \\ & & \dfrac{W_l L_{D65} S_B}{W_l L_{Other} S_B} \end{bmatrix} \tag{8.21}$$

where W_l is a weighting function. The spectra of illuminants L_{D65} and L_{Other} are represented as diagonal matrices so that the matrix operation can be used.

The first tested weighting function is chosen as the *q*-factor curve P_l indicated by Figure 5.2. Initial results do not show this correction matrix has better performance than the previous approach in Section 8.5.4. The result is omitted here. Some other weighting functions have also been tested, e.g. considering the correlation of the illuminants: In Equation (8.21) P_l is replaced with L_{Other} or L_{D65}. Experiment found that L_{D65} as weighting function gave the best correction among the three cases involving weighting functions, and results of correction matrix and color difference were listed in Table 8-18, 8-19 and 8-20. But the performance is not better than that obtained previously in Section 8.5.4.

Table 8–18: Weighted RGB correction matrix before transformation matrix (3CCD 3SS).

	Diagonal Elements in Color Correction Matrix M_d			ΔE^*_{ab}	ΔE^*_{94}	Max ΔE^*_{ab}	Max ΔE^*_{94}
D65				1.50	0.81	8.67	3.57
A	0.696	1.259	3.068	2.88	1.87	13.82	7.44
F2	6.017	8.669	12.667	6.47	3.53	21.29	10.84
F6	6.107	8.669	14.273	7.22	3.96	22.61	12.35

Table 8–19: Weighted RGB correction matrix before transformation matrix (1CCD 3SS).

	Diagonal Elements in Color Correction Matrix M_d			ΔE^*_{ab}	ΔE^*_{94}	Max ΔE^*_{ab}	Max ΔE^*_{94}
D65				2.82	1.63	18.19	5.98
A	0.659	1.277	2.512	7.10	4.50	28.56	13.34
F2	7.968	8.657	13.272	8.92	5.15	41.28	16.93
F6	8.303	8.725	14.952	9.69	5.62	42.47	19.20

Table 8–20: Weighted RGB correction matrix before transformation matrix (Quantix).

	Diagonal Elements in Color Correction Matrix M_d			ΔE^*_{ab}	ΔE^*_{94}	Max ΔE^*_{ab}	Max ΔE^*_{94}
D65				1.71	0.96	8.61	3.48
A	0.693	1.311	2.988	4.00	2.56	18.00	9.87
F2	5.919	9.092	12.497	8.42	4.71	23.44	13.54
F6	5.983	9.200	14.064	9.47	5.30	26.74	15.83

8.7 Discussions

8.7.1 Concatenating Multiple Correction Matrices

When the taking and viewing illuminants are kept the same, the optimal matrix calculated from reference illuminants is assumed applicable to any other illuminant pairs. For the same taking and viewing illuminants, Tastl and Tao gave several approaches to do color correction by employing two white point mapping matrices simultaneously [Tastl2000]. One of the color correction methods can be described as follows:

$$\begin{bmatrix} R_{Other}^{white} \\ G_{Other}^{white} \\ B_{Other}^{white} \end{bmatrix} \xrightarrow[\substack{\text{von-Kries-Type} \\ \text{Color Correction}}]{M_1^d} \begin{bmatrix} R_{D65}^{white} \\ G_{D65}^{white} \\ B_{D65}^{white} \end{bmatrix} \xrightarrow[\substack{\text{Optimized} \\ \text{Transformation} \\ \text{From RGB}\rightarrow\text{XYZ}}]{M_{3\times3}} \begin{bmatrix} X_{D65}^{white} \\ Y_{D65}^{white} \\ Z_{D65}^{white} \end{bmatrix} \xrightarrow[\substack{\text{von-Kries-Type} \\ \text{Color Correction}}]{M_2^d} \begin{bmatrix} X_{Other}^{white} \\ Y_{Other}^{white} \\ Z_{Other}^{white} \end{bmatrix}$$

Therefore the optimal transformation is

$$M_{\text{optimal Other}\rightarrow\text{Other}} = M_2^d M_{\text{optimal D65}\rightarrow\text{D65}} M_1^d \tag{8.22}$$

which may give better color difference performance compared with the direct use of the optimal matrix in Section 8.4. If the taking and viewing illuminants are different, similarly, an additional white point mapping can be concatenated on the right side:

$$\begin{bmatrix} R_{Other}^{white} \\ G_{Other}^{white} \\ B_{Other}^{white} \end{bmatrix} \xrightarrow[\text{von-Kries}]{M_1^d} \begin{bmatrix} R_{D65}^{white} \\ G_{D65}^{white} \\ B_{D65}^{white} \end{bmatrix} \xrightarrow[\substack{\text{Optimized} \\ \text{RGB}\rightarrow\text{XYZ}}]{M_{3\times3}} \begin{bmatrix} X_{D65}^{white} \\ Y_{D65}^{white} \\ Z_{D65}^{white} \end{bmatrix} \xrightarrow[\text{von-Kries}]{M_2^d} \begin{bmatrix} X_{Other}^{white} \\ Y_{Other}^{white} \\ Z_{Other}^{white} \end{bmatrix} \xrightarrow[\text{von-Kries}]{M_3^d} \begin{bmatrix} X_{D65}^{white} \\ Y_{D65}^{white} \\ Z_{D65}^{white} \end{bmatrix}$$

Notice that $M_3^d = (M_2^d)^{-1}$, the correction is equivalent to that used in Section 8.5.4.

8.7.2 Illuminant Dependency of Color Correction

Most of the color correction results in Section 8.5 and 8.6 show that the correction matrix works better for CIE A illuminant than for the fluorescent illuminants (F2 and F6). Possible reasons may be that: (1) CIE A Spectrum has better smoothness; (2) CIE A has high correlation with CIE D65; (3) CIE fluorescent illuminants F2 and F6 have emission lines. In this section, the illuminant dependency of color correction matrix will be tested. Color correction approach described in 8.5.4 will be applied to the following tests.

Test 1: Randomly insert several emission lines onto the CIE A spectrum; boost the red end of fluorescent illuminants such that the trend of their spectra is similar to original A spectrum. The SPDs are plotted in Figure 8.5. After the color correction matrix is employed, the color difference performance is calculated. The result in Table 8-21, 8-22 and 8-23 shows that the color differences for the three modified illuminants are better than their correspondence in Section 8.5.4. Evaluation on all three spectral sensitivity sets is consistent. It seems that emission lines in this case is not the reason to cause the low color correction performance.

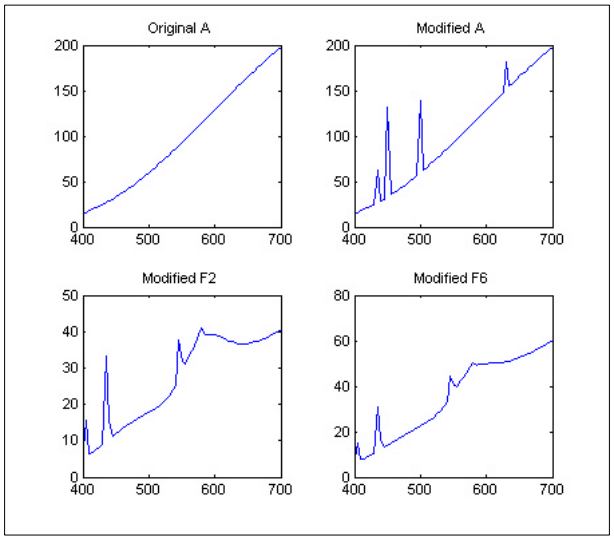

Figure 8.5: Modified illuminant set #1.

Table 8–21: Test #1 of illuminant dependency of correction matrix (3CCD 3SS).

	White Point from SS			Diagonal Elements in Color Correction Matrix M_d			ΔE^*_{ab}	ΔE^*_{94}	Max ΔE^*_{ab}	Max ΔE^*_{94}
D65➔D65	943.480	1481.338	1194.680				1.50	0.81	8.67	3.57
A➔D65	1371.828	1189.018	385.307	0.688	1.246	3.101	2.73	1.77	14.55	7.78
A'➔D65	1385.523	1230.780	495.318	0.681	1.204	2.412	2.30	1.47	11.63	6.27
F2'➔D65	398.297	376.777	154.417	2.369	3.932	7.737	3.23	1.86	13.67	8.35
F6'➔D65	518.229	478.485	175.806	1.821	3.096	6.795	3.06	1.83	13.94	8.50

Table 8–22: Test #1 of illuminant dependency of correction matrix (1CCD 3SS).

	White Point from SS			Diagonal Elements in Color Correction Matrix M_d			ΔE^*_{ab}	ΔE^*_{94}	Max ΔE^*_{ab}	Max ΔE^*_{94}
D65➔D65	647.639	1803.822	1574.265				2.82	1.63	18.19	5.98
A➔D65	1010.238	1441.250	623.507	0.641	1.252	2.525	6.87	4.25	29.96	14.46
A'➔D65	1026.629	1493.063	766.328	0.631	1.208	2.054	6.21	3.81	27.70	11.94
F2'➔D65	266.250	458.795	221.314	2.432	3.932	7.113	6.61	4.09	27.74	14.64
F6'➔D65	356.912	580.738	262.242	1.815	3.106	6.003	6.75	4.20	27.06	14.77

Table 8–23: Test #1 of illuminant dependency of correction matrix (Quanrix).

	White Point from SS			Diagonal Elements in Color Correction Matrix M_d			ΔE^*_{ab}	ΔE^*_{94}	Max ΔE^*_{ab}	Max ΔE^*_{94}
D65➔D65	665.851	517.308	177.248				1.71	0.96	8.61	3.48
A➔D65	971.801	401.629	59.209	0.685	1.288	2.994	3.91	2.40	19.04	10.37
A'➔D65	980.440	417.639	78.419	0.679	1.239	2.260	3.21	2.04	19.16	8.62
F2'➔D65	283.058	126.807	23.503	2.352	4.079	7.542	4.62	2.69	20.64	11.17
F6'➔D65	368.191	160.772	26.850	1.808	3.218	6.601	4.43	2.62	20.81	11.43

Test 2: Multiple emissions are inserted into the spectrum of CIE D65. The modified F6 in Test 1, and equi-energy illuminant are used as test illuminants here. The modified illuminants are shown in Figure 8.6. Only Sony 3CCD 3SS is tested here. Results in Table 8-24 show that all three modified illuminants give good color correction performance.

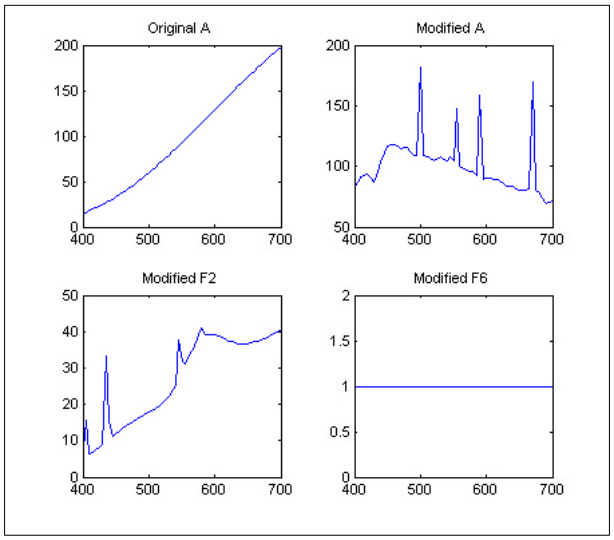

Figure 8.6: Modified illuminant set #2.

Table 8–24: Test #2 of illuminant dependency of correction matrix (3CCD 3SS).

Taking→Viewing	ΔE^*_{ab}	ΔE^*_{94}	Max ΔE^*_{ab}	Max ΔE^*_{94}
D65➔D65	1.50	0.81	8.67	3.57
A➔D65	2.73	1.77	14.55	7.78
A'➔D65	1.53	0.81	9.35	3.53
F2'➔D65	3.23	1.86	13.67	8.35
F6'➔D65	1.52	0.81	7.97	3.79

Test 3: More emission lines are inserted into the spectrum of CIE D65, still the previously modified fluorescent, and a hypothetical illuminant with several dominant emissions together on a weak background spectrum were tested. The spectra of illuminants were shown in Figure 8.7. From the test results in Table 8-25, the first two modified illuminants gave good color correction, the last illuminant gave bad correction. It seems that if the emission lines dominant in the spectrum of illuminant, the color correction performance becomes bad.

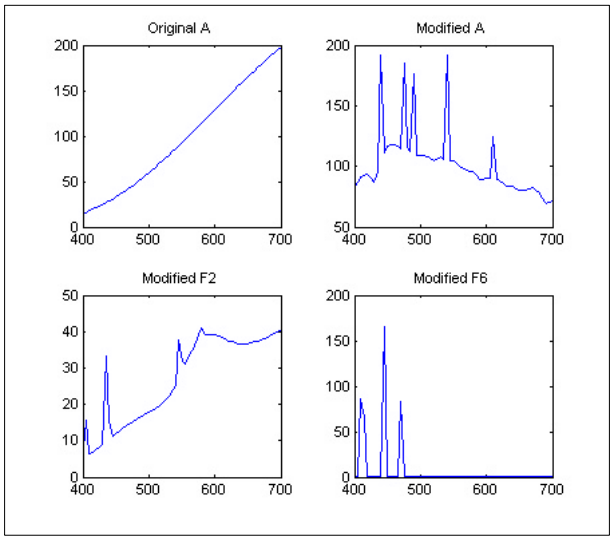

Figure 8.7: Modified illuminant set #3.

Table 8–25: Test #3 of illuminant dependency of correction matrix (3CCD 3SS).

Taking→Viewing	ΔE^*_{ab}	ΔE^*_{94}	Max ΔE^*_{ab}	Max ΔE^*_{94}
D65➔D65	1.50	0.81	8.67	3.57
A➔D65	2.73	1.77	14.55	7.78
A'➔D65	1.54	0.84	8.69	3.55
F2'➔D65	3.23	1.86	13.67	8.35
F6'➔D65	7.11	4.20	19.37	10.80

8.8 Conclusions

The color shifts due to illuminant changes have been discussed in this chapter. Color correction is a method to discount color shifts such that adjusted color approximates its appearance under a reference illuminant. White point mapping has been found to be an effective color correction method.

When the taking illuminant and target illuminant are the same, the color conversion matrix is almost the same even though the illuminant pair changes from among D65, A, F2 and F6. In this case, the color correction matrix is diagnosed as identity matrix.

When the taking illuminant and target illuminant are different, the research assumes the target illuminant is D65, and the color signal under other illuminant is converted to that under D65. Two white point mapping methods were found to be effective. The best color correction matrix is the one obtained as the ratio of camera output signals of white from the reference illuminant and testing illuminant. The best color correction matrix performing much better than others is illustrated by Equation (8.23):

$$\begin{bmatrix} R_{Other}^{white} \\ G_{Other}^{white} \\ B_{Other}^{white} \end{bmatrix} \xrightarrow[\text{von-Kries-Type Color Correction}]{M_d} \begin{bmatrix} R_{D65}^{white} \\ G_{D65}^{white} \\ B_{D65}^{white} \end{bmatrix} \xrightarrow[\text{Optimized Transformation From D65}\rightarrow\text{D65}]{M_{3\times3}} \begin{bmatrix} X_{D65}^{white} \\ Y_{D65}^{white} \\ Z_{D65}^{white} \end{bmatrix} \tag{8.23}$$

Since color correction matrix is von-Kries-type of transformation, this kind of transformation works better when the sensitivity curves are sharp, and is accurate in extreme case if the curves are delta functions, the RGB spectral sensitivity functions used in this chapter are “sharper” than CIE XYZ color matching functions, therefore the obtained best correction matrix performs much better than others. To see whether some simple modification of white point mapping can improve the color correction, weighing functions on the correction matrix of ratio of RGB white is applied, but no better performance was obtained.

The color correction performance depends on the illuminant spectral power distribution. In order to know what causes this, modification of these illuminants were generated, the optimal conversion and correction matrices were calculated, and color difference values were then compared with their original performance. Some trivial tests found that if the emissions are dominant in the spectrum of illuminant, the color correction performance will not be good. The smoothness of illuminant spectrum was not a source causing color correction performance variation. But no concrete conclusion has been drawn yet. Some further research on illuminant dependency is necessary to find the cause.

9 EXPERIMENTS: OPTIMAL DESIGN OF FILTERS

9.1 Introduction

Cameras have been used widely for archiving the spectral or color information of various objects. The design of spectral sensitivities needs to consider capturing signal under multiple taking illuminants and estimating color under multiple viewing illuminants. The design should also take in account imaging noise and noise propagation. The proposed UMG is a metric that considers all these factors. Furthermore, the filter shape should fulfill the basic requirements as previously defined and the design of spectral sensitivities should be based on the filter fabrication process in order that the difference between the designed and fabricated curves is minimal. This chapter will apply the hierarchical approach into real filter design in order to obtain highly colorimetric spectral sensitivities. With additional channels, the designed camera channels may also achieve highly accurate spectral reproduction.

Two design experiments will be described in this chapter. The first is to compare the effectiveness of UMG with other quality factors, particularly m-factor. The second is to apply the hierarchical approach to obtain a set of spectral sensitivities and practically evaluate the colorimetric characteristics. Furthermore, additional spectral sensitivity functions are optimized to achieve spectral reproduction.

9.2 Experimental One

A B/W digital camera system, Photometrics Quantix with controlling software from Roper Scientific, was purchased recently at the Munsell Color Science Laboratory. It is essentially a black/white camera since the color filters were not yet designed for the camera. In this practical application, multiple channel spectral sensitivity functions will be determined from a set of available bandpass filters, infrared cutoff filters and longpass glass filters by Schott Inc. The

available data are the measured spectral sensitivity curve of the electronic sensor (CCD), and the transmittance spectra of these given filter components. Optimal three spectral sensitivity functions for colorimetric reproduction will be determined.

The normalized total B/W detector spectral sensitivity function is measured, which includes the spectral sensitivity of CCD sensor, the transmittance of the optical lenses and a total IR cut-off filter, as shown in Figure 9.1(a). This curve was measured according to certain camera setup. The sensor sensitivity is assumed constant once the configuration is kept fixed.

There are 14 band-pass glass filters (VG-type and BG-type Glass from Schott). The transmittance with a thickness of 3mm is shown in Figure 9.1(b). The shape of these filters is important to form green and blue channels for digital cameras when combining long-pass filters, also red channel if combined with infrared filters.

There are 7 infrared cut-off glass filters (BG-type and KG-type Glass from Schott), whose transmittance is shown in Figure 9.1(c) with a thickness of 3mm. The two BG-type filters have rich variation from 400nm to 650nm, while the five KG-type filters varies from 600nm to 700nm, but changes slowly between 400nm and 600nm, which is a crucial wavelength interval for color image capturing.

The transmittance of the 19 long-pass cut-off glass filters (GG-type, OG-type and RG-type Schott Glass) is shown in Figure 9.1(d), with a thickness of 3mm. Their transmittance spectra typically have sharp edges and do not vary too much if the filter thickness changes between (1 ~ 3mm)

The transmittance of all these filters is based on a thickness of 3mm, which can be easily varied to 2mm and 1mm according to the manufacturer, and according to Bouguer's Law, the corresponding transmittance with 2mm or 1mm thickness can be represented as:

$$T_{2\text{mm}} = T_{3\text{mm}}^{2/3} \qquad T_{1\text{mm}} = T_{3\text{mm}}^{1/3} \tag{9.1}$$

In addition, the transmittance of the total infrared cutoff filter has been shown in Chapter 3 by Figure 3.13(a).

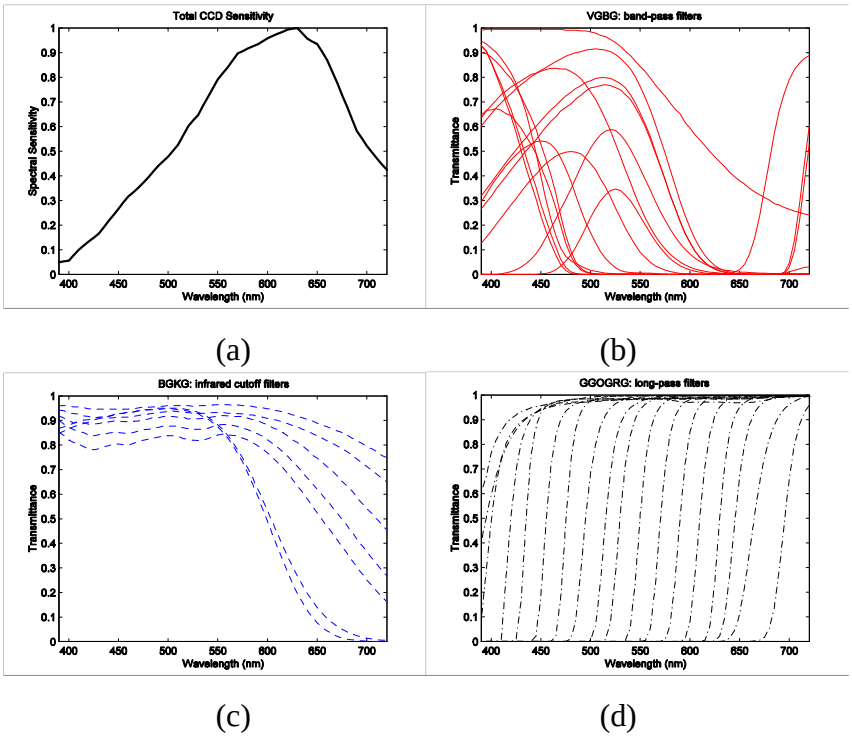

Figure 9.1: (a) Total spectral sensitivity for CCD, optical lens and infrared filter; (b) Transmittance spectra of bandpass filter elements; (c) Transmittance of infrared cutoff filter elements; (d) Transmittance of longpass filter elements.

If a composed filter of certain channel is obtained by superimposing several filter elements with different thickness, its total transmittance can be written as:

$$T_{\text{Total}} = \prod_{i=1}^{k} T_i^{x_i/3} \tag{9.2}$$

where x_i is the thickness of the corresponding filter element. Both Equations (9.1) and (9.2) are simplified prediction model on filter transmittance. Chapter 2 described that more accurate prediction should use internal and external transmittance conversion. Since the primary goal of this experiment is to test the effectiveness of UMG, the simplified prediction does not affect conclusion. So the total spectral sensitivity SS including CCD sensitivity SS_{CCD} is

$$SS = SS_{CCD} \cdot T_{\text{Total}} \tag{9.3}$$

To achieve the transmittance of blue and green channel sensitivities, let the band-pass filters have thickness choices of 3mm, 2mm and 1mm, optionally combined with long-pass filters. The BG-type of IR filters are more useful than the KG filters, and the thickness of each

basic IR can choose from 3mm, 2mm and 1mm, totally 21 IR filters. Thickness variation of long-pass filters does not change their transmittance shape very much, so only thickness of 3mm (or 2mm, 1mm) may be selected to reduce computation amount, but totally there are 57 longpass filters if the thickness changes. To obtain the transmittance of red spectral sensitivity function, use the combination of long-pass filters and IR filters, or the combination of band-pass filters and IR filters. All possible filter combinations can be formed as follows:

Band-pass: 14×3=42 (may be independently used)

IR: 7×3=21 (assuming not used independently)

Long-pass: 19×3=57 (may be independently used)

Band-pass × IR: 42×21=882

Band-pass × Long-pass: 42×57=2934

Long-pass × IR: 57×21=1197

The total number of all filters is 4572 (Pure IR cutoff filters are not counted here). To find the optimal K filters from among these filters, the total combination is 4572^K, as shown in Table 9-1, for example, the computation iterations would be 9.56×10^{10} for K=3. It is obvious that even searching for three optimal filters, the computation will take too much time. Some pre-analysis on the filter information has to be carried out in order to reduce the search range.

Table 9–1: Computation load.

Finding *K* Channels	3	4	5
Computation Times	9.56×10^{10}	4.37×10^{14}	1.99×10^{18}

9.2.1 Pre-Selection of Spectral Sensitivity Functions

It is a huge computational load to obtain an optimal set with a brute force search. It is necessary to pre-select filters in the first step to reduce computation. Previous research discussed in Chapter 6 on general optimization of hypothetical spectral sensitivities shows that filters with single primary peaks are preferred, and the possible peak position of blue channel is located between about 420nm ~ 470nm, that of green channel between about 520nm ~ 560nm, that of

red channel between about 570nm ~ 620nm, as shown in Figure 9.2(a), which is obtained with *q*-factor calculation. The choices of blue channel become 517, and for green channel, 1869, for red channel, 1368 if the extended peak position ranges are applied. This will lead to the reduction of the amount of computation to $517\times1869\times1368=1.3219\times10^9$, much less than the raw brute force search, but it is still too many. If the strict peak position ranges of the three channels are used, the three numbers are further reduced to 391, 1075 and 1049. The corresponding computation load (4.409×10^8) is even less because the search range is even smaller.

For better performance under noisy environment, the widths of sensitivity functions cannot be too wide, or too narrow. From the result of previous research, optimal sensitivity functions should limit their half-peak width to less than 120nm. By assuming the area of the enclosed rectangle be half of the area under the single-peaked sensitivity curve, the full-width at peak-peak can be easily estimated (Figure 9.2(b)), the possible filters with width of less than 120nm and strict peak position ranges are then obtained. The possible choices for blue, green and red channels are now reduced to 384, 601 and 402. They contribute total enumeration to 9.2×10^7, which is a reasonable computation amount able to be finished within days for current desktop personal computers. It is possible that some good combinations outside of the reduced range may be discarded, but it is sufficient that a satisfactory solution is found within this range.

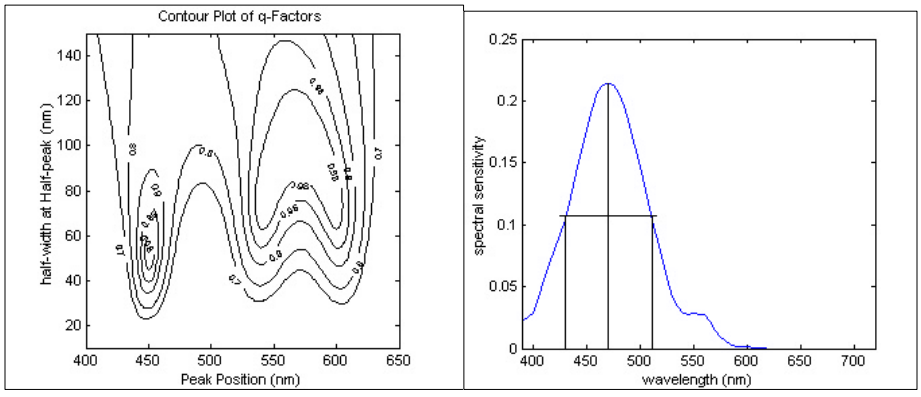

(a) (b)

Figure 9.2: (a) Preferred peak positions and half-width obtained with *q*-factor by setting a confidence level of 0.95; (b) Estimating the width at half-maximum for any spectral sensitivity functions with single primary peak.

9.2.2 Optimization with *m*-Factor

In the initial trial (Figure 9.3), 400 optimal combinations will be obtained from among the reduced collections with *m*-factor since the evaluation of *m*-factor is much faster. The corresponding UMG values are calculated for the 400 sets by assuming signal-to-noise ratio (SNR) be 45dB, which is more or less a reasonable noise performance for most color imaging devices, or 80dB (ideal condition, noise≅0), as shown in Figure 9.4(a). Assuming noise is signal-independent, zero-mean white noise, the SNR is defined as

$$\mathrm{SNR(dB)} = 10\log_{10}\left(\frac{\mathrm{trace}(G^T K_r G)}{J s_h^2}\right) \tag{9.4}$$

The notations in Equation (9.4) are the same as described in Chapter 5. Therefore the noise variance (per channel) is specified as

$$s_h^2 = \frac{1}{J}\frac{\mathrm{trace}(G^T K_r G)}{10^{\mathrm{SNR(dB)}/10}} \tag{9.5}$$

The most favorable set of three filters in terms of *m*-factor is shown in Figure 9.4(b), but this kind of shapes is weird and not preferred from human intuition, since the total sensitivity of green channel is totally enveloped under the red channel. Examining all 400 sets, most of them have such kind of unfavorable shapes. They all have high *m*-factor (>0.98), but the UMG values are not good (<0.70) when SNR=45dB. When the noise is free from the system (SNR=80dB), it is no surprise that the set of sensitivity functions with high *m*-factor corresponds to high UMG values, although their shapes are not ideal such as the “optimal” set given here. It seems the true optimal and desired filter sets with smaller *m*-factor values are buried among those “pseudo” optimal sets.

In order to dig out the optimal set, reduce the searching range by using only one width for the longpass filters, i.e. 2mm, because width of those filters does not affect their cutoff properties very much. The choices for red, green and blues channels are now reduced to 114, 206 and 150. Still search the 400 optimal candidates in terms of *m*-factor in the first step, and then calculate the corresponding UMG for the 400 sets by setting SNR at 45dB (Figure 9.5).

Figure 9.6(a) demonstrates the different trends of *m*-factor and UMG values. The *m*-factor values are very close for all of these sets (>0.965), but obviously, some sets have much higher UMG values than the others. The set of filters with highest UMG value among the 400 sets are shown in Figure 9.6(b), which will be referred as designed set one. Its UMG is 0.82 (45dB) and *m*-factor is 0.966. Quite a few similar sets have close UMG and *m*-factor values. Their shapes are very similar to this optimal one and can be treated as alternative optimums. Most of the other sets with high *m*-factor values but low UMG values do not have such kind of reasonable shape, but their shapes are like Figure 9.4(a), which are not preferred, but sensitivity sets such as Figure 9.6(a) are better results than that from the first trial.

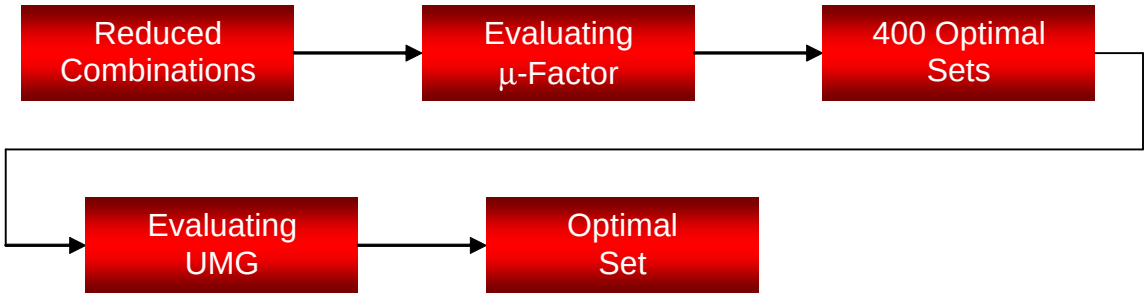

Figure 9.3: Flow chart of optimization trial one.

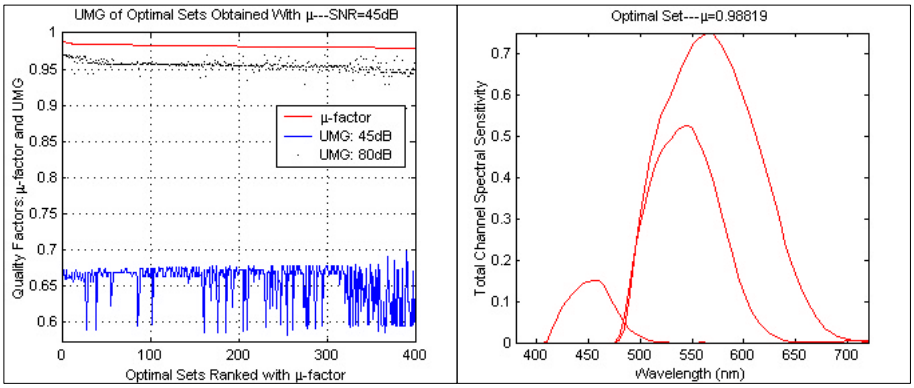

(a) (b)

Figure 9.4: (a) The "optimal" sensitivity function set obtained with *m*-factor, shape is not optimal; (b) the UMG and *m*-factor values of the 400 "optimal" sets.

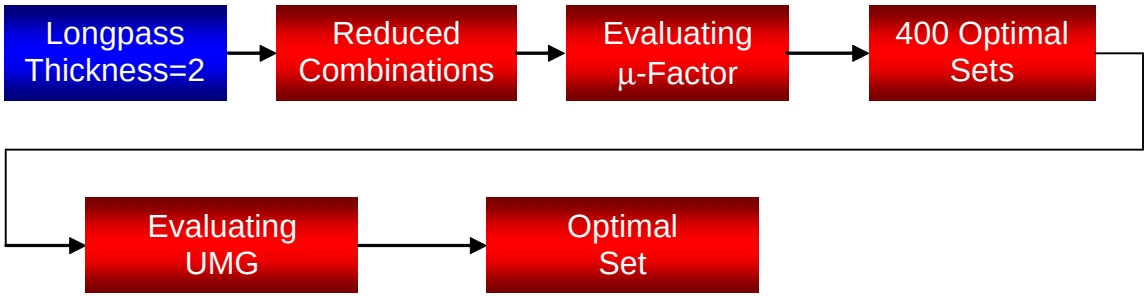

Figure 9.5: Flow chart of optimization trial two.

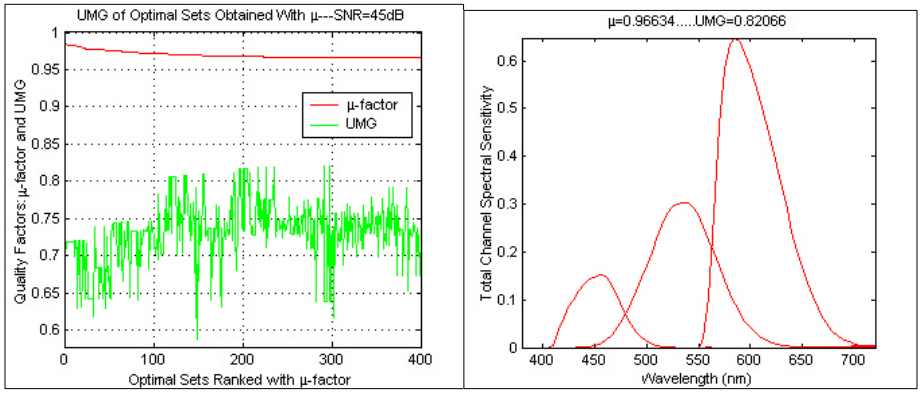

(a) (b)

Figure 9.6**:** (a) UMG and *m*-factor values of the 400 sets obtained with *m*-factor, only a thickness of 2mm is used for longpass filters; (b) The optimal set with highest UMG values among the 400 sets.

This result showed that when the noise is superimposed onto signal like in real world (the signal-to-noise ratio is about 30~50dB), the optimal sets such as Figure 9.6(b) can perform better than the other sets such as Figure 9.4(b). Furthermore, when the noise becomes too much (the signal-to-noise ratio reduces to about 15dB, i.e. in dark illumination), they do not show overwhelming noise proofing any more, since the noise has overshadowed the input signal. If the SNR goes too high (>70dB), the noise can be omitted, most filter sets with high *m*-factor values tend to perform well in ideal condition.

9.2.3 Optimization with UMG

The third trial is to optimize the spectral sensitivities functions by directly evaluating UMG for the 92 million combinations (Figure 9.7). Since UMG depends on data set, illuminants, and noise

level, these parameters are kept the same as the previous experiments. As expected, it takes very long to go through all combinations, a Pentium III 550MHz computer required about forty days, comparatively, it only required about one day to finish the evaluation with *m*-factor. Figure 9.8(a) shows the optimal set obtained from this approach, which is selected with *m*-factor from among the 400 sets obtained with UMG. This optimal set has a *m*-factor value of 0.935, smaller than the optimal set shown in Figure 9.6(b), but its UMG performance is much better, 0.933, denoted as designed set two. The difference between the two sets is that, the sensitivities in Figure 9.8(b) have closer peak sensitivities than that in Figure 9.6(b). It would be interesting to know, which would perform better in practice. This has to be further determined with additional properties, or chosen by professional manufacturers.

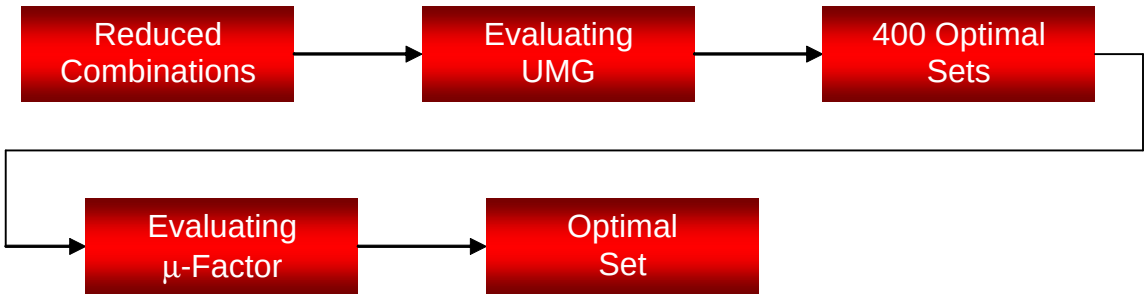

Figure 9.7: Flow chart of optimization trial three.

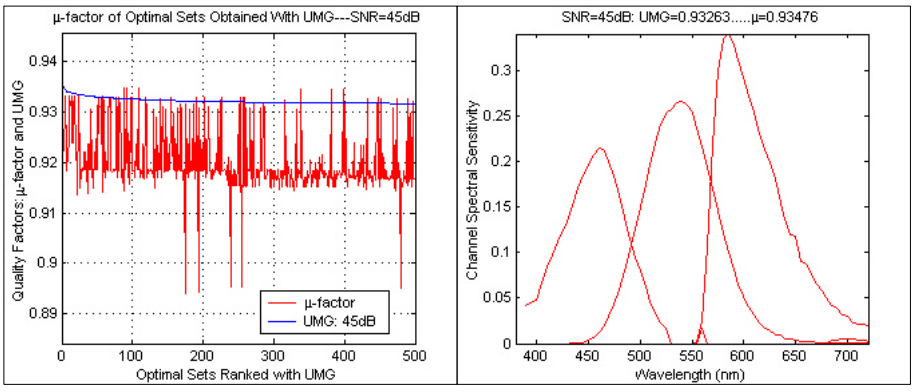

(a) (b)

Figure 9.8: (a) *m*-Factor and UMG values of the 500 optimal filter sets obtained with UMG; (b) The optimal set with maximal UMG value.

9.2.4 Experimental Results and Discussions

The optimal filter set obtained in the second trial was fabricated by the glass filter manufacturer, and the total spectral sensitivities for all three channels were measured and compared with the theoretical counterpart (Figure 9.9(a)). Results showed that they agree very well with each other. An simulated experiment of imaging Macbeth ColorChecker patches is carried out in order to compare the performance for four spectral sensitivity sets: designed set one from trial two, fabricated set one, designed set two from trial three and the measured IBM Pro/3000 spectral sensitivity functions (Figure 9.9(b)). Since different camera has different signal-to-noise performance, all SNRs are assumed at 45dB. The simulated results were list in Table 9-2. For comparison, the various quality factor values were also listed in the table. Table 9-2 showed that the simulated performance of designed and fabricated set one is very close, and the designed set two is very close to the IBM camera, but the latter has a large blue sensitivity which makes it a good choice when tungsten light is used. The practical performance of the manufactured Quantix Set One has been shown in Chapter by Table 3-2 and Table 3-3.

In the other aspect, the predicted and camera output digital counts should have good consistency and linear relationship. An experiment was done by taking images of the Kodak GrayScale. Figure 9.10 showed the predicted and measured digital counts from Quantix camera, all three channels have very high linearity. The color difference of transforming RGB signals to CIE XYZ is 0.03 (average) and 0.108 (maximum) for the predicted digital counts and 1.01 (average) and 4.22 (maximum) for camera output digital counts. It is reasonable that the later has larger color difference because of practical system uncertainties, such as the measurement of CCD sensitivity, the difference between the fabricated and designed filters, and other unexpected noise. The further selection from candidates of optimal spectral sensitivities may require extra metrics. But color difference metrics in Table 9-2 show that designed set two is better.

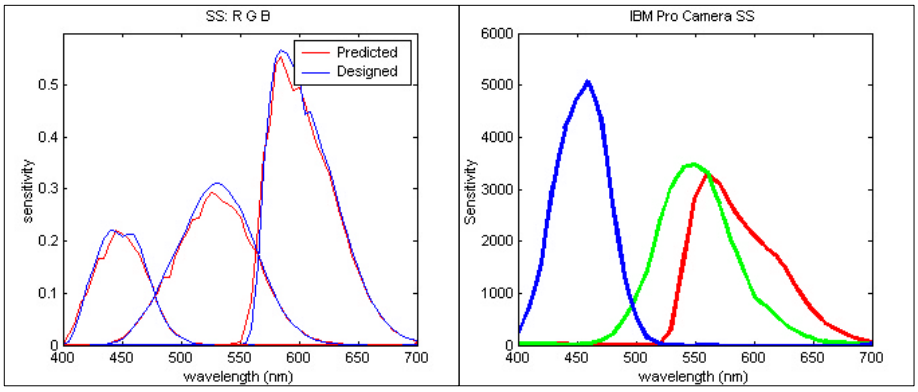

(a) (b)

Figure 9.9: (a) The designed and fabricated spectral sensitivity set; (b) IBM Pro/3000 SS.

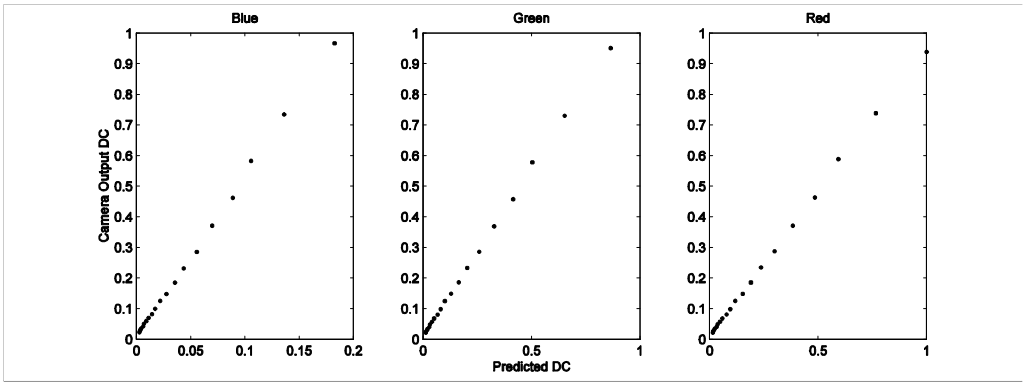

(a) (b) (c)

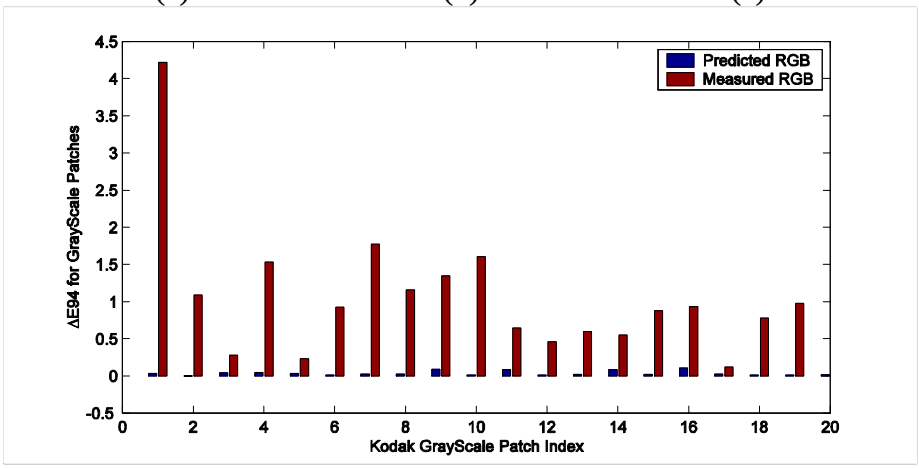

(d)

Figure 9.10**:** The linearity relationship between predicted and camera output digital counts for each channel (Blue, Green and Red), and color difference performance.

Table 9–2: Quality factors and color difference comparison for four sets of spectral sensitivities. Four taking and viewing illuminant pairs are used (D65, A, F2 and Scanlite). Scanlite is the practical light source used with the Photometrics Quantix camera.

		(D65 – D65)	(A – A)	(F2 – F2)	(S – S)
	m-Factor	UMG	UMG	UMG	UMG
Designed Set 1	0.967	0.861	0.653	0.780	0.668
Fabricated Set 1	0.956	0.891	0.745	0.859	0.759
Designed Set 2	0.937	0.935	0.858	0.910	0.866
IBM Pro/3000	0.932	0.934	0.912	0.928	0.916
Color Difference Performance for Macbeth ColorChecker Patches					
Designed Set 1	Mean ΔE^*_{94}	0.80	1.82	0.87	1.65
	Max ΔE^*_{94}	2.40	3.13	2.63	2.98
Fabricated Set 1	Mean ΔE^*_{94}	1.24	1.23	1.12	1.23
	Max ΔE^*_{94}	4.02	4.23	3.88	4.20
Designed Set 2	Mean ΔE^*_{94}	0.70	0.92	0.62	0.91
	Max ΔE^*_{94}	1.72	2.13	1.52	2.13
IBM Pro/3000	Mean ΔE^*_{94}	0.65	0.52	0.66	0.53
	Max ΔE^*_{94}	1.53	1.36	1.53	1.34

9.2.5 Optimization of 4- or 5-Filter Set

The optimization of four or five spectral sensitivities for colorimetric reproduction can be carried out based on the optimization results of three channels. Since the optimal three channels can have good colorimetric performance, adding one or two channels can obtain more information on object colors, and have a larger quality factor, but will not be as efficient as the optimized first three. The peak positions of the additional spectral sensitivity functions should locate differently from the peak positions of the available ones in order to reduce noise amplification and maximize acquisition information for multi-spectral imaging of object reflectance.

9.2.6 Conclusions

An optimal set of filters should satisfy both conditions: first, the subspace of the camera spectral sensitivity functions should approximate that of color matching functions; and second, the

estimation of object colors from noise-mixed channel signals should be close to their measurement in uniform color space. m-Factor indicates whether a sensitivity set is colorimetric or not ideally. By taking account of more practical factors, UMG is able to pick out genuine colorimetric sensitivity functions. A set of sensitivity functions with small m-factor but reasonably good UMG can reproduce object colors quite well; and a set of sensitivity functions with high m-factor but low UMG value is not a good candicate to be implemented in practice.

9.3 Experimental Two

In this experiment, the optimal design procedure followed the hierarchical approach. The sensor sensitivity was priorly accurately measured (Figure 3.12(b)), which is greatly different from the shape shown in Figure 9.1(a). A more accurate prediction model on the transmittance spectra of combined filters described in Chapter 2 was implemented. The total external transmittance spectra T of the basic Schott glass filters with thickness of 1mm are obtained from the Schott filter software. The corresponding internal transmittance is calculated as [Allen1980]

$$T_i = \frac{2T}{(1-K_1)^2 + [(1-K_1)^4 + 4K_1^2 T^2]^{1/2}} \tag{9.6}$$

where T and T_i are the external and internal transmittance, K_1 is a constant associated with the refractive index of the filter. Assuming the combined filters are cemented well enough without in-between air layer, the transmittance of the combined filters fulfill Beer's Law, which means the total internal transmittance is the product of the components:

$$T_{i\text{Total}} = \prod_{j=1}^{k} T_j^{d_j} \tag{9.7}$$

where k is the number of filter components, d_j is the thickness of the component filter, in this application, the thickness can vary among 1, 2 and 3mm. Finally the total internal transmittance spectra is converted to get the total external transmittance:

$$T = (1-K_1)^2 T_{i\text{Total}} (1 - K_1^2 T_{i\text{Total}}^2) \tag{9.8}$$

Generally the difference between internal transmittance and external transmittance can be over 10%, as shown in Figure 9.11.

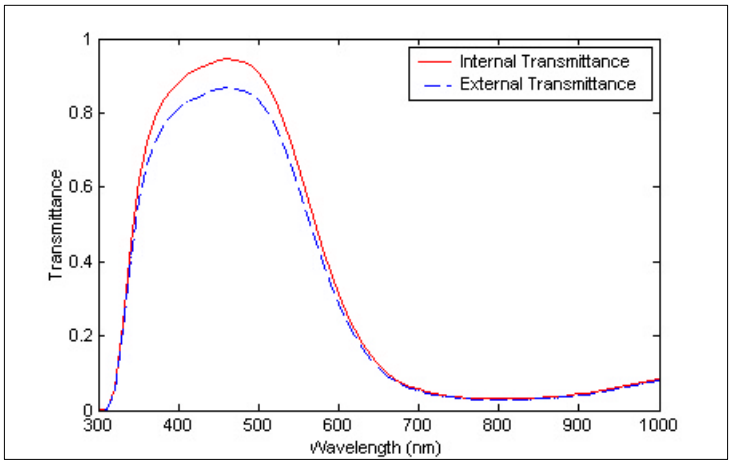

Figure 9.11: Difference between internal and external transmittance spectra for a filter.

9.3.1 Optimization Process

The optimization process is described as follows. There are totally 4593 basic and combined filters (IR cutoff filters are also counted here). The transmittance spectra of these filters are multiplied by CCD sensitivity function to obtain total spectral sensitivity functions. If red, green and blue channels are directly selected from them, the complete combinations are 9.69×10^{10} (4593^3). The pre-selection process with constraints as follows drastically reduces computation.

The primary peak wavelength of red ranges from 570nm to 620nm, that of green ranges from 520nm to 560nm, and that of blue ranges from 420nm to 470nm. Full-width at half peak height is less than 120nm, the sensitivity of primary peak should be over 0.2 (CCD with only IR cutoff filter has a maximum sensitivity of 1.0), and the sensitivity of possible secondary peak in the blue side should be less than 20% of the sensitivity of primary peak. Such constraints return 138 choices for red, 133 for green and 246 for blue. The number of total combinations to be evaluated is $133\times138\times246=4.52\times10^6$. The amount of computation is just about 4.66×10^{-5} of the amount of computation with brute search. It takes about less than two days for a current Pentium computer to evaluate these combinations with UMG.

After pre-selection, evaluate those combinations with UMG. The taking and viewing illuminants are set as equi-energy. The Vrhel-Trussell data set is still used as object colors. Since the practical noise model in UMG equation considers both signal-independent Gaussian-

distributed noise and signal-dependent Poison-distributed noise, while the experimental noise model for this specific camera is unavailable at the moment of optimal design, an assumed noise model described in Section 4.4.3 is applied in the UMG selection process. Five hundred optimal spectral sensitivity set candidates will be obtained based on the UMG values. Then calculate the *m*-factor and UMG values by setting the taking and viewing illuminants as CIE D65, CIE A, CIE F2, CIE F6 and Scanlite while the same noise level was applied. The *m*-factor and the UMG without noise consideration are also calculated. A weighted metric

$$q_w = w_1 UMG_{\mathrm{D65}} + w_2 UMG_{\mathrm{A}} + w_3 UMG_{\mathrm{F2}} + w_4 UMG_{\mathrm{F6}} + w_5 m(UMG_{\mathrm{w/o\ Noise}}) \tag{9.9}$$

was used to re-order the goodness of the 500 candidates, where w_i are weights. The following results were obtained from application of an equal-weighted simplified metric.

9.3.2 Optimization Results

The optimal spectral sensitivity sets were obtained based on the order of secondary evaluation. The ten sets that satisfy the total thickness constraint ($\mathrm{Thickness}_{\mathrm{Total}} \le 4mm$) are plotted in Appendix G with their component parameters.

Other metrics are used to further select the optimal spectral sensitivity set from among these candidates: weighted peak spectral sensitivity $T_{\max}$, the overlapped area between two sensitivity functions (Overalp RB, Overlap RG, Overlap GB), maximal total thickness for the three filter channels (Table 9-3), average color difference $\Delta E^*_{\mathrm{mean}}$, maximal color difference $\Delta E^*_{\max}$, and 90th percentile average ΔE^*_{94} , median value (estimate of the center of color difference, 50th percentile), skewness (A measure of the asymmetry of the data around the sample mean. If skewness is negative, the data are spread out more to the left of the mean than to the right. If skewness is positive, the data are spread out more to the right. The skewness of the normal distribution or any perfectly symmetric distribution is zero [pg. 612 in Press1997]. For color difference, the skewness is usually positive, but the smaller, the better). These statistical values are listed in Table 9-4.

$$T_{\max} = \frac{2T_{\max}^{Blue} + T_{\max}^{Green} + T_{\max}^{Red}}{4} \tag{9.10}$$

where $T_{\max}^{red}$, $T_{\max}^{green}$ and $T_{\max}^{blue}$ are the peak sensitivity for red, green and blue channel respectively. More weight was placed on blue since blue sensitivity is comparatively lower than the others.

Table 9–3: Properties of optimal filter candidates.

Filter Set	UMG (EE)	*m*-Factor	Overlap RG	Overlap RB	Overlap GB	Peak RGB	Thickness (*mm*)
19	0.935	0.941	3.921	0.133	2.712	0.294	4
20	0.935	0.940	3.921	0.207	4.070	0.303	4
21	0.935	0.940	3.921	0.243	2.821	0.297	3
22	0.935	0.940	3.922	0.243	2.821	0.297	3
23	0.935	0.940	3.889	0.207	3.850	0.302	4
24	0.935	0.940	3.889	0.207	3.850	0.302	4
27	0.935	0.940	3.921	0.144	2.758	0.298	3
28	0.935	0.940	3.922	0.144	2.758	0.298	3
29	0.936	0.940	3.921	0.207	2.983	0.302	4
30	0.936	0.940	3.922	0.207	2.983	0.302	4

RGB signals and XYZ values are calculated with the information of illumination (scanlite light source), Macbeth ColorChecker and corresponding camera spectral sensitivity functions. To calculate the conversion matrix from RGB signals to XYZ values, the RGB signals were normalized by setting the maximum of RGB signals to one, and XYZ values were normalized by setting the Y value of illuminant color (scanlite) to 100. The preliminary matrix was obtained via direct pseudo-inverse operation from RGB signals to XYZ values, and final matrix was obtained by refinement through minimization of average CIE ΔE_{94} color difference of samples by setting the starting matrix as the preliminary conversion matrix. In Table 9-5, matrix $\mathbf{M}_1$ was obtained for Macbeth ColorChecker samples, which is close to the matrix $\mathbf{M}_2$ obtained for Vrhel-Trussell data sets. In Table 9-4, three sets of color difference values are calculated. The first was obtained with $\mathbf{M}_1$ for Macbeth ColorChecker samples, the second was obtained with $\mathbf{M}_2$ for Vrhel-Trussell dataset, and the third was obtained with $\mathbf{M}_1$ for Vrhel-Trussell dataset. The purpose of

calculation of the third set of color difference values was to examine the validity of applying a conversion matrix from a small popularity of dataset onto a much larger popularity of dataset.

After careful comparison among these metrics, the set #30 was chosen subjectively and was fabricated by Schott Inc. But in fact, the performance of these sets of spectral sensitivities are not different from each other very much. The simulated performance of this spectral sensitivity set is compared with other spectral sensitivity set candidates in Appendix H.

Table 9–4: Color difference Performance Comparison.

Filter Set	Mean ΔE^*_{94}	Max ΔE^*_{94}	Z-score 90%	Median ΔE^*_{94}	Skew-ness	Mean ΔE^*_{94}	Max ΔE^*_{94}	Z-score 90%	Median ΔE^*_{94}	Skew-ness
19	0.671	2.087	1.569	0.387	0.898	0.633	3.624	1.606	0.405	2.085
20	0.666	2.328	1.624	0.431	1.213	0.660	4.047	1.477	0.455	2.151
21	0.653	1.992	1.376	0.521	0.788	0.702	6.467	1.599	0.466	2.897
22	0.657	2.005	1.382	0.523	0.795	0.704	6.443	1.614	0.467	2.877
23	0.665	2.286	1.616	0.428	1.172	0.657	4.043	1.475	0.452	2.158
24	0.670	2.297	1.623	0.438	1.165	0.660	4.046	1.478	0.449	2.165
27	0.674	2.095	1.588	0.389	0.911	0.638	3.672	1.634	0.412	2.081
28	0.680	2.112	1.592	0.394	0.905	0.641	3.703	1.631	0.411	2.094
29	0.646	2.026	1.472	0.490	0.933	0.629	3.998	1.443	0.424	2.232
30	0.651	2.042	1.479	0.497	0.932	0.632	4.000	1.452	0.425	2.240

Filter Set	Mean ΔE^*_{94}	Max ΔE^*_{94}	Z-score 90%	Median ΔE^*_{94}	Skew-ness
19	0.705	3.464	1.681	0.466	1.556
20	0.751	3.916	1.788	0.542	1.573
21	0.780	6.465	1.714	0.559	2.392
22	0.784	6.440	1.720	0.559	2.371
23	0.747	3.916	1.771	0.535	1.581
24	0.751	3.920	1.774	0.537	1.591
27	0.711	3.501	1.700	0.482	1.554
28	0.715	3.539	1.706	0.479	1.567
29	0.708	3.937	1.644	0.523	1.660
30	0.712	3.941	1.647	0.519	1.670

Table 9–5: Conversion matrices from RGB to XYZ.

Filter Set	M_1 Calculated from Macbeth ColorChecker			M_2 Calculated from Vrhel-Trussell Data		
19	68.109	24.802	0.015	66.754	23.480	-0.072
	39.923	100.934	-4.636	39.892	101.287	-4.573
	4.652	-12.195	136.014	11.304	-6.747	135.984
20	68.295	25.353	-0.633	66.948	23.895	-0.733
	39.351	99.534	-4.529	38.732	99.370	-4.542
	1.072	-19.552	126.788	8.335	-12.969	127.036
21	68.052	24.921	-1.407	67.280	23.953	-1.437
	40.023	100.908	-3.618	38.916	100.462	-3.912
	4.370	-11.991	132.088	11.404	-6.060	132.936
22	67.927	24.872	-1.405	67.173	23.908	-1.435
	40.329	101.148	-3.626	39.156	100.670	-3.916
	4.182	-12.082	132.280	11.334	-6.090	133.111
23	68.276	25.308	-0.631	66.959	23.876	-0.730
	39.783	100.618	-4.578	39.156	100.460	-4.596
	1.597	-18.217	126.726	8.768	-11.745	126.986
24	68.151	25.259	-0.631	66.830	23.823	-0.727
	40.089	100.859	-4.585	39.432	100.686	-4.601
	1.397	-18.320	126.908	8.674	-11.799	127.154
27	68.107	24.809	-0.059	66.746	23.480	-0.120
	39.920	100.924	-4.572	39.851	101.250	-4.544
	4.555	-11.899	132.817	11.111	-6.528	132.735
28	67.980	24.760	-0.059	66.614	23.433	-0.116
	40.226	101.164	-4.578	40.133	101.466	-4.555
	4.369	-11.988	133.006	11.036	-6.555	132.927
29	68.082	24.853	-0.615	67.041	23.674	-0.700
	39.962	100.966	-4.579	39.355	100.990	-4.608
	4.243	-11.412	126.402	10.645	-6.142	126.692
30	67.956	24.804	-0.615	66.913	23.621	-0.697
	40.269	101.206	-4.587	39.628	101.214	-4.616
	4.064	-11.498	126.583	10.571	-6.178	126.864

9.3.3 Simulated Performance of Fabricated Filter Set

The filter components of each channel and their non-cemented combination were predicted with Schott glass filter software and measured with Macbeth ColorEye 7000. Figure 9.12 shows the predicted and measured filter transmittance. The prediction and measurement for Blue and Green channels overlap very well, but there is quite large difference for Red channel. Figure 9.13 shows the theoretically designed spectral sensitivity functions (cemented), the predicted spectral sensitivity functions (cemented), the predicted spectral sensitivity functions (non-cemented), and the measured spectral sensitivity functions (non-cemented). The theoretical design overlaps with cemented prediction very well, which means the transmittance prediction model works very well.

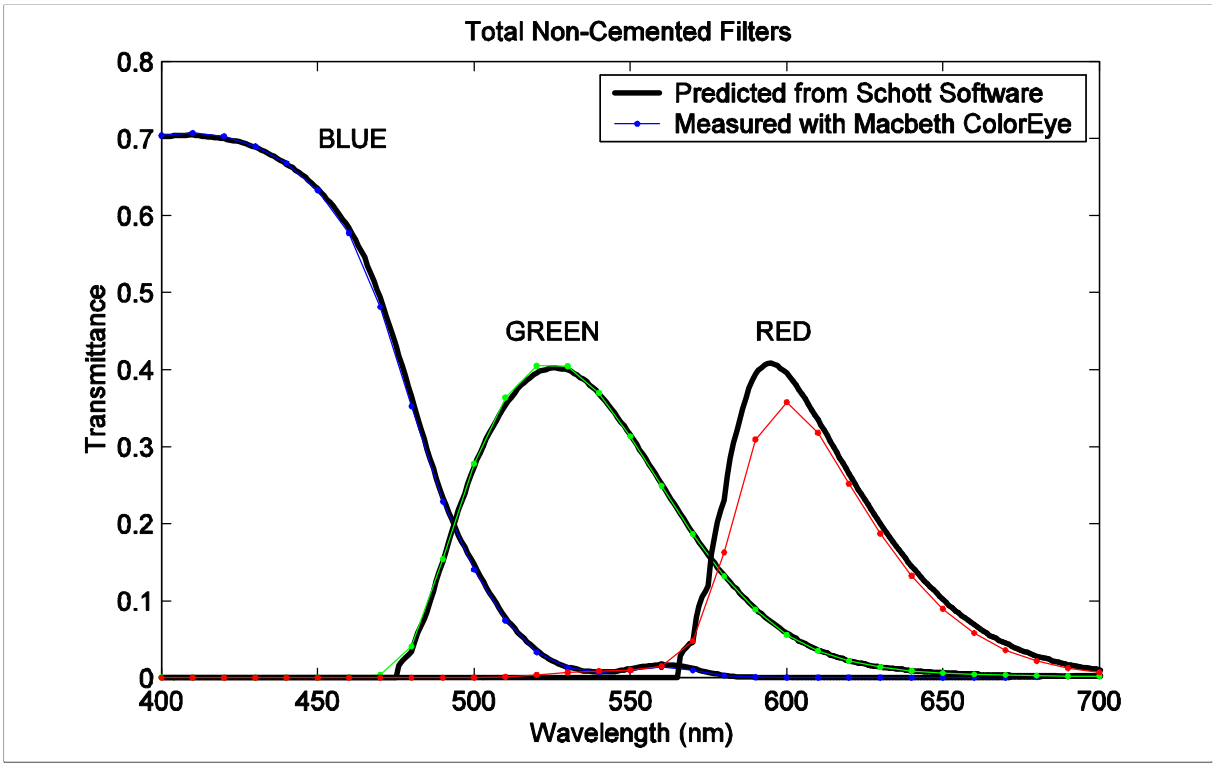

Figure 9.12: Filter transmittance predicted and measured (filter combination is non-cemented). The dotted solid lines are measured transmittance, and the solid lines are predicted spectra of transmittance.

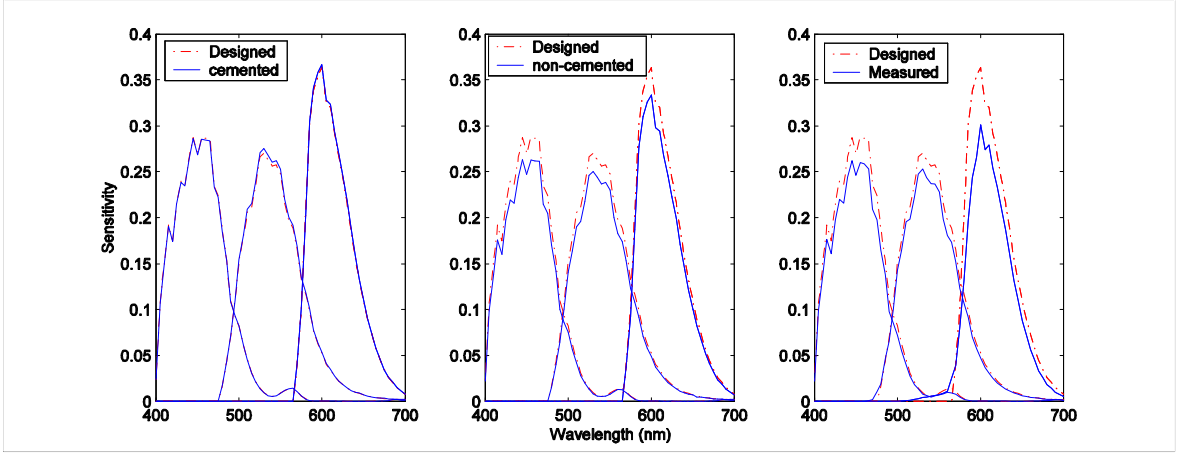

(a) (b) (c)

Figure 9.13: Theoretical designed spectral sensitivities functions compared with (a) predicted cemented; (b) predicted non-cemented; (c) measured sensitivities.

The colorimetric quality factors and the color difference performance of spectral sensitivities functions from predicted non-cemented filters, cemented filters and measured cemented filters were simulated and listed in Table 9-6 to 9-8. The dataset used is Vrhel-Trussell as usual, and the quality factors listed are *m*-factor and UMG under D65, A, F2, F6, Scanlite and EikoFlood illuminants. With imaging noise consideration, the performance of three sets of spectral sensitivity functions is almost the same. In practice, the cemented filters should give better performance than the non-cemented filters since the optimization is based on the requirement that the filters be cemented.

Table 9–6: Simulation: spectral sensitivities from predicted non-cemented filters.

Quality Factors	0.9401	0.9215	0.8312	0.9144	0.9084	0.8418	0.9094
Illuminant Pair	Mean	ΔE^*_{ab}	ΔE^*_{94}		Max	ΔE^*_{ab}	ΔE^*_{94}
D65-D65		1.41	0.96			6.74	3.28
A-A		1.71	1.27			7.16	4.32
F2-F2		1.06	0.73			4.53	2.72
F6-F6		1.06	0.73			4.39	2.65
Scanlite-Scanlite		1.58	1.17			6.48	4.12
Other-Other		1.64	1.13			8.05	4.45

Table 9–7: Simulation: spectral sensitivities from predicted cemented filters.

Quality Factors	0.940	0.922	0.829	0.914	0.910	0.840	0.909
Illuminant Pair	Mean	ΔE^*_{ab}	ΔE^*_{94}		Max	ΔE^*_{ab}	ΔE^*_{94}
D65-D65		1.41	0.96			6.73	3.27
A-A		1.73	1.29			7.28	4.34
F2-F2		1.06	0.73			4.52	2.71
F6-F6		1.06	0.73			4.39	2.64
Scanlite-Scanlite		1.59	1.18			6.58	4.13
Other-Other		1.64	1.13			8.03	4.45

Table 9–8: Simulation: spectral sensitivities from measured cemented filters.

Quality Factors	0.943	0.920	0.841	0.915	0.910	0.851	0.911
Illuminant Pair	Mean	ΔE^*_{ab}	ΔE^*_{94}		Max	ΔE^*_{ab}	ΔE^*_{94}
D65-D65		1.46	0.99			6.95	3.41
A-A		1.54	1.16			4.73	3.87
F2-F2		1.12	0.78			5.05	2.96
F6-F6		1.11	0.78			4.91	2.89
Scanlite-Scanlite		1.45	1.09			4.83	3.71
Other-Other		1.59	1.10			7.95	3.83

9.3.4 Experimental Performance of Fabricated Filter Set

In this experiment, the test target is the Macbeth ColorChecker. The illuminant was Scanlite, which is close to CIE A. The filter components are non-cemented. The predicted digital counts and measured digital counts for Red, Green and Blue channels have great linearity ($R^2 > 0.99$), as shown in Figure 9.14. But the linearity for Red channel is not so good as green and blue channel. Without prior white balance, a comprehensive 3×3 transformation matrix was derived to transfer RGB digital counts to CIE XYZ values by minimizing CIE ΔE^*_{94} color difference. The color difference for each patch is listed in Table 9-9 and plotted in Figure 9.14(d). The average and maximal color difference is very good.

Table 9–9: Experimental color difference performance on Macbeth ColorChecker.

MCC	DC R	DC G	DC B	X	Y	Z	ΔE^*_{94}	ΔE^*_{ab}
Dark Skin	0.188	0.120	0.086	14.496	10.901	2.107	2.551	3.681
Light Skin	0.582	0.387	0.292	49.341	38.560	9.298	0.430	0.712
Blue Sky	0.185	0.235	0.358	17.286	17.659	11.723	2.536	3.290
Foliage	0.132	0.171	0.092	12.005	12.720	2.452	2.210	2.433
Blue Flower	0.291	0.277	0.447	27.477	23.772	15.352	0.561	0.785
Bluish Green	0.286	0.541	0.499	32.379	38.747	16.214	1.833	2.008
Orange	0.657	0.307	0.098	50.763	35.636	2.130	1.657	3.650
Purplish Blue	0.106	0.137	0.362	11.375	10.453	12.447	0.905	2.067
Moderate Red	0.535	0.188	0.159	40.191	24.140	4.679	0.067	0.146
Purple	0.123	0.076	0.146	9.741	6.913	4.723	1.032	1.093
Yellow Green	0.419	0.552	0.168	41.088	43.505	4.578	1.936	3.360
Orange Yellow	0.725	0.463	0.129	62.341	49.207	3.198	1.459	2.059
Blue	0.056	0.068	0.251	5.902	5.170	10.006	1.529	3.771
Green	0.137	0.304	0.134	15.973	21.637	3.722	1.813	3.082
Red	0.446	0.111	0.073	31.066	16.272	1.789	1.700	2.625
Yellow	0.834	0.678	0.171	74.923	64.624	4.102	0.530	1.023
Magenta	0.515	0.191	0.305	38.753	23.101	9.936	0.292	0.304
Cyan	0.096	0.240	0.394	11.955	16.114	14.097	2.185	5.298
White	0.992	1.000	0.971	96.341	88.749	33.218	1.021	1.021
N8	0.639	0.646	0.630	63.442	58.428	21.991	1.541	1.541
N6.5	0.392	0.394	0.389	38.827	35.820	13.527	1.482	1.485
N5	0.221	0.228	0.223	22.013	20.307	7.671	1.105	1.127
N3.5	0.102	0.106	0.103	9.960	9.235	3.541	0.564	0.570
Black	0.041	0.041	0.040	3.602	3.338	1.317	1.309	1.315
						Mean	1.344	2.019
						Max	2.551	5.298

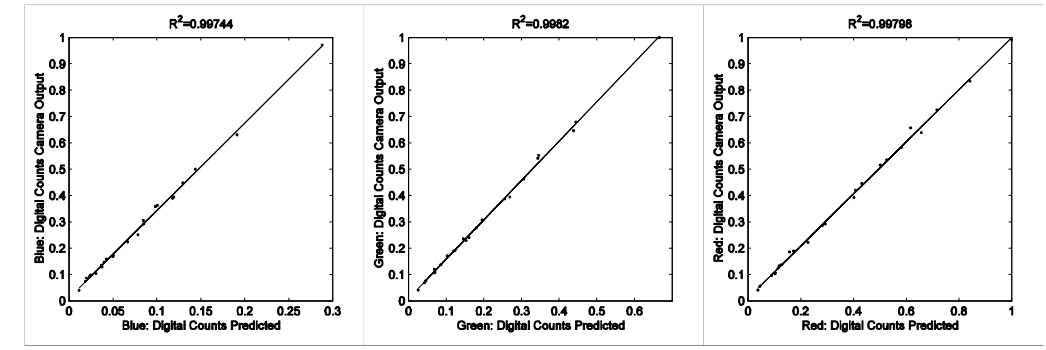

(a) (b) (c)

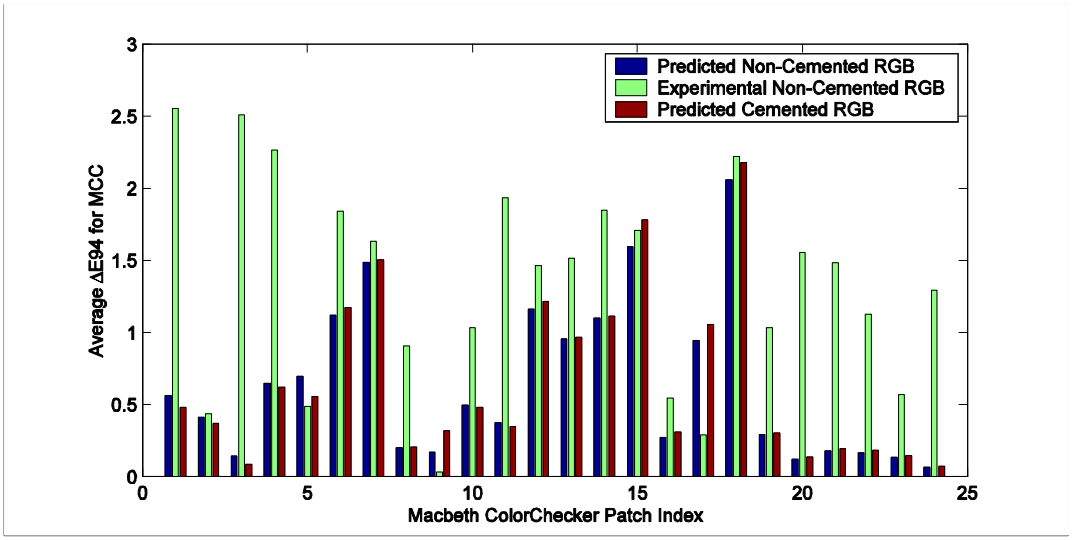

(d)

Figure 9.14: (a,b,c) The linearity relationship between predicted digital counts and measured digital counts. Red channel is not so good as green and blue channel. (d) Predicted and experimental color difference performance on Macbeth ColorChecker.

The experimental color difference performance is quite promising, but it is not so good as theoretically predicted. The possible reasons may be: (1) The transmittance of non-cemented red combination is quite different from that predicted from Schott software. (2) Filters are not cemented, which means it is not as optimal as designed yet.

Based on the optimal spectral sensitivities obtained, additional three imaging channels were designed to achieve spectral reproduction, which forms a complete system consisting of six channels for both colorimetric and spectral performance. The result was shown in Appendix I.

9.4 Conclusions

The effectiveness of UMG as a metric for optimal design of spectral sensitivities is experimentally verified in this chapter. Filters are designed, fabricated and experimentally tested for a specific camera. Results show that UMG is qualified as an efficient metric, and hierarchical optimization approach is very effective in practically designing filters for digital color imaging.

10 SUMMARY AND CONCLUSIONS

The primary work in this dissertation is the characterization, evaluation and optimal design of spectral sensitivity functions for color imaging devices. In Chapter 2, the fundamentals of color vision and color imaging were described, which consists of spectrum of physical stimulus, color space, color and image difference metrics, color appearance models, some mathematical backgrounds, such as vector space method, linear models, singular value decomposition, principal components analysis.

Chapter 3 describes the conventional and spectral characterization methods for color input devices. The conventional characterization builds relationship between device output signals and color coordinates in device-independent color space. Linear and multiple regression as well as neural network mapping are the typical approaches to carry out conventional device characterization. Spectral characterization is realized by directly measuring the spectral sensitivity functions, which requires special equipments to accomplish. Some “quick and dirty” estimation approaches on spectral sensitivities are then discussed and compared in this chapter. Depending on the characteristics of testing targets, illumination, practical sensitivity functions, the estimation methods may or may not work.

The noise characteristics of electronic sensors are discussed in Chapter 4. There are many noise sources in digital electronic imaging, but the consideration of noise types depend on the specific application. In this dissertation, electronic noise is modeled as summation of signal-independent noise and signal-dependent noise, which are represented by white noise and shot noise respectively, experimental noise measurement and characterization verifies that this model fulfills application requirement. Noise is described by its mean and variance, which can be calculated from the first and second order moments of random variables. The noise in the input end will be propagated and amplified while signals are transformed step by step. Noise

propagation rules are obtained with linear transformation and nonlinear transformation. The RMS noise in the target space can be formulated as a function of the variance-covariance matrix in the target color space. Some signal transformation and noise propagation processes usually found in color imaging applications were described briefly.

Chapter 5 addressed the colorimetric performance evaluation of spectral sensitivity functions. Colorimetric quality factors have been found to be appropriate measures to describe various aspects of spectral sensitivity functions. q-Factor and m-factor are simple metrics to describe how the sensitivity functions approximate color matching functions in geometrical space. They were formulated with least-squares approach and used to explore the characteristics of hypothetical spectral sensitivities. FOM was emerged as the most extensive metric, the only shortcoming is that it lacks the capability to handle signal-dependent noise. The proposed UMG metric is more like a practically useful metric as an improvement of FOM. The noise model and multi-illuminant color correction are embedded in this metric.

In chapter 6, generic approaches to the optimal design of spectral sensitivity functions are described. Direct optimization on around one hundred variable would meet practical problem. Three practically feasible approaches are the optimal subset searching among a set, parameterization of spectral sensitivity functions such that the optimization is implemented with a small number of variables, and optimization of single spectral sensitivity functions upon available channels in which case the optimization is also implemented with a small number of variables. In the second part of this chapter, by assuming the spectral sensitivity function is asymmetric gaussian function, the optimal region of peak positions and widths of spectral sensitivity functions are obtained by setting certain quality factor at a confidence level. The region was found to be a continuous solid in high dimension and has some other properties. The region provides fabrication tolerance if the filter fabrication process is unknown.

Chapter 7 outlined a practically feasible and systematic approach to the optimal design of spectral sensitivity functions for colorimetric reproduction. Most of optimization gave virtual optimal curves, which need be approximated with manufacturer's filter component set during

fabrication process. Such approximation will induce error resulting that the fabricated curves are deviated from the ideally optimal ones, which may make the theoretically optimal set practically not optimal at all. The hierarchical approach directly optimizes on the parameters of fabrication, such as the thickness of filters and the selected components. After pre-selection process based on the optimal range obtained in Chapter 6, multiple metrics will be applied in order to obtain the optimal spectral sensitivity set. UMG has been chosen as the primary selection criterion since it considers more properties in color imaging. The secondary criteria are geometrical-difference based quality factor and RMS noise. A two-dimensional decision is desired to find out the final optimal set. The approach is further extended to design spectral sensitivity functions for accurate spectral reproduction.

The color correction in color imaging is explored in Chapter 8. It is impractical to calculate a transformation matrix in real time for a camera, generally a static conversion matrix is built in for reference illuminants and a correction matrix that can be easily calculated is used to adjust color due to illuminant changes. The possible correction matrix forms are proposed in the chapter and the influence of illuminant on the color correction performance is discussed.

Chapter 9 describes the effectiveness of UMG as a metric to optimization of spectral sensitivities. Filters are designed, fabricated and experimentally tested for a specific camera. Results show that UMG is qualified as a useful metric, and hierarchical optimization approach is effective in practical application.

10.1 Contributions

The major contributions of this dissertation are:

- The characterization methods for color imaging devices are comprehensively described. Experiments demonstrating the conventional characterization and spectral characterization are reported. Spectral estimation approaches from common imaging targets are analyzed and experimental results are reported.

- A new colorimetric quality matric (UMG) is proposed for the evaluation of color imaging devices. UMG is based on an average color error in linearized perceptually uniform color space, which could be CIELAB, S-CIELAB, or color appearance space. Signal-independent noise and signal-dependent noise are incorporated in UMG. The newly developed color difference formulae can also be applied in the metric. It is a practically useful metric to evaluate and design spectral sensitivities, with high degree of perceptual relevance and accounts for real noise characteristics.
- The optimal region of widths and peak positions of gaussian-type spectral sensitivity functions are determined by setting a confidence level on certain quality factors. The region is found to be a continuous solid in high-dimensional space and be narrower when the confidence level is stronger.
- Generic feasible approaches to the optimal design of spectral sensitivities functions are discussed, which includes subset searching, parameterization of sensitivities and optimization of additional sensitivity.
- A hierarchical approach to the optimal design of spectral sensitivities is proposed. The basic principles of this approach are that optimization should be based on a model of filter fabrication parameters and the optimal spectral sensitivity functions should be evaluated and be recognized as optimum with multiple metrics. After pre-selection process, the reduced combinations will be evaluated with primary metric and secondary metrics. A few optimal candidates will be judged subjectively to select the final optimal set.
- Optimal design of spectral sensitivities for spectral reproduction has been considered in the dissertation. A normalized metric based on Wiener estimation for spectral reproduction is proposed and applied to obtain additional imaging channels for spectral imaging applications.

10.2 Directions for Future Study

Some of the issues that are interesting but are not fully explored include:

- UMG is not implemented in a more advanced color space than CIELAB yet, the interested color spaces are S-CIELAB and some recognized color appearance space. A more advanced color difference or image difference formula may replace the standard Euclidean color difference equation.
- The hierarchical approach has not been fully implemented yet, that is, the two-dimensional decision is implemented with only one-dimensional decision since the weights for the two metrics (color accuracy and noise perception) are undetermined.
- The ultimate image quality evaluation may need subjective methods. A few optimal spectral sensitivity sets should be fabricated or simulated side-by-side to let observers to judge the image quality among them. Final optimal set may be selected after analyzing the observers' responses. Some relationship between objective and subjective metrics may exist but are unknown yet.

10.3 Conclusions

To develop a colorimetric quality factor that comprehensively considers noise propagation, color accuracy, and color correction. To propose a practically feasible approach to the optimal design of spectral sensitivity functions for color imaging devices. These two core goals are accomplished in the dissertation and verified in practice.

REFERENCES

[Abatsoglou1991] Theagenis J. Abatzoglou, Jerry M. Mendel and Gail A. Harada, The Constrained Total Least Squares Technique and its Applications to Harmonic Superresolution, *IEEE Transactions on Signal Processing*, **39**, 1070-1087 (1991).

[Adkins1993] D. Adkins, V. S. Cherkassky and E. S. Olson, Color Mapping Using Neural Network, *Proc. IS&T/SID's 2nd Color Imaging Conference*, 45-48 (1993).

[Allen1980] Eugene Allen, Colorant Formulation and Shading, *Optical Radiation Measurement*, edited by Franc Grum, Academic Press, 289-335 (1980).

[Angelopoulou1999] Elli Angelopoulou, The reflectance Spectrum of Human Skin, Technical Report MS-CIS-99-29, University of Pennsylvania (1999).

[Angelopoulou2001] Elli Angelopoulou, Rana Molana and Kostas Daniilidis, Multispectral Skin Color Modeling, Technical Report MS-CIS-01-22, University of Pennsylvania (2001).

[Arai1996] Yoshifumi Arai, Shigeki Nakauchi and Shiro Usui, Color Correction Method Based on the Spectral Reflectance Estimation using a Neural Network, *Proc. IS&T/SID the 4th Color Imaging Conference*, 5-9 (1996).

[Barnard1999] Kobus Barnard, *Practical Color Constancy*, PhD Dissertation, School of Computing, Simon Fraser University, Canada (1999).

[Barnard2001] Kobus Barnard, Florian Ciurea and Brian Funt, Sensor Sharpening for Computational Color Constancy, *J. Opt. Soc. Am. A*, **18**, 2728-2743 (2001).

[Berns1988] Roy S. Berns and Kelvin H. Petersen, Empirical Modeling of Systematic Spectrophotometric Errors, *Color Research and Application*, **13**(4), 243-256 (1988).

[Berns1993a] Roy S. Berns, Ricardo J. Motta and Mark E. Gorzynski, CRT Colorimetry. Part I: Theory and Practice, *Color Research and Application*, **18**, 299-314 (1993).

[Berns1993b] Roy S. Berns, Ricardo J. Motta and Mark E. Gorzynski, CRT Colorimetry. Part II: Metrology, *Color Research and Application*, **18**, 315-325 (1993).

[Berns1994] Roy S. Berns and M. J. Shyu, Colorimetric Characterization of a Desktop Drum Scanner via Image Modeling, *Proc. IS&T's 2nd Color Imaging Conference*, 41-44 (1994).

[Berns1998] Roy S. Berns, Francisco H. Imai, Peter D. Burns and Di-Yuan Tseng, Multi-Spectral-Based Color Reproduction Research at the Munsell Color Science Laboratory, *Proc. SPIE Conference on Electronic Imaging*, **3409**, 14-25, (1998).

[Berns2000] Roy S. Berns, *Billmeyer and Saltzman's Principles of Color Technology*, John Wiley & Sons Inc. (2000).

[Boie1992] Robert A. Boie and Ingemar J. Cox, An analysis of Camera Noise, *IEEE Transactions on Pattern Analysis and Machine Intelligence*, **14**, 671-674 (1992).

[Brainard1989] David H. Brainard, Brian A. Wandell and William Cowan, Black Light: How Sensors Filter Spectral Variation of the Illuminant, *IEEE Transactions on Biomedical Engineering*, **36**, 140-149 (1989).

[Brainard1995] David H. Brainard and Doron Sherman, Reconstructing Images from Trichromatic Samples: From Basic Research to Practical Applications, *Proc. IS&T/SID 1995 Color Imaging Conference* (1995).

[Brainard1997a] David H. Brainard and William T. Freeman, Bayesian Color Constancy, *J. Opt. Soc. Am. A*, **14**, 1393-1411 (1997).

[Brainard1997b] David H. Brainard, Wendy A. Brunt and Jon M. Speigle, Color Constancy in the Nearly Natural Image. I. Asymmetric Matches, *J. Opt. Soc. Am. A*, **14**, 2091-2110 (1997).

[Brainard1998] David H. Brainard, Color Constancy in the Nearly Natural Image. 2. Achromatic Loci, *J. Opt. Soc. Am. A*, **15**, 307-325 (1998).

[Buchsbaum1984] G. Buchsbaum and A. Gottschalk, Chromaticity Coordinates of Frequency-Limited Functions, *J. Opt. Soc. Am. A*, **1**, 885-887 (1984).

[Burningham2000] Norman Burningham, Edul Dalal, Status of the Development of International Standards of Image Quality, *Proc. IS&T's 2000 PICS Conference*, 121-123 (2000).

[Burns1987] Peter D. Burns, Analysis of DQE and NEQ Measurement Errors for Medical Imaging Systems, *Proc. SPIE on Medical Imaging*, **767**, 259-270 (1987).

[Burns1996] Peter D. Burns and Roy S. Berns, Analysis Multispectral Image Capture, *Proc. IS&T/SID 4th Color Imaging Conference*, 19-22 (1996).

[Burns1997a] Peter D. Burns and Roy S. Berns, Error Propagation Analysis in Color Measurement and Imaging, *Color Research and Application*, **22**, 280-289 (1997).

[Burns1997b] Peter D. Burns, *Analysis of Image Noise in Multispectral Color Acquisition*, PhD Dissertation, Rochester Institute of Technology (1997).

[Burns1998] Peter D. Burns and Roy S. Berns, Image Noise and Colorimetric Precision in Multispectral Image Capture, *Proc. IS&T's 6th Color Imaging Conference*, 83-85 (1998).

[Chang1988] Yuh-Lin Chang, Ping Liang and Susan Hackwood, Unified Study of Color Sampling, *Applied Optics*, **28**, 809-813 (1988).

[Chen1995] Paul Chen and H. Joel Trussell, Color Filter Design for Multiple Illuminants and Detectors, *Proc. IS&T/SID 1995 Color Imaging Conference*, 67-70 (1995).

[Cheng1998] Fang-Hsuan Cheng, Wen-Hsing Hsu and Te-Wei Chen, Recovering Colors in an Image with Chromatic Illuminant, *IEEE Transactions on Image Processing*, **7**, 1524-1533 (1998).

[Cogno1988] J. A. Cogno, D. Jungman and J. C. Conno, Linear and Quadratic Optimization Algorithms for Computer Color Matching, *Color Research and Application*, **13**, 40-42 (1988).

[Cohen1985] Jozef B. Cohen and William E. Kappauf, Color Mixture and Fundamental Metamers: Theory, Algebra, Geometry, Application, *American Journal of Psychology*, **98**, 171-259 (1985).

[Cohen1988] Jozef B. Cohen, Color and Color Mixture: Scalar and Vector Fundamentals, *Color Research and Application*, **13**, 5-39 (1988).

[Combettes1990] P. L. Combettes and H. J. Trussell, Set Theory and Projection onto Convex Set, *Journal of Optimization Theory and Applications*, **67**, 487-507 (1990).

[Dantzig1998] George B. Dantzig, *Linear Programming and Extensions*, Princeton University Press (1998).

[Davies1962] W. E. R. Davies and G. Wyszecki, Physical Approximation of Color-Mixture Functions, *J. Opt. Soc. Am.*, **52**, 679-685 (1962).

[Debevec2000] Paul Debevec, Tim Hawkins, Chris Tchou, Haarm-Pieter Duiker and Westley Sarokin, Acquiring the Reflectance Field of a Human Face, *Proc. SIGGRAPH 2000 Conference* (2000).

[Deguchi1998] Tatsuya Deguchi and Naoya Katoh, The Effect of User Controls on CRT Monitor Characteristics, *Proc. SPIE 3300*, 219-230 (1998).

[Drew1994] Mark S. Drew and Graham D. Finlayson, Device-Independent Color via Spectral Sharpening, *Proc. IS&T's 2nd Color Imaging Conference*, 121-126 (1994).

[Eem1994] Jae Kwon Eem and Hyun Duk Shin, Reconstruction of Surface Spectral Reflectances using Characteristic Vectors of Munsell Colors, *Proc. IS&T's 2nd Color Imaging Conference*, 127-131 (1994).

[Engeldrum1988] Peter G. Engeldrum, Almost Color Mixture Functions, *Journal of Imaging Technology*, **14**, 108-110 (1988).

[Engeldrum1993] Peter G. Engeldrum, Color Scanner Colorimetric Design Requirements, *Proc. SPIE on Device-Independent Color Imaging and Imaging Systems Integration*, **1909**, 75-83 (1993).

[Engeldrum2000] Peter G. Engeldrum, *Psychometric Scaling: A Toolkit for Imaging Systems Development*, Imcotek Press (2000).

[Engeldrum2001] Peter G. Engeldrum, Psychometric Scaling: Avoiding the Pitfalls and Hazards, *Proc. IS&T's 2001 PICS Conference*, 101-107 (2001).

[Engelhardt1993] Kai Engelhardt and Peter Seitz, Optimum Color Filters for CCD Digital Cameras, *Applied Optics*, **32**, 3015-3023 (1993).

[Evans1953] Ralph M. Evans, W. T. Hanson, Jr. and W. Lyle Brewer, *Principles of Color Photography*, John Wiley and Sons, Inc. (1953).

[Fairchild1991] Mark D. Fairchild and Lisa Reniff, Propagation of Random Errors in Spectrophotometric Colorimetry, *Color Research and Application*, **16**, 360-367 (1991).

[Fairchild1998] Mark D. Fairchild, *Color Appearance Models*, Addison-Wesley (1998).

[Fairchild2001] Mark D. Fairchild, A Revision of CIECAM97s for Practical Applications, *Color Research and Application*, **26**, 418-427 (2001).

[Farrell1993] Joyce E. Farrell and Brian A. Wandell, Scanner Linearity, *Journal of Electronic Imaging*, **2**, 225-230 (1993).

[Farrell1996] Joyce Farrell, Spectral Based Color Image Editing (SBCIE), *Proc. IS&T/SID 4th Color Imaging Conference*, 104-107 (1996).

[Fernandez2001] Scot R. Fernandez and Mark D. Fairchild, Preferred Color Reproduction of Images with Unknown Colorimetry, *Proc. IS&T/SID 9th Imaging Conference*, 274-279 (2001).

[Finlayson1994] G. D. Finlayson, M. S. Drew and B. V. Funt, Spectral Sharpening: Sensor Transformations for Improved Color Constancy, *J. Opt. Soc. Am. A*, **11**, 1553-1563, (1994).

[Finlayson1995] G. D. Finlayson, S. S. Chatterjee and B. V. Funt, Color Angle Invariants for Object Recognition, *Proc. IS&T/SID 1995 Color Imaging Conference*, 44-47 (1995).

[Finlayson1997] Graham D. Finlayson and Mark S. Drew, White-Point Preserving Color Correction, *Proc. IS&T's 5th Color Imaging Conference*, 258-261 (1997).

[Finlayson1998] Graham D. Finlayson, Steven Hordley and Paul M. Hubel, Recovering Device Sensitivities with Quadratic Programming, *Proc. IS&T's 6th Color Imaging Conference*, 90-95 (1998).

[Funt1995] Brian Funt, Linear Models and Computational Color Constancy, *Proc. IS&T/SID 1995 Color Imaging Conference*, 26-29 (1995).

[Giorgianni1998] Edward J. Giorgianni and Thomas E. Madden, *Digital Color Management: Encoding Solutions*, Addison-Wesley (1998).

[Golub1996] Gene H. Golub and Charles F. Van Loan, *Matrix Computations*, Third Edition, The Johns Hopkins University Press (1996).

[Gordon1993] James J. Gordon and Richard A. Holub, On the Use of Linear Transformations for Scanner Calibration, *J. Imaging Sci. Tech*. **18**, 218-219 (1993).

[Gorzynski1999] Mark Gorzynski, Performance of Optimized MultiChannel Image Noise Filters, *Proc. IS&T's 1999 PICS Conference*, 262-265 (1999).

[Granger1998] Edward M. Granger, Image Quality of Digital Cameras, *Proc. IS&T's 1998 PICS Conference*, 188-191 (1998).

[Gruninger1997] John Gruninger and Robert L. Sundberg, Bounds on Component Spectra of Multispectral Images, *Proc. SPIE Algorithms for Multispectral and Hyperspectral Imagery III*, **3071**, 36-46 (1997).

[Haneishi1997] Hideaki Haneishi, Takayaki Hasegawa, Norimichi Tsumura and Yoichi Miyake, Design of Color Filters for Recording Artworks, *Proc. IS&T's 50th Annual Conference*, 369-372 (1997).

[Hardeberg1998] Jon Yngve Hardeberg, Hans Brettel and Francis Schmitt, Spectral Characterization of Electronic Cameras, *Proc. SPIE Conference on Electronic Imaging*, **3409**, 100-109 (1998).

[Hardeberg2000] Jon Y. Hardeberg, Francis Schmitt and Hans Brettel, Multispectral Image Capture using a Tunable Filter, *Proc. IS&T/SPIE Conference on Color Imaging*, **3963**, 77-88 (2000).

[Hauta-Kasari1999] Markku Hauta-Kasari, *Computational Techniques for Spectral Image Analysis*, PhD Dissertation, Lappeenranta University of Technology, Finland (1999).

[Hauta-Kasari1999] Markku Hauta-Kasari, Kanar Miyazawa, Satoru Toyooka and Jussi Parkkinen, Spectral Vision System for Measuring Color Images, *J. Opt. Soc. Am. A*, **16,** 2352-2361 (1999).

[Herzog1999] Patrick G. Herzog, Dietmar Knipp, Helmut Stiebig and Friedhelm König, Colorimetric Characterization of Novel Multiple-Channel Sensors for Imaging and Metrology, *Journal of Electronic Imaging*, **8**, 342-353 (1999).

[Herzog2000] Patrick G. Herzog, Dietmar Knipp, Friedhelm Konig and Helmut Stiebig, Performance of Amorphous-Silicon Based Multiple-Channel Color Sensors, *Proc. IS&T/SID Conference on Color Imaging*, **3963**, 60-69 (2000).

[Hill1998] Bernhard Hill, Multispectral Color Technology: A Way towards High Definition Color Image Scanning and Encoding, Proc. *SPIE Conference on Electronic Imaging*, **3409**, 2-13 (1998).

[Holm2000] Jack Holm, Ingeborg Tastl and Steven Hordley, Evaluation of DSC (Digital Still Camera) Scene Analysis Error Metrics – Part 1, *Proc. IS&T/SID's 8th Color Imaging Conference*, 279-287 (2000).

[Holst1998] Gerald C. Holst, *CCD Arrays, Cameras and Displays*, Second Edition, SPIE Optical Engineering Press (1998).

[Horn1984] Berthold K. P. Horn, *Exact Reproduction of Colored Images*, Academic Press (1984).

[Hosoi1999] Asako Hosoi, Kimiyoshi Miyata, Hideaki Haneishi and Yoichi Miyake, Filter Design of Multispectral Camera Based on CCD Sensor Noise Analysis, *Proc. International Symposium on Multispectral Imaging and Color reproduction for Digital Archives*, 159-162 (1999).

[Hubel1994] Paul M. Hubel, Doron Sherman and Joyce E. Farrell, A Comparison of Methods of Sensor Spectral Sensitivity Estimation, *Proc. IS&T's 2nd Color Imaging Conference*, 45-48 (1994).

[Hubel1999] Paul M. Hubel, Color Image Quality in Digital Cameras, *Proc. IS&T's 1999 PICS Conference*, 153-157 (1999).

[Hubel2000] Paul M. Hubel, The Perception of Color at Dawn and Dusk, *J. Imaging Science and Technology*, **44**, 371-375 (2000).

[Huffel1991] Sabine Van Huffel and Joos Vandewalle, *The Total Least Squares Problem: Computational Aspects and Analysis*, Sociaty for Industrial and Applied Mathematics, Philadelphia, 1-91 (1991).

[Hung1993] Po-Chieh Hung, Colorimetric Calibration in Electronic Imaging Devices using a Look-Up-Table Model and Interpolations, *Journal of Electronic Imaging*, **2**, 53-61 (1993).

[Hung2000] Po-Chieh Hung, Comparison of Camera Quality Indexes, *Proc. IS&T/SID's 8th Color Imaging Conference*, 167-171 (2000).

[Hunt1995] R. W. G. Hunt, *The Reproduction of Colour*, Fountain Press, England (1995).

[IEC1998] International Electrotechnical Commission, 100/PT61966(PL)55, *Color Measurement and Management in Multimedia Systems and Equipment – Part 9: Digital Cameras* (1998).

[IEC1999] International Electrotechnical Commission, 100/PT61966(PL)84, *Color Measurement and Management in Multimedia Systems and Equipment* (1999).

[Iino1998a] Koichi Iino and Roy S. Berns, Building Color-Management Modules Using Linear Optimization I. Desktop Color System, *Journal of Imaging Science and Technology*, **42**, 79-94 (1988).

[Iino1998b] Koichi Iino and Roy S. Berns, Building Color-Management Modules Using Linear Optimization II. Prepress System for Offset Printing, *Journal of Imaging Science and Technology*, **42**, 99-114 (1988).

[Imai1996a] Francisco H. Imai, Norimichi Tsumura, Hideaki Haneishi and Yoichi Miyake, Spectral Reflectance of Skin Color and its Applications to Color Appearance Modeling, *Proc. IS&T/SID 4th Color Imaging Conference*, 121-124 (1996).

[Imai1996b] Francisco Hideki Imai, Norimichi Tsumura, Hideaki Haneishi and Yoichi Miyake, Principal Component Analysis of Skin Color and Its Application to Colorimetric Color Reproduction on CRT Display and Hardcopy, *Journal of Imaging Science and Technology*, **40**, 422-430 (1996).

[Imai1997] Francisco Hideki Imai, Norimichi Tsumura, Hideaki Haneishi and Yochi Miyake, Prediction of Color Reproduction for Skin Color Under Different Illuminants Based on Color Appearance Models, *Journal of Imaging Science and Technology*, **41**, 166-173 (1997).

[Imai1999] Francisco H. Imai, *Multispectral Image Acquisition and Spectral Reconstruction using a Trichromatic Digital Camera System Associated with Absorption Filters*, Research Report of Munsell Color Science Laboratory, Rochester Institute of Technology (1999).

[Imai2001] Francisco H. Imai, Shuxue Quan, Mitchell R. Rosen and Roy S. Berns, Digital Camera Filter Design for Colorimetric and Spectral Accuracy, *Proc. 3rd International Conference on Multispectral Color Science*, 13-16 (2001).

[Janssen2001] Ruud Janssen, *Computational Image Quality*, SPIE Press, Vol. PM101 (2001).

[Jaramillo1993] Andres B. Jaramillo and Kazuo Yamaba, An Artificial Neural Network for Classification of Color Images, *Proc. IS&T/SID's 2nd Color Imaging Conference*, 167-173(1993).

[Johnson1998] Richard A. Johnson and Dean W. Wichern, *Applied Multivariate Statistical Analysis*, Fourth Edition, Prentice Hall (1998).

[Johnson2000] Garrett M. Johnson and Mark D. Fairchild, Sharpness Rules, *Proc. IS&T/SID 8th Imaging Conference*, 24-30 (2000).

[Johnson2001] Garrett M. Johnson and Mark D. Fairchild, Darwinism of Color Image Difference Models, *Proc. IS&T/SID 9th Color Imaging Conference*, 108-112 (2001).

[Juenger1998] Andrew Juenger, Color Sensitivity Selection for Electronic Still Cameras Based on Noise Considerations in Photographic Speed Maximization, *Proc. IS&T's 1998 PICS Conference*, 79-83 (1998).

[Jung2001] J. Jung, R. Gleelen and D. Vandenbroucke, The Virtual Image Chain: A Powerful Tool for the Evaluation of the Perceived Image Quality: a Function of Imaging System Parameters, *Proc. IS&T's 2001 PICS Conference*, 128-131 (2001).

[Kang1992a] Henry R. Kang, Color Scanner Calibration of Reflected Samples, *Proc. SPIE Color Hard Copy and Graphic Arts*, **1670**, 468-477 (1992).

[Kang1992b] Henry R. Kang, Color Scanner Calibration, *Journal of Imaging Science and Technology*, **36**, 162-170 (1992).

[Katoh1997] Naoya Katoh and Tatsuya Deguchi, Reconsideration of CRT Monitor Characteristics, *Proc. IS&T's 5th Color Imaging Conference*, 33-40 (1997).

[Kawata1987a] S. Kawata, K. Sasaki and S. Minami, Component Analysis of Spatial and Spectral Patterns in Multispectral Images. I. Basis, *J. Opt. Soc. Am. A*, **4**, 2101-2106 (1987).

[Kawata1987b] S. Kawata, K. Sasaki and S. Minami, Component Analysis of Spatial and Spectral Patterns in Multispectral Images. II. Entropy Minimization, *J. Opt. Soc. Am. A*, **6**, 73-79 (1987).

[Keusen1995] Thomas Keusen and Werner Praefcke, Multispectral Color System with an Encoding Format Compatible to the Conventional Tristimulus Model, *Proc. IS&T/SID 1995 Color Imaging Conference*, 112-114 (1995).

[Kim1994] Jeong-Yeop Kim, Sung-Ho Bae, Eung-Joo Lee and Yeong-Ho Ha, Color Image Enhancement Based on Land's Color Constancy Algorithm, *Proc. IS&T's 2nd Color Imaging Conference*, 131-136 (1994).

[König1997] Friedhelm König, Reconstruction of Natural Spectra from a Color Sensor Using Nonlinear Estimation Methods, *Proc. IS&T's 50th Annual Conference*, 454-458 (1997).

[König1998] Friedhelm König and Werner Praefcke, The Practice of Multispectral Image Acquisition, *Proc. SPIE Conference on Electronic Imaging*, 3409, 34-41, 1998

[König2000] Friedhelm König and Patrick G. Herzog, Spectral Scanner Characterization using Linear Programming, *Proc. IS&T/SPIE Conference on Color Imaging*, **3963**, 36-46 (2000).

[Kotera1994] Hiroaki Kotera, Quality Measure of Color Scanning Filters, *Proc. IS&T's 2nd Color Imaging Conference*, 58-61 (1994).

[Kotera1996] Hiroaki Kotera, Hideta Motomura and Teruo Fumoto, Recovery of Fundamental Spectrum from Color Signals, *Proc. IS&T/SID 4th Color Imaging Conference*, 141-144 (1996).

[Kotera1999] Hiroaki Kotera, Chen Hung-Shing and Ryoich Saito, Generation of Virtual Spectral Color Target and Its Application, *Proc. IS&T/SID 7th Color Imaging Conference*, 36-41 (1999).

[Kotera2001] Hiroaki Kotera, RGB to Spectral Image Conversion with Spectral Pallet and Compression by SVD, *Proc. 3rd International Conference on Multispectral Color Science*, 45-48 (2001).

[Kraft1999] J. M. Kraft and D. H. Brainard, Mechanisms of Color Constancy under Nearly Natural Viewing, *Proc. Natl. Acad. Sci. USA*, **96**, 307-312 (1999).

[Kriss1996] Michael A. Kriss, Color Filter Arrays for Digital Electronic Still Cameras, *Proc. IS&T's 49th Annural Conference*, 272-278 (1996).

[Laflaquière1998] Ph. Laflaquière, D. Lafon, O. Eterradossi and P. Slangen, Characterization of Color Texture – CIELAB calibration of CCD device, *Proc. EUROPTO Conference on Electronic Imaging*, SPIE **3409**, 118-127 (1998).

[Lake1998] Don W. Lake, CMOS Image Capture for Digital Still Cameras, *Proc. IS&T's 1998 PICS Conference*, 87-90 (1998).

[Lee2000] Eul Hwan Lee, Suk Chul Ahn and Jae Ho Kim, Color Reproduction Based on Spectral Reflectance, *Proc. IS&T/SID Conference on Color Imaging*, **3963**, 101-108 (2000).

[Lehmann2001] Thomas M. Lehmann and Christoph Palm, Color Line Search for Illuminant Estimation in Real-World Scenes, *J. Opt. Soc. Am. A*, **18**, 2679-2691 (2001).

[Lenz1996] U. Lenz, Dr. Habil and R. Lenz, Digital Camera Color Calibration and Characterization, *Proc. IS&T/SID 4th Color Imaging Conference*, 23-24 (1996).

[Liu1991] Yan Liu, Roy S. Berns and Yuexin Shu, Optimization algorithm for designing colored glass filters to simulate CIE illuminant D65, *Color Research and Application*, **16**, 89-96 (1991).

[Longère2001] Philippe Longère and David Brainard, Simulation of Digital Camera Images from Hypotheticall Input, In *Vision Models and Applications to Image and Video Processing*. C. van den Branden Lambrecht (ed.)., Kluwer (2001).

[Lopez-Estrada2000] Alex A. Lopez-Estrada and Peter D. Burns, Propagation of Noise Statistics in Digital Photofinishing Image Processing, *Proc. IS&T 2000 PICS Conference*, 297-300 (2000).

[Luenberger1969] David G. Luenberger, *Optimization by Vector Space Methods*, John Wiley and Sons, Inc. (1969).

[Luther1927] R. Luther, Aus Dem Gebiet der Farbreizmetrik, *Z. Technol. Phys.*, **8**, 540-558 (1927).

[Magnus1999] Jan R. Magnus and Heinz Neudecker, *Matrix Differential Calculus with Applications in Statistics and Econometrics*, Revised Edition, John Wiley and Sons Inc. (1999).

[Mahy1994] M. Mahy, P. Wambacq, L. Van Ekcken and A. Oosterlinck, Optimal Filters for the Reconstruction and Discrimination of Reflectance Curves, *Proc. IS&T's 2nd Color Imaging Conference*, 140-143 (1994).

[Maloney1986] Laurence T. Maloney and Brian Wandell, Color Constancy: A Method for Recovering Surface Spectral Reflectance, *J. Opt. Soc. Am. A*, **3**, 29-33 (1986).

[Manabe2001] Yoshitsugu Manabe, Shinichi Kurosaka and Kunihiro Chihara, Simultaneous Measurement of Spectral Distribution and Shape using Imaging Spectrograph, *Proc. 3rd International Conference on Multispectral Color Science*, 37-40 (2001).

[Marchant2001] J. A. Marchant and C. M. Onyango, Color Invariant for Daylight Changes: Relaxing the Constraints on Illuminants, *J. Opt. Soc. Am. A*, **18**, 2704-2706 (2001).

[Marcu1994] Gabriel Marcu and Satoshi Abe, CRT and Ink Jet Printer Models for Device Independent Color Reproduction in Image Transmission, *Proc. IS&T's 2nd Color Imaging Conference*, 143-147 (1994).

[Marimont1992] David H. Marimont and Brian A. Wandell, Linear Models of Surface and Illuminant Spectra, *J. Opt. Soc. Am. A*, **9**, 1905-1913 (1992).

[Martinez-Verdu2002] Francisco Martinez-Verdu, Jaume Pujol and Pascual Capilla, Calculation of the Color Matching Functions of Digital Cameras from Their Complete Spectral Sensitivities, *J. Imag. Sci. Tech.*, **46**, 15-25 (2002)

[Martinkauppi2001] J. B. Martinkauppi and M. N. Soriano, Basis Functions of the Color Signal of Skin under Diferent Illuminants, *Proc. 3rd International Conference on Multispectral Color Science*, 21-24 (2001).

[Matsushiro2001] Nobuhito Matsushiro, Francisco H. Imai and Noboru Ohta, Principal Component Analysis of Spectral Images Based on the Independence of the Color Matching Function Vectors, *Proc. 3rd International Conference on Multispectral Color Science*, 77-80 (2001).

[McCurnin1993] Thomas W. McCurnin, Larry C. Schooley and Gary R. Sims, Charge-coupled device signal processing models and comparisons, *Journal of Electronic Imaging*, **2**, 100-107 (1993).

[Mendez-Diaz1988] I. Mendez-Diaz and J. A. Cogno, Mixed-Integer Programming Algorithms for Computer Color Matching, *Color Research and Application*, **13**, 43-45 (1988).

[Mesarovic1995] Vladimir Z. Mesarovic, Nikolas P. Galatsanos and Aggelos K. Katsaggelos, Regularized Constrained Total Least Squares Image Restoration, *IEEE Transactions on Image Processing*, **4**, 1096-1108 (1995).

[Miyake1998] Yoichi Miyake and Yasuaki Yokoyama, Obtaining and Reproduction of Accurate Color Images Based on Human Perception, *Proc. SPIE 3300*, 190-197 (1998).

[Montag2001] Ethan D. Montag and Hirokazu Kasahara, Multidimensional Analysis Reveals Importance of Color for Image Quality, *Proc. IS&T/SID 9th Imaging Conference*, 17-21 (2001).

[Morimont1995] David H. Morimont and Brian A. Wandell, Chromatic Aberration, Linear Models and Matching Color Images, *Proc. IS&T/SID 1995 Color Imaging Conference*, 41-44 (1995).

[Morovic1998] Ján Morovic, *To Develop a Universal Gamut Mapping Algorithm*, PhD Dissertation, University of Derby, UK (1998).

[Neugebauer1956] H. E. J. Neugebauer, Quality Factor for Filters Whose Spectral Transmittances are Different from Color Mixture Curves, and Its Application to Color Photography, *J. Opt. Soc. Am.*, **46**, 821-824 (1956).

[Nishio2000] Kenichi Nishio, *Color in CCD Cameras*, Internal Research Report of Sony Corp., Japan (2000).

[Ohta1971] Noboru Ohta, The Color Gamut Obtainable by the Combination of Subtractive Color Dyes, *Photographic Science and Engineering*, **15**, 399-415 (1971).

[Ohta1975] Noboru Ohta and G. Wyszecki, Theoretical Chromaticity-Mismatch Limits of Metamers Viewed under Different Illuminants, *J. Opt. Soc. Am.*, **65**, 327-333 (1975).

[Ohta1981a] Noboru Ohta, Evaluation of Spectral Sensitivities, *Photographic Science and Engineering*, **25**, 101-107 (1981).

[Ohta1981b] Noboru Ohta, A simplified Method for Formaulating Pseudo-Object Colors, *Color Research and Application*, **7**,78-81 (1981).

[Ohta1982] Noboru Ohta, Practical Transformations of CIE Color-Matching Functions, *Color Research and Application*, **8**, 53-56 (1982).

[Ohta1983] Noboru Ohta, Optimization of Spectral Sensitivities, *Photographic Science and Engineering*, **27**, 193-201 (1983).

[Ohta1991] Noboru Ohta, Interrelation between Spectral Sensitivities and Interimage Effects, *J. Imaging Science*, **35**, 94-103 (1991).

[Ohta1992] Noboru Ohta, Colorimetric Analysis in the Design of Color Films: A Perspective, *J. Imaging Science and Technology*, **36**, 63-72 (1992).

[Ohta1997a] Noboru Ohta, *Color Engineering* (in Chinese, Translated by Liu Zhongben), Xi'an Jiaotong University Press, China (1997).

[Ohta1997b] Noboru Ohta, *The Foundamentals of Color Reproduction Engineering*, Published in Tokyo, Japan (1997).

[Ohta2000] Noboru Ohta, Color Reproduction Systems: Basis and Optimization, *Annual Meeting of Society of Photographic Science and Technology of Japan'2000*, 23-26 (2000).

[Okano1997] Yukio Okano, MTF Analysis and its Measurements for Digital Still Camera, *Proc. IS&T's 50th Annual Conference*, 383-387 (1997).

[Pappas2000] Michail Pappas and Ioannis Pitas, Digital Color Restoration of Old Paintings, *IEEE Transactions on Image Processing*, **9**, 291-294 (2000).

[Park1977] Stephen K. Park and Friedrich O. Huck, Estimation of Spectral Reflectance Curves from Multispectral Image Data, *Applied Optics*, **16**, 3107-3114 (1977).

[Park1995] Seung Ok Park, Hong Suk Kim and Jung Man Park, Development of Spectral Sensitivity Measurement System of Image Sensor Devices, *Proc. IS&T/SID 1995 Color Imaging Conference*, 26-29 (1995).

[Pei2001] Soo-Chang Pei, Ching-Long Tseng and Chai-Che Wu, Using Color Histogram Normalization for Recovering Chromatic Illumination-Changed Images, *J. Opt. Soc. Am. A*, **18**, 2641-2657 (2001).

[Praefcke1995] Werner Praefcke and Thomas Keusen, Optimized Basis Functions for Coding Reflectance Spectra Minimizing the Visual Color Difference, *Proc. IS&T/SID 1995 Color Imaging Conference*, 37-40 (1995).

[Praefcke1996] Werner Praefcke, Transform Coding of Reflectance Spectra Using Smooth Basis Vectors, *Journal of Imaging Science and Technology*, **40**, 543-548 (1996).

[Praefcke1998] Werner Praefcke and Friedhelm König, Performance Estimation of Color Printing Models, *Proc. SPIE Conference on Electronic Imaging*, **3409**, 26-33 (1998).

[Pratt1976] William K. Pratt and Clanton E. Mancill, Spectral Estimation Techniques for the Spectral Calibration of a Color Image Scanner, *Applied Optics*, **15**, 73-75 (1976).

[Pratt1991] William K. Pratt, Chapter 12: Spatial Image Restoration Techniques, in *Digital Image Processing*, 2nd Edition, John Wiley and Sons Inc., 351-397 (1991).

[Press1997] William H. Press, Saul A. Teukolsky, William T. Vetterling and Brian P. Flannery, *Numerical Recipes in C: The Art of Scientific Computing*, Second Edition, Cambridge University Press (1997).

[Quan1998] Shuxue Quan, Using RIT-Dupont Data to Test Color Difference Formulae on Color Appearance Models, Term Paper for Color Appearance Course (1998).

[Quan2000a] Shuxue Quan and Noboru Ohta, Evaluating Quality Factors of Hypothetical Spectral Sensitivities, *Proc. IS&T's 2000 PICS Conference*, 37-42 (2000).

[Quan2000b] Shuxue Quan and Noboru Ohta, Optimal Design and Quality Factors of Camera Spectral Sensitivities, *Annual Meeting of Society of Photographic Science and Technology of Japan'2000*, 111-112 (2000).

[Quan2000c] Shuxue Quan and Noboru Ohta, Optimization of Camera Spectral Sensitivities, *Proc. IS&T/SID's 8th Color Imaging Conference*, 273-278 (2000).

[Quan2001a] Shuxue Quan and Noboru Ohta, Optimal Camera Filter Based on Fabrication Process, *Annual Meeting of Society of Photographic Science and Technology of Japan'2001*, 41-42 (2001).

[Quan2001b] Shuxue Quan, Noboru Ohta, Mitchell Rosen and Naoya Katoh, Fabrication Tolerence and Optimal Design of Spectral Sensitivities for Color Imaging Devices, *Proc. IS&T's 2001 PICS Conference*, 277-282 (2001).

[Quan2001c] Shuxue Quan, Noboru Ohta, Roy S. Berns and Naoya Katoh, Optimal Design of Camera Spectral Sensitivity Functions Based on Practical Filter Components, *Proc. IS&T/SID 9th Color Imaging Conference*, 326-331 (2001).

[Quan2001d] Shuxue Quan, Noboru Ohta, Mitchell R. Rosen and Naoya Katoh, *A System And Method For Analyzing, Optimizing And/Or Designing Spectral Sensitivity Curves For An Imaging Device*, US Patent Application, pending (2001).

[Quan2002a] Shuxue Quan and Noboru Ohta, Evaluating Hypothetical Spectral Sensitivities with Quality Factors, *Journal of Imaging Science and Technology*, **46**: 8-14 (2002).

[Quan2002b] Shuxue Quan, Noboru Ohta, Roy S. Berns, Xiaoyun Jiang and Naoya Katoh, Uninified Measure of Goodness and Optimal Design of Spectral Sensitivity Functions, (in Review), *Journal of Imaging Science and Technology* (2002).

[Rasmussen1998] D. René Rasmussen, Peter A. Grean, Fumio Nakaya, Masaari Sato and Edul Dalal, Image Quality Metrics: Applications and Requirements, *Proc. IS&T's 1998 PICS Conference*, 174-178 (1998).

[Ritter1999] Michaela Ritter and Dietmar Wueller, Color Characterization of Digital Cameras by Analyzing the Output Data for Measuring the Spectral Response, *Proc. IS&T's 1999 PICS Conference*, 149-152 (1999).

[Robins1991] Ashley H. Robins, *Biological Perspectives on Human Pigmentation*, Cambridge University Press, 1-122 (1991).

[Roetling1993] Paul G. Roetling, Integrating Scanners into Color Systems, *Proc. IS&T/SID's 2nd Color Imaging Conference*, 92-94 (1993).

[Rosen1999] Mitchell R. Rosen and Xiaoyun Jiang, Lippmann2000: A Spectral Image Database Under Construction, *Proc. International Symposium on Multispectral Imaging and Color reproduction for Digital Archives*, 117-122 (1999).

[Roweis2000] Sam T. Roweis and Lawrence K. Saul, Nonlinear Dimensionality Reduction by Locally Linear Embedding, *Science*, **290**, 2323-2326 (2000).

[Rutherford2000] Melissa Drake Rutherford, *The Role of Illumination Perception in Color Constancy*, PhD Dissertation, University of California at Santa Barbara (2000).

[Rutherford2001] M. D. Rutherford and D. H. Brainard, Lightness Constancy: A Direct Test of the Illumination Estimation Hypothesis, *Psychological Science*, **13**, 142-149, http://color.psych.upenn.edu/brainard/pubs.html (2001).

[Sampat2000] Nitin Sampat, Shyam Venkataraman and Robert Kremens, System Implications of Implementing White Balance on Consumer Digital Cameras, *Proc. SPIE Conference on Sensors and Camera Systems for Scientific, Industrial and Digital Photography Applications*, **3409**, 456-461(2000).

[Sanger1994] Demas Sanger, Takuya Asada, Hideaki Haneishi and Yoichi Miyake, Facial Pattern Detection and Its Preferred Color Reproduction, *Proc. IS&T's 2nd Color Imaging Conference*, 149-153 (1994).

[Sato1996] Takayuki Sato *et al*, Color Reproduction Based on Low Dimensional Spectral Reflectance Using the Principal Component Analysis, *Proc. IS&T/SID 4th Color Imaging Conference*, 185-187 (1996).

[Schreiber1985] William F. Schreiber, *Color Reproduction System*, US Patent, 4500919 (1985).

[Schultz1995] Richard R. Schultz and Robert L. Stevenson, Stochastic Modeling and Estimation of Multispectral Image Data, *IEEE Transactions on Image Processing*, **4**, 1109-1119 (1995).

[Sharma1993] Gaurav Sharma and H. J. Trussell, Characterization of Scanner Sensitivity, *Proc. IS&T/SID's 2nd Color Imaging Conference*, 103-107 (1993).

[Sharma1994] G. Sharma and H. J. Trussell, Decomposition of Fluorescent Illuminant Spectra for Accurate Colorimetry, *IEEE 0-8186-6950-0/94*, 1002-1006 (1994).

[Sharma1996a] G. Sharma and H. J. Trussell, Color Scanner Performance Trade-Offs, Proc. *SPIE 2658*, 270-278 (1996).

[Sharma1996b] Gaurav Sharma and H. Joel Trussell, Measures of goodness for Color Scanners, *Proc. IS&T/SID 4th Color Imaging Conference*, 28-32 (1996).

[Sharma1996c] Gaurav Sharma and H. Joel Trussell, Set Theoretic Estimation in Color Scanner Characterization, *J. Electronic Imaging*, **5**, 479-489 (1996).

[Sharma1996d] Gaurav Sharma, *Color Scanner Characterization, Performance Evaluation and Design*, PhD Dissertation, North Carolina State University (1996).

[Sharma1997a] Gaurav Sharma and H. Joel Trussell, Digital Color Imaging, *IEEE Transactions on Image Processing*, **6**, 901-932 (1997).

[Sharma1997b] Gaurav Sharma and H. Joel Trussell, Figures of Merit for Color Scanners, *IEEE Transactions on Image Processing*, **6**, 990-1001 (1997).

[Sharma1997c] Gaurav Sharma and H. Joel Trussell, Set Theoretic Signal Restoration Using an Error in Variables Criterion, *IEEE Transactions on Image Processing*, **6**, 1692-1697 (1997).

[Sharma1998] Gaurav Sharma, H. Joel Trussell and Michael J. Vrhel, Optimal Nonnegative Color Scanning Filters, *IEEE Transactions on Image Processing*, **7**, 129-133 (1998).

[Sharma1999] Gaurav Sharma, Target-less Scanner Color Calibration, *Proc. IS&T/SID 7th Color Imaging Conference*, 69-74 (1999).

[Shimano2000a] Noriyuki Shimano, Colorimetric Evaluation of Color Image Acquisition Systems I – A Proposal of a New Colorimetric Quality Factor, *Journal of Electronic Photography in Japan*, **29**, 506-516 (2000).

[Shimano2000b] Noriyuki Shimano, Colorimetric Evaluation of Color Image Acquisition Systems II – Experimental Results, *Journal of Electronic Photography in Japan*, **29**, 517-525 (2000).

[Slater1995] David Slater and Glenn Healey, Illumination-Invariant Recognition of Local Color Distributions using Linear Models for Spectral Reflectance, *Proc. IS&T/SID 1995 Color Imaging Conference*, 34-36 (1995).

[Speigle1999] Jon M. Speigle and David H. Brainard, Predicting Color from Gray: the Relationship between Achomatic Adjustment and Asymmetric Matching, *J. Opt. Soc. Am. A*, **16**, 2370-2376 (1999).

[Stark1992] Henry Stark and Elwood T. Olsen, Projection-Based Image Restoration, *J. Opt. Soc. Am. A*, **9**, 1914-1919 (1992).

[Starkweather1993] Gary Starkweather, Integrating Color Printers into Color Systems, *Proc. IS&T/SID's 2nd Color Imaging Conference*, 101-103 (1993).

[Stokes2001] Michael Stokes, Requirement for Digital Still Cameras from the Computer Software Manufacturers' Point of View, *Annual Meeting of Society of Photographic Science and Technology of Japan'2001*, 1-2 (2001).

[Sun2000] Yinlong Sun, *A Spectrum-Based Framework for Realistic Image Synthesis*, PhD Theses, Simon Fraser University, Canada (2000).

[Sun2001] Qun Sun and Mark D. Fairchild, Statistical Characterization of Spectral Reflectances in Spectral Imaging of Human Portraiture, *Proc. IS&T/SID's 9th Color Imaging Conference*, 73-79 (2001).

[Tajima1996] J Tajima, New Quality Measurements for a Set of Color Sensors Weighted Quality Factor, Spectral Characteristic Restorability Index and Color Reproducibility Index, *Proc. 4th IS&T/SID Color Imaging Conference*, 25-28 (1996).

[Tajima1998a] J. Tajima, A Huge Spectral Characteristics Database and Its Application to Color Imaging Device Design, *Proc. IS&T's 6th Color Imaging Conference*, 86-89 (1998).

[Tajima1998b] Johji Tajima, Masato Tsukada, Yoichi Miyake, Hideaki Haneishi, Norimichi Tsumura, *et al*, Development and Standardization of a Spectral Characteristics Data Base for Evaluating Color Reproduction in Image Input Devices, *Proc. SPIE Conference on Electronic Imaging*, **3409**, 42-50 (1998).

[Tajima1999] Johji Tajima, Development and Analysis of Standard Object Color Spectra Database (SOCS), *Proc. International Symposium on Multispectral Imaging and Color reproduction for Digital Archives*, 26-33 (1999).

[Tan2000] Yap-Peng Tan and Tinku Acharya, A Method for Color Correction with Noise Consideration, *Proc. SPIE 3963*, 329-337 (2000).

[Tang1991] Shunqing Tang, *Colorimetry* (in Chinese), Beijing Institute of Technology Press, China (1991).

[Tao2000] Bo Tao and Ingeborg Tastl, Illumination Estimation using Linear Decomposition and Constrained Optimization, *Proc. IS&T/SPIE Conference on Color Imaging*, **3963**, 143-154 (2000).

[Tastl2000] Ingeborg Tastl and Bo Tao, Color Transformations for Digital Camera: a Comparison and a Contribution, *Proc. IS&T/SID Conference on Color Imaging*, **3963**, 89-100 (2000).

[Tenenbaum2000] Joshua B. Tenenbaum, Vin de Silva and John C. Langford, A Global Geometric Framework for Nonlinear Dimensionality Reduction, *Science*, **290**, 2319-2322 (2000).

[Thomson2001] M. Thomson and S. Westland, Colour-Imager Characterization by Parametric Fitting of Sensor Responses, *Color Research and Application*, **26,** 442-449 (2001).

[Tominaga1993] Shoji Tominaga, A Neural Network Approach to Color Reproduction in Color Printers, *Proc. IS&T/SID's 2nd Color Imaging Conference*, 173-177 (1993).

[Tominaga1994] Shoji Tominaga, Dichromatic Reflection Models for a Variety of Materials, *Color Research and Application*, **19**, 277-285 (1994).

[Tominaga1995] Shoji Tominaga, Using Reflectance Models for Surface Estimation, *Proc. IS&T/SID 1995 Color Imaging Conference*, 29-33 (1995).

[Tominaga1996] Shoji Tominaga, Dichromatic Reflection Models for Rendering Object Surfaces, *Journal of Imaging Science and Technology*, **40**, 549-555 (1996).

[Tominaga1998] Shoji Tominaga, Color Conversion Using Neural Network, *Proc. SPIE 3300*, 66-75 (1998).

[Tominaga1999a] Shoji Tominaga, Multi-Channel Cameras and Spectral Image Processing, *Proc. International Symposium on Multispectral Imaging and Color reproduction for Digital Archives*, 18-25 (1999).

[Tominaga1999b] Shoji Tominaga, Satoru Ebisui and Brian A. Wandell, Color Temperature Estimation of Scene Illumination, *Proc. IS&T/SID 7th Color Imaging Conference*, 42-47 (1999).

[Tominaga1999c] Shoji Tominaga, Spectral Imaging by a Multichannel Camera, *Journal of Electronic Imaging*, **8**, 332-341 (1999).

[Tominaga2000] Shoji Tominaga, Lighting System for Color Images, *Proc. IS&T/SPIE Conference on Color Imaging*, **3963**, 15-26 (2000).

[Tominaga2001] Shoji Tominaga, Toshinori Matsumoto and Norihiro Tanaka, 3D Recording and Rendering for Art Paintings, *Proc. IS&T/SID 9th Color Imaging Conference*, 337-341 (2001).

[Trussell1991] H. J. Trussell, Applications of Set Theoretic Methods to Color Systems, *Color Research and Application*, **16**, 31-41 (1991).

[Trussell1994] H. J. Trussell and Manish S. Kulkarni, Estimation of Color under Fluorescent Illuminants, *IEEE 0-8186-6950-0/94*, 1006-1009 (1994).

[Trussell1996] H. J. Trussell and Manish S. Kulkarni, Sampling and Processing of Color Signals, *IEEE Transactions on Image Processing*, **5**, 677-681 (1996).

[Trussell1997] H. J. Trussell and M. J. Vrhel, Color Computation: Consistency or Accuracy, *Proc. IS&T's 5th Color Imaging Conference*, 306-309 (1997).

[Tsumura1997] Norimichi Tsumura, Takaya Tanaka, Hideaki Haneishi and Yoichi Miyake, Optimal Spectraal Transmittance of Color Filters on Single Chip CCD for Electronic Endoscope, *Proc. IS&T's 50th Annual Conference*, 373-376 (1997).

[Tsumura1999] Norimichi Tsumura, Hideki Sato, Takayuki Hasegawa, Hideaki Haneishi and Yoichi Miyake, Limitation of Color Samples for Spectral Estimation from Sensor Responses in Fine Art Painting, *Optical Review*, **6**, 57-61 (1999).

[Tzeng1998] Di-Yuan Tzeng and Roy S. Berns, Spectral-Based Ink Selection for Multiple-Ink Printing I. Colorant Estimation of Original Objects, *Proc. IS&T's 6th Color Imaging Conference*, 106-111 (1998).

[Tzeng1999] Di-Yuan Tzeng, *Spectral-Based Color Separation Algorithm Development for Multiple-Ink Color Reproduction*, PhD Dissertation, Rochester Institute of Technology, New York, USA (1999).

[Viggiano1990] J A Stephen Viggiano, The Comparison of Radiance Ratio Spectra: Assessing a Model's "Goodness of Fit," *Proc. SPSE's 43rd Annual Conference*, 222-225 (1990).

[Viggiano2001] J A Stephen Viggiano, A Perception-referenced Method for Comparison of Radiance Ratio Spectra and its Application as an Index of Metamerism, *Proc. AIC 2001*, 423-424 (2001).

[Vora1993a] P. L. Vora and H. J. Trussell, Measure of Goodness of a Set of Color-Scanning Filters, *J. Opt. Soc. Am. A*, **10**, 1499-1508 (1993).

[Vora1993b] Poorvi L. Vora and H. Joel Trussell, A Mathematical Method for Designing a Set of Color Scanning Filters, *Proc. SPIE Color Hard Copy and Graphic Arts*, **1912**, 322-329 (1993).

[Vora1997a] Poorvi L. Vora, J. E. Farrell, J. D. Tietz and D. Brainard, Linear Models for Digital Cameras, *Proc. IS&T's 50th Annual Conference*, 377-382 (1997).

[Vora1997b] Poorvi L. Vora and H. Joel Trussell, Mathematical Methods for the Design of Color Scanning Filters, *IEEE Trans. on Image Processing*, **6**, 312-320 (1997).

[Vora1997c] Poorvi L. Vora, Joyce E. Farrell, Jerome D. Tietz and David Brainard, *Digital Color Cameras – 1 – Response models*, HP Technical Report (1997).

[Vora1997d] P. L. Vora and H. J. Trussell, Mathematical Methods for the Analysis of Color Scanning Filters, *IEEE Transactions on Image Processing*, **6**, 321-327 (1997).

[Vora1997e] Poorvi L. Vora, Joyce E. Farrell, Jerome D. Tietz and David Brainard, *Digital Color Cameras – 2 – Spectral Response*, HP Technical Report (1997).

[Vora2001] Poorvi L. Vora, Joyce E. Farrell, Jerome D. Tietz and David Brainard, Image Capture: Simulation of Sensor Responses from Hyperspectral Images, *IEEE Trans. on Image Processing*, **10**, 307-316 (2001).

[Vrhel1992] M. J. Vrhel and H. J. Trussell, Color Correction Using Principal Components, *Color Research and Application*, **17**, 328-338 (1992).

[Vrhel1994a] Michael J. Vrhel and H. Joel Trussell, Filter Considerations in Color Correction, *IEEE Transactions on Image Processing*, **3**, 147-161 (1994).

[Vrhel1994b] Michael J. Vrhel, Ron Gershon and Lawrence S. Iwan, Measurement and Analysis of Object Reflectance Spectra, *Color Research and Application*, **19**, 4-9 (1994).

[Vrhel1995a] M. J. Vrhel and H. J. Trussell, Optimal Color Filters in the Presence of Noise, *IEEE Transactions on Image Processing*, **4**, 814-823 (1995).

[Vrhel1995b] Michael J. Vrhel, H. Joel Trussell and Jack Bosch, Design and Realization of Optimal Color Filters for Multi-Illuminant Color Correction, *Journal of Electronic Imagin*g, **4**, 6-14 (1995).

[Vrhel1999] Michael J. Vrhel, Michael Unser, Multichannel Restoration with Limited A Priori Information, *IEEE Transactions on Image Processing*, **8**, 527-536 (1999).

[Wandell1987] Brian A. Wandell, The Synthesis and Analysis of Color Images, *IEEE Transactions on Pattern Analysis and Machine Intelligence*, **PAMI-9**, 2-13, (1987).

[Wandell1995] Brian A. Wandell, *Foundations of Vision*, Sinauer Associates, Inc. (1995).

[Wang1998] Lizhi Wang and Glenn Healey, Using Zernike Moments for the Illumination and Geometry Invariant Classification of Multispectral Texture, *IEEE Transactions on Image Processing*, **7**, 196-203 (1998).

[Wolski1995] Mark Wolski, Charles A. Bouman and Jan P. Allebach, Optimization of Sensor Response Functions for Colorimetry of Reflective and Emissive Objets, *IEEE 0-8186-7310-9/95*, 323-326 (1995).

[Wolski1996] Mark Wolski, Charles A. Bouman, Jan P. Allebach and Eric Walowit, Optimization of Sensor Response Functions for Colorimetry of Reflective and Emissive Objects, *IEEE Transactions on Image Processing*, **5**, 507-517 (1996).

[Wu1999] Wencheng Wu and Jan P. Allebach, Imaging Colorimetry Using a Digital Camera, *Proc. IS&T/SID 7th Color Imaging Conference*, 15-20 (1999).

[Wyszecki1982] Günther Wyszecki and W. S. Stiles, *Color Science: Concepts and Methods, Quantitative Data and Formulae*, Second Edition, John-Wiley and Sons, Inc. (1982).

[Zhang1996a] Xuemei Zhang and Brian A. Wandell, *A Spatial Extension of CIELAB for Digital Color Image Reproduction*, Stanford University Research Report (1996).

[Zhang1996b] Xuemei Zhang and Brian A. Wandell, A Spatial Extension of CIELAB for Digital Color Image Reproduction, http://white.stanford.edu/~brian/refs.html#color, Proc. SID Conference (1996).

[Zhang1997] Xuemei Zhang, D. Amnon Silverstein, Joyce E. Farrell and Brian A. Wandell, Color Image Quality Metric S-CIELAB and Its Application on Halftone Texture Visibility, http://white.stanford.edu/~brian/refs.html#color, *IEEE Compcon* (1997).

[Zhang1998] Xuemei Zhang and Brian A. Wandell, Color Image Fidelity Metrics Evaluated Using Image Distortion Maps, *IEEE Transactions on Signal Processing*, **70**, 201-214 (1998).

[Zhang1999] Xuemei Zhang, D. Amnon Silverstein, Joyce E. Farrell and Brian *A. Wandell, Color Image Quality Metric S-CIELAB and Its Application on Halftone Texture Visibility*, Stanford University Research Report (1999).

11 APPENDICES

11.1 Appendix A: Color and Image Difference Metrics

11.1.1 CMC(*l*:*c*)

Among the most widely used advanced color difference formulae is the CMC(*l*:*c*) color difference formula which apart from improving accuracy also provides a means for changing the relative importance of lightness and chroma. The $\Delta E_{\mathrm{CMC}(l:c)}$ color difference can be calculated by [reviewed in Berns2000]:

$$\Delta E_{\mathrm{CMC}(l:c)} = \sqrt{\left(\frac{\Delta L^*}{lS_L}\right)^2 + \left(\frac{\Delta C^*}{cS_C}\right)^2 + \left(\frac{\Delta H^*}{S_H}\right)^2} \tag{11.1}$$

where

$$S_L = \frac{0.040975L_1^*}{1+0.01765L_1^*} \text{ unless } L_1^* < 16 \text{ then } S_L = 0.511.$$

$$S_C = \frac{0.0638C_1^*}{1+0.0131C_1^*} + 0.638.$$

$$S_H = S_C(Tf + 1 - f).$$

$$f = \sqrt{\frac{C_1^{*4}}{C_1^{*4}+1900}}.$$

$$T = 0.36 + \left|0.4\cos(h_1 + 35)\right| \text{ unless } 164^\circ < h_1 < 345^\circ \text{ then } T = 0.56 + \left|0.2\cos(h_1 + 168)\right|.$$

Here L_1^*, C_1^* and h_1 are calculated in CIELAB. When the *l*:*c* ratio is set to 1:1, the ΔE values are meant to represent the perceptibility of color difference whereas if set to 2:1 they stand for acceptability. CMC(*l*:*c*) is widely used for calculating small color differences in textile industry.

11.1.2 BFD(*l*:*c*)

BFD(*l*:*c*) was derived based on the Luo-Rigg dataset [refer to review in Berns2000]. BFD(*l*:*c*) is a weighted color-difference formula and emphasizes the correlation between chroma and hue:

$$\Delta E_{BFD} = \sqrt{\left(\frac{\Delta L_{BFD}}{l}\right)^2 + \left(\frac{\Delta C^*_{ab}}{cD_c}\right)^2 + \left(\frac{\Delta H^*_{ab}}{D_H}\right)^2 + R_T \frac{\Delta C^*_{ab}}{cD_c}\frac{\Delta H^*_{ab}}{D_H}} \tag{11.2}$$

Detailed parameter description of Equation (11.2) can also be found in literature [Berns2000]. This equation has not been widely used in industry, but its advantages have been incorporated into the latest CIEDE2000 formula.

11.1.3 CIE DE94 Formula

A modification of the ΔE^*_{ab} formula was released by CIE in 1994 based on new experimental data [RIT-DuPont dataset, reviewed on pg. 119 in Berns2000]. The new formula was found to predict color difference slightly better than the old formula. The new color difference formula, ΔE_{94}, is calculated as a weighted distance between two colors in the lightness, chroma and hue space (*L**, *C**, *H**):

$$\Delta E^*_{94} = \sqrt{\left(\frac{\Delta L^*}{k_L S_L}\right)^2 + \left(\frac{\Delta C^*}{k_C S_C}\right)^2 + \left(\frac{\Delta H^*}{k_H S_H}\right)^2}, \tag{11.3}$$

where

$$\begin{aligned} S_L &= 1, \\ S_C &= 1 + 0.045 C^*_{\text{standard}}, \\ S_H &= 1 + 0.015 H^*_{\text{standard}}. \end{aligned} \tag{11.4}$$

and

$$\begin{aligned} \Delta L^* &= L^*_2 - L^*_1, \\ \Delta C^* &= C^*_2 - C^*_1 = \sqrt{a^{*2}_2 + b^{*2}_2} - \sqrt{a^{*2}_1 + b^{*2}_1}, \\ \Delta H^{*2} &= \Delta a^{*2} + \Delta b^{*2} - \Delta C^{*2} = 2C^*_1 C^*_2 (1 - \cos \Delta h^*), \text{ [in Ohta1997]} \\ \Delta H^{*2} &= \frac{2(a^*_1 b^*_2 - a^*_2 b^*_1)^2}{C^*_1 C^*_2 + a^*_1 a^*_2 + b^*_1 b^*_2}. \text{ [in Berns2000]} \end{aligned} \tag{11.5}$$

The symbols ΔL^*_{ab}, ΔC^*_{ab} and ΔH^*_{ab} represent the differences between the two colors to be compared along the lightness, chroma and hue dimensions, S_L, S_C and S_H represent weighting factors calculated from the chroma coordinates of the standard of the two colors compared, and

k_L, k_C and k_H are parameters specific to experimental conditions. In general, if the experimental conditions are unknown, the values of k_L, k_C and k_H are set to be one. The values of S_C and S_H are calculated from the chroma coordinates C^*_{ab} of the colors in the original reference images.

As shown in Figure 11.1, for CMC(l:c) and ΔE^*_{94} color difference formulae, the ellipsoids corresponding to one unit color difference are projected onto a*-b* plane [Berns2000]. Both color difference formulae are designed to be more uniform than Euclidean color difference. If it is so, in Figure 11.1, the shape of ellipses shows the non-uniformity of CIELAB space.

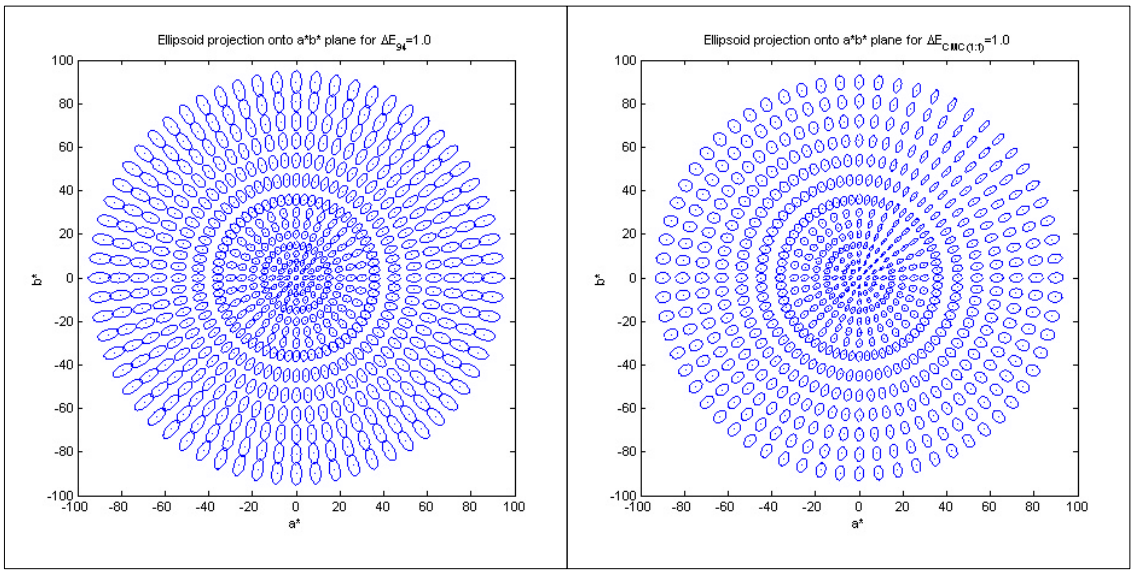

(a) (b)

Figure 11.1: (a) Ellipsoid corresponding to CIE DE^*_{94}=1.0 is projected onto a*-b* plane; (b) Ellipsoid corresponding to CMC $DE^*_{CMC(1:1)}$=1.0 is projected onto a*-b* plane.

11.1.4 S-CIELAB

Since CIELAB system was created in a period when most color reproduction applications were concerned with matching large uniform colored areas, it was tested against data from color appearance judgments of large uniform fields. The aforementioned CIELAB color difference metrics are not suited for image perception difference. Many studies have found that color discrimination and appearance depend on spatial pattern of the images. For example, the human visual system is not as sensitive to color differences in fine details as compared to large patches,

yet the CIELAB color metric will predict the same perceptual difference for the two cases since there is no spatial variable in the CIELAB transformation.

With the growth of digital color imaging, many applications have been developed to process real images. However, most real images are not made up of large uniform patches. Many psychophysical studies show that discrimination and appearance of small-field or fine-patterned colors differ from similar measurements made using large uniform fields. Therefore, applying CIELAB to predict local color reproduction errors in patterned images does not give satisfactory results. For example, when comparing a continuous-tone color image with a halftone version of the image, a point-by-point computation of the CIELAB error produces large errors at most image points. Because the halftone patterns vary rapidly these differences are blurred by the eye, and the reproduction may still preserve the appearance of the original.

Zhang and Wandell introduced a spatial extension of CIELAB for digital color image reproduction recently [Zhang1996a], as shown in Figure 11.2. In a spatial extension of CIELAB, named S-CIELAB, the spatial-color sensitivity of the human eye is included in the metric. The S-CIELAB metric incorporates the different spatial sensitivities of the three opponent color channels by adding a spatial pre-processing step before the standard CIELAB ΔE calculation. This spatial extension is designed to accounts for human spatial-color sensitivity and thus improves the performance of the CIELAB ΔE metric for patterned targets.

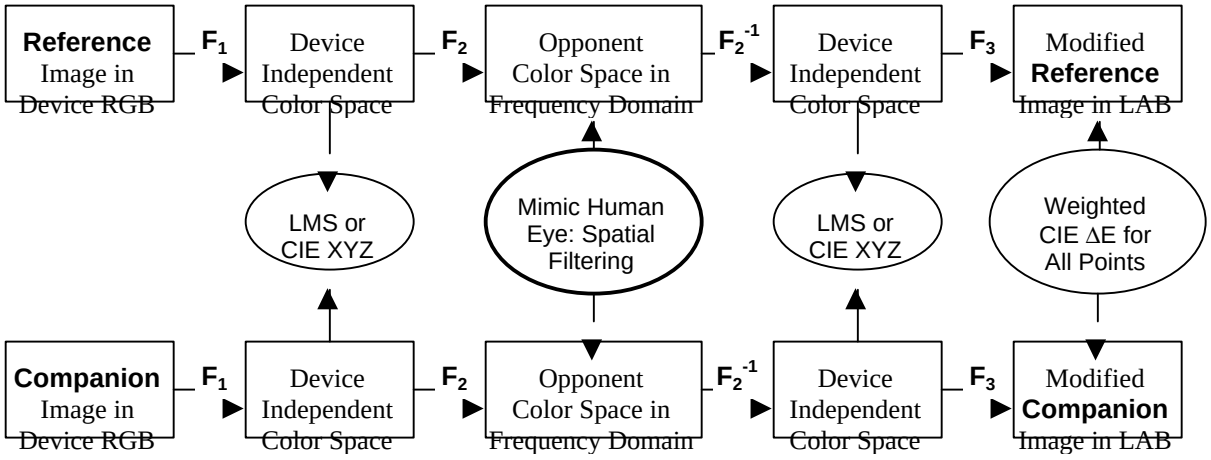

Figure 11.2: Flowchart illustrating definition of S-CIELAB.

There are two goals for S-CIELAB metric. First, a spatial filtering operation to the color image data is applied in order to simulate the spatial blurring by the human visual system. Second, when the inputs are large uniform areas, it is expected the extension to be consistent with the basic CIELAB calculations.

The basic ideas of calculating S-CIELAB can be illustrated by the steps as follows: The image data are transformed into an opponent-colors space; each opponent-colors image is convolved with a kernel whose shape is determined by the visual spatial sensitivity to that color dimension; the area under each of these kernels integrates to one. The calculation is pattern-color separable because the color transformation does not dependent on the image's spatial pattern, and the spatial convolution does not depend on the image's color.

Finally the filtered representation is transformed to a CIE XYZ representation, and this representation is transformed using the CIELAB formula. Thus the S-CIELAB representation includes both the spatial filtering and the CIELAB processing.

Differences between the S-CIELAB representation of an original image and its reproduction measure the reproduction error. The pixel-by-pixel differences are summarized by a quantity *DE,* which is computed precisely as *DE* in color difference formula on CIELAB. The S-CIELAB difference measure reflects both spatial and color sensitivity, and it equals the conventional CIELAB over uniform regions of the image.

In S-CIELAB model, the color transformation converts the input image, specified in terms of CIE 1931 XYZ tristimulus values, into three opponent-colors planes that represent luminance (O_1), red-green (O_2) and blue-yellow (O_3) image. The linear transformation from XYZ to opponent-colors is

$$\begin{aligned} O_1 &= 0.279X + 0.72Y - 0.107Z \\ O_2 &= -0.449X + 0.29Y - 0.077Z \\ O_3 &= 0.086X - 0.59Y + 0.501Z \end{aligned} \tag{11.6}$$

The data in each plane are filtered by 2-D separable spatial kernels of the form

$$f = k\sum_i w_i E_i \tag{11.7}$$

where $E_i = k_i e^{-(x^2+y^2)/s_i^2}$. f, k_i and s_i are chosen to simulate the spatial sensitivity of human eye.

Because the spatial processing stage is separate from the CIELAB calculation, S-CIELAB can be implemented as a pre-processor to existing CIELAB-related software or hardware. The separability of the pattern and color stages makes it straightforward to apply the spatial extension to other color difference calculations.

11.1.5 CIEDE2000

The effort is still continuing to develop a color difference formula in a imperfectly uniform color space that can be more consistent with human vision than available metrics such as ΔE^*_{94} and CMC(*l*:*c*). Recently the CIE has introduced a new color difference formula, CIEDE2000, as a successor to CIE94. Compared with CIE94, this formula include a interactive hue and chroma term to improve performance for the blue region of color space, correcting for perceived constant-hue nonlinearity; an adjusted a^* term to improve performance of low-chroma (gray) colors; a hue dependent function to correct for perceived hue differences. Each step to derive CIEDE2000 is briefly described as follows [Johnson2001].

An adjustment of the a^* axis is introduced to correct for the color difference perception of low chroma colors, as shown in the following equations:

$$C^* = \sqrt{a^{*2} + b^{*2}} \tag{11.8}$$

$$\overline{C}^* = \frac{C^*_{\text{reference}} + C^*_{\text{reproduction}}}{2} \tag{11.9}$$

$$G = 0.5\left(1 - \sqrt{\frac{\overline{C}^{*7}}{\overline{C}^{*7} + 25^7}}\right) \tag{11.10}$$

Equation (11.12)-(11.14) are used to calculate the lightness, chroma and hue rectangular differences on a per-pixel basis for the image pair.

$$a' = (1+G)a^* \tag{11.11}$$

$$L' = L^* \tag{11.12}$$

$$C' = \sqrt{a'^2 + b^{*2}} \tag{11.13}$$

$$h' = \tan^{-1}\left(\frac{b^*}{a'}\right) \tag{11.14}$$

Now the color coordinates difference can be calculated for each pixel pair of the original and reproduced images:

$$\Delta L' = L'_{\text{reference}} - L'_{\text{reproduction}} \tag{11.15}$$

$$\Delta C' = C'_{\text{reference}} - C'_{\text{reproduction}} \tag{11.16}$$

$$\Delta h' = h'_{\text{reference}} - h'_{\text{reproduction}} \tag{11.17}$$

$$\Delta H = 2\sqrt{C'_{\text{reference}} C'_{\text{reproduction}}}\,\sin\left(\frac{\Delta h'}{2}\right) \tag{11.18}$$

Note that if the absolute difference between the hue angles of the original and reproduced images is greater than 180°, the method to calculate hue angle differences would be slightly different, a 360° should be added to the smaller of the hue angles:

$$\text{if } \left|\Delta h'\right| > 180^\circ, \text{ then } \Delta h' = \min(h'_{\text{reference}},\ h'_{\text{reproduction}}) + 360^\circ - \max(h'_{\text{reference}},\ h'_{\text{reproduction}}) \tag{11.19}$$

The average lightness, chroma and hue-angle between the original and reproduced images can be calculated as follows:

$$\bar{L}' = \frac{L'_{\text{reference}} + L'_{\text{reproduction}}}{2} \tag{11.20}$$

$$\bar{C}' = \frac{C'_{\text{reference}} + C'_{\text{reproduction}}}{2} \tag{11.21}$$

$$\bar{h}' = \frac{h'_{\text{reference}} + h'_{\text{reproduction}}}{2} \tag{11.22}$$

Similar correction as Equation (11.19) should be applied to Equation (11.22) if the two hue angles are located in different quadrants:

$$\text{if } \left|\Delta h'\right| > 180^\circ, \text{ then } \bar{h}' = \frac{\min(h'_{\text{reference}},\ h'_{\text{reproduction}}) + 360^\circ - \max(h'_{\text{reference}},\ h'_{\text{reproduction}})}{2} \tag{11.23}$$

Weighting functions are calculated to adjust for the perceived color differences between lightness, chroma and hue in CIELAB space. The lightness and chroma functions S_L and S_C are carried out as follows:

$$S_L = 1 + \frac{0.015(\bar{L}' - 50)^2}{\sqrt{20 + (\bar{L}' - 50)^2}} \tag{11.24}$$

$$S_C = 1 + 0.045\bar{C}' \tag{11.25}$$

The hue weighting function is a function of both hue angle and chroma. First the hue angle dependency is determined as follows

$$T = 1 - 0.17\cos(\bar{h}' - 30) + 0.24\cos(2\bar{h}') + 0.32\cos(3\bar{h}' + 6) - 0.20\cos(4\bar{h}' - 63) \quad (11.26)$$

This is combined with the chroma dependency:

$$S_H = 1 + 0.015\bar{C} * T \quad (11.27)$$

The blue region of CIELAB is known to be highly nonlinear in regards to hue angle and chroma interaction. Thus a rotation has been created to compensate this. First,

$$R_C = 0.5\left(1 - \sqrt{\frac{\bar{C}^7}{\bar{C}^7 + 25^7}}\right) \quad (11.28)$$

This is followed by a hue angle dependency

$$\Delta q = 30^\circ e^{-\left(\frac{\bar{h}' - 275^\circ}{25}\right)^2} \quad (11.29)$$

The rotation function is applied as

$$R_T = -\sin(2\Delta q) R_C \quad (11.30)$$

Finally the total color difference for each pixel can be given by Equation (11.31):

$$\Delta E = \sqrt{\left(\frac{\Delta L'}{K_L S_L}\right)^2 + \left(\frac{\Delta C'}{K_C S_C}\right)^2 + \left(\frac{\Delta H'}{K_H S_H}\right)^2 + R_T\left(\frac{\Delta C' \Delta H'}{K_C S_C K_H S_H}\right)^2} \quad (11.31)$$

The parametric weights, K_L, K_C and K_H can be fit to existing data sets if available, otherwise these weights are all set to be 1.0 by default.

To better predict the color difference for both large isolated color patches and color images, a generalized color difference formula is desirable, which comprehensively extracts the advantages of CIEDE2000 and S-CIELAB. The spatial domain and frequency domain filtering technique is applied to remove high frequency components and enhance local contrast, just like the human visual system [Johnson2001]. It is expected that the conceived color difference metric be compatible with the current ones if simplified.

11.2 Appendix B: Color Appearance Models

The appearance of a given stimulus (as specified in terms of SPD or tristimulus values) depends on the surroundings in which it is viewed. CIEXYZ characterizes the physical properties of colors, but not their appearance, since no any influence of the viewing conditions is considered.

CIELAB is slightly better, which built in compressive nonlinearity, von Kries-type of chromatic-adaptation transform and predicts basic appearance attributes (lightness, hue and chroma), therefore CIELAB can be regarded as a primitive color appearance model. But an ideal color appearance model would consider all major color appearance phenomena, i.e. simultaneous contrast, Hunt effect, Stevens effect, chromatic adaptation, memory colors and predict various color appearance attributes [Fairchild1998]. Some color appearance models, RLAB, LLAB and CIECAM97s, that may be used in the current research are briefly described as follows. They are chosen either because of elegant implementation or rather complete inclusion of color appearance phenomena.

11.2.1 RLAB

This color appearance model [refer to Fairchild1998] is aimed at applications where the speed of transformation is important and where complex images are considered instead of simple color patches. The model consists of two stages: first the tristimulus coordinates of a color are transformed into a set of reference viewing conditions (D65, 2° observer, 318 cd/m2 illumination and hard copy medium) using a chromatic adaptation transform which can allow for incomplete adaptation when visual display units are viewed. Then, appearance attributes are calculated from the adapted cone responses and to obtain tristimulus values for another set of viewing conditions, the model is analytically reversed. To predict the appearance attributes of a color, the following parameters are required:

- Adapted white under source viewing conditions $X_wY_wZ_w$
- Absolute luminance of adapted white Y_n
- Sample under source viewing conditions XYZ
- Information about the medium and the nature of the surround

Note that $X_wY_wZ_w$ is the adapted white in terms of relative tristimulus values (scaled so that Y_w=100). The following steps then describe the implementation of the model:

Step1 Fundamental tristimulus values

$$\begin{bmatrix} L \\ M \\ S \end{bmatrix} = \mathbf{M} \begin{bmatrix} X \\ Y \\ Z \end{bmatrix}; \mathbf{M} = \begin{bmatrix} 0.3897 & 0.6890 & -0.0787 \\ -0.2298 & 1.1834 & 0.0464 \\ 0.0 & 0.0 & 1.0000 \end{bmatrix} \tag{11.32}$$

The elements in the matrix are normalized so as to give equal cone responses (L=M=S=100) for the equi-energy illuminant S_E (X=Y=Z=100). Note that this transformation is also carried out for the adapted white, which results in $L_w M_w S_w$.

Step2 Chromatic adaptation

$$\begin{aligned} A &= \begin{bmatrix} a_L & 0 & 0 \\ 0 & a_M & 0 \\ 0 & 0 & a_S \end{bmatrix}. \\ a_L &= \frac{p_L + D(1.0 - p_L)}{L_n}; \\ p_L &= \frac{1.0 + Y_n^{1/3} + l_E}{1.0 + Y_n^{1/3} + 1.0/l_E}; \\ l_E &= \frac{3L_W}{L_W + M_W + S_W} \end{aligned} \tag{11.33}$$

a_M, a_S, p_M, p_S, m_E and s_E are calculated analogously and D represents the contribution of cognitive chromatic adaptation to the transformation (D=1 for hard copy, D=0 for soft copy and D=0.5 for projected transparency).

Step3 Reference XYZ

$$\begin{bmatrix} X_{ref} \\ Y_{ref} \\ Z_{ref} \end{bmatrix} = \mathbf{RAM} \begin{bmatrix} X \\ Y \\ Z \end{bmatrix}; \mathbf{R} = \begin{bmatrix} 1.9569 & -1.1882 & 0.2313 \\ 0.3612 & 0.6388 & 0.0 \\ 0.0 & 0.0 & 1.0000 \end{bmatrix} \tag{11.34}$$

where **A** is the chromatic adaptation matrix for the reference viewing conditions.

Step4 RLAB coordinates

$$\begin{aligned} L^R &= 100\left(Y_{ref}\right)^s \\ a^R &= 430\left[\left(X_{ref}\right)^s - \left(Y_{ref}\right)^s\right] \\ b^R &= 170\left[\left(Y_{ref}\right)^s - \left(Z_{ref}\right)^s\right] \\ C^R &= \sqrt{a^{R2} + b^{R2}} \\ b^R &= \tan^{-1}(b^R / a^R) \end{aligned} \tag{11.35}$$

The exponent σ depends on the surround ($1/2.3$ for average surround, $1/2.9$ for dim surround and 1/3.5 for dark surround) and is included to model the surround's influence on image contrast. XYZ coordinates for the destination viewing conditions can be obtained by reversing the model in a simple analytical way.

11.2.2 LLAB

LLAB color appearance model was proposed by Luo *et al*. [in Fairchild1998]. The parameters needed by this color appearance model are:

- Adapted white under source viewing conditions $X_wY_wZ_w$
- Luminance of adapted white under source viewing conditions L_S
- Y value of background under source adapting field Y_b
- Sample under source viewing conditions XYZ
- Information about the medium and the nature of the surround

Four parameters need to be predetermined according to the viewing conditions considered, i.e. D (Incomplete adaptation factor), F_s (Surround induction factor), F_L (Lightness induction factor), and F_C (Colorfulness induction factor). These values corresponding to each set of viewing conditions and are shown in Table 11-1:

Table 11–1: Parameters for LLAB.

Viewing Conditions	D	F_S	F_L	F_C
Reflection samples and images in average surround				
Large sample subtending more than 4°	1.0	3.0	0.0	1.0
Small sample subtending less than 4°	1.0	3.0	1.0	1.0
Television and VDU displays in dim surround	0.7	3.5	1.0	1.0
Cut-sheet transparency in dim surround	1.0	5.0	1.0	1.1
35mm projection transparency in dark surround	0.7	4.0	1.0	1.0

The following steps are then carried out to obtain the appearance attributes of a given color:

Step1 Compute corresponding tristimulus values under reference illuminant (S_E)

$$\begin{bmatrix} R \\ G \\ B \end{bmatrix} = \mathbf{M} \begin{bmatrix} X/Y \\ Y/Y \\ Z/Y \end{bmatrix} \text{ where } \mathbf{M} = \begin{bmatrix} 0.8951 & 0.2664 & -0.1614 \\ -0.7502 & 1.7135 & 0.0367 \\ 0.0389 & -0.0685 & 1.0296 \end{bmatrix} \tag{11.36}$$

The RGB cone responses for the adapted whites under reference and source illuminants, and test color under source illuminant are calculated using Equation (11.36) and are labeled as R_{wr}, G_{wr}, B_{wr}; R_{ws}, G_{ws}, B_{ws} and R, G, B respectively.

$$\begin{aligned} &R_r = [D(R_{wr}/R_{ws}) + 1 - D]R \\ &G_r = [D(G_{wr}/G_{ws}) + 1 - D]G \\ &\text{For B} \geq 0,\ B_r = [D(B_{wr}/B_{ws}^b) + 1 - D]B^b \\ &\text{Otherwise, } B_r = -[D(B_{wr}/B_{ws}^b) + 1 - D]|B|^b \\ &\text{where } b = (B_{ws}/B_{wr})^{0.0834} \end{aligned} \tag{11.37}$$

Convert cone signals to CIE tristimulus values, as inverse of Equation (11.36):

$$\begin{bmatrix} X_r \\ Y_r \\ Z_r \end{bmatrix} = \mathbf{M}^{-1} \begin{bmatrix} R_r Y \\ G_r Y \\ B_r Y \end{bmatrix} \tag{11.38}$$

Step2 Calculate appearance attributes

In addition to lightness (L_L), chroma (Ch_L) and hue angle (h_L), which will be shown here, the model also has predictors for colorfulness (C_L), saturation (s_L) and hue composition (H_L), which are of less importance.

$$\begin{aligned} &L_L = 116 f(Y/100)^z - 16 \\ &A = 500[f(X/100) - f(Y/100)] \\ &B = 200[f(Y/100) - f(Z/100)] \\ &\text{where } z = 1 + F_l (Y_b/100)^{1/2} \\ &\text{If } I > 0.008856,\ f(I) = I^{1/F_S} \\ &\text{Otherwise, } f(I) = [(0.008856^{1/F_S} - 16/116)/0.008856]I + 16/116 \\ &Ch_L = 25\ln(1 + 0.05C) \\ &\text{where } C = (A^2 + B^2)^{1/2} \\ &h_L = \tan^{-1}(B/A) \end{aligned} \tag{11.39}$$

11.2.3 CIECAM97s

In order to break through the limitations of CIELAB, many efforts have been made, which produce a bunch of color appearance models in the last two decades. Representative models are the Nayatani *et al*. model, the Hunt model, the RLAB model, the LLAB model, and the ATD model (As reviewed in Fairchild1998). These models are different from each other among the complexity of the model itself, the types of color appearance phenomena and effects predicted, and the level of acceptance by users. But there is a significant amount of interest in the establishment and use of a single, standardized color appearance model, however such a model has not yet been completely formulated. The industrial demand for such a model has led the CIE to speed up its efforts to establish a model to be put into use, tested and perhaps recommended as a standard in the coming years. Some slight but important revisions were made to the Bradford-Hunt 96S model to derive the model agreed upon by CIE TC1-34 to become the CIECAM97s model (i.e., the simple version of the CIE 1997 Interim Color Appearance Model). This model builds upon the work of many researchers in the field of color appearance. Various aspects of the model can be traced to the work of Bartleson, Breneman, Estevez, Fairchild, Hunt, Lam, Luo, Nayatani, Rigg, Seim and Valberg, among others. Details on the model can be found from references including relevant CIE publications.

The input parameters of CIECAM97s are:

- Adapted white under test viewing conditions $X_wY_wZ_w$
- Background under test viewing conditions $X_bY_bZ_b$
- Sample under test viewing conditions XYZ
- Luminance of the test adapting field (cd/m2) L_A
- L_A is normally taken to be 1/5 of the luminance of the adapted white under source conditions
- Information about the medium and the nature of the surround.

Based on the surround, the following parameters need to be chosen in Table 11-2:

Table 11–2: Parameters for CIECAM97s.

SURROUND	F	c	F_{LL}	N_C
Average				
Large sample subtending more than 4°	1.0	0.69	0.0	1.0
Small sample subtending less than 4°	1.0	0.69	1.0	1.0
Dim	0.9	0.59	1.0	1.0
Dark	0.9	0.525	1.0	0.8
Cut-sheet	0.9	0.41	1.0	0.8

Step1 Chromatic adaptation

$$\begin{bmatrix} R \\ G \\ B \end{bmatrix} = M_{BFD} \begin{bmatrix} X/Y \\ Y/Y \\ Z/Y \end{bmatrix} \text{ where } M_{BFD} = \begin{bmatrix} 0.8951 & 0.2664 & -0.1614 \\ -0.7502 & 1.7135 & 0.0367 \\ 0.0389 & -0.0685 & 1.0296 \end{bmatrix} \tag{11.40}$$

Calculate *RGB* values for sample as shown by Equation (11.40), adopted white and background under test conditions, the adopted white under reference conditions $[X_{wr}\ Y_{wr}\ Z_{wr}] = [100\ 100\ 100]$ and the degree of chromatic adaptation *D*.

$$D = F - F/(1 + 2L_A^{1/4} + L_A^{1/4}/300) \tag{11.41}$$

Calculate *RGB* values after chromatic adaptation whereby the adapted values of *RGB* are $R_CG_CB_C$ and those of $R_WG_WB_W$ and $R_bG_bB_b$ are $R_{WC}G_{WC}B_{WC}$ and $R_{bC}G_{bC}B_{bC}$.

$$\begin{aligned} &R_C = [D(R_{wr}/R_w) + 1 - D]R \\ &G_C = [D(G_{wr}/G_w) + 1 - D]G \\ &\text{For B} \geq 0,\ B_C = [D(B_{wr}/B_w^p) + 1 - D]B^p \\ &\text{Otherwise, } B_C = -[D(B_{wr}/B_{ws}^p) + 1 - D]|B|^p \\ &\text{where } p = (B_w/B_{wr})^{0.0834} \\ &F_L = 0.2k^4(5L_A) + 0.1(1-k^4)^2(5L_A)^{1/3} \text{ where } k = 1/(5L_A + 1) \end{aligned} \tag{11.42}$$

Step2 Calculate cone responses and apply dynamic response function

$$\begin{bmatrix} R' \\ G' \\ B' \end{bmatrix} = M_H M_{BFD}^{-1} \begin{bmatrix} R_C Y \\ G_C Y \\ B_C Y \end{bmatrix} \quad \begin{bmatrix} R'_W \\ G'_W \\ B'_W \end{bmatrix} = M_H M_{BFD}^{-1} \begin{bmatrix} R_{WC} Y_W \\ G_{WC} Y_W \\ B_{WC} Y_W \end{bmatrix}$$
$$M_H = \begin{bmatrix} 0.38971 & 0.68898 & -0.07868 \\ -0.33981 & 1.18340 & 0.04641 \\ 0.0 & 0.0 & 1.0 \end{bmatrix} \tag{11.43}$$

$$
\begin{aligned}
&Y_{bC} = (0.43231R_{bC} + 0.51836G_{bC} + 0.04929B_{bC})Y_b \\
&Y_{WC} = (0.43231R_{WC} + 0.51836G_{WC} + 0.04929B_{WC})Y_W \\
&n = Y_{bC} / Y_{WC},\ N_{bb} = 0.725(1/n)^{0.2} \text{ and } N_{cb} = 0.725(1/n)^{0.2}
\end{aligned}
\tag{11.44}
$$

Apply the dynamic response function $R'G'B'$ and $R'_W G'_W B'_W$ which then become $R'_a G'_a B'_a$ and $R'_{aW} G'_{aW} B'_{aW}$ respectively.

$$
\begin{aligned}
&R'_a = 40(F_L R'/100)^{0.73} / [(F_L R'/100)^{0.73} + 2] + 1 \\
&\text{If } R' < 0 \text{ then } R'_a = -40(-F_L R'/100)^{0.73} / [(-F_L R'/100)^{0.73} + 2] + 1
\end{aligned}
\tag{11.45}
$$

G'_a, B'_a, R'_{aW}, G'_{aW}, and B'_{aW} are calculated similarly.

Step3 Calculate Appearance Attributes

In addition to brightness (*Q*), lightness (*J*), chroma (*C*), saturation (*s*) and hue angle (*h*), which will be shown here, the model also has predictors for colorfulness (*M*) and hue composition (*H*), which are less relevant for imaging applications.

First, redness-greenness (*a*) and yellowness-blueness (*b*) are calculated:

$$
\begin{aligned}
a &= R'_a - 12G'_a/11 + B'_a/11 \\
b &= (R'_a + G'_a - 2B'_a)/9
\end{aligned}
\tag{11.46}
$$

This is followed by a calculation of hue:

$$
b = \tan^{-1}(b/a) \tag{11.47}
$$

The eccentricity factor (*e*) is then calculated using the following unique hue data:

	Red	Yellow	Green	Blue
h	20.14	90.00	164.25	237.53
e	0.8	0.7	1.0	1.2

$$
e = e_1 + (e_2 - e_1)(h - h_1)/(h_2 - h_1) \tag{11.48}
$$

where e_1 and h_1 are the values of *e* and *h* for the unique hue having the nearest lower value of *h* and e_2 and h_2 are the values having the nearest higher value of *h*. Next, the value of the achromatic signal is calculated for both the sample and the adopted white:

$$
\begin{aligned}
A &= [2R'_a + G'_a + 0.05B'_a - 2.05]N_{bb} \\
A_W &= [2R'_{aW} + G'_{aW} + 0.05B'_{aW} - 2.05]N_{bb}
\end{aligned}
\tag{11.49}
$$

Finally, lightness, saturation and chroma can be obtained as follows:

$$
J = 100(A/A_W)^{cz} \text{ where } z = 1 + F_{LL} n^{1/2} \tag{11.50}
$$

$$s = \frac{100e(10/13)N_c N_{cb} 50\sqrt{a^2 + b^2}}{R'_a + G'_a + 1.05B'_a} \tag{11.51}$$

$$C = 2.44s^{0.69}(J/100)^{0.67n}(1.64 - 0.29^n) \tag{11.52}$$

11.2.4 Color Appearance Difference Metrics

A color appearance model with too much freedom on parameter selection will reduce its prediction accuracy. It is also believable that a color appearance model that tries to take account of all appearance phenomena may in fact discount its capability to make reasonable prediction. Probably a practically useful color appearance model would take account of only some important phenomena and effects.

Since the color appearance attributes, lightness, brightness, saturation, chroma, and colorfulness, are "predicted" from the model by setting a lot of viewing condition parameters, a color difference formula may be derived upon the model space by the Euclidean distance for two different colors. However, no results have yet been reported whether the color appearance space is uniform or not. Quan has compared the applicability of various color difference formulae on various color appearance models to check their uniformity [Quan1998] and initial results are shown in Table 11-3. In the table, the numbers are standard deviation of color difference, the smaller the better. It seems CIE ΔE_{94} can be applied to all those appearance models and RLAB has better uniformity averagely. Advanced color difference formula similar to CMC(*l*:*c*), CIE94, S-CIELAB, and CIEDE2000 can also be used. At this moment, standard Euclidean distance and modification similar to S-CIELAB for color image difference will be used to indicate the visual difference of two different color patches or images.

Table 11–3: Applying RIT-Dupont data to check the applicability of various color difference formulae and uniformity of color appearance models.

Models	CIE DE^*_{ab}	CIE DE^*_{94}	CMC (1:1)	BFD (1:1)
CIELAB 1976	0.1266	0.0434	0.0867	0.2993
RLAB	0.1288	0.0586	0.0672	0.2769
LLAB	0.0963	0.1016	0.8462	0.3243
ZLAB	0.0605	0.1001	0.1178	0.3304
CIECAM97s	0.5899	0.3689	0.5070	0.5272

11.3 Appendix C: Spectral Estimation Approaches

11.3.1 Smoothing Estimation

Smoothing inverse or estimation was first introduced by Pratt and Mancill [Pratt1976]. It is known that although the generalized pseudo-inverse provides a minimum mean-square error, minimum norm estimate of *s*, ill-conditioning of $\mathbf{R}$ coupled with observational errors can lead to oscillatory estimates. Since $\mathbf{S}$ is generally smooth, it is reasonable to impose some smoothing constraints on the solution. A common type of smoothing estimate is given by:

$$\hat{\mathbf{s}} = M^{-1}\mathbf{R}(\mathbf{R}^T M^{-1}\mathbf{R})^{-1}\mathbf{T} \tag{11.53}$$

where M is a smoothing matrix of the typical form [Pratt1976]

$$M = \begin{bmatrix} 1 & -2 & 1 & 0 & 0 & 0 & 0 & . & . & . & 0 \\ -2 & 5 & -4 & 1 & 0 & 0 & 0 & & & & . \\ 1 & -4 & 6 & -4 & 1 & 0 & 0 & & & & . \\ 0 & 1 & -4 & 6 & -4 & 1 & 0 & & & & . \\ 0 & 0 & 1 & -4 & 6 & -4 & 1 & & & & . \\ . & . & . & . & . & . & . & . & . & . & . \\ . & & & & & 1 & -4 & 6 & -4 & 1 & 0 \\ . & & & & & 0 & 1 & -4 & 6 & -4 & 1 \\ . & & & & & 0 & 0 & 1 & -4 & 5 & -2 \\ 0 & . & . & . & . & 0 & 0 & 0 & 1 & -2 & 1 \end{bmatrix} \tag{11.54}$$

Since M is singular, it must be slightly modified to

$$M' = M + e\mathbf{I} \tag{11.55}$$

where e is a reasonably small constant, i.e. 10^{-10} [Herzog1999].

11.3.2 Wiener Estimation

Another alternative is to apply Wiener estimation method, which has been widely used in spectral reflectance estimation, since the statistical characteristics of reflectance spectra can be easily obtained from natural objects [Vrhel1992, Tsumura1999, and Hosoi2000]. With Wiener estimation, the vector **S** to be estimated is assumed to be a sample of a vector random process with a known correlation matrix K_S. The Wiener estimate is given by [Pratt1976]

$$\hat{\mathbf{s}} = K_s\mathbf{R}(\mathbf{R}^T K_s \mathbf{R} + K_?)^{-1}\mathbf{T} \tag{11.56}$$

where $K_?$ is the covariance matrix of the additive observational noise assumed independent of **S**. As a convenient approximation, the covariance matrix K_S can be modeled as a first-order Markov process covariance matrix of the form.

$$K_s = \frac{s_s^2}{Q}\begin{bmatrix} 1 & r & r^2 & . & . & . & r^{Q-1} \\ r & 1 & r & . & . & . & r^{Q-2} \\ . & . & . & . & . & . & . \\ . & & & & & & . \\ . & & & & & & . \\ r^{Q-1} & . & . & . & . & . & 1 \end{bmatrix} \tag{11.57}$$

where $0 \le r \le 1$ is the adjacent element correlation factor, s_s^2 represents the energy of *s*, and *Q* is the dimensionality of sampling. In case of spectral reflectance estimation, K_S can be calculated from an ensemble of typical reflectance samples. Observation noise is commonly modeled as a white noise process with covariance equal to

$$K_? = \frac{s_?^2}{Q}\mathbf{I} \tag{11.58}$$

where $s_?^2$ is the noise energy and **I** is an identity matrix.

Hubel, *et al*. found that the method gave generally good results, but it produced negative lobes in the sensitivity functions [Hubel1994].

11.3.3 Projection onto Convex Set Estimation

Sharma and Trussell introduced a set theoretic estimation method in spectral characterization of color scanner [Sharma1996c]. All of the above estimation methods fail to take into account the considerable *a priori* knowledge available from the physical situation. For instance, except for

the illuminant, the camera sensitivity is a smooth function of wavelength. Hence if the illuminant is known, the functions $\{s_j = m_j\}_{j=1}^3$ are smooth. However, if the illuminant has sharp peaks in its spectrum, the principal eigenvectors of *LR* will also have sharp peaks and will yield estimates of $\{s_j = m_j\}_{j=1}^3$ that have sharp spectral peaks. On the other hand, if the illuminant is a fluorescent lamp whose spectrum is not known, the function $\{s_j = Lm_j\}_{j=1}^3$ will have sharp spectral peaks, but for typical reflectance samples the principal eigenvectors of *R* will be smooth and therefore yield only smooth estimates of **S**.

In addition to the knowledge of smoothness/impulsiveness, other *a priori* information such as non-negativity of the sensitivity functions and boundedness can be incorporated in set theoretical estimates. Based on each constraint that the camera sensitivity must satisfy, a set can be defined in which the true value must lie. Any element in the intersection of the constraint sets is then a feasible solution and can be used as an estimate of the sensitivity. If only closed convex constraint sets are used, a point in the intersection can be determined by projecting onto the sets in cyclic order starting from an arbitrary point in R^N . This is the well-known method of successive *projections onto convex sets* (POCS). If one has *n* constraint sets, the POCS estimate is the limit of the sequence $\{y_k\}$ defined recursively by,

$$y_{k+1} = P_n(P_{n-1}(...P_2(P_1(y_k))...)), \tag{11.59}$$

where y_0 is an arbitrary starting point, and $P_i(z)$ denotes the projection of z onto the i^{th} constraint set close to z. The iterative process of successive projections is guaranteed to converge to a point in the intersection, provided the intersection is nonempty.

POCS is guaranteed to give a solution that satisfies all the constraints, but the solution might not be optimal since POCS solution is very sensitive to the choice of the initial iteration point. In addition, its accuracy is about the same as that of PE estimation [Sharma1996c].

11.3.4 Other Approaches

Finlayson, *et al.* presented an alternative approach to recovering spectral sensitivities with quadratic programming [Finlayson1998]. This approach formulates the problem as constrained

regression: a non-unique approximation $\hat{\mathbf{s}}$ to $\mathbf{S}$ is found such that this approximation minimizes the residual squared error

$$\min\left\{e = \left\|\mathbf{T} - \mathbf{R}^T\hat{\mathbf{s}}\right\|^2\right\}, \tag{11.60}$$

by satisfying the following constraints:

Positivity: Sensitivities at all wavelength samplings are larger than or equal to zero.

Modality: All sensitivity functions are uni-modal or "plausible" multi-modal.

Band-limitedness: All functions are linear combinations of band-limited basis functions.

After implementing this linear constrained quadratic programming, the experimental results showed that the recovered sensor curves are very close to the actual curves.

König and Herzog proposed linear programming approach to estimating sensitivity functions with linear constraints [König2000, Herzog2000]. The linear objective function is chosen as the average absolute error, and the constraints applied are non-negativity and smoothness:

$$\begin{aligned} S(l_i) &\geq 0 \\ \left|S(l_{i-1}) - 2(l_i) + S(l_{i+1})\right| &\leq \Delta S_{\max} \end{aligned} \tag{11.61}$$

where $S(l)$ is spectral sensitivity, and $\Delta S_{\max}$ is smoothness tolerance. This approach has roughly the same performance as that proposed by Finlayson, *et al*.

Thomson and Westland introduced a new sensitivity estimation approach by parameterizing the sensitivity function [Thomson2001]. Since most published data on the response characteristics of color input devices suggest that they are generally smooth, band-limited, uni-modal or bi-modal, asymmetric with respect to the wavelength axis, they can be approximated with low-dimensional parametric model, i.e.

$$s(l) \approx (s_r \cdot l + 2k_r \cdot l^2)a_r \exp\left(-\frac{l - p_r}{w_r}\right) \tag{11.62}$$

where $p_r, a_r, w_r, s_r,$ and k_r are called the peak wavelength, amplitude, width, skewness and kurtosis terms of the gaussian function. The Imaging target was the 18 chromatic color patches of Macbeth ColorChecker. A Levenberg-Marquardt algorithm was used to minimize non-linear objective function similar to Equation (11.60) and obtain parameters in Equation (11.62). Their

results show that the predicted digital counts and the recorded digital counts are not well located in a straight line, which may induce that the parametric model limits the degree of freedom too much.

Barnard modified Sharma and Trussell's approach by minimizing the relative RMS error instead of the absolute error, and the constraints were rewritten so that the entire problem became a least squares fit with linear constraints which can be easily handled with available numerical methods [Barnard1999]. Smoothness and uni-modal constraints were also used. The performance was about the same as POCS.

11.4 Appendix D: Q_{st} and Q_{sf}

The tristimulus values of a set of spectral reflectance samples are

$$t = A^T L_v R = A_L^T R \tag{11.63}$$

Without noise consideration, the corresponding camera output signals are

$$t_c = S^T L_c R = G^T R \tag{11.64}$$

The notations in the following equations are the same as those appeared in Chapter 5. In order to approximate the tristimulus values from camera output signals, a linear matrix B is to be decided so that the mean-squared error is minimized:

$$\min\left\{e = E\left[\left\|t - Bt_c\right\|^2\right]\right\} \tag{11.65}$$

The solution to Equation (11.65) is readily obtained with pseudo-inverse operation,

$$B = t \cdot t_c^T (t_c \cdot t_c^T)^{-1} \tag{11.66}$$

Therefore the minimal error in Equation (11.65) can be obtained as

$$e_{\min} = E\left[\left\|t - Bt_c\right\|^2\right] = E\left[\left\|t - t \cdot t_c^T (t_c t_c^T)^{-1} t_c\right\|^2\right] \tag{11.67}$$

Applying Equations (11.63) and (11.64) onto Equation (11.67),

$$\begin{aligned} e_{\min} &= E\left[\left\|t - t \cdot t_c^T (t_c t_c^T)^{-1} t_c\right\|^2\right] \\ &= E\left[\left\|A_L^T R - A_L^T R R^T G (G^T R R^T G)^{-1} G^T R\right\|^2\right] \\ &= \text{trace}(A_L^T K_r A_L) - \text{trace}(A_L^T K_r G (G^T K_r G)^{-1} G^T K_r A_L) \end{aligned} \tag{11.68}$$

Therefore, Q_{st} is defined as

$$Q_{st} = \frac{\text{trace}(A_L^T K_r G (G^T K_r G)^{-1} G^T K_r A_L)}{\text{trace}(A_L^T K_r A_L)} \tag{11.69}$$

Q_{sf} is defined by replacing human visual illuminant subspace A_L in Equation (11.69) with its orthonormal fundamental subspace U_L.

11.5 Appendix E: Mathematics of Unified Measure of Goodness

The measurement result on imaging noises of a camera has been demonstrated in Chapter 4. The noise property in an imaging process is not white noise. The shot noise dominates when the signal is strong, and the dark noise dominates when the signal is week. By incorporating this noise property, as well as multi-illuminant color correction, minimizing color error in a perceptually uniform color space or color appearance space, FOM is extended to unified measure of goodness. Compared with Figure of Merit, Unified Measure of Goodness is a more practice-oriented colorimetric quality factor.

11.5.1 The Least-Squares Approach

The derivation of FOM / UMG is based on a simple fact that, for a least-squares problem

$$\min\left\{e = \|x - Yb\|^2\right\} \tag{11.70}$$

where *e* is regression error, measurement *x* is fitted with *Y*. The solution of *b* is obtained with Moore-Penrose (MP) pseudo-inverse

$$b = (Y^T Y)^{-1} Y^T x \tag{11.71}$$

Therefore the minimized mean squared error is

$$\begin{aligned} e_{\min} &= \|x - Yb\|^2 = \left\|x - Y(Y^T Y)^{-1} Yx\right\|^2 \\ &= (x - Y(Y^T Y)^{-1} Yx)^T (x - Y(Y^T Y)^{-1} Yx) \\ &= x^T x - x^T Y (Y^T Y)^{-1} Yx = a(x) - t(x, Y) \end{aligned} \tag{11.72}$$

where $a(x) \equiv x^T x$ and $t(x, Y) \equiv x^T Y (Y^T Y)^{-1} Yx$. The ratio

$$q = \frac{t(x, Y)}{a(x)}$$

defines goodness of fit. If $q \to 1$, $e_{\min} \to 0$, the fit becomes perfect.

11.5.2 The Derivation of Unified Measure of Goodness

For a pair of taking-viewing illuminants, the first stage of UMG is quite similar to Sharma and Trussell's FOM. The difference is in the second stage this quality factor includes a signal-dependent imaging noise model rather than assumes the noise is signal-independent white noise. Detailed mathematics is described as follows.

The CIE *XYZ* tristimulus values defining the color are given by

$$t = A^T L r = A_L^T r \tag{11.73}$$

where A is the matrix of CIE *XYZ* color matching functions $[\bar{x} \quad \bar{y} \quad \bar{z}]$, L is the diagonal illuminant matrix with diagonal entries from samplings of illuminant *l*, and $L = L^T$, $A_L = LA$.

For sensors commonly used in digital cameras, the response at a single spatial location can be modeled as:

$$t_i^c = \int_{-\infty}^{\infty} f_i(l) d(l) r(l) l_c(l) dl + x_i = \int_{-\infty}^{\infty} m_i(l) r(l) l_c(l) dl + x_i \quad i = 1, 2, ...J \tag{11.74}$$

where t_i^c denotes the camera measurement obtained from the i^{th} channel, $f_i(l)$ is the spectral transmittance of the i^{th} channel color filter, $d(l)$ is the sensitivity of the detector used in the measurements, $l_c(l)$ is the spectral radiance of the camera taking illuminant, $r(l)$ is the spectral reflectance of the object, x_i represents recording noise (dark noise and shot noise, as discussed in Chapter 4), J is the number of camera recording channels, and $m_i(l) = f_i(l) d(l)$ is the product of the i^{th} filter transmittance and detector sensitivity. $m_i(l)$ may often be referred to as the i^{th} filter-transmittance since the detector sensitivity is fixed in camera sensitivity design issue.

The above integral can be represented in terms of their samples in the visible range:

$$t_i^c = m_i^T L_c r + x_i, \quad i = 1, 2, ...J \tag{11.75}$$

where m_i is the $N \times 1$ vector of samples of $m_i(l)$, r is the $N \times 1$ vector of reflectance samples, and L_c is the $N \times N$ diagonal matrix with samples of the camera taking-illuminant, $l_c(l)$, along the diagonal. In a like manner, this discreet equation may be rewritten using matrix notation as

$$t_c = M^T L_c r + h = G^T r + x \tag{11.76}$$

where t_c is the $J \times 1$ vectors of camera measurements, $M_{N \times J} = [m_1, m_2, ..., m_j]$, x is the $K \times 1$ recording noise vector, and $G = L_c M$.

In the absence of noise, the camera measurements determine the projection of the reflectance spectra, *r*, onto the column space of $G = L_c M$. Using the analogy with the *HVISS*, the space of *G* will be called the camera *sensitivity visual subspace* (*SVS*).

Consider the estimation of the CIE tristimulus values of a captured object from the measurements made with a camera as an optimal linear transformation:

$$\hat{t} = Bt_c \tag{11.77}$$

where $\hat{t}$ are the estimates of the true tristimulus values, t_c is the $J\times1$ vector of measurements from the camera and the linear transformation *B* is used to estimate the tristimulus values. The average magnitude of "color difference" between the true color *t* and the estimate $\hat{t}$ may be used as an error metric for quantifying the camera performance under the given color correction transformation, *B*. Different color spaces may be used in the computation of the "color difference." To encompass several cases in a unified treatment, it will be assumed that the error magnitude can be expressed mathematically in the form $\left\|F(t)-F(\hat{t})\right\|$ where $F(\cdot)$ is a 3×3 (possibly nonlinear) transformation of the tristimulus values, and $\|\cdot\|$ denotes the Euclidean vector norm. For color difference formulae such as ΔE^*_{94}, additional transformations can convert it into Euclidean vector norm. Such a metric is motivated by the uniform color spaces, in which equal Euclidean distances correspond to approximately equal perceptual color errors. In such a scenario, $F(\cdot)$ represents the transformation from the CIE *XYZ* space into a uniform color space.

In terms of the above notation, the camera's mean squared color error e_0 under the color-correction transformation *B* is given by

$$e_0(A_L, G, B) = \left(E\left\{ \left\| F(t) - F(\hat{t}) \right\|^2 \right\} \right)^{1/2} \tag{11.78}$$

where $E\{\ \}$ denotes the expectation over the ensemble of objects to be captured and A_L and *G* are defined as viewing-illuminant-color matching function space and taking-illuminant-camera spectral sensitivity space. As an alternative to the mean squared value, the maximum error over the ensemble, or a variety of other means may be used in the above expression. The mean

squared value, however, has the advantage that it preserves differentiability which is desirable in design applications making use of gradient based methods.

The above error metric quantifies the performance of a camera "specified by" *G* when the transformation *B* is used. An error metric for the camera alone can be obtained by replacing the generic transformation, *B*, with the optimal transformation that minimizes the error. However, such an error metric is not readily computable since the optimal transformation cannot be determined in closed form for a general non-linear transformation, $F(\cdot)$. If the transformation $F(\cdot)$ is differentiable, with continuous first partial derivatives, a first order Taylor series provides a fairly accurate locally linear approximation for $F(\cdot)$. If $\|t-\hat{t}\|$ is small over the captured ensemble, this first order Taylor series expansion can be used to approximate the error metric by the expected mean-squared linearized color error,

$$e(A_L, G, B) = e_0^2(A_L, G, B) \approx e_l(A_L, G, B) = E\left\{\left\| J_F(t)(t-\hat{t})\right\|^2\right\} \tag{11.79}$$

where $J_F(t)$ denotes the Jacobian matrix of the transformation $F(\cdot)$ at *t*. In this case, $F(\cdot)$ is a linearized transformation. The transformation that minimizes the linearized error metric, viz.,

$$B_{opt}(A_L, G) = \arg\min_B e_l(A_L, G, B) \tag{11.80}$$

can be used to obtain a camera error-metric as $e_{\min}(A_L, G) = e_l(A_L, G, B_{opt}(A_L, G))$. The advantage of using the linearized error metric is that closed-form expressions can be obtained for the optimal transformation and also for the camera error metric.

In this part, the linearized camera error metric $e_l(A_L, G, B)$ is considered. Expressions are derived for the optimal linear color-correction transformation, $B_{opt}(A_L, G)$, that minimizes this error metric and for the resulting minimum mean-squared linearized color error $e_{\min}(A_L, G)$.

From Equations (11.78) and (11.79), the linearized color error metric for a scanner with sensitivity matrix *G* under the color correction transformation *B* can be written as

$$e_l(A_L, G, B) = E\left\{\left\| J_F(t)(t-\hat{t})\right\|^2\right\} = E\left\{\left\| J_F(t)\left[A_L^T r - B(G^T r + x)\right]\right\|^2\right\} \tag{11.81}$$

where *x* is the variable denoting imaging noise and the other terms are as defined previously.

In order to simplify Equation (11.81) and apply the least-squares approach, it is useful to introduce the *vec*(·) operator that transforms a matrix into a vector by stacking the columns of the matrix one underneath the other in sequence. It is also useful to state some properties of the *vec*(·) operator and the Kronecker product. For arbitrary matrices, *T*, *U*, *V*, and *W* with appropriate sizes, the following results hold:

$$\begin{aligned}
(T+U)\otimes(V+W) &= T\otimes V + T\otimes W + U\otimes V + U\otimes W \\
(T\otimes U)(V\otimes W) &= TV\otimes UW \\
(T\otimes U)^T &= T^T\otimes U^T \\
vec(UVW) &= (W^T\otimes U)vec(V) \\
(T\otimes U)(V\otimes W) &= TV\otimes UW \\
(T\otimes U)^{-1} &= T^{-1}\otimes U^{-1} \\
\text{trace}(TUVW) &= (vecW^T)^T(V^T\otimes T)vecU
\end{aligned} \tag{11.82}$$

where ⊗ denotes the Kronecker product and it is assumed that the matrices satisfy rank and size restrictions for all the relevant operations to be defined. Backgrounds on Equations (11.82) can be found in [Magnus1999]. Application of locally linearized approximation, *vec* operator, and Kronecker production onto color imaging can also be found in [Wolski1995, Wolski1996, Sharma1996b and Sharma1997b]. Using Equations (11.82),

$$\begin{aligned}
J_F(t)A_L^T r &= vec(J_F(t)A_L^T r) = (r^T\otimes J_F(t))vec(A_L^T) \\
J_F(t)B[G^T r + x] &= vec(J_F(t)B[G^T r + x]) = [(G^T r + x)^T\otimes J_F(t)]vec(B)
\end{aligned} \tag{11.83}$$

For notational simplicity, denote

$$b = vec(B),\ x = (r^T\otimes J_F(t))vec(A_L^T),\ Y = (G^T r + x)^T\otimes J_F(t)$$

Then

$$e_l(A_L, G, B) = E\left\{\|x - Yb\|^2\right\} = E\{\|x\|^2\} - 2E\{x^T Y\}b + b^T E\{Y^T Y\}b \tag{11.84}$$

is a quadratic function of *b*. Notice that Equation (11.84) has similar form to Equation (11.70), least-squares approach similar to Equations (11.71)-(11.72) can be applied. Clearly a minimum exists, and a necessary and sufficient condition for the minimum is

$$\frac{\partial e_l}{\partial b} = 2\left[E\{Y^T Y\}b - E\{Y^T x\}\right] = 0 \tag{11.85}$$

Note that Equations (11.85) are a variation of the normal equations for linear least-squares approach. These equations are guaranteed to have a solution. There is a unique solution, if and only if $E\{Y^T Y\}$ is full rank. In further treatment, it will be assumed that $E\{Y^T Y\}$ is full rank. In the presence of noise, it can be shown that this holds.

The optimum value of *b* (*B*) is then given by the solution to Equations (11.85)

$$vec(B_{opt}) = b_{opt} = \left[E\left\{Y^T Y\right\}\right]^{-1} E\left[Y^T x\right] \tag{11.86}$$

Note also that the orthogonality conditions in Equations (11.85) imply that

$$\left[E\left\{Y^T Y\right\} b_{opt} - E\left\{Y^T x\right\}\right] = 0 \tag{11.87}$$

from which it follows that,

$$\begin{aligned} e_l(A_L, G, B_{opt}) &= E\left\{\|x\|^2\right\} - E\left\{x^T Y\right\} b_{opt} + b_{opt}^T \left[E\left\{Y^T Y\right\} b_{opt} - E\left\{Y^T x\right\}\right] \\ &= E\left\{\|x\|^2\right\} - E\left\{x^T Y\right\} b_{opt} \\ &= E\left\{\|x\|^2\right\} - E\left\{x^T Y\right\}\left[E\left\{Y^T Y\right\}\right]^{-1} E\left[Y^T x\right] \end{aligned} \tag{11.88}$$

Note that Equation (11.88) is similar to Equation (11.72). Hence, it can be readily seen that,

$$\begin{aligned} E\left\{Y^T Y\right\} &= E\left\{\left[\left(G^T r + x\right) \otimes J_F^T(t)\right]\left[\left(G^T r + x\right)^T \otimes J_F(t)\right]\right\} \\ &= E\left\{\left(G^T r + x\right)\left(G^T r + x\right)^T \otimes J_F^T(t) J_F(t)\right\} \\ &= E\left\{\left[G^T r r^T G + G^T r x^T + x r^T G + x x^T\right] \otimes J_F^T(t) J_F(t)\right\} \\ &= E\left\{G^T r r^T G \otimes J_F^T(t) J_F(t)\right\} + \cdots \\ &= \left(G^T \otimes I_3\right) E\left\{r r^T \otimes J_F^T(t) J_F(t)\right\}\left(G \otimes I_3\right) + \left(G^T \otimes I_3\right) E\left\{r x^T \otimes J_F^T(t) J_F(t)\right\} \\ &\quad + E\left\{x r^T \otimes J_F^T(t) J_F(t)\right\}\left(G \otimes I_3\right) + E\left\{x x^T \otimes J_F^T(t) J_F(t)\right\} \end{aligned} \tag{11.89}$$

where I_3 denotes the 3×3 identity matrix. Also,

$$\begin{aligned} E\left\{Y^T x\right\} &= E\left\{\left[\left(G^T r + x\right) \otimes J_F^T(t)\right]\left[r^T \otimes J_F(t)\right] vec(A_L^T)\right\} \\ &= E\left\{\left[G^T r r^T + x r^T\right] \otimes J_F^T(t) J_F(t)\right\} vec(A_L^T) \\ &= \left(G^T \otimes I_3\right) E\left\{r r^T \otimes J_F^T(t) J_F(t) + x r^T \otimes J_F^T(t) J_F(t)\right\} vec(A_L^T), \end{aligned} \tag{11.90}$$

$$\begin{aligned} E\left\{\|x\|^2\right\} &= E\left\{vec(A_L^T)^T (r \otimes J_F^T(t))(r^T \otimes J_F(t)) vec(A_L^T)\right\} \\ &= vec(A_L^T)^T E\left\{r r^T \otimes (J_F^T(t) J_F(t))\right\} vec(A_L^T) \end{aligned} \tag{11.91}$$

According to the CCD imager noise model discussed in Chapter 4, the recording noise, x, is zero-mean and dependent of r. The normalized total noise variance for specific r is

$$E[x_i x_i^T] = s_x^2 = s_d^2 + k_1 m_i = s_d^2 + \frac{k}{G_0^T \mathbf{1}} G_i^T r \tag{11.92}$$

For some spectral sensitivity, $s_d^2 \approx 10^{-7}$ and $k_1 \approx 10^{-4}$ as specified by Equation (4.35). $G_0^T \mathbf{1}$ calculates the camera output signal of illuminant white for the reference spectral sensitivity (S_0) under the reference illumination L_{ref} (i.e. CIE D65), $G_0 = L_{ref} S_0$. Then the noise variance-covariance matrix can be represented as

$$E\left[xx^T\right] = \begin{bmatrix} s_d^2 & & & \\ & s_d^2 & & \\ & & \ddots & \\ & & & s_d^2 \end{bmatrix} + \frac{k}{G_0^T \mathbf{1}} \begin{bmatrix} G_1^T r & & & \\ & G_2^T r & & \\ & & \ddots & \\ & & & G_m^T r \end{bmatrix} = K_{s_d} + \frac{k}{G_0^T \mathbf{1}} diag(G^T r) \tag{11.93}$$

And the noise mean is

$$E[x] = 0 \tag{11.94}$$

For the same r, the noise can be treated as independent variable of input signal since the variance for fixed input signal is constant, thus:

$$E\{x r^T \otimes J_F^T(t) J_F(t)\} = \frac{1}{n_{sample}} \sum_{i=1}^{n_{sample}} E\{x_i\} E\{r_i^T\} \otimes E\{J_F^T(t_i) J_F(t_i)\} = 0 \tag{11.95}$$

$$E\{r x^T \otimes J_F^T(t) J_F(t)\} = [E\{x r^T \otimes J_F^T(t) J_F(t)\}]^T = 0 \tag{11.96}$$

$$\begin{aligned} E\{xx^T \otimes J_F^T(t) J_F(t)\} &= \frac{1}{n_{sample}} \sum_{i=1}^{n_{sample}} E\{x_i x_i^T\} \otimes E\{J_F^T(t_i) J_F(t_i)\} \\ &= \frac{1}{n_{sample}} \sum_{i=1}^{n_{sample}} diag(s_d^2 + k \frac{G^T r_i}{G_0^T \mathbf{1}}) \otimes [J_F^T(t_i) J_F(t_i)] \\ &= \frac{1}{n_{sample}} \sum_{i=1}^{n_{sample}} diag(s_d^2) \otimes [J_F^T(t_i) J_F(t_i)] + \frac{k}{G_0^T \mathbf{1}} \frac{1}{n_{sample}} \sum_{i=1}^{n_{sample}} diag(G^T r_i) \otimes [J_F^T(t_i) J_F(t_i)] \\ &= K_{s_d} \otimes E\{J_F^T(t) J_F(t)\} + \frac{k}{G_0^T \mathbf{1}} E\{diag(G^T r) \otimes [J_F^T(t) J_F(t)]\} \end{aligned} \tag{11.97}$$

where K_{s_d} is the dark noise covariance matrix. The optimal transformation in Equation (11.86) is:

$$\begin{aligned} vec(B_{opt}(A_L, G)) &= \arg\min_B e_l(A_L, G, B) = b_{opt} \\ &= \left[\left(G^T \otimes I_3\right) S_r (G \otimes I_3) + S_x\right]^{-1} \left(G^T \otimes I_3\right) S_r vec(A_L^T) \end{aligned} \tag{11.98}$$

where

$$S_r = E\left\{\left(rr^T\right)\otimes\left(J_F^T(t)J_F(t)\right)\right\} \tag{11.99}$$

$$\begin{aligned} S_x &= E\left\{xx^T \otimes J_F^T(t)J_F(t)\right\} \\ &= K_{s_d}\otimes E\{J_F^T(t)J_F(t)\} + \frac{k}{G_0^T\mathbf{1}}E\{diag(G^T r_i)\otimes[J_F^T(t_i)J_F(t_i)]\} \end{aligned} \tag{11.100}$$

By straightforward simplification of the corresponding value of the minimum mean-squared linearized color error is given by

$$e_{\min}(A_L,G) = e_l(A_L,G,B_{opt}) = a(A_L) - t(A_L,G) \tag{11.101}$$

where

$$a(A_L) = vec(A_L^T)^T S_r vec(A_L^T) \tag{11.102}$$

$$t(A_L,G) = vec(A_L^T)^T S_r(G\otimes I_3)\left[\left(G^T\otimes I_3\right)S_r\left(G\otimes I_3\right)+S_x\right]^{-1}\left(G^T\otimes I_3\right)S_r vec(A_L^T) \tag{11.103}$$

$a(A_L)$ may be interpreted as the total colorimetric information of object colors, and $t(A_L,G)$ is the colorimetric information that can be recovered with color imaging device. The error metric for digital imaging derived above is useful for comparing the color accuracy of different filter sets in a chosen color space, i.e., for a given $F(\cdot)$. Since different color spaces may have very different scales, a normalized measure of goodness is more useful for the comparison of error metrics in different spaces. It can be readily seen that

$$0 \le t(A_L,G) \le a(A_L) \tag{11.104}$$

In like wise of *m*-factor definition in Section 5.4, the ratio

$$q(A_L,G,F) = \frac{t(A_L,G)}{a(A_L)} \tag{11.105}$$

defines a normalized quality factor for imaging application. The normalization ensures that the quality factor is bounded between 0 and 1 with $q(A_L,G,F)=1$ representing a "perfect" colorimetric imaging whose error metric is zero.

Note that the initial objective function is Equation (11.78), in order to correct the result from objective function of Equation (11.79), a measure of goodness for specified taking-viewing-illuminant pair can be defined as:

$$q = 1-\sqrt{1-q(A_L,G,F)} \tag{11.106}$$

in order to obtain linear relationship between the average color difference for an ensemble of objects and the quality factor. Since the taking (recording) and viewing illuminants may be different, a quality factor for any taking-viewing illuminant pair can be defined. If the illuminant pair can be chosen from a set of illuminants, a quality factor matrix is defined. An illuminant-color-correction strategy is outlined as follows.

The above derivations are based on single taking-viewing illuminant pair. For *m* taking and *n* viewing illuminants, a quality factor matrix M can be defined by considering combinations of any illuminant pairs:

$$\mathrm{M}=\begin{bmatrix} q_{11} & q_{12} & q_{13} & \cdots & q_{1m} \\ q_{21} & q_{22} & q_{23} & \cdots & \vdots \\ q_{11} & q_{11} & q_{11} & \cdots & \vdots \\ \vdots & \vdots & \vdots & \ddots & \vdots \\ q_{n1} & q_{n2} & q_{n3} & \cdots & q_{nm} \end{bmatrix} \tag{11.107}$$

Therefore the comprehensive quality factor UMG for all illuminant pairs may be defined as the weighted average of elements of the above matrix:

$$\Theta=\frac{1}{mn}\sum_{j=1}^{m}\sum_{i=1}^{n}w_{ij}q_{ij} \tag{11.108}$$

where w_{ij} is the weight preset by camera manufacturers for the corresponding quality factor q_{ij} defined for viewing-taking-illuminant pair $(L_{v_i},\ L_{t_j})$, and $\sum_{i=1}^{n}\sum_{j=1}^{m}w_{ij}=1$.

The reason of proposing such a strategy is that, for some color imaging devices, like a color scanner, there is only one fixed recording illuminant, but there may be several viewing (target) illuminants; for some other imaging devices, like a digital camera, there may be more than one recording illuminant (working under different illuminations), which is quite usual, but colorimetric information under single or multiple viewing illuminants is desired to know. For some other imaging devices, in most cases, it is only required that the recording illuminant and viewing illuminant are the same, although there could be multiple. Then the comprehensive quality factor Θ can be defined as the weighted average of the diagonal elements of the quality factor matrix M.

For specific device, UMG for the illuminant set may be defined as the weighted average of elements of one column, one row, or diagonal elements of the above matrix:

$$\Theta = \frac{1}{n}\sum_{i=1}^{n} w_i q_{ij} \text{ or } \Theta = \frac{1}{m}\sum_{j=1}^{m} w_j q_{ij} \text{ or } \Theta = \frac{1}{n}\sum_{i=1}^{n} w_i q_{ii} \tag{11.109}$$

11.6 Appendix F: Designing Spectral Sensitivities for Spectral Reproduction

As an extension to the above approach to the design of colorimetric filters, additional channels can be designed for the goal of spectral reproduction. Filter design for only spectral reproduction has been studied before [Haneishi1997, Hosoi1999], but it is preferred to have the camera system to achieve both colorimetric and spectral reproduction, simultaneously, if possible. Here metrics for evaluating the goodness of sensitivities for spectral reproduction are defined.

The candidate metrics to define spectral difference are:

Candidate 1: Mean square error of reflectance spectra

$$MSE = E\left\{\left\| R - \hat{R} \right\|^2\right\} \tag{11.110}$$

where R is the measured reference spectral reflectance, $\hat{R}$ is the recovered spectral reflectance.

Candidate 2: Weighted mean square error of reflectance spectra

$$MSE_w = E\left\{\left\| w_l (R - \hat{R}) \right\|^2\right\} \tag{11.111}$$

where w_l is a diagonal matrix with diagonal elements from samplings of weighting function, which may be related to the human visual system, for example, the *q*-factor curve obtained in Chapter 5 which emphasizes the "prime wavelengths" characteristics of the human visual system. Viggiano also introduced a weighting function by linearized approximation of CIELAB space [Viggiano1990, Viggiano2001], this weighting function is in fact close to the shape of *q*-factor curve.

11.6.1 Principal Components Imaging

Assuming the object reflectance spectra can be approximated with limited number of eigenvectors, the recovering of spectral reflectance may be carried out with principal component analysis.

$$t_c = S^T L_c R = S^T L_c \mathbf{B} a \tag{11.112}$$

$$a = (S^T L_c \mathbf{B})^{-1} t_c \tag{11.113}$$

where S is the spectral sensitivities, L_c is the taking illuminant, $\mathbf{B}$ is the principal component vectors, and a is the weighting for each principal component, t_c is camera output signal. Therefore the recovered spectral reflectance is represented as

$$\hat{R} = \mathbf{B} a = \mathbf{B}(S^T L_c \mathbf{B})^{-1} t_c \tag{11.114}$$

The minimized mean square error of spectral difference is

$$MSE = E\left\{ \left\| R - \mathbf{B}(S^T L_c \mathbf{B})^{-1} t_c \right\|^2 \right\} \tag{11.115}$$

A quality factor similar to *m*-factor can be defined to represent the difference between spectral sensitivities S and principal components for accurate spectral reproduction.

$$m(\mathbf{B}, S) = \frac{\text{trace}(\mathbf{B}S(S^T S)^{-1} S^T \mathbf{B}^T)}{\text{trace}(\mathbf{B}^T \mathbf{B})} \tag{11.116}$$

where function $m(\bullet)$ calculates the difference of fundamental subspaces of $\mathbf{B}$ and S.

11.6.2 Wiener Estimation on Spectral Reflectance

The camera output signal with noise consideration is expressed as

$$t_c = S^T L_c R = G^T R + h \tag{11.117}$$

where $G = L_c S$. The estimation of R is given by

$$\hat{R} = F \cdot t_c \tag{11.118}$$

where F is a linear matrix. Minimizing MSE in Equation (11.110), explicit form of F is given as

$$F = K_R G (G^T K_R G + K_h)^{-1} \tag{11.119}$$

where K_R and K_h are the correlation matrix of ensemble of object spectra and noise respectively. More details on Equation (11.119) can refer to [Pratt1991].

$$K_R = E[RR^T] = \frac{1}{n_{sample}} \mathbf{R}\mathbf{R}^T$$

$$K_h = E[h h^T]$$

Noise correlation matrix K_h can be estimated from detail measurement of noise for CCD cameras actually used. Therefore the minimal mean squared error can be represented as

$$\begin{aligned} MSE_{\min} &= E\left\{\left\| R-\hat{R}\right\|^2\right\} \\ &= E\left\{\left\| R-K_R G(G^T K_R G+K_h)^{-1} t_c\right\|^2\right\} \\ &= a(R)-t(R,G,h) \end{aligned} \tag{11.120}$$

where

$$a(R)=\text{trace}\left[K_R\right] \tag{11.121}$$

$$t(R,G,h)=\text{trace}\left[K_R G(G^T K_R G+K_h)^{-1} G^T K_R\right] \tag{11.122}$$

The meaning of $a(\bullet)$ and $t(\bullet)$ can be interpreted as the total spectral information of objects and the recovered spectral information of objects. A normalized metric

$$q_{SR}=\frac{t(R,G,h)}{a(R)} \tag{11.123}$$

can evaluate spectral sensitivities in terms of spectral reproduction and will be referred as *spectral quality factor*, or quality factor of spectral reproduction.

Besides the mean squared error of spectral reflectance as a primary metric, the mean color difference under a standard illuminant can be a secondary metric to the optimal design of spectral reproduction filters. Usually the primary metric will generate a collection of optimal candidates to be lately refined with secondary metric.

11.6.3 Wiener Estimation with Weighting Function

By minimizing MSE_w in Equation (11.111), the reflectance spectra is estimated as

$$\hat{R}=K_R G(G^T K_R G+K_h)^{-1} \tag{11.124}$$

and the minimal mean squared error of spectra is

$$\begin{aligned} MSE_w &= E\left\{\left\| w_l(R-\hat{R})\right\|^2\right\} \\ &= E\left\{\left\| w_l(R-K_R G(G^T K_R G+K_h)^{-1})\right\|^2\right\} \\ &= a(R,w_l)-t(R,G,h,w_l) \end{aligned} \tag{11.125}$$

where w_l is a spectral weighting function, and

$$a(R,w_l)=\text{trace}\left[w_l^2 K_R\right] \tag{11.126}$$

$$t(R,G,h,w_l) = \text{trace}\left[w_l^2 K_R G (G^T K_R G + K_h)^{-1} G^T K_R \right] \tag{11.127}$$

Thus a normalized metric can be defined as

$$q_{SRW} = \frac{t(R,G,h,w_l)}{a(R,w_l)} \tag{11.128}$$

which also indicates the performance of spectral sensitivities in terms of spectral reproduction. Both Equations (11.123) and (11.128) can be used as criteria to design a set of spectral sensitivities for spectral reproduction.

11.7 Appendix G: Optimization Results

The optimal spectral sensitivity sets are obtained based on the order of secondary evaluation (*m*-factor). The ten sets that satisfy the total thickness constraint ($\text{Thickness}_{\text{Total}} \le 4\text{mm}$) are plotted here with their component parameters.

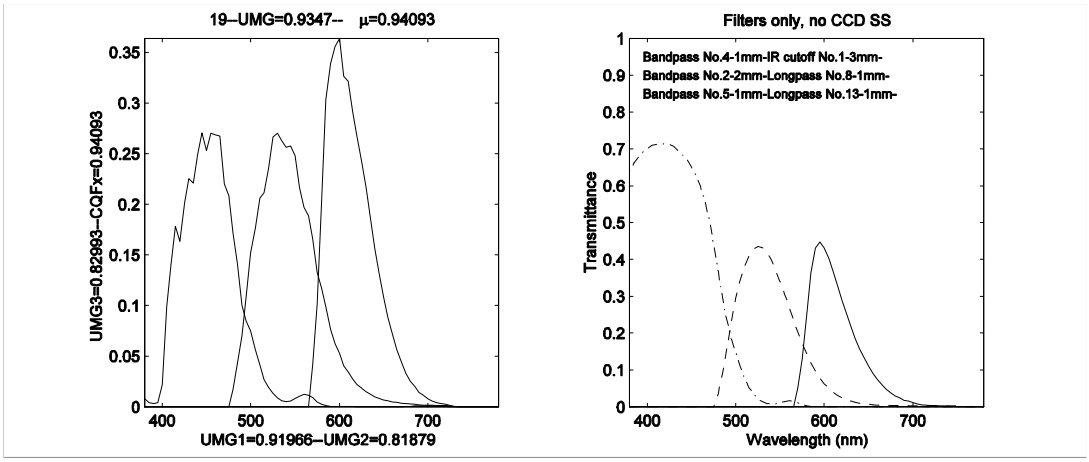

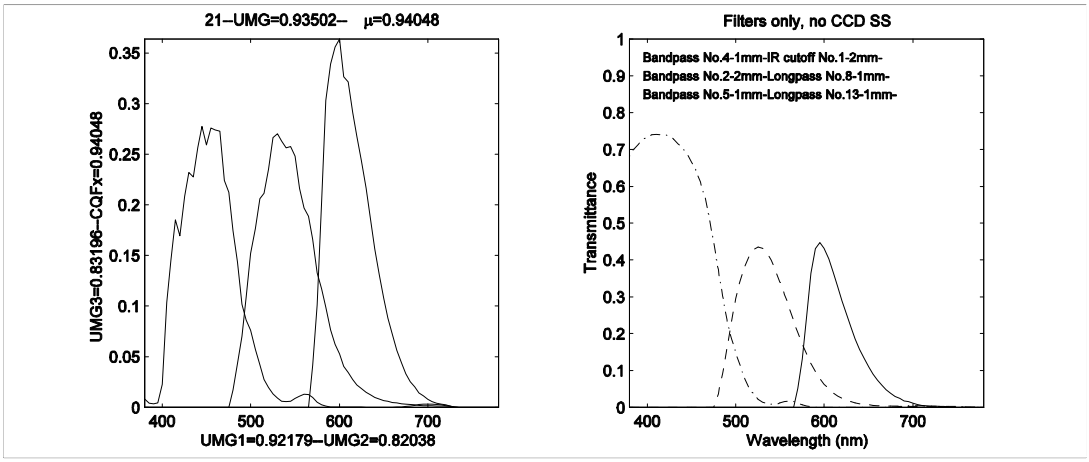
21--UMG=0.93502-- μ=0.94048
UMG3=0.83196--CQFx=0.94048
UMG1=0.92179--UMG2=0.82038
Filters only, no CCD SS
Bandpass No.4-1mm-IR cutoff No.1-2mm-
Bandpass No.2-2mm-Longpass No.8-1mm-
Bandpass No.5-1mm-Longpass No.13-1mm-
Transmittance
Wavelength (nm)

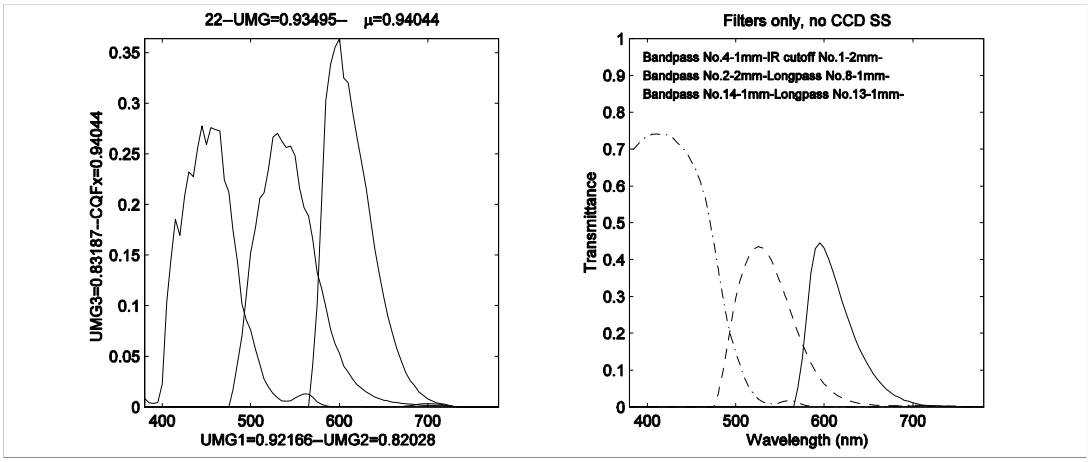
22--UMG=0.93495-- μ=0.94044
UMG3=0.83187--CQFx=0.94044
UMG1=0.92166--UMG2=0.82028
Filters only, no CCD SS
Bandpass No.4-1mm-IR cutoff No.1-2mm-
Bandpass No.2-2mm-Longpass No.8-1mm-
Bandpass No.14-1mm-Longpass No.13-1mm-
Transmittance
Wavelength (nm)

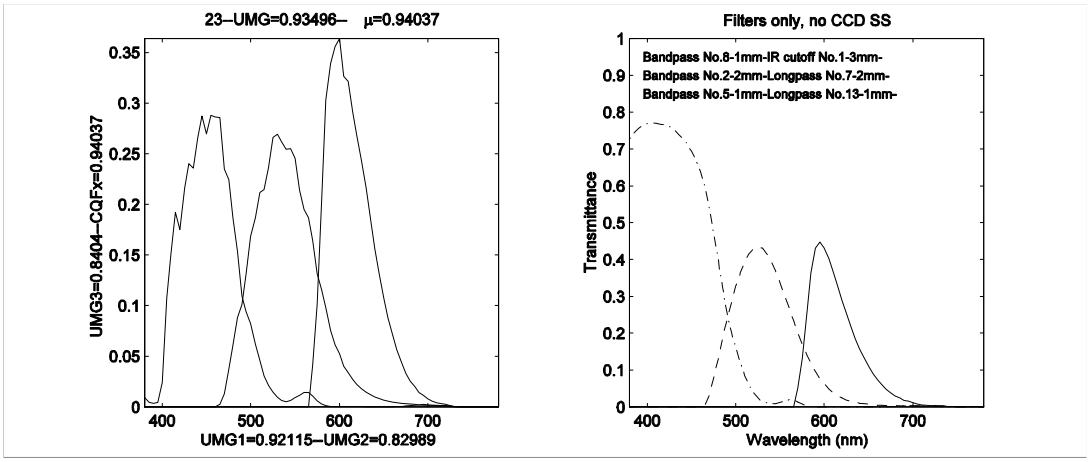
23--UMG=0.93496-- μ=0.94037
UMG3=0.8404--CQFx=0.94037
UMG1=0.92115--UMG2=0.82989
Filters only, no CCD SS
Bandpass No.8-1mm-IR cutoff No.1-3mm-
Bandpass No.2-2mm-Longpass No.7-2mm-
Bandpass No.5-1mm-Longpass No.13-1mm-
Transmittance
Wavelength (nm)

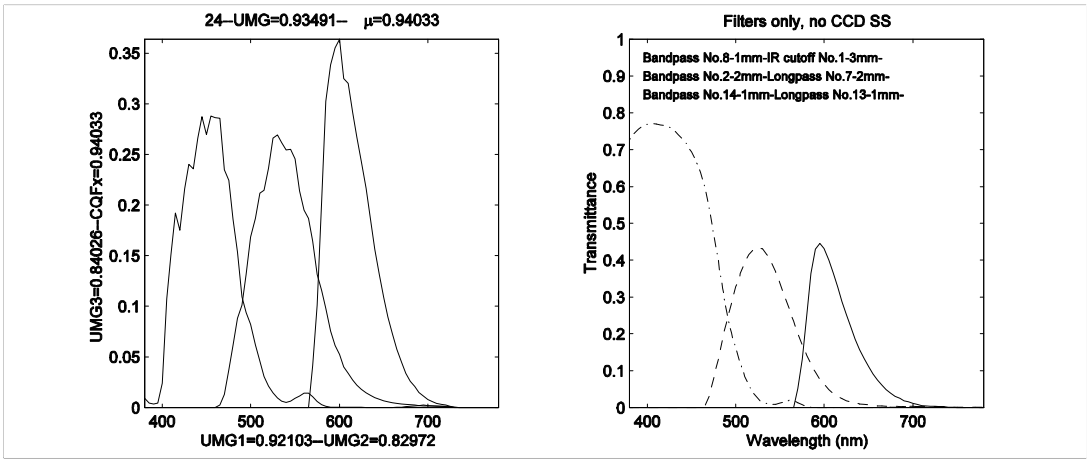
24--UMG=0.93491-- μ=0.94033
UMG3=0.84026--CQFx=0.94033
UMG1=0.92103--UMG2=0.82972
Filters only, no CCD SS
Bandpass No.8-1mm-IR cutoff No.1-3mm-
Bandpass No.2-2mm-Longpass No.7-2mm-
Bandpass No.14-1mm-Longpass No.13-1mm-
Transmittance
Wavelength (nm)

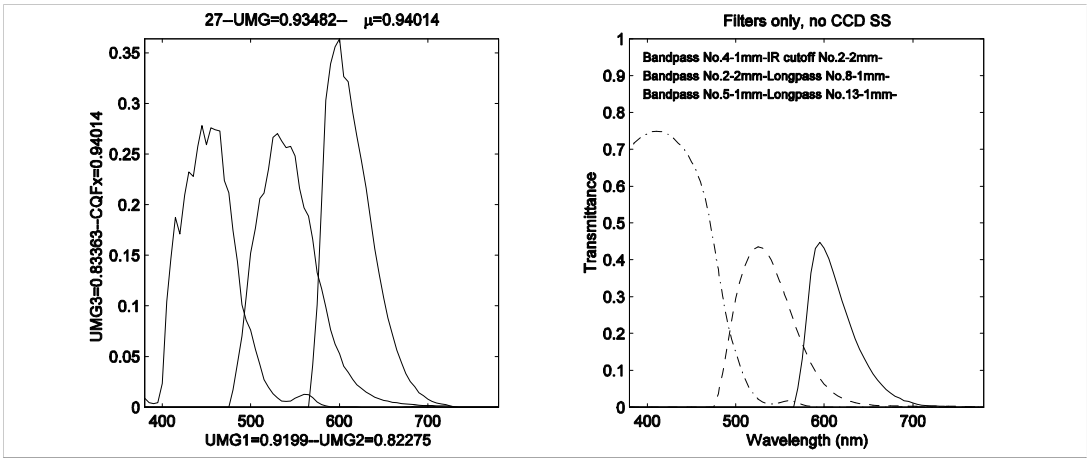
27--UMG=0.93482-- μ=0.94014
UMG3=0.83363--CQFx=0.94014
UMG1=0.9199--UMG2=0.82275
Filters only, no CCD SS
Bandpass No.4-1mm-IR cutoff No.2-2mm-
Bandpass No.2-2mm-Longpass No.8-1mm-
Bandpass No.5-1mm-Longpass No.13-1mm-
Transmittance
Wavelength (nm)

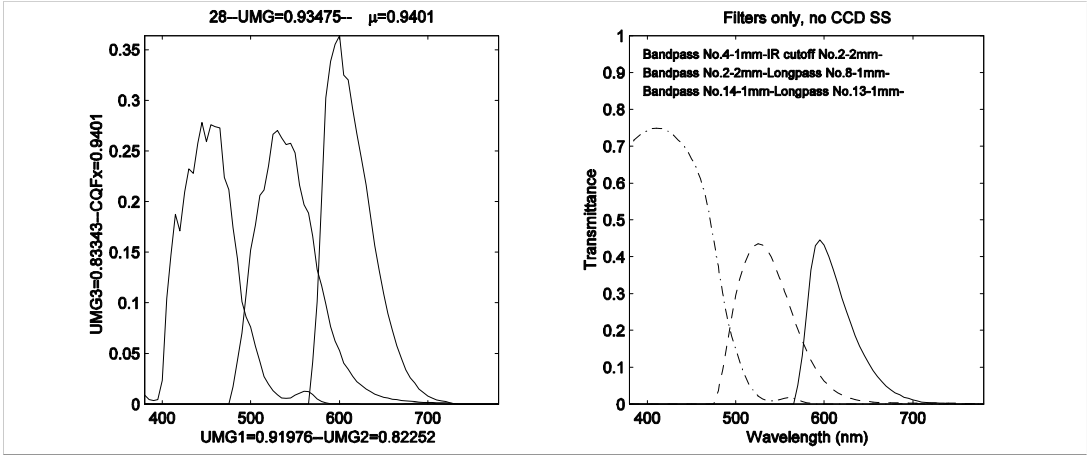
28--UMG=0.93475-- μ=0.9401
UMG3=0.83343--CQFx=0.9401
UMG1=0.91976--UMG2=0.82252
Filters only, no CCD SS
Bandpass No.4-1mm-IR cutoff No.2-2mm-
Bandpass No.2-2mm-Longpass No.8-1mm-
Bandpass No.14-1mm-Longpass No.13-1mm-
Transmittance
Wavelength (nm)

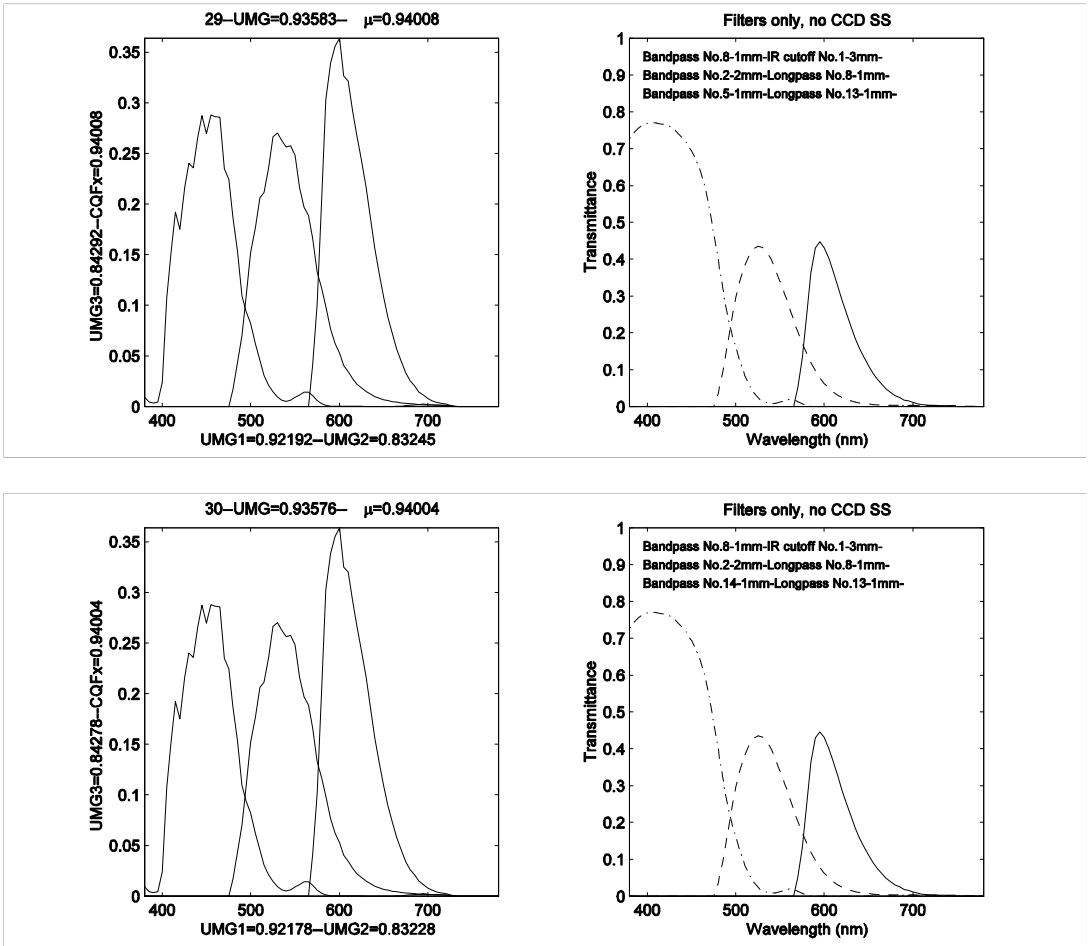

Figure 11.3: Candidates of optimal spectral sensitivity set from experiment 2.

11.8 Appendix H: Comparison of Multiple Spectral Sensitivity Sets

The performance of the newly designed spectral sensitivities (Figure 9.13) was compared with Sony 3CCD (Figure 8.3(b)) and IBM Pro/3000 sensitivities (Figure 9.9(b)). The colorimetric quality factors calculated were *m*-factor, UMG(D65, D65), UMG(A,A), UMG(F2,F2), UMG(F6,F6), UMG(Scanlite, Scanlite), UMG(S, S) in the following tables. Scanlite is an illuminant very close to CIE illuminant A, "S" illuminant is EikoFlood, close to illuminant D65.

Table 11–4: Colorimetric performance for SONY 3CCD 3SS (45dB).

Quality Factors	0.9500	0.9068	0.8236	0.8923	0.8857	0.8321	0.8955
Taking-Viewing	Mean	ΔE^*_{ab}	ΔE^*_{94}	Max	ΔE^*_{ab}	ΔE^*_{94}	
D65-D65		1.5461	0.9091		7.1427	3.6594	
A-A		2.2141	1.4477		8.1264	3.7021	
F2-F2		1.5033	0.9307		7.1709	3.3651	
F6-F6		1.5076	0.9459		7.0868	3.3447	
Scanlite-Scanlite		2.1194	1.3669		8.1021	3.6579	
Other-Other		1.6917	0.9546		7.4568	3.8641	

Table 11–5: Colorimetric performance for IBM Pro/3000 (45dB).

Quality Factors	0.9322	0.9297	0.8639	0.9132	0.9052	0.8716	0.9295
Taking-Viewing	Mean	ΔE^*_{ab}	ΔE^*_{94}	Max	ΔE^*_{ab}	ΔE^*_{94}	
D65-D65		1.1651	0.7737		5.3990	3.1581	
A-A		1.2784	0.8831		4.7900	1.9953	
F2-F2		1.1703	0.7789		5.3107	2.8677	
F6-F6		1.2019	0.8061		5.3539	2.7836	
Scanlite-Scanlite		1.2257	0.8328		4.8138	2.0687	
Other-Other		1.0505	0.6563		5.0893	2.9530	

Table 11–6: Colorimetric performance of newly designed Quantix (45dB).

Quality Factors	0.9400	0.9218	0.8323	0.9149	0.9090	0.8428	0.9100
Taking-Viewing	Mean	ΔE^*_{ab}	ΔE^*_{94}	Max	ΔE^*_{ab}	ΔE^*_{94}	
D65-D65		1.4111	0.9609		6.7228	3.2728	
A-A		1.7015	1.2600		7.2783	4.3046	
F2-F2		1.0616	0.7309		4.5186	2.7154	
F6-F6		1.0581	0.7301		4.3866	2.6485	
Scanlite-Scanlite		1.5738	1.1610		6.5812	4.0976	
Other-Other		1.6414	1.1280		8.0217	4.4627	

Table 11–7: Colorimetric performance of previous Quantix 1 (45dB).

Quality Factors	0.9665	0.8067	0.4941	0.6773	0.6508	0.5093	0.7723
Taking-Viewing	Mean	ΔE^*_{ab}	ΔE^*_{94}	Max	ΔE^*_{ab}	ΔE^*_{94}	
D65-D65		2.1033	1.5170		6.5857	3.9998	
A-A		13.4856	10.4627		28.2308	24.6985	
F2-F2		4.7041	3.7648		9.8642	7.9816	
F6-F6		5.4757	4.4063		11.2059	9.5553	
Scanlite-Scanlite		12.4236	9.6800		25.1849	22.6507	
Other-Other		2.6890	1.9636		7.8797	4.7238	

Table 11–8: Colorimetric performance of previous Quantix 2 (45dB).

Quality Factors	0.9372	0.9198	0.7748	0.8784	0.8658	0.7877	0.8806
Taking-Viewing	Mean	ΔE^*_{ab}	ΔE^*_{94}	Max	ΔE^*_{ab}	ΔE^*_{94}	
D65-D65		1.1244	0.7490		4.7443	3.1686	
A-A		2.6565	2.0159		9.0102	5.6739	
F2-F2		1.2921	0.8700		4.5682	3.5523	
F6-F6		1.3662	0.9423		4.4460	3.5802	
Scanlite-Scanlite		2.4284	1.8278		8.4836	5.2839	
Other-Other		2.0724	1.3854		10.4973	6.3724	

Table 11–9: Colorimetric performance of newly designed Quantix (no noise).

Quality Factors	0.9401	0.9381	0.9550	0.9541	0.9550	0.9549	0.9301
Taking-Viewing	Mean	ΔE^*_{ab}	ΔE^*_{94}	Max	ΔE^*_{ab}	ΔE^*_{94}	
D65-D65		1.3973	0.9425		6.7229	3.2825	
A-A		0.9940	0.6711		4.6821	2.8498	
F2-F2		1.0207	0.6823		4.5262	2.7519	
F6-F6		1.0010	0.6647		4.3904	2.6868	
Scanlite-Scanlite		0.9981	0.6760		4.5750	2.7360	
Other-Other		1.6046	1.0884		8.0072	3.9214	

Table 11–10: Colorimetric performance of previous Quantix 1 (no noise).

Quality Factors	0.9665	0.9362	0.9271	0.9381	0.9392	0.9290	0.9354
Taking-Viewing	Mean	ΔE^*_{ab}	ΔE^*_{94}		Max	ΔE^*_{ab}	ΔE^*_{94}
D65-D65		1.3488	0.8005			5.7309	3.2375
A-A		1.5236	0.8148			11.7576	5.3854
F2-F2		1.2988	0.7809			5.5412	2.9147
F6-F6		1.2724	0.7644			5.4753	2.8023
Scanlite-Scanlite		1.4991	0.8073			10.7602	4.9021
Other-Other		1.3655	0.7623			7.7030	3.6804

Table 11–11: Colorimetric performance of previous Quantix 2 (no noise).

Quality Factors	0.9372	0.9505	0.9329	0.9511	0.9506	0.9350	0.9077
Taking-Viewing	Mean	ΔE^*_{ab}	ΔE^*_{94}		Max	ΔE^*_{ab}	ΔE^*_{94}
D65-D65		1.0980	0.7179			4.7770	2.9272
A-A		1.4522	0.8749			10.1801	6.2328
F2-F2		1.1374	0.6994			4.0666	2.8421
F6-F6		1.1485	0.7055			4.1084	2.7342
Scanlite-Scanlite		1.4171	0.8571			9.4785	5.8772
Other-Other		2.0139	1.3215			10.5913	6.4915

11.9 Appendix I: Designing Additional Channels for Spectral Reproduction

Designing additional channels for spectral reproduction was not the primary goal of this research. In Appendix F, spectral quality factors to evaluate the goodness of spectral sensitivities for spectral reproduction performance are proposed. A preliminary experiment is described as follows. In Section 9.3, a set of three spectral sensitivities was designed to achieve colorimetric reproduction. Three more channels work with them together to achieve spectral accuracy. If Wiener estimation is applied to recover spectral reflectance, Vrhel-Trussell dataset is used to represent the spectral characteristics, and peak wavelengths are chosen as 470~530nm, 530~570nm and 570~720nm due to the peak locations of available three are about 450nm, 530nm and 570nm, the width was limited to 80nm, the set of three SS that maximal Equation

(11.123) were plotted in Figure 11.4. These filters were very preliminary results. No further test or optimization has been done yet.

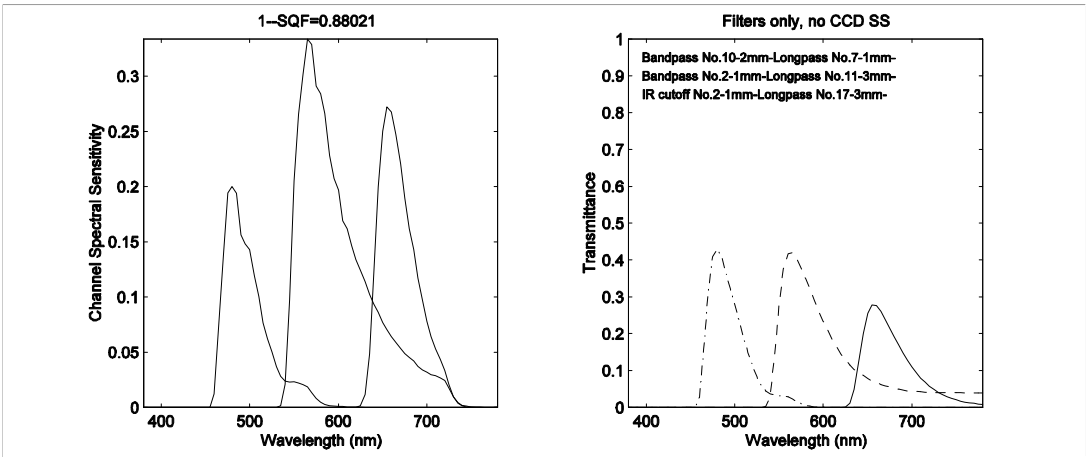

Figure 11.4: Three spectral sensitivities to achieve spectral reproduction when working with the three designed sensitivities for colorimetric reproduction.

11.10 Appendix J: MATLAB Source Codes for Optimal Design of Spectral Sensitivities

11.10.1 Part One – Optima Search

```
%
% Hierarchical optimization of spectral sensitivities for digital color imaging devices
% Three or more imaging channels are obtained from the combination of given basic filter components
%
% The optimization is divided into two procedures:
%       OptimUMG1part1: Pre-Selection, UMG Optimization for single illuminant pair (EE-EE), Saving into a file
%       OptimUMG1part2: Loading the file saved by OptimUMG1part1, UMG evaluation for other illuminant pairs,
%                       mu-factor calculation, RMS noise calculation, and Secondary Optimization
%
% This file is OptimUMG1part1.m, which must be run at first before OptimUMG1part2.m
%
% calculate using UMG and mu-factor:
%
% refer to Shuxue Quan's PhD Thesis: chapter 5, chapter 7 and chapter 9 for background knowledge
%
% N e w   O p t i m i z a t i o n   N e w   D a t a b a s e   N e w   J a c o b i a n M a t r i x
%
% Schott glass filters in QuantixDatabase.mat
%
% bandpass filters: VGBG  : 14x3 (3mm 2mm 1mm)
% longpass filters: GGOGRG: 19x3 (3mm 2mm 1mm)
% IR cut   filters: BGKG  :  7x3 (3mm 2mm 1mm)
%
% April 23, 2002     copyright (c) Shuxue Quan of MCSL CIS RIT EDU
%
% databases:
% colorDatabase.mat: contains CIE specified spectra, i.e. color matching functions, illuminants etc. --> Ohta's book
%
```

```
%           Tc_xDyD_M1M2      56x5      : x, y and multiplier scalaer M1, M2 of daylight of corresponding CCT
%           originalA         107x1     : CIE A
%           originalC         91x1      : CIE C
%           originalD55       54x1      : CIE D55
%           originalD65       107x1     : CIE D65
%           originalD75       54x1      : CIE D75
%           originalDye       81x3      : Fuji Color Film Dye Sensitivity - by Dr. Ohta
%           originalF1F12     81x12     : CIE Fluorescent F1-F12
%           originalMacbeth   81x24     : Macbeth Color Checker
%           originalS0S1S2    54x3      : Mean Relative Radiant SPD S0(lamda) and First Two eigen vectors
%           originalXYZ1931   95x3      : CIE xyz 1931
%           originalXYZ1964   95x3      : CIE xyz 1964
%           waveA             107x1     : visible wavelength range for CIE A
%           waveC             91x1      : visible wavelength range for CIE C
%           waveD55           54x1      : visible wavelength range for CIE D55
%           waveD65           107x1     : visible wavelength range for CIE D65
%           waveD75           54x1      : visible wavelength range for CIE D75
%           waveDye           81x1      : visible wavelength range for Fuji Color Film Dye Sensitivity
%           waveF             81x1      : visible wavelength range for CIE Fluorescent Illuminants
%           waveMacbeth       81x1      : visible wavelength range for Macbeth Color Checker
%           waveS0S1S2        54x1      : visible wavelength range for CIE Daylight S0S1S2
%           waveXYZ1931       95x1      : visible wavelength range for CIE xyz 1931
%           waveXYZ1964       95x1      : visible wavelength range for CIE xyz 1964
%
% QuantixDatabase.mat: contains Schott Filters and CCD sensitivity  --> Schott Glass Software
% ============== The transmittance spectra are external tranmittance spectra of 1 mm thickness glass filters
%
%           BGKG              901x7     : Transmittance spectra of 7 Schott IR cutoff filters
%           CCD02             201x5     : Measured Quantix CCD sensitivity  2nm sampling
%           CCD10             36x3      : Measured Quantix CCD sensitivity 10nm sampling
%           EikoFloodRawSpectra  186x4  : Radiance SPD of some illuminant: EikoFlood
%           GGOGRG            901x19    : Transmittance spectra of 19 Schott longpass cutoff filters
%           HalonSpectra      186x4     : Halon's reflectance spectra
%           ScanliteRawSpectra   186x4  : Radiance SPD of some illuminant: Scanlite, used for Quantix
%           VGBG              901x14    : Transmittance spectra of 14 Schott bandpass filters
%           waveCCD02         201x1     : Visible wavelength range for CCD SS with  2nm sampling
%           waveCCD10         36x1      : Visible wavelength range for CCD SS with 10nm sampling
%           waveSchott        901x1     : Visible wavelength range for transmittance of Schott glass filters
%
%    Name of    #   bandpass  IR   longpass filters      :      basic given Schott glass filters (1mm)
%
%           1      VG6        BG38   GG385
%           2      VG9        BG40   GG395
%           3      BG7        KG1    GG400
%           4      BG12    KG2       GG420
%           5      BG18    KG3       GG435
%           6      BG23    KG4       GG455
%           7      BG24A   KG5       GG475
%           8      BG25              GG495
%           9      BG26              OG515
%           10     BG28              OG530
%           11     BG3                  OG550
%           12     BG39              OG570
%           13     BG4                  OG590
%           14     BG42              RG1000
%           15                          RG610
%           16                          RG630
%           17                          RG645
%           18                          RG665
%           19                          RG695
```

```
% filterData20010301.mat; filterDataTotal.mat: precious database for Schott Filters
%                Some other SS of camera (3) channels are supplied in these files
%                New filter transmittance spectra in Quantix database are recommendeded rather than this
%
% VrhelDatabase.mat: contains 354 samples prepared by Vrhel-Trussell --> refer to their publications
%
%             VrhelDupont      171x120     : Reflectance spectra of 120 Dupont patches
%             VrhelMunsell     171x64      : Reflectance spectra of 64 Munsell Color chips (9 from MCC)
%             VrhelObject      171x170     : Reflectance spectra of 170 natural objects, i.e. leaves etc.
%             waveVrhel        171x1       : Visible wavelength tange: [390: 2: 730]'
%
% measuredFilter.mat: The measured transmittance spectra of 6 filters designed in Year2001
%
%      measuredBlue         40x1     : Transmittance spectra of BLUE
%      measuredClear        40x1     : Transmittance spectra of CLEAR channel, only IR cutoff filter exists
%      measuredGreen         40x1     : Transmittance spectra of GREEN
%      measuredIRcut        40x1     : Transmittance spectra of IR cutoff
%      measuredNIR          40x1     : Transmittance spectra of Near IR, or Far RED (long red)
%      measuredNUV           40x1     : Transmittance spectra of Near UV, or Far BLUE (short blue)
%      measuredRed          40x1     : Transmittance spectra of RED
%      measuredStandard      40x1     : Transmittance spectra of AIR
%      waveMeasured          40x1     : Visible wavelength range [360:10:750]'

%
% Subroutines
%
% TransmittanceE2I.m: convert external transmittance spectra into internal transmittance spectra
% TransmittanceI2E.m: convert internal transmittance spectra into external transmittance spectra
% statisticsReflectance.m: [Sr,EJFtJF]=statisticsReflectance(AL,R), calculate Sr and E[JF'*Jf] for reflectance samples R
%                        under (diagonal) viewing illuminant L and CMF A: AL=diag(L)*A
% UMGSingle.m: [umg,bopt]=UMGSingle(AL,GG,Sr,Se), calculate UMG value 'umg' and vector of optimal conversion matrix
'bopt'
%             AL: viewing illuminant and color matching functions: AL=diag(Lv)*xyz31
%             GG: taking illuminant and spectral sensitivities: GG=diag(Lt)*ssRGB
%             Sr: a variable contains statistical information of reflectance samples
%             Se: a variable contains statistical information of recording noise: Se=kron(Ke,EJFtJF)
%             Bopt: matrix form (i.e. 3 x 3) of transformation from XYZ -> LAB after 'bopt' (i.e. 9 x 1) is obtained
% sigmaLab.m: [dLabBurns,dLab]=sigmaLab(sigmaXYZ), calculate the average RMS noise in CIELAB space,
%            both Burns-Berns noise formula and diagonal RMS noise formula are used
% cameraColorError.m: dEUMG2=cameraColorError(AL,GG,Bopt,R), calculates the CIE DE94 and DEab color difference of
%                    samples R for AL and GG and Bopt, which are defined the same as those in UMGSignle.m
% u_xyz_ss.m: u_xyz_ss(xyz31,ss), calculates the mu-factor of spectral sensitivity set ss against CMF xyz31
% q_xyz_ss.m: q_xyz_ss(xyz31,ss), calculates the mu-factor of single spectral sensitivity ss against CMF xyz31
% JacobianLab.m: JLab=JacobianLab(x,y,z,Xn,Yn,Zn), calculate the Jacobian matrix for tristimulus values XYZ
%               XnYnZn are the corresponding tristimulus values of illuminant white, sometimes appeared as XwYwZw
% XYZ2Lab.m: XYZ2Lab(X,Y,Z,Xw,Yw,Zw), calculate the CIELAB attributes for vectors of X, Y, Z and illuminant XwYwZw
% CIE94Lab.m: CIE94lab(L1, a1, b1, L2, a2, b2,flag), calculate the DE94 for two sets of CIELAB coordinates Lab1 and Lab2
%            flag determines the selection of SL, SC and SH. Look into the details of the function
% vec.m: B=vec(A), if A is a mxn matrix, column vector B (mnx1) is obtained by stacking all columns of A one after another
%

clear all;

% ========== load CIE database, all spectra are related to the corresponding wavelength samplings ======

load colorDatabase.mat;

% ======= specify the working visible range, typical 400-700nm, 390-720nm, or 380-780nm by 5 or 10nm ===========

  wave=[380:5:780]';
% wave=[400:5:700]';
% wave=[390:5:720]';
```

```
nWave=length(wave);

% ================ all spectra will be interpolated with the working visible range !!!!! ==========
% ====== if you are going to introduce a new spectrum, make sure to do the interpolation at first ========

xyz31=interp1(waveXYZ1931,originalXYZ1931,wave);                    % CIE 1931 color matching functions
xlamda=xyz31(:,1); ylamda=xyz31(:,2); zlamda=xyz31(:,3);            % CIE 1931 color matching functions
M33=[3.2406 -1.5372 -0.4986; -0.9689 1.8758 0.0415; 0.0557 -0.2040 1.0570];     % matrix convert 1931cmf -> iso sRGB
sRGB31=xyz31*M33';                                                  % iso sRGB primaries
AAA=interp1(waveA,originalA,wave); D65=interp1(waveD65,originalD65,wave);       % CIE illuminant A and D65
LightAAA=diag(AAA); LightD65=diag(D65);                             % diagonal format of A and D65

% ====== loading measuredFilter.mat which contains a IR cutoff filter that is commonly used at MCSL ======

load measuredFilter;      msdIRcut=interp1(waveMeasured,measuredIRcut,wave)/100.00;          % wavelength range: 360nm-750nm
if nWave==81, msdIRcut(76:81,:)=[1/5; 1/10; 1/15; 1/20; 1/25; 1/50]*msdIRcut(75,:); end;  % extrapolation to wave

% ========== loading QuantixDatabase.mat which contains Schott glass filters and measured CCD spectra =======
% ================ Transmittance is external transmittance of 1mm thickness ================

load QuantixDatabase;  % load filterData20010301.mat;  % load filterDataTotal.mat; % these are former database ==========

CCD=interp1(waveCCD02,CCD02(:,1),wave);                 % CCD SS, including lens and IR cutoff influence
VGBG0=interp1(waveSchott,VGBG,wave);                    % external transmittance of bandpass filters, 14
BGKG0=interp1(waveSchott,BGKG,wave);                    % external transmittance of IR cutoff filters, 7
GGOGRG0=interp1(waveSchott,GGOGRG,wave);                % external transmittance of longpass cutoff filters, 19

RI=1.52; K1=(RI-1)^2/(RI+1)^2;                          % refractive index of glass, calculate K1, reflective factor
VGBG1=TransmittanceE2I(VGBG0,K1);                       % internal transmittance of bandpass filters
BGKG1=TransmittanceE2I(BGKG0,K1);                       % internal transmittance of IR cutoff filters
GGOGRG1=TransmittanceE2I(GGOGRG0,K1);                   % internal transmittance of longpass cutoff filters

% ================ graph of some spectra, 1931 CMF, CCD, bandpass, IR cutoff and longpass filters

figure('Units','centimeters','Position',[2 2 12 10]); set(gcf,'PaperPositionMode','auto');
plot(wave,xyz31);  xlabel('wavelength (nm)'); ylabel('CIE CMFs');
figure('Units','centimeters','Position',[2 2 12 10]); set(gcf,'PaperPositionMode','auto');
plot(wave,CCD);    xlabel('wavelength (nm)'); ylabel('Total CCD QE');
figure('Units','centimeters','Position',[2 2 12 10]); set(gcf,'PaperPositionMode','auto');
plot(wave,VGBG0);   xlabel('wavelength (nm)'); ylabel('VGBG: band-pass');
figure('Units','centimeters','Position',[2 2 12 10]); set(gcf,'PaperPositionMode','auto');
plot(wave,BGKG0);   xlabel('wavelength (nm)'); ylabel('BGKG: IR');
figure('Units','centimeters','Position',[2 2 12 10]); set(gcf,'PaperPositionMode','auto');
plot(wave,GGOGRG0); xlabel('wavelength (nm)'); ylabel('GGOGRG: long-pass');

% ================ the thickness of basic filters can select 1mm, 2mm and 3mm ================
% ================ The internal transmittance fulfills Beer's Law ==============

VGBG2=[VGBG1 VGBG1.^2 VGBG1.^3];       BGKG2=[BGKG1 BGKG1.^2 BGKG1.^3];       GGOGRG2=[GGOGRG1 GGOGRG1.^2 GGOGRG1.^3];
nBandpass=size(VGBG2,2);          nIR=size(BGKG2,2);              nLongpass=size(GGOGRG2,2);

% ================ Three filter sets: 42 bandpass, 21 IR cutoff and 57 longpass cutoff filters ===

filterSet1=VGBG2;               filterSet2=BGKG2;               filterSet3=GGOGRG2;

% ================ The external transmittance of these filters are calculated =========

VGBG3=TransmittanceI2E([VGBG1 VGBG1.^2 VGBG1.^3],K1);
BGKG3=TransmittanceI2E([BGKG1 BGKG1.^2 BGKG1.^3],K1);
```

```
GGOGRG3=TransmittanceI2E([GGOGRG1 GGOGRG1.^2 GGOGRG1.^3],K1);

% ================== combination of filters: bandpass x IR; bandpass x longpass; longpass x IR ======
% ================== internal transmittance of filterSet12, filterSer13 and filterSet23  =========
% ================== The numbers of combinations: 42 x 21; 42 x 57; 57 x 21 ===============

% Combination of Bandpass-Filter x IR-Cutoff-Filter
for i=1:nIR,
   filterSet12(:,(i-1)*nBandpass+1:i*nBandpass)=VGBG2.*(BGKG2(:,i)*ones(1,nBandpass));
end;

% Combination of Bandpass-Filter x Longpass-Filter
for i=1:nLongpass,
   filterSet13(:,(i-1)*nBandpass+1:i*nBandpass)=VGBG2.*(GGOGRG2(:,i)*ones(1,nBandpass));
end;

% Combination of longpass-Filter x IR-Cutoff-Filter
for i=1:nIR,
   filterSet23(:,(i-1)*nLongpass+1:i*nLongpass)=GGOGRG2.*(BGKG2(:,i)*ones(1,nLongpass));
end;

% A total filter set contains the pure bandpass, IR, longpass filters and their cross combinations ==========

filterSetInternal=[filterSet1 filterSet2 filterSet3 filterSet12 filterSet13 filterSet23];

% The internal transmittance of these filters are converted to obtain external transmittance ===========

filterSet0=TransmittanceI2E(filterSetInternal,K1);       nFilterSet=size(filterSet0,2);

% By multiplying sensitivity of CCD (plus lens and total IR cutoff filtet), total sensitivity functions are obtained
% each colomn of filterSet is a total spectral sensitivity function

filterSet=filterSet0.*(CCD*ones(1,nFilterSet));

% ========= For each total spectral sensitivity function, find its peak wavelength 'waveIndex' =============

filterSetMax=max(filterSet,[],1);                    [filterSetMax,maxIndex]=max(filterSet);
waveIndex=wave(maxIndex);                              dWave=wave(2)-wave(1);

% ========= Estimate 'ssWidth', the full-width at half peak of each spectral sensitivity function ===========

for i=1:nFilterSet, ssWidth(i,:)=sum(filterSet(:,i))*dWave/(filterSetMax(i)+10^(-8)); end; % estimate width

% ========= Pre Selection Procedure ============================================
% ========= It's unnecessary if the computer speed is fast enough ==================
% ========= But it's required to greatly reduce the computation scale, otherwise it takes years to search for an ====
% ========= optimal SS set with brute force from 'filterSet' ====================

% ========= The Pre-Selection generally limits the peak wavelength and width to reasonable range according to =======
% ========= previous research, refer to Chapter 6 of my PhD Thesis ====================
% ========= Other constraints are: sensitivity of secondary peak of SS is less than 20% of that of primary peak =====
% ========= The sensitivity of blue SS at infrared and of red SS at ultraviolet can also be limited to low enought ==

% ========= Find the index of those SS in 'filterSet' that are qualified as BLUE SS ========

j=0; % blueIndex=find(waveIndex>=420&waveIndex<=470&ssWidth<120);
for i=1:nFilterSet,
   secondMax=max(filterSet(round(4/5*nWave):nWave,i));
   firstMax=filterSetMax(i);
   if (secondMax<0.2*firstMax) & (waveIndex(i)>=420) & (waveIndex(i)<=470) & (ssWidth(i)<120) & (firstMax>0.2),
      j=j+1;        blueIndex(j,:)=i;
   end;
```

```
end;

% ========= Find the index of those SS in 'filterSet' that are qualified as GREEN SS ===========

j=0; % greenIndex=find(waveIndex>=510&waveIndex<=560&ssWidth<120);
for i=1:nFilterSet,
   secondMax=max(filterSet(round(3/4*nWave):nWave,i));
   thirdMax=max(filterSet(1:round(1/4*nWave),i));
   firstMax=filterSetMax(i);
   if (thirdMax<0.2*firstMax) &(secondMax<0.2*firstMax) & (waveIndex(i)>=520) & (waveIndex(i)<=560) & ...
         (ssWidth(i)<120) & (firstMax>0.2),
      j=j+1;       greenIndex(j,:)=i;
   end;
end;

% ========= Find the index of those SS in 'filterSet' that are qualified as RED SS =========

j=0; % redIndex=find(waveIndex>=570&waveIndex<=620&ssWidth<120);
for i=1:nFilterSet,
   secondMax=max(filterSet(round(5/6*nWave):nWave,i));
   firstMax=filterSetMax(i);
   if (secondMax<0.2*firstMax) & (waveIndex(i)>=570) & (waveIndex(i)<=620) & (ssWidth(i)<120) & (firstMax>0.2),
      j=j+1;       redIndex(j,:)=i;
   end;
end;

% ========= Construct the sets of SS for RED, GREEN and BLUE candidates respectively ==========

filterSetR=filterSet(:,redIndex);
filterSetG=filterSet(:,greenIndex);
filterSetB=filterSet(:,blueIndex);

% ========= Count the number of SS for RED, GREEN and BLUE candidates respectively ========

nFilterSetR=size(filterSetR,2);
nFilterSetG=size(filterSetG,2);
nFilterSetB=size(filterSetB,2);

% ========= Plot the spectra of SS for RED, GREEN and BLUE candidates respectively ======

 figure('Units','centimeters','Position',[2 2 20 16]); set(gcf,'PaperPositionMode','auto');
 subplot(2,2,1); plot(wave,filterSetR); axis([wave(1) wave(nWave) 0 max(max(filterSetR))]); title('RED');
 subplot(2,2,2); plot(wave,filterSetG); axis([wave(1) wave(nWave) 0 max(max(filterSetG))]); title('GREEN');
 subplot(2,2,3); plot(wave,filterSetB); axis([wave(1) wave(nWave) 0 max(max(filterSetB))]); title('BLUE');
 subplot(2,2,4); plot(wave,CCD);       axis([wave(1) wave(nWave) 0 max(max(CCD))]);       title('CCD QE');


% %%%%%%%%%%%%%%%%%% loading one set of standardobject color ensemble
%%%%%%%%%%%%%%%%%%%%%%%%%%%%%%%%%%%%%%%%%%%%%%%
% ============== Vrhel-Trussell's 354 reflectance samples are repeatedly used in my study =======
% ============== As alternative, the 24 Macbeth ColorChecker can be used instead ============
% ============== Make sure the same set is used if comparing the goodness of various SS sets =====

% This is Vrhel-Trussell dataset, interpolated to standard wavelength samplings
% Original visible wavelength of 354 Vrhel-Trussell samples: 390:2:730

load VrhelDatabase; R1=interp1(waveVrhel,[VrhelMunsell VrhelObject VrhelDupont],wave); R=R1'; nSample=size(R,1);
if nWave==81, R(:,72:81)=R(:,71)*ones(1,10); R(:,1:2)=R(:,3)*ones(1,2); end;       % extrapolation to [380:5:780]'

% This is macbeth color checker, if this is used, un-comment the following line, and comment the above lines on Vrhel....

% R1=interp1(waveMacbeth,originalMacbeth,waveNew); R=R1'; nSample=size(R,1);
```

```
% ========= Equi-Energy illuminant is used as standard taking-viewing illuminant pair to UMG evaluation =========
% ========= alternatively CIE D65 or D50 may be used instead of EE (equi-energy illuminant) ====================

EE=100*ones(nWave,1); diagEE=100*eye(nWave);          % Generate SPD of Equi-Energy illuminant

% AL is defined as the diagonal format of illuminant spectrum (L) multiplied by CIE 1931 color matching functions (xyz31) ===

AL=diagEE*xyz31;   %  AL=LightD65*xyz31;

% Kr: Correlation of reflectance samples

Kr=R'*R/nSample;

% Calculate Sr and E[JF'*JF], the definition of Sr is the same as Chapter 5 in my Thesis,
% JF is Jacobian Matrix from CIE XYZ to CIELAB, E{.} means statistical expectation.

[Sr,EJFtJF]=statisticsReflectance(AL,R);

% if no noise is considered, noise matrix Ke is a zero matrix, the dimension of Ke is the number of channels

Ke=zeros(3,3); % noise characteristics, I(3,3) or 0(3,3)

% Assuming evaluation of UMG quality factor generates 500 optimal candidates, which can be varied depennding on application

nUMG=500;

% The UMG values will be stored in vector umgMax

umgMax=zeros(nUMG,1);

% The index of these 500 sets of optimal SS combination (i,j,k) will be stored in umgIndex
% M3x3 may be used to store the 3x3 optimal conversion matrix from CIE XYZ to CIELAB

umgIndex=zeros(nUMG,3);
M3x3=cell(nUMG,1);

% Noise is assumed to be 45dB, to check the noise influence on filter selection, change the SNR from 15dB to 85dB

mdB=4.5;   % generally 1.5~8.5, that is 15dB to 85dB. Reasonable SNR should be around 35-55dB

clear i j k l ii;

% ========== Evaluating SS combinations in          filterSetB x filterSetG x filterSetR ============
% ========== Find the first 500 optimal combinations, recording their filter indexes in filterSetR(G or B) ====

for i=1:nFilterSetB,
   [i,floor(umgMax(1)*1000)]
   for j=1:nFilterSetG,
      for k=1:nFilterSetR,

         % Each i, j, k contributes a combination of SS

         ssRGB=[filterSetB(:,i) filterSetG(:,j) filterSetR(:,k)];

         % GG is defined as the diagonal format of taking illuminant multiplied by sensor spectral sensitivities
         % refer to Chapter 5 in my Thesis

         GG=diagEE*ssRGB;   % The taking illuminant has been assumed to be EE, the same as viewing illuminant

         % ===== Ke: diagonal noise is assumed, otherwise noise correlation between channels can be applied ======
```

```
        Ke=trace(GG'*Kr*GG)/10^mdB*eye(size(ssRGB,2))/size(ssRGB,2);          % diagonal noise; using matlab function eye
        % Ke=trace(GG'*Kr*GG)/10^mdB*ones(size(ssRGB,2))size(ssRGB,2);       % noise correlation between channels, 'ones'

        % Se: Noise characteristics, refer to Chapter 5 in my thesis

        Se=kron(Ke,EJFtJF);

        % calculate UMG for single pair of taking-viewing illuminants

        [umg,bopt]=UMGSingle(AL,GG,Sr,Se);

        % bopt is the vectorization of Bopt, the conversion matrix from XYZ to LAB, reconstruct of Bopt as follows

        % Bopt=zeros(size(AL,2),size(GG,2)); for ii=1:size(GG,2), Bopt(:,ii)=bopt((ii-1)*size(AL,2)+1:ii*size(AL,2)); end;

        % Normaling UMG as specified in Chapter 5

        UMG=1-sqrt(1-umg);

        % If the calculated UMG is larger than some of the UMG values in the 500 combinations,
        % Insert this combination into the position so that the UMG values are placed in order, larger --> smaller
        % Also the indexes of spectral sensitivity functions are recorded into 'umgIndex'

        for l=1:nUMG,
           if UMG>umgMax(l),
              umgMax(l+1:nUMG)=umgMax(l:nUMG-1);
              umgMax(l)=UMG;
              umgIndex(l+1:nUMG,:)=umgIndex(l:nUMG-1,:);
              umgIndex(l,:)=[i,j,k];
              % M3x3(l+1:nUMG,:)=M3x3(l:nUMG,-1:); M3x3(l,:)={Bopt};
              break;
           end;
        end;
     end;
  end;
  save c:\download\BernsCameraUMG08New2;   % save the intermediate computation results for intermediate analysis ======
  % save c:\download\BernsCameraUMG08;   % save the intermediate computation results for intermediate analysis ======
end;

% ============= All variables and optimization results are saved into one *.MAT file ======
% ============= Very important to be analyzed further ========================

save c:\download\BernsCameraUMG08New2;          % for diagonal noise characteristics
% save c:\download\BernsCameraUMG08;          % for full noise characteristics, assuming noise correlation between channels

% ========================================================================
%                    The Part One of Optimization with UMG ends here !!!
% ====================================


break;

% ==================================== OptimUMG1part2.m ============

% load c:\download\BernsCameraUMG08New2;
```

11.10.2 Part Two – Analysis and Refinement

```
%
% Hierarchical optimization of spectral sensitivities for digital color imaging devices
% Three or more imaging channels are obtained from the combination of given basic filter components
```

```
%
% The optimization is divided into two procedures:
%         OptimUMG1part1: Pre-Selection, UMG Optimization for single illuminant pair (EE-EE), Saving into a file
%         OptimUMG1part2: Loading the file saved by OptimUMG1part1, UMG evaluation for other illuminant pairs,
%                   mu-factor calculation, RMS noise calculation, and Secondary Optimization
%
% This file is OptimUMG1part2.m, make sure that OptimUMG1part1.m is run at first
%

% ========== load the computation results from OptimUMG1part1.m ====================
% ========== make sure the filename and filepath is the same as that used in OptimUMG1part1 ===

% load c:\download\BernsCameraUMG08New;                  % diagonal noise characterisrics
  load c:\download\BernsCameraUMG08New1;                % diagonal noise characterisrics
% load c:\download\BernsCameraUMG08;                     % noise characteristics: noise correlation between channels

% ========== plot the filters, spectral sensitivities of the 500 combinations obtained in OptimUMG1part1.m ==========
% ========== generally plot (the first) several each time, don't plot 500 combinatios, due to computer limitation ====

clear i j a b c d x y z;
for i=1:10,  % if you want to plot others, you may change this line such as     for i=50:60,       etc.
   figure('Units','centimeters','Position',[2 2 18 16]); set(gcf,'PaperPositionMode','auto');
%   a=[filterSetR(:,umgIndex(1+nUMG-i,3)) filterSetG(:,umgIndex(1+nUMG-i,2)) filterSetB(:,umgIndex(1+nUMG-i,1))];
   a=[filterSetR(:,umgIndex(i,3)) filterSetG(:,umgIndex(i,2)) filterSetB(:,umgIndex(i,1))];
   x=pinv(a)*xyz31;            % x is a 3x3 matrix transforms spectral sensitivity set ss (a) to xyz31
   subplot(2,2,1); plot(wave,xyz31,'b--',wave,a*x,'r-','LineWidth',2);
   title(strcat('Approximating CIE CMF: ---','UMG=',num2str(umgMax(i))));
   axis([wave(1) wave(nWave) -0.5 2]);
   subplot(2,2,2); plot(wave,a,'r','LineWidth',2);
   axis([wave(1) wave(nWave) min(min(a)) max(max(a))]); title('Total Spectral Sensitivity: CCD+Filter');
   b=[a(:,1)./CCD a(:,2)./CCD a(:,3)./CCD];                    % b: filter transmittance only, no CCD QE
   c=[a(:,1)/max(a(:,1)),a(:,2)/max(a(:,2)),a(:,3)/max(a(:,3))];   % c: normalizing ss (a) such that peak of each is 1.0
   title(strcat('UMG=',num2str(umgMax(i))));
   subplot(2,2,3); plot(wave,b(:,1),'r',wave,b(:,2),'g',wave,b(:,3),'b');
   axis([wave(1) wave(nWave) 0 1]); title('Filter only, no CCD QE');
   y=pinv(b)*xyz31;     z=pinv(c)*xyz31;
   subplot(2,2,4);      plot(wave,c(:,1),'r',wave,c(:,2),'g',wave,c(:,3),'b');
   axis([wave(1) wave(nWave) min(min(c)) max(max(c))]); title('Normalized Total Spectral Sensitivity');
end;

%%%%%%%%%%%%%%%%%%%%% calculate UMG  values %%%%%%%%%%%%%%%%

% ==================== UMGe4: taking illuminant (EE), viewing illuminant (EE), noise (45dB): mdB=4.5 ========

AL=xyz31; Kr=R'*R/nSample; [Sr,EJFtJF]=statisticsReflectance(AL,R);
mdB=4.5; clear i j a d;
for j=1:nUMG,
   d=[filterSetR(:,umgIndex(j,3)) filterSetG(:,umgIndex(j,2)) filterSetB(:,umgIndex(j,1))];
   GG=d;

   miu0(j,:)=u_xyz_ss(xyz31,d);

   Ke=trace(GG'*Kr*GG)/10^mdB*eye(size(d,2))/size(d,2);          %     diagonal noise characteristics, matlab function 'eye'
   % Ke=trace(GG'*Kr*GG)/10^mdB*ones(size(d,2))/size(d,2);       % non-diagonal noise characteristics, matlab function 'ones'
   Se=kron(Ke,EJFtJF);
   [umg,bopt]=UMGSingle(AL,GG,Sr,Se);
   UMGe4(j,:)=1-sqrt(1-umg);
end;

% ========== UMGe3: taking illuminant (EE), viewing illuminant (EE), noise (35dB): mdB=3.5 ========

AL=xyz31; Kr=R'*R/nSample; [Sr,EJFtJF]=statisticsReflectance(AL,R);
```

```
mdB=3.5; clear i j a d;
for j=1:nUMG,
   d=[filterSetR(:,umgIndex(j,3)) filterSetG(:,umgIndex(j,2)) filterSetB(:,umgIndex(j,1))];
   GG=d;

   Ke=trace(GG'*Kr*GG)/10^mdB*eye(size(d,2))/size(d,2);          %     diagonal noise characteristics, matlab function 'eye'
   % Ke=trace(GG'*Kr*GG)/10^mdB*ones(size(d,2))/size(d,2);      % non-diagonal noise characteristics, matlab function 'ones'
   Se=kron(Ke,EJFtJF);
   [umg,bopt]=UMGSingle(AL,GG,Sr,Se);
   UMGe3(j,:)=1-sqrt(1-umg);
end;

% ======== UMGe2: taking illuminant (EE), viewing illuminant (EE), noise (25dB): mdB=2.5 ========

AL=xyz31; Kr=R'*R/nSample; [Sr,EJFtJF]=statisticsReflectance(AL,R);
mdB=2.5; clear i j a d;
for j=1:nUMG,
   d=[filterSetR(:,umgIndex(j,3)) filterSetG(:,umgIndex(j,2)) filterSetB(:,umgIndex(j,1))];
   GG=d;

   Ke=trace(GG'*Kr*GG)/10^mdB*eye(size(d,2))/size(d,2);          %     diagonal noise characteristics, matlab function 'eye'
   % Ke=trace(GG'*Kr*GG)/10^mdB*ones(size(d,2))/size(d,2);      % non-diagonal noise characteristics, matlab function 'ones'
   Se=kron(Ke,EJFtJF);
   [umg,bopt]=UMGSingle(AL,GG,Sr,Se);
   UMGe2(j,:)=1-sqrt(1-umg);
end;

% ========== UMGe1: taking illuminant (EE), viewing illuminant (EE), noise (15dB): mdB=1.5 ========

AL=xyz31; Kr=R'*R/nSample; [Sr,EJFtJF]=statisticsReflectance(AL,R);
mdB=1.5; clear i j a d;
for j=1:nUMG,
   d=[filterSetR(:,umgIndex(j,3)) filterSetG(:,umgIndex(j,2)) filterSetB(:,umgIndex(j,1))];
   GG=d;

   Ke=trace(GG'*Kr*GG)/10^mdB*eye(size(d,2))/size(d,2);          %     diagonal noise characteristics, matlab function 'eye'
   % Ke=trace(GG'*Kr*GG)/10^mdB*ones(size(d,2))/size(d,2);      % non-diagonal noise characteristics, matlab function 'ones'
   Se=kron(Ke,EJFtJF);
   [umg,bopt]=UMGSingle(AL,GG,Sr,Se);
   UMGe1(j,:)=1-sqrt(1-umg);
end;

% ====== UMGe5: taking illuminant (EE), viewing illuminant (EE), noise (55dB): mdB=5.5 ========

AL=xyz31; Kr=R'*R/nSample; [Sr,EJFtJF]=statisticsReflectance(AL,R);
mdB=5.5; clear i j a d;
for j=1:nUMG,
   d=[filterSetR(:,umgIndex(j,3)) filterSetG(:,umgIndex(j,2)) filterSetB(:,umgIndex(j,1))];
   GG=d;

   Ke=trace(GG'*Kr*GG)/10^mdB*eye(size(d,2))/size(d,2);          %     diagonal noise characteristics, matlab function 'eye'
   % Ke=trace(GG'*Kr*GG)/10^mdB*ones(size(d,2))/size(d,2);      % non-diagonal noise characteristics, matlab function 'ones'
   Se=kron(Ke,EJFtJF);
   [umg,bopt]=UMGSingle(AL,GG,Sr,Se);
   UMGe5(j,:)=1-sqrt(1-umg);
end;

% ======== UMGe6: taking illuminant (EE), viewing illuminant (EE), noise (65dB): mdB=6.5 ========

AL=xyz31; Kr=R'*R/nSample; [Sr,EJFtJF]=statisticsReflectance(AL,R);
mdB=6.5; clear i j a d;
for j=1:nUMG,
```

```
   d=[filterSetR(:,umgIndex(j,3)) filterSetG(:,umgIndex(j,2)) filterSetB(:,umgIndex(j,1))];
   GG=d;

   Ke=trace(GG'*Kr*GG)/10^mdB*eye(size(d,2))/size(d,2);          %     diagonal noise characteristics, matlab function 'eye'
   % Ke=trace(GG'*Kr*GG)/10^mdB*ones(size(d,2))/size(d,2);       % non-diagonal noise characteristics, matlab function 'ones'
   Se=kron(Ke,EJFtJF);
   [umg,bopt]=UMGSingle(AL,GG,Sr,Se);
   UMGe6(j,:)=1-sqrt(1-umg);
end;

% ========== UMGe7: taking illuminant (EE), viewing illuminant (EE), noise (75dB): mdB=7.5 ========

AL=xyz31; Kr=R'*R/nSample; [Sr,EJFtJF]=statisticsReflectance(AL,R);
mdB=7.5; clear i j a d;
for j=1:nUMG,
   d=[filterSetR(:,umgIndex(j,3)) filterSetG(:,umgIndex(j,2)) filterSetB(:,umgIndex(j,1))];
   GG=d;

   Ke=trace(GG'*Kr*GG)/10^mdB*eye(size(d,2))/size(d,2);          %     diagonal noise characteristics, matlab function 'eye'
   % Ke=trace(GG'*Kr*GG)/10^mdB*ones(size(d,2))/size(d,2);       % non-diagonal noise characteristics, matlab function 'ones'
   Se=kron(Ke,EJFtJF);
   [umg,bopt]=UMGSingle(AL,GG,Sr,Se);
   UMGe7(j,:)=1-sqrt(1-umg);
end;

% break; The above section calculates UMG values for 500 optimal combinations under various noise level

% ============= RMS noise propagation from recording noise in device/RGB space to CIE XYZ then to CIELAB ===

AL=LightD65*xyz31;                        % product of diagonal format of illuminant and CIE color matching functions
Kr=R'*R/nSample;                          % correlation matrix of reflectance samples
[Sr,EJFtJF]=statisticsReflectance(AL,R);      % statistical information of spectral reflectance samples

mdB=4.5;                                  % noise level: SNR
clear i j a d;

% ===== calculate the reference CIE XYZ tristimulus values for reflectance samples R (vrhel-trussell or MCC) ==
% ============= CIE D65, CIE xyz31 ================================

XYZ0=D65'*xyz31; Yn=100; temp=Yn/XYZ0(2); XYZn=temp*XYZ0; % Normalize raw XYZ so that Yn=100
XYZraw=[LightD65*xyz31]'*R'; XYZraw=temp*XYZraw;         % for all samples XYZ values are normalized proportionally
M2XYZ=temp*eye(3);                                % M2XYZ is the 3x3 normalization matrix

% ============= calculate the RMS noise properties for all 500 SS combinations =========
for j=1:nUMG,
   d=[filterSetR(:,umgIndex(j,3)) filterSetG(:,umgIndex(j,2)) filterSetB(:,umgIndex(j,1))];    % spectral sensitivity set
   GG=LightD65*d;                                                    % GG:
   RGBraw=GG'*R';                                                    % RGB raw singal, un-normalized

   Ke=zeros(size(d,2),size(d,2));                                    % if noise is assumed to be zero
   Se=kron(Ke,EJFtJF);                                               % calculate Se, see chapter 5 in my thesis
   [umg,bopt]=UMGSingle(AL,GG,Sr,Se);                                % calculate umg and bopt
   Bopt=zeros(size(AL,2),size(GG,2)); for i=1:size(GG,2), Bopt(:,i)=bopt((i-1)*size(AL,2)+1:i*size(AL,2)); end; % from bopt
(vector) --> Bopt (matrix)
   UMG0(j,:)=1-sqrt(1-umg);     miu0(j,:)=u_xyz_ss(xyz31,d);         % calculate normalized UMG (from umg) and mu-factor

   % ============== since SS is known, its ability to predict XYZ is described by color difference of samples
   dEUMG1=cameraColorError(AL,GG,Bopt,R);                            % calculate color differences for reflectance samples R
   MeanDE1(j,:)=mean(dEUMG1);                                        % mean color difference for samples in R
   MaxDE1(j,:)=max(dEUMG1);                                          % max  color difference for samples in R
```

```
   M3x3=M2XYZ*Bopt;      % since Bopt is the 3x3 matrix from raw RGB to raw XYZ, M2XYZ is diagonal 3x3 matrix from raw XYZ
                         % to normalized XYZ (Yw=100), M3x3 is the concatenated matrix

   Ke=trace(GG'*Kr*GG)/10^mdB*eye(size(d,2))/size(d,2);       % assuming a diagonal noise in raw RGB space, specified by SNR mdB
   % Ke=[4 0 0; 0 4 0; 0 0 4];                                % assuming a static diagonal noise, may be too small for some raw signal
                                                              % or maybe too large for some other raw RGB signal (scale problem)
   Se=kron(Ke,EJFtJF);
   [umg,bopt]=UMGSingle(AL,GG,Sr,Se);
   Bopt=zeros(size(AL,2),size(GG,2)); for ii=1:size(GG,2), Bopt(:,ii)=bopt((ii-1)*size(AL,2)+1:ii*size(AL,2)); end;
   UMG1(j,:)=1-sqrt(1-umg);                                   % calculate UMG and conversion matrix Bopt under noise

   dEUMG2=cameraColorError(AL,GG,Bopt,R);                     % calculate color difference performance
   MeanDE2(j,:)=mean(dEUMG2);
   MaxDE2(j,:)=max(dEUMG2);

   sigmaRGB=Ke;                                               % RMS noise in raw RGB space is the same as Ke
   sigmaXYZ=M3x3*sigmaRGB*M3x3';                              % RMS noise in raw RGB space is propagated to CIE XYZ space, chapter 4
   [dLabBurns,dLab]=sigmaLab(sigmaXYZ);                       % RMS noise is calculated from the noise variance-covariance matrix
   rmsNoiseXYZ(j,:)=[dLabBurns,dLab];                         % Both Burns-Berns and diagonal RMS noise definitions are calculated

   % calculate noise propagation from CIE XYZ to CIELAB, the Jacobian matrix from XYZ to LAB is sample dependent
   % calculate the RMS noise in CIELAB for each sample, and take the average of all samples as the final RMS noise in CIELAB

   rmsTemp=[0 0];
   for ii=1:nSample,
      t1=XYZraw(1,ii); t2=XYZraw(2,ii); t3=XYZraw(3,ii);
      JLab=JacobianLab(t1,t2,t3,XYZn(:,1),XYZn(:,2),XYZn(:,3));
      [dLabBurns,dLab]=sigmaLab(JLab*sigmaXYZ*JLab');
      rmsTemp=rmsTemp+[dLabBurns,dLab];
   end;
   rmsNoise(j,:)=rmsTemp/nSample;                             % This is the averaged RMS noise in CIELAB color space for all sampels
end;

% ========= plot the relationship between UMG without noise consideration and mean color difference ===========

figure('Units','centimeters','Position',[2 2 12 10]); set(gcf,'PaperPositionMode','auto');
plot(UMG0,MeanDE1(:,1),'r.');
xlabel('UMG without noise consideration');
ylabel('average color difference: \DeltaE');
xdata=UMG0; ydata=MeanDE1(:,1); kk=convhull(xdata,ydata); hold on; plot(xdata(kk),ydata(kk),'b-');

% ====== plot the relationship between UMG with noise consideration and mean color difference ===========

figure('Units','centimeters','Position',[2 2 12 10]); set(gcf,'PaperPositionMode','auto');
plot(UMG1,MeanDE2(:,1),'r.');
xlabel('UMG with noise consideration');
ylabel('average color difference: \DeltaE');
xdata=UMG1; ydata=MeanDE2(:,1); kk=convhull(xdata,ydata); hold on; plot(xdata(kk),ydata(kk),'b-');

% ======= plot the relationship between UMG without noise consideration and RMS noise in CIELAB ===========

figure('Units','centimeters','Position',[2 2 12 10]); set(gcf,'PaperPositionMode','auto');
plot(UMG0,rmsNoise(:,1),'r.');
xlabel('UMG without noise consideration');
ylabel('RMS noise in CIE L*a*b*');
title('Burns-Berns RMS Noise Formula')
xdata=UMG0; ydata=rmsNoise(:,1); kk=convhull(xdata,ydata); hold on; plot(xdata(kk),ydata(kk),'b-');
```

```
% ===== plot the relationship between UMG without noise consideration and RMS noise in CIELAB ===========

figure('Units','centimeters','Position',[2 2 12 10]); set(gcf,'PaperPositionMode','auto');
plot(UMG0,rmsNoise(:,2),'r.');
xlabel('UMG without noise consideration');
ylabel('RMS noise in CIE L*a*b*');
title('Diagonal RMS Noise Formula');
xdata=UMG0; ydata=rmsNoise(:,2); kk=convhull(xdata,ydata); hold on; plot(xdata(kk),ydata(kk),'b-');

% ============== plot the relationship between UMG with noise consideration and RMS noise in CIELAB ===========

figure('Units','centimeters','Position',[2 2 12 10]); set(gcf,'PaperPositionMode','auto');
plot(UMG1,rmsNoise(:,1),'r.');
xlabel('UMG with noise consideration');
ylabel('RMS noise in CIE L*a*b*');
title('Burns-Berns RMS Noise Formula')
xdata=UMG1; ydata=rmsNoise(:,1); kk=convhull(xdata,ydata); hold on; plot(xdata(kk),ydata(kk),'b-');

% ======= plot the relationship between UMG with noise consideration and RMS noise in CIELAB ===========

figure('Units','centimeters','Position',[2 2 12 10]); set(gcf,'PaperPositionMode','auto');
plot(UMG1,rmsNoise(:,2),'r.');
xlabel('UMG with noise consideration');
ylabel('RMS noise in CIE L*a*b*');
title('Diagonal RMS Noise Formula');
xdata=UMG1; ydata=rmsNoise(:,2); kk=convhull(xdata,ydata); hold on; plot(xdata(kk),ydata(kk),'b-');

% ======= plot the relationship between Burns-Berns Noise and diagonal RMS noise ===========

figure('Units','centimeters','Position',[2 2 12 10]); set(gcf,'PaperPositionMode','auto');
plot(rmsNoise(:,1),rmsNoise(:,2),'r.');
xlabel('Burns-Berns RMS Noise Formula');
ylabel('Diagonal RMS Noise Formula');

% ===== plot the relationship between UMG without noise consideration and RMS noise in CIE XYZ ===========

figure('Units','centimeters','Position',[2 2 12 10]); set(gcf,'PaperPositionMode','auto');
plot(UMG0,rmsNoiseXYZ(:,1),'r.');
xlabel('UMG without noise consideration');
ylabel('RMS noise in CIE XYZ');
title('Burns-Berns RMS Noise Formula')
xdata=UMG0; ydata=rmsNoiseXYZ(:,1); kk=convhull(xdata,ydata); hold on; plot(xdata(kk),ydata(kk),'b-');

% ====== plot the relationship between UMG without noise consideration and RMS noise in CIE XYZ ===========

figure('Units','centimeters','Position',[2 2 12 10]); set(gcf,'PaperPositionMode','auto');
plot(UMG0,rmsNoiseXYZ(:,2),'r.');
xlabel('UMG without noise consideration');
ylabel('RMS noise in CIE XYZ');
title('Diagonal RMS Noise Formula');
xdata=UMG0; ydata=rmsNoiseXYZ(:,2); kk=convhull(xdata,ydata); hold on; plot(xdata(kk),ydata(kk),'b-');

% ============== plot the relationship between mu-factor and RMS noise in CIELAB ===========

figure('Units','centimeters','Position',[2 2 12 10]); set(gcf,'PaperPositionMode','auto');
plot(miu0,rmsNoise(:,1),'r.');
xlabel('\mu-factor');
ylabel('RMS noise in CIE L*a*b*');
title('Burns-Berns RMS Noise Formula')
xdata=miu0; ydata=rmsNoise(:,1); kk=convhull(xdata,ydata); hold on; plot(xdata(kk),ydata(kk),'b-');

% ============== plot the relationship between mu-factor and RMS noise in CIELAB ===========
```

```
figure('Units','centimeters','Position',[2 2 12 10]); set(gcf,'PaperPositionMode','auto');
plot(miu0,rmsNoise(:,2),'r.');
xlabel('\mu-factor');
ylabel('RMS noise in CIE L*a*b*');
title('Diagonal RMS Noise Formula');
xdata=miu0; ydata=rmsNoise(:,2); kk=convhull(xdata,ydata); hold on; plot(xdata(kk),ydata(kk),'b-');

% ============== plot the relationship between UMG without noise consideration and mu-factor ===========

figure('Units','centimeters','Position',[2 2 12 10]); set(gcf,'PaperPositionMode','auto');
plot(UMG0,miu0,'r.');
xlabel('UMG without noise consideration');
ylabel('\mu-factor');
xdata=UMG0; ydata=miu0; kk=convhull(xdata,ydata); hold on; plot(xdata(kk),ydata(kk),'b-');


%%%%%%%%%%%%%%%% calculate UMG  values %%%%%%%%%%%%%%%%%%%%%%%%


miu0=zeros(nUMG,1);          % mu-factors of the 500 optimum candidates
UMG0=zeros(nUMG,1);          % UMG without noise consideration, illuminant pair: D65 - D65
UMG1=zeros(nUMG,1);          % UMG with    noise consideration, illuminant pair: D65 - D65 SNR=45dB
UMG2=zeros(nUMG,1);          % UMG with    noise consideration, illuminant pair: A   - A   SNR=45dB
UMG3=zeros(nUMG,1);          % UMG with    noise consideration, illuminant pair: ScanLite - Scanlite SNR=45dB

% ============================ calculate miu0, UMG0, UMG1 ======================

AL=LightD65*xyz31; Kr=R'*R/nSample; [Sr,EJFtJF]=statisticsReflectance(AL,R);
mdB=4.5; clear i j a d;
for j=1:nUMG,
   d=[filterSetR(:,umgIndex(j,3)) filterSetG(:,umgIndex(j,2)) filterSetB(:,umgIndex(j,1))];
   GG=LightD65*d;

   Ke=zeros(size(d,2),size(d,2));
   Se=kron(Ke,EJFtJF);
   [umg,bopt]=UMGSingle(AL,GG,Sr,Se);
   % Bopt=zeros(size(AL,2),size(GG,2)); for i=1:size(GG,2), Bopt(:,i)=bopt((i-1)*size(AL,2)+1:i*size(AL,2)); end;

   UMG0(j,:)=1-sqrt(1-umg);
   miu0(j,:)=u_xyz_ss(xyz31,d);

   Ke=trace(GG'*Kr*GG)/10^mdB*eye(size(d,2))/size(d,2);          %     diagonal noise characteristics, matlab function 'eye'
   % Ke=trace(GG'*Kr*GG)/10^mdB*ones(size(d,2))/size(d,2);      % non-diagonal noise characteristics, matlab function 'ones'
   Se=kron(Ke,EJFtJF);
   [umg,bopt]=UMGSingle(AL,GG,Sr,Se);
   % Bopt=zeros(size(AL,2),size(GG,2)); for ii=1:size(GG,2), Bopt(:,ii)=bopt((ii-1)*size(AL,2)+1:ii*size(AL,2)); end;
   UMG1(j,:)=1-sqrt(1-umg);
end;

% ============================== calculate UMG2 ========================

AL=LightAAA*xyz31; Kr=R'*R/nSample; [Sr,EJFtJF]=statisticsReflectance(AL,R);
mdB=4.5; clear i j a d;
for j=1:nUMG,
   d=[filterSetR(:,umgIndex(j,3)) filterSetG(:,umgIndex(j,2)) filterSetB(:,umgIndex(j,1))];
   GG=LightAAA*d;

   Ke=trace(GG'*Kr*GG)/10^mdB*eye(size(d,2))/size(d,2);          %     diagonal noise characteristics, matlab function 'eye'
   % Ke=trace(GG'*Kr*GG)/10^mdB*ones(size(d,2))/size(d,2);      % non-diagonal noise characteristics, matlab function 'ones'
   Se=kron(Ke,EJFtJF);
   [umg,bopt]=UMGSingle(AL,GG,Sr,Se);
```

```
   % Bopt=zeros(size(AL,2),size(GG,2)); for ii=1:size(GG,2), Bopt(:,ii)=bopt((ii-1)*size(AL,2)+1:ii*size(AL,2)); end;
   UMG2(j,:)=1-sqrt(1-umg);
end;


% ========= Scanlite is the illumination that is used with Quantix camera at MCSL ==========

% load mcc4Quan01; % QuantixDatabase.mat already contains the spectra of Scanlite; resampling these spectra ====

EikoFlood=interp1(EikoFloodRawSpectra(:,1),EikoFloodRawSpectra(:,4),wave);
Scanlite=interp1(ScanliteRawSpectra(:,1),ScanliteRawSpectra(:,4),wave);
if nWave==81,    EikoFlood(76:81,:)=EikoFlood(75)*ones(6,1); Scanlite(76:81,:)=Scanlite(75)*ones(6,1);   end;
diagScanlite=diag(Scanlite);

% ================================ calculate UMG3 ============================

AL=diagScanlite*xyz31; Kr=R'*R/nSample; [Sr,EJFtJF]=statisticsReflectance(AL,R);
mdB=4.5; clear i j a d;
for j=1:nUMG,
   d=[filterSetR(:,umgIndex(j,3)) filterSetG(:,umgIndex(j,2)) filterSetB(:,umgIndex(j,1))];
   GG=diagScanlite*d;

   Ke=trace(GG'*Kr*GG)/10^mdB*eye(size(d,2))/size(d,2);          %     diagonal noise characteristics, matlab function 'eye'
   % Ke=trace(GG'*Kr*GG)/10^mdB*ones(size(d,2))/size(d,2);       % non-diagonal noise characteristics, matlab function 'ones'
   Se=kron(Ke,EJFtJF);
   [umg,bopt]=UMGSingle(AL,GG,Sr,Se);
   % Bopt=zeros(size(AL,2),size(GG,2)); for ii=1:size(GG,2), Bopt(:,ii)=bopt((ii-1)*size(AL,2)+1:ii*size(AL,2)); end;
   UMG3(j,:)=1-sqrt(1-umg);
end;

% ==================== plot the relationship between ======================
%
%           UMG(EE,EE) ~ UMG(D65,D65) ~ UMG(A,A) ~ UMG(Scanlite, Scanlite) ~ mu-factor
%
% ========================================================================

figure('Units','centimeters','Position',[2 2 18 16]); set(gcf,'PaperPositionMode','auto');
subplot(2,2,1); k1 = convhull(umgMax,UMG1); plot(umgMax,UMG1,'r.',umgMax(k1),UMG1(k1),'b');
xlabel('UMG(default illuminant)'); ylabel('UMG(D65)'); axis([min(umgMax) max(umgMax) min(UMG1) max(UMG1)]);
subplot(2,2,2); k2 = convhull(umgMax,UMG2); plot(umgMax,UMG2,'r.',umgMax(k2),UMG2(k2),'b');
xlabel('UMG(default illuminant)'); ylabel('UMG(A)'); axis([min(umgMax) max(umgMax) min(UMG2) max(UMG2)]);
subplot(2,2,3); k3 = convhull(umgMax,UMG3); plot(umgMax,UMG3,'r.',umgMax(k3),UMG3(k3),'b');
xlabel('UMG(default illuminant)'); ylabel('UMG(Scanlite)'); axis([min(umgMax) max(umgMax) min(UMG3) max(UMG3)]);
subplot(2,2,4); k4 = convhull(umgMax,miu0); plot(umgMax,miu0,'r.',umgMax(k4),miu0(k4),'b');
xlabel('UMG(default illuminant)'); ylabel('\mu-factor'); axis([min(umgMax) max(umgMax) min(miu0) max(miu0)]);

% ========= plot the UMG(EE,EE) and mu-factors of the 500 combinations ========================

figure('Units','centimeters','Position',[2 2 12 10]);
set(gcf,'PaperPositionMode','auto');
plot([1:nUMG]',miu0,'-r.'); hold on;
plot([1:nUMG]',umgMax,'-b.');
legend('\mu-factor','UMG: 45dB');
title(strcat('\mu-factor of Optimal Sets Obtained With UMG---','SNR=',num2str(10*mdB),'dB'));
xlabel('Optimal Sets Ranked with UMG');
ylabel('Quality Factors: \mu-factor and UMG');
grid on; axis([0 nUMG min([miu0; umgMax])-0.01 max([miu0; umgMax])+0.01]);

% ============ choose one of the following weight-averaged metric as comprehensive quality factor for =========
%                  secondary optimization among 500 sets
% currently mu-factor may be used as the secondary metric, but using others is easy as eating a cake
% The only problem is ----------- how to define the weights ----------------
```

```
% ==========================================================================

% CQFx=1/5*(miu0+UMG1+UMG2+UMG3+umgMax);
% CQFx=1/4*(umgMax+UMG1+UMG2+UMG3);
% CQFx=1/8*(UMG1+UMG2+UMG3+umgMax)+0.5*miu0;
% CQFx=0.5*UMG3+0.5*miu0;
% CQFx=umgMax;
% CQFx=miu0+1/rmsNoise(:,1);
  CQFx=miu0;

% ================ re rank the order of the 500 sets according to the comprehensive quality factor =======
% ================ MATLAB function 'sort' put the best choice in the last place ===

[tempMu,tempIndex]=sort(miu0); miuIndex=umgIndex(tempIndex,:);
[tempCQFx,tempIndex]=sort(CQFx); CQFxIndex=umgIndex(tempIndex,:);

% %%%%%%%%%%%%%%%%%%%%%%%%%%%% Find the components of each filter
% %%%%%%%%%% the index to filterSet %%%%%%%%%%
%
% The component filter information is saved as [a b c d e]
% 'a' - the a-th filter in filterSet 1-6: 1: filterSet1,  2: filterSet2,  3: filterSet3,
%                                  4: filterSet12, 5: filterSet13, 6: filterSet23
% 'b' - the b-th filter in filterSet which is specified by 'a'
% 'c' - the c-th bandpass filter, 0 if no
% 'd' - the e-th IR filter,       0 if no
% 'e' - the d-th longpass filter, 0 if no

% blueIndexOpt=blueIndex(umgIndex(:,1)); greenIndexOpt=greenIndex(umgIndex(:,2)); redIndexOpt=redIndex(umgIndex(:,3));
%                       blueIndexUMG=blueIndex(CQFxIndex(:,1));                       greenIndexUMG=greenIndex(CQFxIndex(:,2));
redIndexUMG=redIndex(CQFxIndex(:,3));

nSet1=size(filterSet1,2);
nSet2=nSet1+size(filterSet2,2);
nSet3=nSet2+size(filterSet3,2);
nSet4=nSet3+size(filterSet12,2);
nSet5=nSet4+size(filterSet13,2);
nSet6=nSet5+size(filterSet23,2);

  save c:\download\temp;                % save the intermediate results into a file so that next time
% load c:\download\temp;                  % load the intermeduate results and do following analysis

% ____________________________________________________________________________
%
%              The last set is the    O P T I M A L  !
% ____________________________________________________________________________
%
% finalIndex_CQFx: 'cell' data structure. The filter components used in each channel as indexed as [a,b,c,d,e]
% i.e. finalIndex_CQFx{1,2}=[5        1121          29          0          27]
%         here, a=5, means the filter components are in filterSet5, b=1121, the 1121st filter in filterSet5
%               c=29, means the 29th bandpass filter, d=0 means no IR cutoff filter, e=27, the 27th longpass filters
% lastIndex_CQFx : The filter components used in each channel by specifying the # of position in bandpass, IR or longpass
% i.e. lastIndex_CQFx{1,2}='bandpass No.1-3mm-Longpass No.8-2mm-', further specify the filter components in
%                 finalIndex_Cqfx{1,2}
% maxThickness   : The maximum total thickness of three channels
%

blueIndexCQFx=blueIndex(CQFxIndex(:,1));                                    greenIndexCQFx=greenIndex(CQFxIndex(:,2));
redIndexCQFx=redIndex(CQFxIndex(:,3));
rgbIndex=[blueIndexCQFx greenIndexCQFx redIndexCQFx];

for i=1:nUMG,
   for j=1:3,
```

```
if rgbIndex(i,j)<nSet1,
   finalIndex(i,j)={[1 rgbIndex(i,j)]};
   temp=rgbIndex(i,j);
   if temp<=nBandpass/3,
      lastIndex(i,j)={strcat('bandpass No.',num2str(temp),'-1mm-')};
      thickness(i,j)=1;
   elseif temp<=2*nBandpass/3,
      lastIndex(i,j)={strcat('bandpass No.',num2str(temp-nBandpass/3),'-2mm-')};
      thickness(i,j)=2;
   else
      lastIndex(i,j)={strcat('bandpass No.',num2str(temp-2*nBandpass/3),'-3mm-')};
      thickness(i,j)=3;
   end;
   clear temp;
elseif rgbIndex(i,j)<nSet2,
   finalIndex(i,j)={[2 rgbIndex(i,j)-nSet1]};
   temp=rgbIndex(i,j)-nSet1;
   if temp<=nIR/3,
      lastIndex(i,j)={strcat('IR cutoff No.',num2str(temp),'-1mm-')};
      thickness(i,j)=1;
   elseif temp<=2*nBandpass/3,
      lastIndex(i,j)={strcat('IR cutoff No.',num2str(temp-nIR/3),'-2mm-')};
      thickness(i,j)=2;
   else
      lastIndex(i,j)={strcat('IR cutoff No.',num2str(temp-2*nIR/3),'-3mm-')};
      thickness(i,j)=3;
   end;
   clear temp;
elseif rgbIndex(i,j)<nSet3,
   finalIndex(i,j)={[3 rgbIndex(i,j)-nSet2]};
   temp=rgbIndex(i,j)-nSet2;
   if temp<=nLongpass/3,
      lastIndex(i,j)={strcat('Longpass No.',num2str(temp),'-1mm-')};
      thickness(i,j)=1;
   elseif temp<=2*nBandpass/3,
      lastIndex(i,j)={strcat('Longpass No.',num2str(temp-nLongpass/3),'-2mm-')};
      thickness(i,j)=2;
   else
      lastIndex(i,j)={strcat('Longpass No.',num2str(temp-2*nLongpass/3),'-3mm-')};
      thickness(i,j)=3;
   end;
   clear temp;
elseif rgbIndex(i,j)<nSet4,
   temp1=floor((rgbIndex(i,j)-nSet3-0.1)/nBandpass)+1;
   temp2=rgbIndex(i,j)-nSet3-nBandpass*(temp1-1);
   finalIndex(i,j)={[4 rgbIndex(i,j)-nSet3 temp2 temp1 0]};
   if temp2<=nBandpass/3,
      str1=strcat('bandpass No.',num2str(temp2),'-1mm-');
      thickness(i,j)=1;
   elseif temp2<=2*nBandpass/3,
      str1=strcat('bandpass No.',num2str(temp2-nBandpass/3),'-2mm-');
      thickness(i,j)=2;
   else
      str1=strcat('bandpass No.',num2str(temp2-2*nBandpass/3),'-3mm-');
      thickness(i,j)=3;
   end;
   if temp1<=nIR/3,
      str2=strcat('IR cutoff No.',num2str(temp1),'-1mm-');
      thickness(i,j)=thickness(i,j)+1;
   elseif temp1<=2*nIR/3,
      str2=strcat('IR cutoff No.',num2str(temp1-nIR/3),'-2mm-');
      thickness(i,j)=thickness(i,j)+2;
```

```
        else
            str2=strcat('IR cutoff No.',num2str(temp1-2*nIR/3),'-3mm-');
            thickness(i,j)=thickness(i,j)+3;
        end;
        lastIndex(i,j)={strcat(str1,str2)};
        clear temp1 temp2;
    elseif rgbIndex(i,j)<nSet5,
        temp1=floor((rgbIndex(i,j)-nSet4-0.1)/nBandpass)+1;
        temp2=rgbIndex(i,j)-nSet4-nBandpass*(temp1-1);
        finalIndex(i,j)={[5 rgbIndex(i,j)-nSet4 temp2 0 temp1]};
        if temp2<=nBandpass/3,
            str1=strcat('bandpass No.',num2str(temp2),'-1mm-');
            thickness(i,j)=1;
        elseif temp2<=2*nBandpass/3,
            str1=strcat('bandpass No.',num2str(temp2-nBandpass/3),'-2mm-');
            thickness(i,j)=2;
        else
            str1=strcat('bandpass No.',num2str(temp2-2*nBandpass/3),'-3mm-');
            thickness(i,j)=3;
        end;
        if temp1<=nLongpass/3,
            str2=strcat('Longpass No.',num2str(temp1),'-1mm-');
            thickness(i,j)=thickness(i,j)+1;
        elseif temp1<=2*nLongpass/3,
            str2=strcat('Longpass No.',num2str(temp1-nLongpass/3),'-2mm-');
            thickness(i,j)=thickness(i,j)+2;
        else
            str2=strcat('Longpass No.',num2str(temp1-2*nLongpass/3),'-3mm-');
            thickness(i,j)=thickness(i,j)+3;
        end;
        lastIndex(i,j)={strcat(str1,str2)};
        clear temp1 temp2;
    elseif rgbIndex(i,j)<nSet6,
        temp1=floor((rgbIndex(i,j)-nSet5-0.1)/nLongpass)+1;
        temp2=rgbIndex(i,j)-nSet5-nLongpass*(temp1-1);
        finalIndex(i,j)={[6 rgbIndex(i,j)-nSet5 0 temp1 temp2]};
        if temp1<=nIR/3,
            str1=strcat('IR cutoff No.',num2str(temp1),'-1mm-');
            thickness(i,j)=1;
        elseif temp1<=2*nIR/3,
            str1=strcat('IR cutoff No.',num2str(temp1-nIR/3),'-2mm-');
            thickness(i,j)=2;
        else
            str1=strcat('IR cutoff No.',num2str(temp1-2*nIR/3),'-3mm-');
            thickness(i,j)=3;
        end;
        if temp2<=nLongpass/3,
            str2=strcat('Longpass No.',num2str(temp2),'-1mm-');
            thickness(i,j)=thickness(i,j)+1;
        elseif temp2<=2*nLongpass/3,
            str2=strcat('Longpass No.',num2str(temp2-nLongpass/3),'-2mm-');
            thickness(i,j)=thickness(i,j)+2;
        else
            str2=strcat('Longpass No.',num2str(temp2-2*nLongpass/3),'-3mm-');
            thickness(i,j)=thickness(i,j)+3;
        end;
        lastIndex(i,j)={strcat(str1,str2)};
        clear temp1 temp2;
    end;
  end;
end;
finalIndex_CQFx=finalIndex;
```

```
lastIndex_CQFx=lastIndex;
maxThickness=max(thickness,[],2);

% ================== load Macbeth ColorChecker (MCC) and Vrhel-Trussell data sets again ============

R1=interp1(waveMacbeth,originalMacbeth,wave); mccR=R1'; nSample1=size(mccR,2);
load VrhelDatabase; R1=interp1(waveVrhel,[VrhelMunsell VrhelObject VrhelDupont],wave); vrhelR=R1';
nSample2=size(vrhelR,1);
if nWave==81, vrhelR(:,72:81)=vrhelR(:,71)*ones(1,10); vrhelR(:,1:2)=vrhelR(:,3)*ones(1,2); end;

% ================== calculate the color difference performance of those 500 combinations ===========

global rgbM xyzM Wn;
Wn=xyz31'*Scanlite; scaleK=100/Wn(2); Wn=scaleK*Wn;
mccXYZ=mccR*[diag(Scanlite)*xyz31];                 % raw XYZ of MCC patches
mccXYZ=scaleK*mccXYZ;                               % normalized XYZ of MCC, Yw=100
vrhelXYZ=vrhelR*[diag(Scanlite)*xyz31];             % raw XYZ of Vrhel-Trussell samples
vrhelXYZ=scaleK*vrhelXYZ;                           % normalized XYZ of Vrhel-Trussell samples, Yw=100

clear overlapRG overlapRB overlapGB;

% ============================================================================

% load c:\download\UMG08New2;          % load the final results, copy-paste-run the following analysis if necessary
for i=1:200,                           % The optimal 200 sets are analyzed, you may choose 1:50, or even 1:500 etc.
   if maxThickness(nUMG+1-i)<5,        % total thickness in each channel is limited to 4mm for Quantix filter wheel
      i                                % The thickness constraint might not be necessary for other cameras

      % ========= plot the total spectral sensitivities and the filters only, post the filter index and thickness

      figure('Units','centimeters','Position',[2 2 20 10]); set(gcf,'PaperPositionMode','auto');
      a=[filterSet(:,rgbIndex(nUMG+1-i,3)) filterSet(:,rgbIndex(nUMG+1-i,2)) filterSet(:,rgbIndex(nUMG+1-i,1))];
      x=pinv(a)*xyz31;
      subplot(1,2,1);
      plot(wave,a,'r','LineWidth',2);
      axis([wave(1) wave(nWave) min(min(a)) max(max(a))]);
      title(strcat(num2str(i),'--UMG=',num2str(umgMax(tempIndex(nUMG+1-i))),'--\mu=',num2str(miu0(tempIndex(nUMG+1-
i)))));
      xlabel(strcat('UMG1=',num2str(UMG1(tempIndex(nUMG+1-i))),'--UMG2=',num2str(UMG2(tempIndex(nUMG+1-i)))));
      ylabel(strcat('UMG3=',num2str(UMG3(tempIndex(nUMG+1-i))),'--CQFx=',num2str(CQFx(tempIndex(nUMG+1-i)))));
      % xlabel('Wavelength (nm)');     ylabel('Channel Spectral Sensitivity'); % axis([wave(1) wave(nWave) -0.5 2]);
      % text(wave(10),max(max(a))/2+0.05,lastIndex_CQFx{nUMG+1-i,1});
      % text(wave(10),max(max(a))/2+0.00,lastIndex_CQFx{nUMG+1-i,2});
      % text(wave(10),max(max(a))/2-0.05,lastIndex_CQFx{nUMG+1-i,3});
      b=[a(:,1)./CCD a(:,2)./CCD a(:,3)./CCD];
      subplot(1,2,2); plot(wave,b(:,1),'r',wave,b(:,2),'g',wave,b(:,3),'b');
      axis([wave(1) wave(nWave) 0 1]); title('Filters only, no CCD QE');
      text(wave(4),0.9+0.05,lastIndex_CQFx{nUMG+1-i,1},'FontSize',8);
      text(wave(4),0.9+0.00,lastIndex_CQFx{nUMG+1-i,2},'FontSize',8);
      text(wave(4),0.9-0.05,lastIndex_CQFx{nUMG+1-i,3},'FontSize',8);

      % ================ calculate the overlapping area for RGB sensitivities

      sR=a(:,1); sG=a(:,2); sB=a(:,3);
      for j=1:nWave,
         if sR(j)<sG(j), sRG(j)=sR(j); else sRG(j)=sG(j); end;
         if sR(j)<sB(j), sRB(j)=sR(j); else sRB(j)=sB(j); end;
         if sG(j)<sB(j), sGB(j)=sG(j); else sGB(j)=sB(j); end;
      end;
      overlapRG(i,:)=sum(sRG)*dWave;
      overlapRB(i,:)=sum(sRB)*dWave;
      overlapGB(i,:)=sum(sGB)*dWave;
```

```
% ================ calculate the averaged peak senstivity for RGB channels

maxSS(i,:)=(2*max(a(:,3))+max(a(:,2))+max(a(:,1)))/4;

% Thickness of the SS with satisfactory thickness requirements

maxFilterThick(i,:)=maxThickness(nUMG+1-i);

% calculate the normalized RGB signals for both MCC and Vrhel-Trussell data set

mccDC=mccR*[diag(Scanlite)*a];
maxDC=max(max(mccDC));
mccDC=mccDC/maxDC;
vrhelDC=vrhelR*[diag(Scanlite)*a];
vrhelDC=vrhelDC/maxDC;

% ================================================================
% for MCC, calculate the color difference and obtain 3x3 conversion matrix
% x1: convert normalized RGB digital counts to normalized XYZ values

rgbM=mccDC; xyzM=mccXYZ;                        % rgbM: matrix of rgb dc, xyzM: matrix of XYZ
x0=pinv(rgbM'*rgbM)*rgbM'*xyzM;                 % x0: initial matrix of x1, by pseudo-inverse
[x,DE]=fminunc('TestFiltersOptFun',x0); x1=x; DE        % x1: obtained by minimizing CIE DE94
XYZ1=rgbM*x1; XYZ2=xyzM; XYZ0=Wn;                       % XYZ2: reference XYZ = xyzM; XYZ1: estimated XYZ
from RGB
[L1,a1,b1,c1,h1]=XYZ2Lab(XYZ1(:,1),XYZ1(:,2),XYZ1(:,3),XYZ0(1),XYZ0(2),XYZ0(3));          % convert XYZ1 to
CIELAB
[L2,a2,b2,c2,h2]=XYZ2Lab(XYZ2(:,1),XYZ2(:,2),XYZ2(:,3),XYZ0(1),XYZ0(2),XYZ0(3));          % convert XYZ2 to
CIELAB
deltaE94 = CIE94lab(L1, a1, b1, L2, a2, b2,1);                  % calculate DE94 for two sets of L*a*b*
deltaELab=sqrt((L2-L1).^2+(a2-a1).^2+(b2-b1).^2);               % calculate DEab for two sets of L*a*b*
meanDE=mean([deltaE94' deltaELab']);                            % calculate mean DE
maxDE=max([deltaE94' deltaELab']);                              % calculate max DE
E_1=deltaE94';
[meanDE maxDE]
meanDE1(i,:)=meanDE; maxDE1(i,:)=maxDE;
z90percent1(i,:)=prctile(E_1,90);                               % calculate 90th percentile
conversionM(i,1)={[x0,x1]};                                     % save conversion matrix

% ================================================================================
% for Vrhel-Trussell dataset, calculate the color difference and obtain 3x3 conversion matrix
% the process is the same as the above one ==============================================

rgbM=vrhelDC; xyzM=vrhelXYZ;
x0=pinv(rgbM'*rgbM)*rgbM'*xyzM;
[x,DE]=fminunc('TestFiltersOptFun',x0); x2=x; DE        % x1: conversion matrix obtained by minimizing DE94
XYZ1=rgbM*x2; XYZ2=xyzM; XYZ0=Wn;
[L1,a1,b1,c1,h1]=XYZ2Lab(XYZ1(:,1),XYZ1(:,2),XYZ1(:,3),XYZ0(1),XYZ0(2),XYZ0(3));
[L2,a2,b2,c2,h2]=XYZ2Lab(XYZ2(:,1),XYZ2(:,2),XYZ2(:,3),XYZ0(1),XYZ0(2),XYZ0(3));
deltaE94 = CIE94lab(L1, a1, b1, L2, a2, b2,1);
deltaELab=sqrt((L2-L1).^2+(a2-a1).^2+(b2-b1).^2);
meanDE=mean([deltaE94' deltaELab']);
maxDE=max([deltaE94' deltaELab']);
E_2=deltaE94';
[meanDE maxDE]
meanDE2(i,:)=meanDE; maxDE2(i,:)=maxDE;
z90percent2(i,:)=prctile(E_2,90);
conversionM(i,2)={[x0,x2]};

% ================================================================================
% applying the conversion matrix from MCC on Vrhel-Trussell dataset
```

```
    % the process is the same as the above one ==================================================

    rgbM=vrhelDC; xyzM=vrhelXYZ;
    x3=x1;
    XYZ1=rgbM*x3; XYZ2=xyzM; XYZ0=Wn;
    [L1,a1,b1,c1,h1]=XYZ2Lab(XYZ1(:,1),XYZ1(:,2),XYZ1(:,3),XYZ0(1),XYZ0(2),XYZ0(3));
    [L2,a2,b2,c2,h2]=XYZ2Lab(XYZ2(:,1),XYZ2(:,2),XYZ2(:,3),XYZ0(1),XYZ0(2),XYZ0(3));
    deltaE94 = CIE94lab(L1, a1, b1, L2, a2, b2,1);
    deltaELab=sqrt((L2-L1).^2+(a2-a1).^2+(b2-b1).^2);
    meanDE=mean([deltaE94' deltaELab']);
    maxDE=max([deltaE94' deltaELab']);
    E_3=deltaE94';
    [meanDE maxDE]
    meanDE3(i,:)=meanDE; maxDE3(i,:)=maxDE; z90percent3(i,:)=prctile(E_3,90);
    conversionM(i,3)={[x0,x3]};

    % save UMG(EE,EE) and miu0 of these satisfactory SS onto CQFs

    CQFs(i,:)=[umgMax(tempIndex(nUMG+1-i)) miu0(tempIndex(nUMG+1-i))];

    % print the figures of these satisfactory SS with their filter components

    print('-depsc','-tiff',strcat('c:/temp/figure',num2str(i)));
  end;
end;

save c:\download\UMG08New2;     % save the final results into a document so that copy-paste-run can be done

==========================      THE END     ==========================
```